



## City Research Online

### City, University of London Institutional Repository

---

**Citation:** Bianchini, D. (2016). Entanglement entropy in integrable quantum systems. (Unpublished Doctoral thesis, City, University of London)

This is the accepted version of the paper.

This version of the publication may differ from the final published version.

---

**Permanent repository link:** <https://openaccess.city.ac.uk/id/eprint/17490/>

**Link to published version:**

**Copyright:** City Research Online aims to make research outputs of City, University of London available to a wider audience. Copyright and Moral Rights remain with the author(s) and/or copyright holders. URLs from City Research Online may be freely distributed and linked to.

**Reuse:** Copies of full items can be used for personal research or study, educational, or not-for-profit purposes without prior permission or charge. Provided that the authors, title and full bibliographic details are credited, a hyperlink and/or URL is given for the original metadata page and the content is not changed in any way.

# Entanglement Entropy in Integrable Quantum Systems



**Davide Bianchini**  
City, University of London  
Department of Mathematics

Thesis submitted for the degree of  
*Doctor of Philosophy*  
August 2016



# Contents

<b>1</b>	<b>Introduction</b>	<b>15</b>
<b>2</b>	<b>Measures of Entanglement</b>	<b>18</b>
2.1	Bipartite Quantum Entanglement . . . . .	18
2.1.1	A classical analogue . . . . .	20
2.1.2	An application: quantum teleportation . . . . .	21
2.2	Measures of Entanglement . . . . .	23
2.2.1	Density matrix . . . . .	23
2.2.2	Reduced density matrix . . . . .	25
2.2.3	What is a good measure of entanglement? . . . . .	26
2.2.4	Entanglement entropy . . . . .	27
2.3	Logarithmic Negativity . . . . .	29
2.4	Why Entanglement? . . . . .	31
2.5	Conclusions . . . . .	32
<b>3</b>	<b>Conformal and Integrable Quantum Field Theory</b>	<b>34</b>
3.1	Critical Systems . . . . .	34
3.1.1	Two dimensional CFT . . . . .	35
3.1.2	Conformal families . . . . .	37
3.1.3	Minimal models . . . . .	40
3.1.4	Modular transformations and conformal characters . . . . .	42
3.1.5	Non unitary CFT . . . . .	44
3.1.6	The Casimir effect . . . . .	45
3.2	Integrable Quantum Field Theory . . . . .	46
3.2.1	S-matrix . . . . .	46
3.2.2	Form factors . . . . .	49
3.3	Form Factor Equations . . . . .	52
3.3.1	Correlation functions . . . . .	56
3.3.2	Ultraviolet limit . . . . .	58

3.3.3	Non unitary case . . . . .	61
3.4	Operator Product Expansion . . . . .	63
3.5	Conclusions . . . . .	63
<b>4</b>	<b>Entanglement in Quantum Field Theory</b>	<b>65</b>
4.1	Entanglement Entropy and Partition Functions . . . . .	66
4.2	Branch Point Twist Fields . . . . .	71
4.3	Entropy in Conformal Field Theory . . . . .	73
4.3.1	Entanglement entropy . . . . .	75
4.3.2	Beyond criticality . . . . .	76
4.4	Conclusions . . . . .	77
<b>5</b>	<b>Entanglement in Non Unitary Conformal Field Theory</b>	<b>79</b>
5.1	Entanglement Entropy in Non Unitary CFT . . . . .	80
5.1.1	Two Virasoro algebras . . . . .	82
5.1.2	Partition functions . . . . .	83
5.1.3	Interpretation in terms of twist fields . . . . .	85
5.2	Entanglement Entropy in Logarithmic CFT . . . . .	86
5.3	Numerical Checks . . . . .	87
5.4	Comments about Non Hermiticity . . . . .	88
5.5	Conclusions . . . . .	90
<b>6</b>	<b>Entanglement in Non Unitary Quantum Field Theory</b>	<b>91</b>
6.1	Twist Field Form Factors in the Lee-Yang Model . . . . .	92
6.1.1	One- and two-particle form factors . . . . .	95
6.1.2	Higher particle form factors . . . . .	99
6.2	Conformal Perturbation Theory . . . . .	104
6.2.1	Twist field OPEs . . . . .	107
6.3	Numerics . . . . .	111
6.3.1	Short distance scaling . . . . .	112
6.3.2	Vacuum expectation values $\langle \mathcal{T} \rangle$ and $\langle : \mathcal{T} \phi : \rangle$ . . . . .	117
6.3.3	The $n = 3, 4$ cases . . . . .	118
6.3.4	Perturbative CFT vs form factor expansion . . . . .	119
6.4	Entanglement Entropy . . . . .	123
6.4.1	Saturation . . . . .	123
6.4.2	Corrections to saturation . . . . .	126
6.4.3	Leading correction to saturation . . . . .	131
6.4.4	Numerical identification of the universality class . . . . .	132

6.5	Conclusions . . . . .	133
<b>7</b>	<b>Entanglement in Forrester-Baxter RSOS Models</b>	<b>135</b>
7.1	The FB RSOS Models . . . . .	135
7.2	Entanglement Using Corner Transfer Matrix . . . . .	139
7.2.1	Hamiltonian limit . . . . .	139
7.2.2	Corner transfer matrix . . . . .	140
7.2.3	Reduced density matrix using CTMs . . . . .	143
7.3	Entanglement in Forrester-Baxter Models . . . . .	145
7.3.1	Thermodynamic limit . . . . .	147
7.3.2	“Unusual” corrections . . . . .	151
7.3.3	Off-critical logarithmic minimal models . . . . .	154
7.4	RSOS Quantum Hamiltonians . . . . .	155
7.4.1	Multiplying face operators . . . . .	157
7.4.2	The $r = 5$ case (the $T_2$ quantum chains) . . . . .	159
7.4.3	The generic case . . . . .	166
7.5	Conclusions . . . . .	168
<b>8</b>	<b>Logarithmic Negativity and Entanglement Entropy in Free Boson Theories</b>	<b>170</b>
8.1	Logarithmic Negativity . . . . .	170
8.1.1	The $\langle \mathcal{T}(0)\tilde{\mathcal{T}}(r) \rangle$ short distance scaling . . . . .	172
8.1.2	The $\langle \mathcal{T}(0)\mathcal{T}(r) \rangle$ short distance scaling . . . . .	172
8.2	Form Factor Expansion of Twist Field Correlation Functions . . . . .	173
8.2.1	Form factors in the massive free boson theory . . . . .	173
8.2.2	Connected correlation functions . . . . .	174
8.3	Short Distance Scaling . . . . .	178
8.3.1	The two-point function $\langle \mathcal{T}(0)\tilde{\mathcal{T}}(r) \rangle$ . . . . .	178
8.3.2	The two-point function $\langle \mathcal{T}(0)\mathcal{T}(r) \rangle$ . . . . .	185
8.4	The Vacuum Expectation Value $\langle \mathcal{T} \rangle$ and The Structure Constant $C_{\mathcal{T}\mathcal{T}}^{\mathcal{T}^2}$ . . . . .	187
8.4.1	The $\langle \mathcal{T}(0)\tilde{\mathcal{T}}(r) \rangle$ correlation function . . . . .	188
8.4.2	The $\langle \mathcal{T}(0)\mathcal{T}(r) \rangle$ correlation function . . . . .	189
8.4.3	The $C_{\mathcal{T}\mathcal{T}}^{\mathcal{T}^2}$ structure constant . . . . .	191
8.5	Interpretation of Divergent Series . . . . .	197
8.5.1	Three-point structure constant of $C_{\mathcal{T}\mathcal{T}}^{\mathcal{T}^2}$ and logarithmic negativity . . . . .	200
8.5.2	Three-point structure constant of $C_{\mathcal{T}\mathcal{T}}^{\mathcal{T}^2}$ and out of equilibrium systems . . . . .	202
8.6	Conclusions . . . . .	203

<b>9</b>	<b>Conclusions</b>	<b>206</b>
<b>A</b>	<b>Values of <math>A_i</math></b>	<b>211</b>
<b>B</b>	<b>Structure Constants</b>	<b>212</b>
B.1	Structure Constants of Twist Fields $\mathcal{T}$ . . . . .	213
B.1.1	The $C_{\mathcal{T}\tilde{\mathcal{T}}}^{\Phi_1}$ structure constant . . . . .	213
B.1.2	The $C_{\mathcal{T}\tilde{\mathcal{T}}}^{\Phi_{1j}}$ structure constant . . . . .	214
B.1.3	Higher-point structure constants . . . . .	215
B.2	Structure Constants of Composite Twist Fields : $\mathcal{T}\phi$ : . . . . .	215
<b>C</b>	<b>Monte Carlo Integration Algorithm</b>	<b>219</b>
<b>D</b>	<b>Jacobi Elliptic Theta Functions</b>	<b>222</b>
<b>E</b>	<b>Summation Formulæ</b>	<b>224</b>
<b>F</b>	<b>Numerical Fit</b>	<b>226</b>
F.1	Fitting Algorithm - Polynomial . . . . .	226
F.2	Fitting Algorithm - Logarithm . . . . .	227
<b>G</b>	<b>Numerical Implementations</b>	<b>229</b>

# List of Figures

3.1	The three-particle scattering (first diagram) can be factorised into three two-particle processes (second and third diagrams). The only difference between the two factorisations is the order of the individual scattering processes.	47
3.2	Form factors of the operator $\mathcal{O}$ with $\ell$ incoming particles . . . . .	52
3.3	Graphical representation of the first Watson equation. In the form factor on the right the two particles $i$ and $i + 1$ have been exchanged. Since these particles live in a two-dimensional space-time, the scattering is unavoidable.	53
3.4	Graphical representation of the second Watson equation. A shift by $2\pi i$ in the first rapidity implies a complete rotation of the particle around the operator $\mathcal{O}$ . The initial order of particles can be restored by making the first particle scatter with all others. . . . .	53
4.1	Propagator using path integrals. . . . .	67
4.2	Partition function . . . . .	67
4.3	Reduced density matrix. . . . .	68
4.4	Surface $\mathcal{M}_3$ for $n = 3$ . . . . .	71
4.5	Surface $\mathcal{M}_3$ for $n = 3$ and $\beta = \infty$ . Picture taken from [14] with permission from authors. . . . .	71
5.1	Space-time representation of the system. . . . .	80
5.2	The system mapped to a cylinder . . . . .	81
5.3	Different cylinders. . . . .	82
5.4	Scaling of entanglement entropy in the Lee-Yang chain with $N = 24$ sites against the length $r$ of the subsystem $A$ (normalised by the correlation length $\xi$ - see text). The blue squares represent the numerical data, while the red dashed line corresponds to the fit (5.26). . . . .	87
5.5	Scaling of entanglement entropy in the Lee-Yang chain with $N = 12$ sites against the length $r$ of the subsystem. In this case the finite size gap is too large to extract meaningful critical information. . . . .	89

6.1	Second Watson equation for twist field. The branch cut (red dashed line) modifies particles when they cross it. . . . .	93
6.2	The twist field $\mathcal{T}$ creates a branch cut (red dashed line) which moves particles between adjacent copies. . . . .	94
6.3	The twist field $\tilde{\mathcal{T}}$ creates a branch cut (green dashed line) which moves particles between adjacent copies. Notice that the orientation of this branch cut is reversed compared to $\mathcal{T}$ (Figure 6.2). . . . .	94
6.4	When both twist fields are present, a finite branch cut (red dashed line) is created. . . . .	94
6.5	Scaling of the correlator $\langle \mathcal{T}(0)\tilde{\mathcal{T}}(r) \rangle$ . The CFT prediction is given by the black solid line, while the one-, two- and three- particle form factor expansion are given respectively by the red squares, blue circles and green triangles. . . . .	113
6.6	Scaling of the correlator $\langle : \mathcal{T}\phi:(r) : \tilde{\mathcal{T}}\phi:(0) \rangle$ . The CFT prediction is given by the black solid line, while the one-, two- and three- particle form factor expansion are given respectively by the red squares, blue circles and green triangles. . . . .	114
6.7	Comparison between the perturbative (solid black line) and form factor (coloured points) expansion using linear (left) and logarithmic (right) scales.	120
6.8	Comparison between the perturbative (solid black line) and form factor (coloured points) expansion using linear (left) and logarithmic (right) scales.	121
6.9	Comparison between the perturbative (solid black line) and form factor (coloured points) expansion using linear (left) and logarithmic (right) scales.	122
6.10	Comparison between the perturbative (solid black line) and form factor (coloured points) expansion using linear (left) and logarithmic (right) scales.	122
6.11	Scaling of entanglement entropy at different scales. Near the critical point ( $mr \ll 1$ ) it scales logarithmically according to the CFT prediction. At the other end of the scale, in the infrared regime ( $mr \gg 1$ ), the entropy is constant. Less is known about the behaviour of the entropy in the intermediate region. The form factor expansion can be used to estimate how the entropy tends to its saturation value. . . . .	124
7.1	Square tile. . . . .	136
7.2	A row-to-row transfer matrix between two spin configurations. . . . .	140
7.3	A double-row-to-row transfer matrix between two spin configurations. The intermediate spins (black dots) are summed over all possible configurations.	141

7.4	Diamond shaped lattice divided into four corners. Each Corner Transfer Matrix depends on the values of the local height on the two edges (denoted by $\circ$ ). The internal sites ( $\bullet$ ) should be considered already summed over all possible configurations. . . . .	142
7.5	Tadpole diagram $T_2$ . . . . .	159
8.1	Tripartite system. Using logarithmic negativity we can compute the amount of entanglement between the subsystems $A$ and $B$ even though they are embedded into $C$ . . . . .	171
8.2	Tripartite system in Figure 8.1 in the limit $A = [-\infty, 0]$ , $B = [r, \infty[$ . . . . .	171
8.3	Difference between fully connected and not fully connected diagrams. The diagram on the left (right) corresponds to terms like the second (third) line of (8.18). Even though equation (8.18) refers to a $\langle \mathcal{T}(0)\tilde{\mathcal{T}}(r) \rangle$ correlator, four operators appear in this picture instead of just two. This discrepancy is corrected by the fact that the form factors we are taking into account are normalised by the VEV of $\mathcal{T}$ . . . . .	177
8.4	Numerical evaluation of the scaling dimension $-4x_{\mathcal{T}\mathcal{T}}$ for integer and non integer values of $n$ . In order to compute the sum (8.44) for a very high value of $\ell$ , the actual values have been computed through a numerical fit. We computed and summed the first 150 terms of (8.44), then we completed the sum by fitting the logarithm of each term from $\ell=20$ to $\ell=150$ against $\log \ell$ . . . . .	184
8.5	Values of $u_\ell(3)$ and $u_\ell(5)$ in linear-logarithmic scale. . . . .	189
8.6	Values (rescaled) of $u_\ell(3)$ and $u_\ell(5)$ (red dots) in linear scale checked against the fit (8.59) (blue line). . . . .	190
8.7	The values of the integrals $v_\ell$ in linear-logarithmic scale. . . . .	191
8.8	The (rescaled) values of $v_\ell$ (red dots) checked against the interpolating function (8.63) (blue line) in linear scale. . . . .	192
8.9	Numerical values of $\kappa_{\mathcal{T}\mathcal{T}}^o$ (red dots) for different integer and non integer values of $n$ . The blue line represent the best fit $-0.34 + 0.215n + 0.13/n$ . . . . .	193
8.10	Numerical values of $-\log C_{\mathcal{T}\mathcal{T}}^{\mathcal{T}^2}$ for some even values of $n$ (red dots). Both interpolating functions (blue and green lines) provide a very good fit of the data. . . . .	195
8.11	Numerical values (red dots) of the logarithm of the three-point structure constant computed using equation (8.68). The blue and green solid line the $-1.0 + 0.27n + 0.9/n$ and $-0.31 + 0.31n - 0.46 \log n$ fitting functions, respectively. These values are checked against $\log \tilde{P}_n$ (yellow dashed line). . . . .	201

8.12 Time evolution of logarithmic negativity after a quench at equal temperature  $\beta^{-1}$ . Picture taken from [15] with permission from the authors. . . . 202

# List of Tables

6.1	Scaling of the $\langle \mathcal{T}(0)\tilde{\mathcal{T}}(r) \rangle$ correlation function. The perturbative CFT prediction is presented together with the one-, two- and three-particle form factor computation. Clearly, adding more particles, the form factors expansion approaches the perturbative prediction. . . . .	113
6.2	Scaling of the $\langle : \mathcal{T}\phi : (0) : \tilde{\mathcal{T}}\phi : (r) \rangle$ correlation function. The perturbative CFT prediction is presented together with the one-, two- and three-particle form factor computation. Clearly, adding more particles, the form factors expansion approaches the perturbative prediction. . . . .	114
8.1	Numerical evaluation of (8.39). The sum has been truncated at $\ell = 2000$ and it shows a very good agreement with the expected scaling dimension (8.5). . . . .	182
8.2	Numerical values of $\kappa_{\mathcal{T}\mathcal{T}}^o = -\log\left(\frac{c_{\mathcal{T}\mathcal{T}}}{\langle \mathcal{T} \rangle_n}\right)$ for $n$ odd. These values have been computed from equation (8.61) summing up to $\ell = 1000$ using the interpolation (8.63). . . . .	192

# Acknowledgements

My first thanks must go to my supervisor Dr Olalla Castro-Alvaredo for her invaluable help and guidance during my doctoral studies. I want to thank her also for her patience and her support with which she accompanied my growth both as a scientist and as a person. The end of path is always the moment to thank those who have been with us from the very beginning. Thanks to my family who has been supportive and encouraging whatever the physical distance between us. The PhD is of course a beautiful and demanding challenge and every challenge is better faced with the help of friends and colleagues. Both in and outside the University, in UK and abroad, to all of you, thank you! My last thoughts goes to my wife: her love, her kindness and her trust has made the most tough choices easier.

# Declaration

I hereby grant powers of discretion to the University Librarian to allow the thesis to be copied in whole or in part without further reference to the author. This permission covers only single copies made for study purposes, subject to normal conditions of acknowledgment.

# Abstract

In this thesis I present the results I have been developing during my PhD studies at City University London. The original results are based on D Bianchini *et al* [1], D Bianchini, O Castro-Alvaredo and B Doyon [2], D Bianchini and F Ravanini [3], D Bianchini *et al* [4] and D Bianchini and O Castro-Alvaredo [5]. In all but one ([4]) publications, we compute the entanglement [6] of various systems. Using the celebrated “replica trick” [7, 8] we compute the entanglement entropy of non unitary systems using integrable tools in continuum ([1, 2]) and discrete ([3]) models. In particular, in [1] we generalise the method described in [7] in order to take into account non unitary conformal systems. In [2] we use a form factor expansion [9, 10] to probe a non unitary system outside the critical point. In [4] we derive the explicit expressions of one dimensional quantum Hamiltonians which provide a lattice realisation of off critical non unitary minimal models. Using a Corner Transfer Matrix approach [11, 12, 13] we compute the scaling of the entanglement of such spin chains [3]. In [5] we study the scaling of various twist field correlation functions in order to compute the entanglement entropy and the logarithmic negativity in free boson massive theories.

# Chapter 1

## Introduction

Since the emergence of Quantum Mechanics at the beginning of the 20<sup>th</sup> century many questions have been posed by scientists and philosophers about its intrinsic nature and how it will affect the deterministic and accepted view of Nature. Among the numerous quantum features of the Universe, entanglement is maybe the most intriguing and the most manifestly quantum phenomenon [6]. Quantum entanglement, an intrinsic quantum correlation, is what makes quantum phenomena really quantum and - for the last hundred years or so - has been unlocking the doors to new possibilities and opportunities which have no classic counterpart. Like many other physical quantities, the need of an operative definition of a measure of entanglement arises naturally. The main focus of this thesis is the evaluation of such measures using one of the most successful tools of modern physics: quantum field theory. In particular, we will focus on a particular class of models, the so-called integrable systems. Like the name suggests, integrable systems enjoy an infinite number of conservation laws which make the model integrable. When dealing with such systems, various physical quantities, including entanglement, can be computed exactly. Unfortunately, apart from some free theories and non local models, integrable systems exist only in two dimensions. These two dimensions can be arranged either as a 2+0 or 1+1 dimensional systems. While a Wick's rotation connects the two cases, they represent quite different situations. In particular, we refer to 2+0 dimensional theories as classical statistical bi-dimensional systems. On the other hand, 1+1 systems are unidimensional quantum models with a time evolution. After having introduced the main tools of integrable quantum field theories, we briefly review the known results in the literature regarding entanglement in 1+1 dimensional integrable theories. In the second part of the thesis we present some new results in the evaluation of entanglement in a particular class of theories, called non unitary. The thesis is structured as follows:

- In Chapter 2 we introduce quantum entanglement and its measures. In particular, we focus on entanglement entropy and logarithmic negativity, two among the most

---

common measures used in the context of integrable theories.

- In Chapter 3 we briefly review conformal field theories (CFT) and integrable quantum field theories (IQFT). These theories can be used to successfully describe a large class of critical and off-critical systems. We describe some objects and tools we use in the following chapters for the evaluation of entanglement. In particular we describe the so-called “form factor expansion”, a powerful tool for the evaluation of correlation functions in massive theories.
- In Chapter 4 we present some known results on the evaluation of entanglement entropy in (unitary) CFT and IQFT. We introduce the so-called “replica trick”, which can be used to represent entanglement measures as partition functions on particular geometries. We discuss how to represent entanglement measures as correlation functions of a special kind of field, called “branch point twist field”. We review how the “central charge”, a physical quantity related to the universality class of the critical point, affects the scaling of the entropy when the system can be described using a CFT. Moreover, we present some known results on the scaling of entanglement entropy in the massive regime, with a particular focus on the so-called “corrections to saturation”.
- In Chapter 5 we present the first original result of this thesis. We compute the entanglement entropy in non unitary CFT. The main result of this chapter is the extension of unitary results to the non unitary case. In particular, we show that the so-called “effective central charge” replaces the central charge in the scaling of entanglement entropy. Moreover, we present a numerical simulation supporting our analytical results. Additionally, we compute the entanglement entropy for the so-called logarithmic CFTs. We will return to this class of models in Chapter 8, when studying the uncompactified massless free boson. We show also how a new kind of branch point twist fields can be used to compute entanglement entropy in non unitary theories.
- In Chapter 6 we extend the previous result to massive non unitary integrable field theories. In particular, we use the form factor expansion to probe the entanglement entropy in the massive Lee-Yang model, the simplest non unitary IQFT. We show how the non unitarity of the model affects the scaling of entanglement entropy and we interpret such a difference in terms of a new kind of branch point twist fields.
- In Chapter 7 we perform another computation of entanglement entropy in a non unitary system. While in other chapters we rely on quantum field theory techniques to study the amount of entanglement in a system, in this chapter we present a lat-

---

tice computation. In particular, we compute the entanglement entropy of some one dimensional quantum chains associated to the so-called Forrester Baxter Restricted-Solid-On-Solid (FB RSOS) model. The FB RSOS model is a classical lattice model which, in the thermodynamic limit and in a particular regime, provides a lattice realisation of the off critical minimal models, a large class of perturbed CFTs. Using the “Corner Transfer Matrix” approach, we show how the scaling of the entropy differs from the unitary case. In particular, we compute both the principal term and the leading corrections to the scaling of entanglement. Moreover, we extend our computations to the so-called “off critical logarithmic minimal models”. Additionally, using a tool called “Hamiltonian limit” we compute the quantum Hamiltonian associated to the FB RSOS model.

- In Chapter 8 we consider the entanglement entropy and the logarithmic negativity of the massive free boson theory. Using the form factor expansion of some correlation functions of branch point twist fields, we study the scaling of entanglement in such systems. The simple nature of the free boson theory allows very precise form factor studies. While in many theories only few terms of the form factor expansion can be computed explicitly, in this case we could sum thousands of contributions (in some cases even an infinite number). Using form factor expansion, we recover a number of short distance results derived in CFT. Moreover, we find some very interesting divergences in some correlation functions associated to entanglement entropy and logarithmic negativity. We interpret these divergences as a signal of extra double logarithmic terms in the scaling of entanglement. Such double logarithmic corrections are in agreement with the CFT prediction of the scaling of entanglement entropy in logarithmic CFT presented in Chapter 5. Moreover, we compute the “three point structure constant” of twist field, which, in this context, represents an important universal constant in the scaling of logarithmic negativity.

## Chapter 2

# Measures of Entanglement

In this chapter we introduce quantum entanglement and its properties. In particular, after having introduced the qualitative features of entanglement, we will discuss some physical quantities which can be used to measure the amount of entanglement in a physical system.

### 2.1 Bipartite Quantum Entanglement

Let us start with a very simple example. Consider a two-particle system and two observers, called Alice and Bob. Alice and Bob share a quantum state made by the two particles. In particular, both of them have a one-half spin particle<sup>1</sup>. Let us denote by  $|\uparrow\rangle$  positive  $+\frac{1}{2}$  spin and by  $|\downarrow\rangle$  the negative  $-\frac{1}{2}$  spin. Let us now consider two different cases, namely  $\phi$  and  $\psi$ :

$$|\phi\rangle = |\uparrow\rangle_A \otimes |\downarrow\rangle_B \quad (2.1)$$

$$|\psi\rangle = \frac{|\uparrow\rangle_A \otimes |\downarrow\rangle_B - |\downarrow\rangle_A \otimes |\uparrow\rangle_B}{\sqrt{2}} \quad (2.2)$$

Even though both cases might seem similar (for instance, the total spin in the two cases is zero), they behave quite differently. Consider the  $\phi$  case first. If Alice measures the spin of the particle  $A$ , she finds  $1/2$  and she does not get any *additional* piece of information regarding the other particle. Of course, the same situation happens if Bob measures its particle. In this case the two particles are not “connected” or entangled and the state is said *separable* (or *factorisable*). The case  $\psi$  is definitely more interesting. As soon as Alice performs a measure of the spin of her particle, she immediately knows the value of the spin of Bob’s particle, even if they are far apart. This feature, commonly referred to as *entanglement*, is intrinsic in the structure of the quantum state of the two particles. A

---

<sup>1</sup>For the purpose of the example, the actual kind of quantum system is not relevant. For instance, it could be the spin of an electron, the nuclear spin of an atom or even the helicity of a photon.

quantum state is separable if it can be written as a single tensor product between single-particle states, like  $|\phi\rangle$ , while states like  $|\psi\rangle$  are called *entangled* (such a decomposition does not exist). This concept can be extended to systems with larger Hilbert spaces and more particles, but, of course, it does not make any sense talking about entanglement if there is only one particle.

Consider now a quantum system composed by  $N$  particles and define  $\mathcal{H}_i$  as the single-particle Hilbert space, the quantum states of the  $i$ -th particle. The total Hilbert space would be given by:

$$\mathcal{H}_N = \bigotimes_{a=1}^N \mathcal{H}_a \quad (2.3)$$

A generic quantum state  $|\Psi\rangle \in \mathcal{H}_N$  can be represented as

$$|\Psi\rangle = \sum_{i_1, \dots, i_N} C_{i_1, \dots, i_N} |\psi_{i_1}\rangle_1 \otimes \dots \otimes |\psi_{i_N}\rangle_N \quad (2.4)$$

where the  $C$ s are complex numbers and  $|\psi_i\rangle_a \in \mathcal{H}_a$ . In the above expression, each index  $i_a$  runs from 1 to  $\dim(\mathcal{H}_a)$  (which can be either finite or infinite). Like in the two-particle examples, states can be factorisable or entangled. For instance, the state

$$|\Psi\rangle = \frac{|\psi_1\rangle_1 \otimes |\psi_1\rangle_2 \otimes |\psi_{i_3}\rangle_3 \otimes \dots \otimes |\psi_{i_N}\rangle_N + |\psi_2\rangle_1 \otimes |\psi_1\rangle_2 \otimes |\psi_{i_3}\rangle_3 \otimes \dots \otimes |\psi_{i_N}\rangle_N}{\sqrt{2}} \quad (2.5)$$

is entangled. Interestingly, if we rearrange the above state, it seems now factorisable<sup>2</sup>

$$\begin{aligned} |\Psi\rangle &= \left[ \frac{|\psi_1\rangle_1 \otimes |\psi_2\rangle_2 + |\psi_2\rangle_1 \otimes |\psi_1\rangle_2}{\sqrt{2}} \right] \otimes |\psi_{i_3}\rangle_3 \otimes \dots \otimes |\psi_{i_N}\rangle_N \\ &= |\Phi\rangle_{12} \otimes |\Omega\rangle_{34\dots N} \end{aligned} \quad (2.7)$$

In this case the state does not look entangled, even if it is the very same state as before! From this example it is clear that a given quantum state can be either entangled or factorisable according to the partition chosen. In particular, a system described by the state (2.5) is entangled when considering the partitions  $A = 1$  and  $B = 2 \cup 3 \cup \dots \cup N$ . On the other hand, choosing a different partition like  $A = 1 \cup 2$  and  $B = 3 \cup \dots \cup N$  the state

---

<sup>2</sup>Here we define  $\Phi$  and  $\Omega$  as

$$\begin{aligned} |\Phi\rangle_{12} &= \frac{|\psi_1\rangle_1 \otimes |\psi_2\rangle_2 + |\psi_2\rangle_1 \otimes |\psi_1\rangle_2}{\sqrt{2}} \\ |\Omega\rangle_{34\dots N} &= |\psi_{i_3}\rangle_3 \otimes \dots \otimes |\psi_{i_N}\rangle_N \end{aligned} \quad (2.6)$$

is separable. From this example it is clear that entanglement is a feature that does not depend only on the explicit expression of the state but also on the partition chosen.

### 2.1.1 A classical analogue

Let us consider a classical analogue of the Alice’s and Bob’s measurements of quantum states. Suppose Alice (who lives in London) decides to visit her friend Bob in Sidney. She then prepares her suitcase and takes a plane to Australia. Once she has arrived at Bob’s place, she opens her luggage and finds out that she has only one red sock and she *immediately* realises that the other sock has been left in a drawer in London. In the same way, if she performs a measure on the particle  $A$  of the state (2.2) and finds ‘up’, she *immediately* knows that Bob’s spin is pointing down. Of course, the main difference between the two cases is that quantum particles “live” in both states as long as a measure has been performed on them. On the other hand, the second red sock has never left London. In both cases the result is uncertain before making a measure (‘which is the spin of the first particle?’ - ‘are there two red socks in my suitcase?’). While in the socks’ case one of the two possibilities (‘one sock’ or ‘two socks’) is chosen with a classical random distribution at the time of packing the suitcase, in the quantum case one of the two options (‘up’ or ‘down’) is selected at the time of the measure. During the last century there have been some attempts to interpret quantum mechanics using classical models. One of the most important of these formulations is the theory of *hidden variables*<sup>3</sup>. In such theory there is no quantum superposition and the result of a measure (say ‘up’ or ‘down’ for a spin system) is already determined at the time of creation of the quantum state. In particular, quantum particles have some degrees of freedom which are not experimentally accessible, called hidden variables, which determine the outcome of a measure. To explain this concept better, we can consider the celebrated Stern-Gerlach experiment [17]. In this experiment a beam of electrons is sent through an inhomogeneous magnetic field that deflects the trajectory of each electron according to its spin. Each electron of the beam has its spin pointing up or down. In standard quantum mechanics, we represent this situation as a superposition using the (not normalised) state  $|\uparrow\rangle + |\downarrow\rangle$ . The state collapses to one of the two options when a measure is performed. In the hidden variables interpretation each electron has an hidden variable  $\lambda$  uniformly distributed between 0 and 1 such that the electron points up or down according to its value. For instance, it points up if  $\lambda \in [0, 1/2[$  and down if  $\lambda \in [1/2, 1]$ . In a Stern-Gerlach experiment there is no way to rule out one of the two interpretations. In particular, we can consider the beam of

---

<sup>3</sup>During the last century a number of hidden variable theories has been introduced. Probably the first attempt to define such a theory was due to Louis de Broglie [16] in 1927.

electrons as truly quantum particles or as classical particles whose spin point up or down according to some classical probability distribution. In order to solve this ambiguity, in 1964 J S Bell proposed an ideal experiment [18], when an entangled two-particle state is taken into account. Bell discovered an inequality (the celebrated *Bell inequality*) which holds *only* in the hidden variables set up. On the other hand if the particles are truly quantum the inequality is not satisfied. Almost twenty years later, in 1981 A Aspect, P Grangier and G Roger performed an experiment [19] to check whether Bell's inequalities are satisfied or not. The experiment found a strong violation of Bell's inequality and ruled out any (local) hidden variable theory. Further and more recent experiments [20] ruled out some possible loopholes [21] which could have affected Aspect's experiment [19].

From the qualitatively point of view we can then say that there is entanglement between two parts  $A$  and  $B$  of a system if the state is not completely factorisable. While this definition is intuitive and gives a good grasp of the quantum nature of this feature, it is hardly quantifiable and does not distinguish between different levels of entanglement. For instance, the state <sup>4</sup>

$$\sqrt{0.001}|\uparrow\downarrow\rangle - \sqrt{0.999}|\downarrow\uparrow\rangle \quad (2.8)$$

is *almost* separable, but, according to our definition, it is entangled exactly as  $\frac{|\uparrow\downarrow\rangle - |\downarrow\uparrow\rangle}{\sqrt{2}}$ . In order to differentiate between those states, we need to introduce some quantitative measures of entanglement. Before that we would like to illustrate a celebrated quantum protocol which intrinsically exploits the entangled nature of certain quantum states.

### 2.1.2 An application: quantum teleportation

Probably, one of the most interesting protocols which exploit the entanglement of a state is the so-called *quantum teleportation*. Using such a protocol [22] it is possible to copy a given quantum state without knowing its internal structure. Consider the familiar situation when Alice and Bob share a quantum state of two particles  $A$  and  $B$ :

$$|\phi_{\text{shared}}\rangle_{AB} = \frac{|\uparrow\downarrow\rangle_{AB} + |\downarrow\uparrow\rangle_{AB}}{\sqrt{2}} \quad (2.9)$$

Each of them can perform operations and measures on one particle. Moreover, suppose Alice has an additional unknown quantum state  $|\phi_{\text{unknown}}\rangle_I = \alpha_0|\uparrow\rangle_I + \alpha_1|\downarrow\rangle_I$ <sup>5</sup>. The total

---

<sup>4</sup>In the following we will use a more compact notation for states:  $|\psi\phi\rangle \equiv |\psi\rangle_1 \otimes |\phi\rangle_2$ .

<sup>5</sup>For unknown state we mean that neither Alice or Bob know the value of the constants  $\alpha_i$ .

state describing the system (shared+unknown) is then

$$|\Psi_{\text{total}}\rangle = |\phi_{\text{unknown}}\rangle \otimes |\phi_{\text{shared}}\rangle = \frac{\alpha_0|\uparrow\downarrow\rangle + \alpha_0|\uparrow\uparrow\rangle + \alpha_1|\downarrow\downarrow\rangle + \alpha_1|\downarrow\uparrow\rangle}{\sqrt{2}} \quad (2.10)$$

This state can be rearranged in the following way:

$$\begin{aligned} |\Psi_{\text{total}}\rangle_{IAB} &= \frac{1}{2} \frac{|\downarrow\downarrow\rangle_{IA} + |\uparrow\uparrow\rangle_{IA}}{\sqrt{2}} \mathbf{1} [\alpha_0|\uparrow\rangle_B + \alpha_1|\downarrow\rangle_B] \\ &+ \frac{1}{2} \frac{|\uparrow\downarrow\rangle_{IA} + |\downarrow\uparrow\rangle_{IA}}{\sqrt{2}} \sigma^x [\alpha_0|\uparrow\rangle_B + \alpha_1|\downarrow\rangle_B] \\ &+ \frac{1}{2} \frac{|\uparrow\downarrow\rangle_{IA} - |\downarrow\uparrow\rangle_{IA}}{\sqrt{2}} (i\sigma^y) [\alpha_0|\uparrow\rangle_B + \alpha_1|\downarrow\rangle_B] \\ &+ \frac{1}{2} \underbrace{\frac{|\downarrow\downarrow\rangle_{IA} - |\uparrow\uparrow\rangle_{IA}}{\sqrt{2}}}_{\text{Alice}} \underbrace{\sigma^z [\alpha_0|\uparrow\rangle_B + \alpha_1|\downarrow\rangle_B]}_{\text{Bob}} \end{aligned} \quad (2.11)$$

where  $\sigma^a$  are Pauli's matrices.

The above state is nothing but a rearrangement of the three particle state Alice and Bob share (one each from  $\phi_{\text{shared}}$  plus the unknown state Alice has). Alice now performs a measure on her side of the quantum state (i.e. on the first two sites of the above equation - denoted by 'Alice'). Before performing the measure, the quantum system is in a superposition of different states. When performing the measure, Alice simply make the system collapse to one state. This measure (called *projective measure*) can be performed in a number of ways. For instance, Alice can check whether her two spins are both pointing up. In this set up, it is more convenient to Alice to perform a bit more complicated measure. In particular, she measures in which of the four states of (2.11) the systems collapses after the measure. In this way, there are four possible results for Alice's measure: the state can collapse in one of the four lines of (2.11). After the measure she communicates the result (classically - even with a normal phone call) to Bob. Once Bob receives the result of Alice's measure, he can perform a simple operation on its side of the quantum state to recover the original unknown state. For instance, if Alice measures that the system has collapsed onto the first state, Bob's state is identical to the unknown state  $|\phi_{\text{unknown}}\rangle$ . On the other hand, if Alice finds out that the system has collapsed onto the state on the second line of (2.11), Bob's state is equal to the unknown state multiplied by  $\sigma^x$ . To recover the unknown state  $|\phi_{\text{unknown}}\rangle$ , Bob must simply perform a  $\sigma^x$  operation - that is, a flipping of the spin - on his state. Of course, this argument can be extended to the third and fourth lines of (2.11). Such a protocol has been experimentally implemented at the end of the last century [23, 24] with successful results. It should

be noticed that the shared state  $|\phi_{\text{shared}}\rangle$  used in such protocol is entangled (and, as we will see in next sections is maximally entangled). Entanglement is then a very important feature of quantum protocols and it really adds some intrinsic advantages with respect to classical protocols. Moreover, it is possible to show that if a state like (2.8) - an almost separable state- has been used to implement the teleportation protocol, the results, i.e. the transmission of the unknown quantum state from Alice to Bob, would have been less precise. In particular, the scalar product (called *fidelity*) between the initial unknown state and the final Bob state is equal to one (perfect transmission) if the state (2.9) is used, while it is close to zero (bad transmission) if (2.8) is used. This protocol shows not only how entanglement is very important in making a system truly quantum but also it is clear that a quantitative measure of it is important to discriminate states with different amounts of entanglement.

## 2.2 Measures of Entanglement

In order to quantify entanglement and to distinguish between differently entangled states we have to define a way to measure it. Before discussing the possible options to define entanglement measures, we would like to introduce the density matrix, a useful mathematical object to study quantum states.

### 2.2.1 Density matrix

States like (2.5) are usually called *pure* states. Pure states can describe only a fraction of all possible quantum states. Pure states are enough to describe a system at zero temperature (since the system is in the ground state of the Hamiltonian), but they cannot describe systems at finite temperature, in which a complete mixture of states with different energies play a role. An isolated system at equilibrium at temperature  $T$  can be described using the so-called *density matrix*  $\rho$ :

$$\rho = \frac{1}{Z} \sum_n \exp\left[-\frac{E_n}{kT}\right] |\psi_n\rangle\langle\psi_n| \quad (2.12)$$

where  $|\psi_n\rangle$  is the  $n$ -th eigenvector of the Hamiltonian of the system,  $E_n$  is the corresponding eigenvalue,  $Z = \sum_n e^{-\frac{E_n}{kT}}$  is the partition function and  $k$  is the Boltzmann constant (which will be set to one in the following).

Quantum states like (2.12) are called *mixed* since they take into account more than one vector of the Hilbert space. Thermal systems are just an example: a density matrix is

defined by a convex combination of projectors  $|\psi_i\rangle\langle\psi_i|$ . The operator

$$\rho = \sum_i p_i |\psi_i\rangle\langle\psi_i| \quad (2.13)$$

is a density matrix if  $p_i \geq 0$  and  $\sum_i p_i = 1$ . Notice that the coefficients  $p_i$  play here the role of **classic** probabilistic weights. Of course, density matrices can also describe pure states. For instance, if a quantum system is in the quantum state  $|\psi\rangle$  its density matrix is simply given by

$$\rho = |\psi\rangle\langle\psi| \quad (2.14)$$

As we have just seen, density matrices can describe a wider variety of quantum states than simple vectors in the Hilbert space. Moreover, they can be used to define expectation values of operators, since

$$\langle\mathcal{O}\rangle_\rho \equiv \text{tr}[\rho\mathcal{O}] \quad (2.15)$$

From its definition, it is easy to show that the following properties hold for a density matrix:

$$\rho = \rho^\dagger \quad (2.16)$$

$$\text{tr}\rho = 1 \quad (2.17)$$

$$\langle\phi|\rho|\phi\rangle \geq 0 \quad \forall \phi \in \mathcal{H} \quad (2.18)$$

Density matrices can be used also to define thermodynamic and statistical properties of many-body quantum systems. In particular the *von Neumann Entropy*  $S$  of a quantum state described by a density matrix  $\rho$  is given by [25]

$$S(\rho) = -\text{Tr}[\rho \log \rho] = -\sum_i p_i \log p_i \quad (2.19)$$

von Neumann Entropy is positive-definite, it vanishes for pure states ( $\rho = |\psi\rangle\langle\psi|$ ) and has its maximum when the  $p_i$  are all equal (all states are equally probable).

### Rényi entropy

Since the definition (2.19) involves the logarithm of an operator, its computation could be challenging. Using the density matrix, it is possible to define another Entropy:

$$S_n(\rho) = \frac{1}{1-n} \log \text{tr} \rho^n \quad (2.20)$$

which is called *Rényi Entropy* [26]. In some circumstances (like in the majority of systems studied in this thesis), this quantity is easier to compute than (2.19). The two entropies are also related by

$$S(\rho) = \lim_{n \rightarrow 1} S_n(\rho) \quad (2.21)$$

### 2.2.2 Reduced density matrix

Consider now a system divided into two parts  $A$  and  $B$ . As we have just seen, we can use a density matrix  $\rho$  to define the state of the system. This density matrix is an operator acting on the Hilbert space  $\mathcal{H} = \mathcal{H}_A \otimes \mathcal{H}_B$  of the whole system, while a generic vector  $\Psi \in \mathcal{H}$  can be written as ( $\phi_i \in \mathcal{H}_A$  and  $\chi_j \in \mathcal{H}_B$ )

$$|\Psi\rangle = \sum_{i,j} C_{ij} |\phi_i \chi_j\rangle \quad (2.22)$$

If  $\{\chi_j\}_j$  form a basis of  $\mathcal{H}_B$ , we can define a partial trace over  $\mathcal{H}_B$  of an operator  $\mathcal{O} \in \text{End}(\mathcal{H})$  by

$$\mathcal{O}_A \equiv \text{tr}_B \mathcal{O} \equiv \sum_j \langle \chi_j | \mathcal{O} | \chi_j \rangle \quad (2.23)$$

This new operator  $\mathcal{O}_A \in \text{End}(\mathcal{H}_A)$  can be used to focus only on the subsystem  $A$  and to consider  $B$  just an environment.

Of course we can reproduce this procedure of tracing over some degrees of freedom of a system for any operator in  $\mathcal{H}$ . In particular, if we consider the density matrix  $\rho$ , the new operator  $\rho_A$  is the so-called *reduced density matrix*:

$$\rho_A \equiv \text{tr}_B \rho \quad (2.24)$$

This new object is a density matrix of the subsystem  $A$ : properties (2.16) hold and the expectation values of operators  $\mathcal{O}_A$  defined on the subsystem  $A$  (2.23) are given by

$$\langle \mathcal{O}_A \rangle = \text{tr}_A(\rho_A \mathcal{O}_A) \quad (2.25)$$

The reduced density matrix is then a very useful tool to focus only on a part of a system and regard the rest as an environment or a thermal bath. Notice that the reduced density matrix of a subsystem can be mixed even if the state of the whole system was pure.

### 2.2.3 What is a good measure of entanglement?

Before looking for a good measure of entanglement, we should define which properties such a measure must satisfy [27]. In the following we will refer to a quantum state using its density matrix  $\rho$ .

1. **Normalisation.** Separable states are not entangled:

$$E(\rho) = 0 \tag{2.26}$$

if  $\rho$  represents a separable (not entangled) state.

2. **Not increasing under LOCC.** Entanglement is a genuine quantum phenomenon and its amount cannot be increased by any classical operation (or *classical communication* CC). Additionally, since entanglement is also a feature of the partition chosen, the action of local operator should not change the value of entanglement. Let  $U = U_A \otimes U_B$  an operator associated with a local operation (LO) on the quantum state, its action leaves the entanglement unaffected:

$$E(U\rho U^\dagger) = E(\rho) \tag{2.27}$$

We can incorporate both non increasing properties under LOCC:

$$E(\Theta(\rho)) \leq E(\rho) \tag{2.28}$$

where  $\Theta$  is a map associated with a LOCC transformation.

3. **Convexity.** Entanglement cannot be created by *classically mixing* two quantum states. Consider two states (mixed or pure) described by density matrices  $\rho_1$  and  $\rho_2$ . A mixture of these two states can be simply obtained by  $\rho_{1+2} = \alpha\rho_1 + (1 - \alpha)\rho_2$ . Of course, we should not expect the entanglement to increase under this operation. Entanglement must then be convex:

$$E(\alpha\rho_1 + (1 - \alpha)\rho_2) \leq \alpha E(\rho_1) + (1 - \alpha)E(\rho_2) \tag{2.29}$$

4. **Sub-additivity.** Suppose we have **two different** quantum systems, each of them defined by a density matrix, say  $\rho$  and  $\rho'$ . Entanglement should not increase by

joining these two systems together:

$$E(\rho \otimes \rho') \leq E(\rho) + E(\rho') \quad (2.30)$$

**Note: difference between convexity and sub-additivity**

In the above requirements for a quantity to be a good measure of entanglement the last two properties might seem equivalent. In fact they describe two quite different situations. The third property regards the classical mixture of two quantum states. The two density matrices are defined on the same Hilbert space  $\mathcal{H}$  and their sum implies a mixture. For instance, consider a quantum system with inverse temperature  $\beta$  and two energy levels  $E_1$  and  $E_2$ . The two density matrices relative to the two energy levels are respectively  $\rho_1 = |\psi_1\rangle\langle\psi_1|$  and  $\rho_2 = |\psi_2\rangle\langle\psi_2|$ . The thermal state (a classical mixture) is then given by  $\rho = Z^{-1}(e^{-\beta E_1}\rho_1 + e^{-\beta E_2}\rho_2)$ . In this case the convexity property implies that entanglement should not increase under classical (thermal) correlations:

$$E(\rho) \leq Z^{-1}e^{-\beta E_1}E(\rho_1) + Z^{-1}e^{-\beta E_2}E(\rho_2) \quad (2.31)$$

On the other hand, the sub-additivity property takes into account quite a different situation. Consider two quantum systems and their Hilbert spaces  $\mathcal{H}_1$  and  $\mathcal{H}_2$ . Let  $\rho_1$  and  $\rho_2$  identify two quantum states, one for each system. Of course, the two systems can be joint together. The new Hilbert space is given by  $\mathcal{H}_1 \otimes \mathcal{H}_2$  and the new density matrix by  $\rho = \rho_1 \otimes \rho_2$ . Since the operation of joining the two systems together does not create any quantum interaction between the two systems, entanglement must not increase:

$$E(\rho_1 \otimes \rho_2) \leq E(\rho_1) + E(\rho_2) \quad (2.32)$$

**2.2.4 Entanglement entropy**

As seen in the previous section 2.1.2, the more entangled a state is, the more quantum information can be compressed into it, in the same way a classical message is less compressed the more entropic it is. For this reason, entropy can be a good measure for entanglement. If a system is described by a density matrix  $\rho$ , the entanglement between two subsections  $A$  and  $B$  can be represented as the von Neumann Entropy of the reduced density matrix  $\rho_A$ :

$$E_{A \cup B}(\rho) = S(\rho_A) = - \text{Tr}_{\mathcal{H}_A}[\rho_A \log \rho_A] \quad (2.33)$$

Moreover it satisfies almost all the 2.2.3 requirements to be a good measure of entanglement.

1. **Normalisation.** Consider the state  $|\Psi\rangle = |\phi\rangle_A \otimes |\chi\rangle_B$ . It is separable (not entangled) for the partition  $A \cup B$  and its reduced density matrix is simply given by  $\rho_A = |\phi\rangle_A \langle\phi|$ . Since  $\rho_A$  represents a pure state, its von Neumann entropy vanishes. Thus  $S(\rho_A) = 0$  if  $\rho$  is separable.
2. **Not increasing under LOCC.** In the previous section we represented a LO as a unitary operator  $U = U_A \otimes U_B$ . Thanks to the cyclic property of the trace, von Neumann entropy is invariant under such transformations:

$$E_{A \cup B}(U\rho U^\dagger) = S(U_A \rho_A U_A^\dagger) = S(\rho) = E_{A \cup B}(\rho) \quad (2.34)$$

3. **Concavity.** An explicit computation shows that<sup>6</sup>

$$\begin{aligned} S(\alpha\rho_1 + (1-\alpha)\rho_2) &= \alpha S(\rho_1) + (1-\alpha)S(\rho_2) - \log[\alpha(1-\alpha)] \\ &\geq \alpha S(\rho_1) + (1-\alpha)S(\rho_2) \end{aligned} \quad (2.35)$$

Such a simple argument makes it clear that the von Neumann entropy cannot be a good measure of entanglement for generic states. On the other hand, the above inequality becomes an equality in the  $\alpha = 0, 1$  case, i.e. when pure states are considered. Fortunately the ground state of a system can be represented by a pure state, and then the von Neumann entropy can be used as a measure of entanglement in such a case.

4. **Sub-additivity.** Suppose to have a quantum system  $A \cup B$  with density matrix  $\rho$ . The entropy of the entire system is less than the sum of the entropy of the two parts of the system:

$$S(\rho) \leq S(\rho_A) + S(\rho_B) \quad (2.36)$$

When comparing these properties with the requirements (2.2.3) for a good measure of entanglement it is clear that the von Neumann entropy measures properly the entanglement of a pure state. Even though it can sound very restrictive, it covers a large number of physically interesting cases, like ground states. In following chapters we will refer to such measure as von Neumann entropy or as *entanglement entropy* (EE)

---

<sup>6</sup>It can be easily proved by considering the diagonalised version of the matrices  $\rho_{1,2}$ :

$$\begin{aligned} \rho_1 &= \sum_i a_i \mathbb{P}_i \\ \rho_2 &= \sum_i b_i \mathbb{P}_i \end{aligned}$$

As we said in Section 2.1.2, different states provide different levels of precision in the teleportation protocol. Truly entangled states, like

$$|\psi\rangle = \frac{|\uparrow\downarrow\rangle - |\downarrow\uparrow\rangle}{\sqrt{2}} \quad (2.37)$$

allow a perfect transmission of a unknown state, On the other hand, almost separable states, like:

$$|\phi\rangle = \sqrt{0.001}|\uparrow\downarrow\rangle - \sqrt{0.999}|\downarrow\uparrow\rangle \quad (2.38)$$

makes the teleportation less precise. The amount of entanglement reflects this difference:

$$\begin{aligned} E(|\psi\rangle\langle\psi|) &= \log 2 = 0.693147\dots \\ E(|\phi\rangle\langle\phi|) &= 0.007907\dots \end{aligned} \quad (2.39)$$

The von Neumann entropy distinguishes the two states and clearly represents the amount of entanglement encapsulated in them.

As we have just seen, the von Neumann entropy cannot be used to measure entanglement in thermal systems (described by mixed states) or, as we will see in the next section, the entanglement between two subsystems embedded in a larger environment<sup>7</sup>. In addition to these features, von Neumann entropy encapsulates also another important property of bipartite entanglement. Since entanglement is related to the amount of quantum correlations between two parts of a system, the measure of entanglement must not depend on the order in which we perform the traces. In other words, considering  $A$  as a system and  $B$  as an environment must be the same as considering  $B$  the system and  $A$  the environment. For bipartite systems, von Neumann entropy guarantees this symmetry, since  $S(\rho_A) = S(\rho_B)$ .

## 2.3 Logarithmic Negativity

As we said in previous sections, the entanglement can be measured using the von Neumann entropy only if two conditions are satisfied. First of all, the system (as a whole) has to be in a pure state. Moreover, the entropy is a good measure of entanglement only for bipartite systems. Whenever one of these two conditions is not satisfied, the von Neumann entropy

---

<sup>7</sup>From a mathematical point of view, the two cases are similar. Suppose to have a tripartite system  $A \cup B \cup C$ . To compute the entanglement between  $A$  and  $B$  we need to trace over the degrees of freedom of  $C$  (to create a bipartite system). Such a procedure will create (in most of the cases) a mixed states, even if the initial state  $\rho_{ABC}$  was pure.

does not satisfy all the necessary conditions for being a good measure of entanglement (see Section 2.2.3). Since the entanglement measures the genuine quantum correlations between two subsystems, any thermal noise has to be factored out. As soon as the system becomes mixed, both quantum and classical effect contribute to the von Neumann entropy and the actual amount of quantum entanglement cannot be isolated. As we said before, a tripartite system in a pure state can be seen as a mixed state of a bipartite system, once the degrees of freedom of the third subsystem have been traced over. For these reasons a new measure of entanglement has to be introduced, the so-called *logarithmic negativity* (LN) [28, 29, 30].

Logarithmic negativity measures the amount of entanglement even in the particular situations when the von Neumann entropy fails. Let  $A \cup B \cup C$  be a quantum system in a pure state  $\rho = |\Psi\rangle\langle\Psi|$ . As usual, we can define a reduced density matrix tracing over only degrees of freedom belonging to  $C$ .

$$\rho_{A \cup B} = \text{tr}_C \rho \quad (2.40)$$

Once we have traced the degrees of freedom of  $C$ , we have an object which focuses only on the regions  $A$  and  $B$ . Of course, we cannot compute the entanglement by simply tracing over also the degrees of freedom of  $B$ , otherwise we will end up with the very same difficulties of the von Neumann entropy discussed in the previous paragraph. In order to study the quantum correlations between  $A$  and  $B$ , we should find a way to “distinguish” them. In other words, we need to perform some operations on one side of the system without losing degrees of freedom. One way to do so is to perform the so-called *partial transposition*, when only some degrees of freedom are transposed. For instance, consider an operator  $\mathcal{O}$  which acts on the Hilbert space  $\mathcal{H}_A \otimes \mathcal{H}_B$ . Its matrix elements are given by

$$\langle i'_A j'_B | \mathcal{O} | i_A j_B \rangle \quad (2.41)$$

When partially transposing on  $\mathcal{H}_B$ 's degrees of freedom, only the  $j_B$  indexes will be exchanged. We denote the partial transposition of the  $B$ 's degrees of freedom by  $\mathcal{O}^{T_B}$ :

$$\langle i'_A j'_B | \mathcal{O}^{T_B} | i_A j_B \rangle = \langle i'_A j_B | \mathcal{O} | i_A j'_B \rangle \quad (2.42)$$

The resulting operator  $\mathcal{O}^{T_B}$  is still acting on  $\mathcal{H}_A \otimes \mathcal{H}_B$  but the two sets of degrees of freedom are somehow “marked”. Once the partial transposition has been performed on the reduced density matrix, the logarithmic negativity  $\mathcal{E}$  can be defined in a very similar

way to the von Neumann entropy:

$$\mathcal{E} = \log \text{Tr} \left| \rho_{AUB}^{TB} \right| = \log \left( \sum_i |\lambda_i| \right) \quad (2.43)$$

where  $\lambda_i$  are the eigenvalues of  $\rho_{AUB}^{TB}$ .

Like entanglement entropy, it is possible to define logarithmic negativity as a limit [31]:

$$\mathcal{E} = \lim_{n_e \rightarrow 1} \log \text{tr}_{AUB} \left( \rho_{AUB}^{TB} \right)^{n_e} \quad (2.44)$$

Apart from the partial transposition, one of the main differences between the logarithmic negativity and the entanglement entropy is that the above limit has to be performed once the function  $\log \text{tr}_{AUB} \left( \rho_{AUB}^{TB} \right)^{n_e}$  has been analytically continued for the even values of  $n$ . While in the entanglement entropy case there is no intrinsic difference between the even and the odd  $n$  series, in the negativity case there is a substantial difference. In particular, while any density matrix is positive definite, this is no more the case once a partial transposition has been performed. For this reason, while the even series of  $\text{tr}_{AUB} \left( \rho_{AUB}^{TB} \right)^{n_e}$  is simply given by series of positive elements, thus it is no more the case for the odd series.

Like the von Neumann entropy, it is possible to show [28] that logarithmic negativity satisfies all the requirements for being a good measure of entanglement.

Even though logarithmic negativity has been defined for tripartite systems, it perfectly describes also the bipartite thermal case. In particular, consider a quantum system with Hilbert space  $\mathcal{H}$  in a mixed state described by a density matrix  $\rho$ . This density matrix can be interpreted as a reduced density matrix relative to  $\mathcal{H}$  of a larger Hilbert space  $\mathcal{H} \otimes \mathcal{H}_{\text{extra}}$ :

$$\rho = \text{tr}_{\text{extra}} |\Psi\rangle\langle\Psi| \quad (2.45)$$

In this way LN is a good measure of entanglement also for the bipartite mixed case.

## 2.4 Why Entanglement?

Apart from its unique properties of describing truly quantum phenomena, entanglement is a very important resource also in the study of many-body quantum systems. The scaling of entanglement entropy can be used also to probe the critical and off critical properties of quantum systems which can be described by a quantum field theory. One of the most important features of entanglement is its scaling in one dimensional quantum systems. Consider a critical one dimensional quantum system of length  $R$  with periodic boundary conditions. Suppose we are interested in evaluating the entanglement entropy between

two parts of the system  $A$  and  $B$  of length  $r$  and  $R - r$ , respectively. It has been shown [7, 8] that it scales as

$$S(\rho_A) = \frac{c}{3} \log \left( \frac{R}{\pi} \sin \frac{r\pi}{R} \right) + \text{const.} \quad (2.46)$$

where  $c$  is the central charge of the system (a number associated with the universality class of the critical point - see Chapter 3). Suppose now we study the problem from a different perspective. Consider some quantum system, like a spin chain with a very large number of sites. Suppose we know that the system is critical but we would like to find out which is the underlying universality class (which depend on the central charge  $c$ ). If we perform some kind of numerical analysis of the spin chain, like a DMRG simulation [32], it is possible to estimate the value of the entanglement entropy at various sizes of the subsystem. Fitting these data with the theoretical prediction (2.46), it is possible to extract the value of the central charge with very good precision.

This kind of analysis and identification of the central charge using the scaling of some physical quantity is not limited to entanglement. It has been known for a long time that the ground state energy  $E_0$  scales with the size  $R$  of the system (with periodic boundary conditions) [33, 34]:

$$E_0 \sim R\epsilon_0 - v \frac{\pi c}{6R} \quad (2.47)$$

where  $\epsilon_0$  is the energy density and  $v$  is the sound velocity.

Of course, a similar numerical analysis can be performed to compute the value of the central charge from the scaling of the ground state energy. Unfortunately, to isolate the central charge  $c$  we need to know the sound velocity  $v$ <sup>8</sup>. On the other hand, once the entanglement scaling has been evaluated, the central charge can be directly extracted using (2.46).

## 2.5 Conclusions

In this chapter we introduced the basic notions of entanglement and its features. We showed how entanglement clearly reflects the truly quantum nature of some systems. In order to quantify the amount of entanglement, we introduced two *measures of entanglement*: entanglement entropy and logarithmic negativity. Even though there are many more suitable measures for entanglement (like the *entanglement of formation* [36]), these two aforementioned measures are the most suitable for the study of many-body one dimensional quantum systems. In the following Chapters we will study the scaling of the

---

<sup>8</sup>For instance, the speed of the sound can be computed performing a Bethe ansatz [35].

entanglement entropy in a variety of quantum systems (Chapters 4, 5, 6 and 7), while in the last chapter we will investigate the scaling of logarithmic negativity in free theories.

## Chapter 3

# Conformal and Integrable Quantum Field Theory

In this chapter we review some known results of conformal field theory (CFT) [37, 38, 39, 40] and Integrable Quantum Field Theory (IQFT) [41, 42, 43, 44, 45, 46]. In particular, we set up the framework for some of the CFT ideas we will use in the following chapters. Additionally, we will briefly introduce the form factor program, a very useful tool for the evaluation of correlation functions in massive field theories. This chapter is not intended to be a complete review of CFT and IQFT. Our aim is to give some physical grasp of ideas, formulæ and concepts which will be used in the following chapters.

### 3.1 Critical Systems

A typical feature of second order phase transitions is the absence of a length scale. If a system is scale invariant it looks the same at every scale. It means that all the (quasi)particles interact with each other and the system is completely “connected”. From the correlation functions point of view, it means that the decay is no more exponential, like  $G(r) \sim e^{-mr}$ , but algebraic,  $G(r) \sim r^{-d}$ , where  $m$  is the lightest mass of the system and  $r$  is the distance between two points. In particular, non critical correlators decay exponentially, and each particle is affected only by other particles inside a ball of radius  $\sim \xi = m^{-1}$ . At the critical point the parameter  $m$  will vanish, the “ball of influence” will diverge and all parts of the system will become connected. Furthermore, the majority of systems are Poincaré invariant (invariance under rotations, translations and Lorentz boost). With the exception of some rare cases [47], most scale and Poincaré invariant systems are also *conformally invariant*. Conformal transformations can be defined as maps which act as dilations of

the metric:

$$g_{\mu\nu}(\mathbf{x}) \rightarrow g'_{\mu\nu}(\mathbf{x}') = \Lambda(\mathbf{x}) g_{\mu\nu}(\mathbf{x}) \quad (3.1)$$

Conformal invariance encapsulate not only Poincaré and scale invariance, but also the so-called *special conformal invariance*<sup>1</sup>.

In the following chapters we will make large use of conformal invariance in the study of critical systems. In particular, since we are interested in 1+1 dimensional systems, we specialise our introduction to two dimensional conformal field theories.

### 3.1.1 Two dimensional CFT

When specialising to the two dimensional case it is useful to replace the two real coordinates  $(x^0, x^1)$  with a complex variable  $z$  and its conjugate  $\bar{z}$ :

$$\begin{aligned} z &= x^0 + ix^1 \\ \bar{z} &= x^0 - ix^1 \end{aligned} \quad (3.2)$$

Fundamental objects in CFT are the so-called *primary fields*, which transform as:

$$\phi(z, \bar{z}) = \left(\frac{df}{dz}\right)^\Delta \left(\frac{d\bar{f}}{d\bar{z}}\right)^{\bar{\Delta}} \phi'(z', \bar{z}') \quad (3.3)$$

where  $z' = f(z)$  and  $f$  is an *arbitrary* conformal transformation and the constants  $\Delta$  and  $\bar{\Delta}$  are called *conformal weights* or *conformal dimensions*. One of the most peculiar features of conformal invariance in two dimensions is that conformal transformations are represented by holomorphic and anti-holomorphic functions [37]. The above condition for primary fields can be slightly relaxed. We can define *quasi primary* fields as objects which transform like (3.3) under *global* conformal transformations<sup>2</sup>. Conformal weights affect also the scaling of two point functions and (for spinless fields) the two components are equal ( $\Delta = \bar{\Delta}$ ) and they coincide with the *scaling dimension*:

$$\langle \phi(z, \bar{z}) \phi(w, \bar{w}) \rangle = \frac{1}{|z - w|^{4\Delta}} \quad (3.4)$$

---

<sup>1</sup>A special conformal transformation is nothing but a translation preceded and followed by an inversion  $x^\mu \rightarrow x^\mu/|x|^2$  [37].

<sup>2</sup>From an intuitive point of view, global conformal transformations are conformal transformations whose parameters are fixed and do not depend on the point  $z$  they are transforming. On the other hand, local conformal transformations (which include global transformations) are conformal transformations that depend on the point  $z$ .

Let us now consider a conformal theory with lagrangian density  $\mathcal{L}$ . Of course, it is possible to define a stress energy tensor  $T_{\mu\nu}(\mathbf{x})$ . As we said before, in two dimensional CFT it comes natural to use a single complex coordinate instead of two real ones. In these new coordinates, it is convenient to rearrange the stress energy tensor in the following way:

$$\begin{aligned} T &\equiv \frac{1}{4}(T_{00} - T_{11} + 2iT_{01}) \\ \bar{T} &\equiv \frac{1}{4}(T_{00} - T_{11} - 2iT_{01}) \\ \Theta &\equiv T_{\mu}^{\mu} = T_{00} + T_{11} \end{aligned} \tag{3.5}$$

In complex coordinates, the familiar Noether conservation law  $\partial^{\mu}T_{\mu\nu} = 0$  becomes:

$$\begin{aligned} \partial_z \bar{T} + \frac{1}{4} \partial_{\bar{z}} \Theta &= 0 \\ \partial_{\bar{z}} T + \frac{1}{4} \partial_z \Theta &= 0 \end{aligned} \tag{3.6}$$

Since at the critical point  $\Theta = 0$ , the above conservation laws become holomorphicity conditions for the stress-energy tensor:

$$\partial_z \bar{T} = 0 = \partial_{\bar{z}} T \tag{3.7}$$

Another important property of the stress energy tensor is how it transforms under conformal transformations  $z \mapsto z' = f(z)$

$$T'(z') = \left(\frac{dz'}{dz}\right)^{-2} \left[ T(z) - \frac{c}{12} \{z'; z\} \right] \tag{3.8}$$

where the symbol  $\{\cdot, \cdot\}$  is the so-called Schwarzian derivative:

$$\{z'; z\} = \frac{d^3 z'}{dz'^3} - \frac{3}{2} \left( \frac{d^2 z'}{dz'^2} \frac{dz'}{dz} \right)^2 \tag{3.9}$$

The constant  $c$  appearing in (3.8) is called *central charge* and it is a number which depends on the universality class of the CFT. From an intuitive point of view, the central charge measures the number of degrees of freedom in the system. For instance, the central charge of a free boson is equal to one, while the one of a free fermion is one half. Of course, both field theories have infinite degrees of freedom, but, from a very naive point of view, two (Majorana) fermions create a boson. Additionally, the stress energy tensor has a very precise action on fields when inserted in correlators. Let  $X$  be a string of  $n$  primary fields:

$$X = \phi_1(z_1, \bar{z}_1) \cdots \phi_n(z_n, \bar{z}_n) \tag{3.10}$$

The action of  $T$  on  $X$  is given by the Conformal Ward identity:

$$\langle T(z)X \rangle = \sum_{i=1}^n \left[ \frac{\Delta_i}{(z-z_i)^2} + \frac{\partial_{z_i}}{z-z_i} \right] \langle X \rangle \quad (3.11)$$

After this very short review of some important properties of two dimensional CFT, let us discuss the Hilbert space structure in such theories.

### 3.1.2 Conformal families

The structure of the Hilbert space in two dimensional CFT is very simple and elegant. In order to quantise the system, it is worth moving from the complex plane to a cylinder geometry. Consider then a one dimensional quantum system with periodic boundary condition and size  $R$ . The time evolution of this system can be chosen along the vertical direction of the cylinder. The actual map from the complex plane to the cylinder is given by

$$z = e^{\frac{2\pi(t+ix)}{R}} \quad (3.12)$$

where  $x$  and  $t$  are the space and time coordinates, respectively. We can now quantise the system with the time flowing from the bottom to the top of the cylinder.

The asymptotic past ( $t \rightarrow -\infty$ ) is then associated with the point  $z = 0$  while the asymptotic future with the point  $z = \infty$ . Asymptotic states can then be represented as the action of primary fields on the conformal vacuum:

$$|\phi\rangle \equiv |\Delta, \bar{\Delta}\rangle \equiv \lim_{z, \bar{z} \rightarrow 0} \phi(z, \bar{z})|\emptyset\rangle \quad (3.13)$$

where  $|\emptyset\rangle$  is the *conformal vacuum*.

Of course, it is possible to define asymptotic future states as hermitian conjugates of asymptotic past states. Using equation (3.12) it is clear that the maps  $t \rightarrow -t$  is equivalent, in complex coordinates, to  $z \rightarrow \bar{z}^{-1}$ . In order to avoid ill defined norms, we can define the hermitian conjugation of a (quasi primary) field as:

$$[\phi(z, \bar{z})]^\dagger = z^{-2\bar{\Delta}} \bar{z}^{-2\Delta} \phi\left(\frac{1}{\bar{z}}, \frac{1}{z}\right) \quad (3.14)$$

Like other fields, also the stress energy tensor can be interpreted as a quantum operator.

The Laurent expansion of the operator  $T$  is then given by

$$\begin{aligned} T(z) &= \sum_{n=-\infty}^{\infty} z^{-n-2} L_n \\ \bar{T}(z) &= \sum_{n=-\infty}^{\infty} \bar{z}^{-n-2} \bar{L}_n \end{aligned} \quad (3.15)$$

The stress energy tensor can be seen as the Noether current associated with conformal invariance. For this reason, its coefficients  $L_n$  are the actual generators of local conformal transformations. In particular,  $L_0 + \bar{L}_0$  generates the dilations  $z \mapsto \lambda z$ . Since, according to the map (3.12), dilations are nothing but time translations, the quantum Hamiltonian is given by  $\frac{2\pi}{\hbar}(L_0 + \bar{L}_0)$ . On the other hand, operators  $L_{-1}$  and  $L_1$  generate translations and special conformal transformations, respectively. While three operators (and their antiholomorphic counterparts) are enough to generate *global* conformal transformations, in order to generate *local* transformations all the generators must be taken into account. The explicit expressions of the operators  $L_n$  can be obtained inverting the above Laurent expansion:

$$\begin{aligned} L_n &= \frac{1}{2\pi i} \oint dz z^{n+1} T(z) \\ \bar{L}_n &= \frac{1}{2\pi i} \oint d\bar{z} \bar{z}^{n+1} \bar{T}(z) \end{aligned} \quad (3.16)$$

These operators, also-called *Virasoro generators*, satisfy the celebrated *Virasoro algebra*  $\mathfrak{Vir}$ :

$$\begin{aligned} [L_n, L_m] &= (n-m)L_{n+m} + \frac{c}{12} (n^3 - n) \delta_{n+m,0} \\ [L_n, \bar{L}_m] &= 0 \\ [\bar{L}_n, \bar{L}_m] &= (n-m)\bar{L}_{n+m} + \frac{c}{12} (n^3 - n) \delta_{n+m,0} \end{aligned} \quad (3.17)$$

The study of the representations of such algebra can then be used to understand the Hilbert space structure of systems enjoying conformal symmetry.

### Conformal towers

Let us start from the conformal vacuum  $|\emptyset\rangle$ . Since it should be invariant under global conformal transformations, it should be annihilated by the three operators responsible for

such transformations:

$$L_n|\emptyset\rangle = 0 \quad \text{for } n = 0, \pm 1 \quad (3.18)$$

Moreover, in order to have a well defined action of the stress energy tensor on the vacuum  $(T(z)|\emptyset\rangle)$ , the above condition can be extended to all  $n$  greater or equal to  $-1$ . Since<sup>3</sup>  $\langle\emptyset|L_n = (L_{-n}|\emptyset\rangle)^\dagger$ , the vacuum expectation value of the stress energy tensor vanishes:

$$\langle\emptyset|T(z)|\emptyset\rangle = 0 \quad (3.19)$$

Having discussed the properties of the conformal vacuum, we can now study the features of the other states of the Hilbert space. Let us consider a primary state  $|\Delta, \bar{\Delta}\rangle$ . It is possible to show that it is also an eigenstate of the operators  $L_0$  and  $\bar{L}_0$ , thus of the Hamiltonian as well:

$$\begin{aligned} L_0|\Delta, \bar{\Delta}\rangle &= \Delta|\Delta, \bar{\Delta}\rangle \\ \bar{L}_0|\Delta, \bar{\Delta}\rangle &= \bar{\Delta}|\Delta, \bar{\Delta}\rangle \end{aligned} \quad (3.20)$$

Moreover, these primary states are annihilated by  $L_n$  with  $n > 0$ :

$$\begin{aligned} L_n|\Delta, \bar{\Delta}\rangle &= 0 \\ \bar{L}_n|\Delta, \bar{\Delta}\rangle &= 0 \end{aligned} \quad (3.21)$$

These two conditions (3.20) and (3.21) can also be used as an alternative definition of primary states (and primary fields). Primary states can then be considered as the *highest weight states* of the Virasoro algebra. In the same way, the highest weight states of the  $\mathfrak{su}_2$  algebra are annihilated by  $J^+$  and they are eigenvectors of  $J^z$  at the same time. In the  $\mathfrak{su}_2$  case, the operator  $J^-$  creates a collection of states starting from the highest weight state. In the same way the operators  $L_{-n}$  (with  $n$  positive) create a family of states starting from a highest weight state of the Virasoro algebra  $\mathfrak{Vir}$ . These states are called *descendants* and the family of all descendants from a single primary state is called a *conformal tower* or *Verma module*. We will denote it by  $V(c, \Delta)$ . For instance, the state

$$L_{-2}L_{-1}|\Delta, \bar{\Delta}\rangle \quad (3.22)$$

---

<sup>3</sup>The explanation of such conjugation relation can be found in the definition of asymptotic states. In particular, since conjugation maps states from the asymptotic past to the asymptotic future and vice versa, it is equivalent to the exchange  $z \leftrightarrow \bar{z}^{-1}$ , which, according to the expansion 3.15, maps  $L_n$  into  $\bar{L}_{-n}$ .

is a descendant of  $|\Delta, \bar{\Delta}\rangle$ .

Thanks to this elegant structure, the study of the representations of the Virasoro algebra is enough to probe the Hilbert space of the states in a CFT.

### 3.1.3 Minimal models

As we saw in the previous section, the Hilbert space of a CFT is formed by all the conformal towers of its primary fields. In principle there is no upper bound to the number of primary fields a CFT can have. However, there is a particular class of models, called *minimal models* in which the number of primary fields is finite. The most peculiar feature of minimal models is the presence of primary-like states among the descendants. These states, which are orthogonal to the entire Verma module, are called *singular* or *null* vectors and they have zero norm. For instance, consider a CFT with central charge  $c$  and a primary state  $|\Delta, \bar{\Delta}\rangle$  with conformal weight  $(\Delta, \bar{\Delta})$ . To simplify the example we can assume a spinless theory, where the holomorphic and anti-holomorphic parts have the same properties<sup>4</sup>. Let  $|\chi\rangle$  be a descendant of  $|\Delta\rangle$ :

$$|\chi\rangle = [L_{-2} + \eta L_{-1}^2] |\Delta\rangle \quad (3.23)$$

It is a null vector if

$$\begin{aligned} \eta &= -\frac{3}{2(2\Delta + 1)} \\ \Delta &= \frac{1}{16} \left[ 5 - c \pm \sqrt{(c-1)(c-25)} \right] \end{aligned} \quad (3.24)$$

Such a choice makes  $\chi$  a primary state at level two:

$$L_n |\chi\rangle = 0 \quad \text{for } n > 0 \quad (3.25)$$

Such a state is then a primary and a descendant at the same time. Additionally, it is clear that  $\chi$  has zero norm:

$$\langle \chi | \chi \rangle = 0 \quad (3.26)$$

---

<sup>4</sup>In spinless theories we can use a shorter notation for states  $|\Delta, \bar{\Delta}\rangle = |\Delta, \Delta\rangle \equiv |\Delta\rangle$ .

Moreover,  $\chi$  is orthogonal to any state  $|\psi\rangle = L_{-k_1}L_{-k_2}\cdots L_{-k_N}|\Delta\rangle^5$  in the Verma module:

$$\langle\chi|\psi\rangle = \langle\chi|L_{-k_1}L_{-k_2}\cdots L_{-k_N}|\Delta\rangle = (\langle\Delta|L_{k_N}\cdots L_{k_2}L_{k_1}|\chi\rangle)^* = 0 \quad (3.27)$$

For this reason, null vectors and their descendant can be safely removed from the Verma module  $V(c, \Delta)$ . Let  $\mathcal{M}(c, \Delta)$  be the Verma module  $V(c, \Delta)$  once all null vectors have been removed. The module  $\mathcal{M}(c, \Delta)$  is then irreducible and it can be used to construct irreducible representations of the Virasoro algebra.

We can now investigate which are the conditions such that null states appear inside a Verma module. Among the various regions of values the central charge can have, we specialise to the  $c < 1$  case. When the central charge is less than one and there exist some Verma modules containing null vectors, the CFT is called a *Minimal Model*. In particular, the central charge can be parametrised by two integer numbers  $m$  and  $m'$  (with  $m$  and  $m'$  coprime and  $2 < m < m'$ ):

$$c = 1 - 6\frac{(m - m')^2}{mm'} \quad (3.28)$$

Of course, the existence condition of null states does not rely only on the value of the central charge, but also on the conformal weight. In order to have some null state among its descendant, a primary state must have a conformal weight of the form (when the value of  $c$  is given by (3.28)):

$$\Delta_{rs} = \frac{(mr - m's)^2 - (m - m')^2}{4mm'} \quad (3.29)$$

with

$$1 \leq r < m' \quad 1 \leq s < m \quad (3.30)$$

Sometimes it is useful to denote the set  $\{(s, r) \in \mathbb{N}^2 \text{ s. t. } 1 \leq r < m' \text{ and } 1 \leq s < m\}$  as  $\mathcal{J}$ . Such models are also-called *rational models* thanks to the rational expressions which define their central charges and conformal weights.

One of the main consequences of the presence of null vectors is the finite number of

---

<sup>5</sup>A generic descendant of  $|\Delta\rangle$  can be represented as a linear combinations of states like  $L_{-k_1}L_{-k_2}\cdots L_{-k_N}|\Delta\rangle$  where  $\{k_1, k_2, \dots, k_N\}$  is a collection of  $N$  positive integers.

conformal families which constitute the Hilbert space:

$$\mathcal{H} = \bigoplus_{(s,r) \in \mathcal{J}} \mathcal{M}(c, \Delta_{r,s}) \otimes \bar{\mathcal{M}}(c, \Delta_{r,s}) \quad (3.31)$$

where the  $\bar{\mathcal{M}}$  refers to the antiholomorphic part of the module. In CFT it is very common to denote a minimal model by  $\mathcal{M}_{mm'}$  which indicates all the conformal families (once the null states have been removed) associated with a particular choice of  $m$  and  $m'$ .

Moreover, minimal models describe a variety of common physical phenomena. For instance, the universality class of the critical Ising model is realised by the  $\mathcal{M}_{34}$  minimal model and that of the three-state Potts model by  $\mathcal{M}_{56}$ .

### 3.1.4 Modular transformations and conformal characters

In previous sections we described the Hilbert space of the conformal states obtained by quantising a CFT on the cylinder. Another natural geometry to quantise a two dimensional fields theory on is the torus, i.e. a space with periodic boundary conditions on both directions. Consider, for example, a cylinder with height  $L$  and circumference  $R$ . A torus can be simply obtained by joining together the two sides of the cylinder. It is possible to choose any of the two directions ( $R$  or  $L$ ) to quantise the system. Of course, the partition functions computed with the different choice of quantisations must be the same. This property is guaranteed by quite an elegant symmetry of the torus, called *modular invariance* [48]. From an intuitive point of view, a torus is modular invariant because there are many equivalent ways to represent it on a complex plane. The simplest one is to consider a rectangle of size  $L \times R$  on the complex plane and identify the opposite edges to recover the torus' geometry. Without any loss of generality, we can set one vertex to one and the other to  $it$  with  $t > 0$ . Our rectangle can then be identified by its four vertices at (anticlockwise order)  $0, 1, 1 + it$  and  $it$ . Since conformal systems are invariant under rotations and dilations, the rectangle can be rotated and dilated without affecting the partition function. Let  $\tau$  be such that  $\text{Im}\tau = t$ , we can deform our rectangle into a parallelogram with vertices  $0, 1, 1 + \tau$  and  $\tau$ . All the transformations of the parallelogram which leave the partition function unchanged are called *modular transformations* and can be represented by the operations  $\mathbb{T}$  and  $\mathbb{S}$ . The action of these operations is given by:

$$\begin{aligned} \mathbb{T} &: \tau \mapsto \tau + 1 \\ \mathbb{S} &: \tau \mapsto -\frac{1}{\tau} \end{aligned} \quad (3.32)$$

The partition function on the torus defined by the parameter  $\tau$  is then given by

$$Z(\tau, \bar{\tau}) = \text{Tr} \exp[-\text{Im}\tau H - i\text{Re}\tau P] \quad (3.33)$$

where  $H$  and  $P$  are the Hamiltonian and the momentum operator, respectively. The Hamiltonian operator on a cylinder of circumference  $R$  has already been computed in previous sections and is given by

$$H = \frac{2\pi}{R} \left( L_0 + \bar{L}_0 - \frac{c}{12} \right) \quad (3.34)$$

where the radius  $R$  is equal to one in the present case. On the other hand, the momentum operator is proportional to  $L_0 - \bar{L}_0$  (see e.g. [42]):

$$P = \frac{2\pi}{R} (L_0 - \bar{L}_0) \quad (3.35)$$

Putting everything together, the partition function is then given by:

$$Z(\tau, \bar{\tau}) = \text{Tr} \exp \left[ q^{L_0 - \frac{c}{24}} \bar{q}^{\bar{L}_0 - \frac{c}{24}} \right] \quad (3.36)$$

with

$$\begin{aligned} q &= e^{2\pi i\tau} \\ \bar{q} &= e^{2\pi i\bar{\tau}} \end{aligned} \quad (3.37)$$

The partition function can also be written as a sum over all primary fields of the theory:

$$Z(\tau, \bar{\tau}) = \sum_{\Delta, \bar{\Delta}} N_{\Delta, \bar{\Delta}} \chi_{\Delta}(q) \chi_{\bar{\Delta}}(\bar{q}) \quad (3.38)$$

where the coefficients  $N$  are integer numbers and the functions  $\chi$  are called *conformal characters* (or *Virasoro characters*):

$$\chi_{\Delta}(q) = \text{Tr}_{\Delta} q^{L_0 - \frac{c}{24}} \quad (3.39)$$

Of course, the above trace is restricted to the conformal family of the primary state  $\Delta$ .

For minimal models it is possible to compute the conformal characters using the Rocha-Caridi formula:

$$\chi_{rs}(q) = \frac{1}{(q)_{\infty}} q^{-\frac{c}{24} + \Delta_{rs}} \sum_{k=-\infty}^{\infty} q^{mm'k} \left[ q^{k(rm' - sm)} - q^{k(rm' + sm)} \right] \quad (3.40)$$

where  $(q)_\infty$  is the q-Pochhammer symbol [49]:

$$(q)_\infty = \prod_{j=1}^{\infty} (1 - q^j) \quad (3.41)$$

Modular transformations have a very simple action on conformal characters in minimal models. The action of  $\mathbb{T}$  is given by (not only for minimal models, but for a generic CFT):

$$\mathbb{T}\chi_\Delta(q) \mapsto e^{2\pi i(\Delta - \frac{c}{24})}\chi_\Delta(q) \quad (3.42)$$

The action of the modular transformation  $\mathcal{S}$  is a bit more complicated. For minimal models, the conformal character transforms under  $\mathcal{S}$  as

$$\chi_{rs}(\tilde{q}) = \sum_{(r's') \in \mathcal{J}} \mathcal{S}_{rs}^{r's'} \chi_{r's'}(q) \quad (3.43)$$

where  $\tilde{q} = e^{-\frac{2\pi i}{\tau}}$  and the modular matrix  $\mathcal{S}_{rs}^{r's'}$  is given by:

$$\mathcal{S}_{rs}^{r's'} = \sqrt{\frac{8}{mm'}} (-1)^{(r+s)(r'+s')} \sin \frac{\pi r r'}{m} \sin \frac{\pi s s'}{m'} \quad (3.44)$$

### 3.1.5 Non unitary CFT

In this section we discuss some features of so-called *non unitary CFT* [50].

For instance, all minimal models  $\mathcal{M}_{n,m}$  with  $m \neq n + 1$  are non-unitary. In the context of CFT, non-unitarity means that there could be some states with negative norm. For instance, setting the norm of all primary states to one ( $\langle \Delta | \Delta \rangle = 1$ ), the state  $|\psi\rangle = L_{-n}|\Delta\rangle$  has negative norm:

$$\langle \psi | \psi \rangle = 2n\Delta + \frac{1}{12}cn(n^2 - 1) \leq 0 \quad (3.45)$$

for negative  $c$  and  $n$  sufficiently large.

Non unitary systems have also another very interesting feature: some conformal weights can be negative. For instance, in the Lee-Yang minimal model  $\mathcal{M}_{25}$  the conformal dimension  $\Delta_\Phi$  of the field  $\Phi$  is equal to  $-1/5$ .

Even though negative conformal dimensions and non positive-definite norms could make non unitary systems seem a bit unphysical, with the right precautions these CFTs can be used to describe a number of physical phenomena. For example, some excitations in the fractional quantum Hall systems with filling  $\nu = 2/5$  are described by the non unitary minimal model  $\mathcal{M}_{35}$  [51].

### 3.1.6 The Casimir effect

From a many-body physics point of view, one of the most interesting features of CFT is the relation between the energy of the lowest quantum states of a critical Hamiltonian and the conformal dimensions of the conformal theory describing the critical point. Consider, for instance, a spin chain with periodic boundary conditions and with large number  $R$  of sites and its quantum Hamiltonian  $H_{\text{spin}}$ . With a suitable choice of parameters, the Hamiltonian describes a quantum critical point in the thermodynamic limit  $R \rightarrow \infty$ . We can now assume that, at least for the lowest energy spectrum, the spin chain Hamiltonian can be described by the CFT Hamiltonian  $H$  (3.34):

$$H_{\text{spin}} \sim vH \quad (3.46)$$

where  $v$  (called *sound velocity*) is a non universal numerical parameter which depends on the actual implementation of the quantum Hamiltonian<sup>6</sup>. The above, together with the CFT Hamiltonian (3.34), gives immediately the scaling of the energy of the ground state and of the first excited states:

$$E(\Delta) \sim \frac{2\pi v}{R} \left( 2\Delta - \frac{c}{12} \right) \quad (3.47)$$

where, for simplicity, we have considered a spinless theory ( $\Delta = \bar{\Delta}$ ).

From the above equation it is clear that, if the system is unitary, the ground state, i.e. the state with the lowest energy, is associated with the identity field ( $\Delta = 0$ ) [33, 34]:

$$E_0 \sim -\frac{\pi v c}{6R} \quad (3.48)$$

such a scaling is sometimes referred to as *Casimir effect*<sup>7</sup>.

On the other hand, if the system is non unitary, there is a conformal dimension  $\Delta_{\text{min}} < 0$ . From equation (3.47) it is clear that the ground state is no more associated with the identity field. In fact, its scaling is associated with the primary field with the smallest conformal dimension  $\Delta_{\text{min}}$  [50]:

$$E_0 \sim -\frac{\pi v c_{\text{eff}}}{6R} \quad (3.49)$$

---

<sup>6</sup>For instance, in the XXZ spin- $\frac{1}{2}$  chain in the critical region (central charge  $c=1$ ) the sound velocity is equal to [52]  $\frac{\pi \sin(\gamma/2)}{2\gamma}$  where  $\cos \gamma$  represent the anisotropy of the model ( $H_{\text{spin}} = -(1/2) \sum \sigma^x \sigma^x + \sigma^y \sigma^y - \cos \gamma \sigma^z \sigma^z$ ).

<sup>7</sup>The name is linked with the celebrated Casimir effect in 3+1 dimension [53]. The vacuum energy (associated with the quantised electromagnetic field) of two infinite parallel metallic plates at distance  $R$  scales with  $R^{-3}$ .

where  $c_{\text{eff}} = c - 24\Delta_{\text{min}}$  is the *effective central charge*. Notice that in the unitary case  $\Delta_{\text{min}} = 0$  and then  $c_{\text{eff}} = c$ .

While the standard central charge  $c$  is directly associated with the CFT describing a particular universality class, its effective counterpart is linked with the scaling of the ground state energy. It is then possible to argue that, in non unitary CFT, the effective central charge has a more **physical role** than its standard version, which is associated with the symmetry underlying the critical point.

## 3.2 Integrable Quantum Field Theory

We have just seen that 2D systems enjoying conformal invariance have an infinite number of integrals of motion thanks to invariance under the Virasoro algebra. In such a case, there are enough integrals of motion to match all the degrees of freedom of the system. In this case the model is called *integrable*, i.e. it can (in principle) be solved exactly.

The conformal invariance is not the only symmetry which gives rise to an infinite number of integrals of motion. There are also some other non critical theories whose underlying symmetry is enough to solve exactly the model and to make it integrable. By solving exactly we mean a computing all correlation functions of local fields, even if it is technically challenging.

An object we are particularly interested in is the evaluation of correlation functions outside the critical point in massive integrable models. Such a computation can be done using the so-called *form factor (FF) programme* [9, 10], which allows us to expand correlation functions as an infinite sum over form factors. Before introducing the form factor program, we will discuss the main features of scattering in integrable QFT (IQFT).

### 3.2.1 S-matrix

While the S-matrix is an object widely used in QFT, we restrict our analysis to the systems which happen to be integrable. In QFT by S-matrix we mean the probability amplitude that a particle state in the asymptotic past ( $t \rightarrow -\infty$ ) evolves into another particle state in the asymptotic future ( $t \rightarrow \infty$ ). In a generic QFT a number of quantum charges are conserved through a scattering process. A Poincaré invariant scattering process preserves the energy and all the spatial and angular momenta <sup>8</sup> but not the number of particles. For instance, a quark down decays into a quark up, an electron and an antineutrino (beta decay) [54]. An integrable scattering process must satisfy many more constraints than a standard relativistic process [55, 56, 57, 58, 59]. In particular, it is

---

<sup>8</sup>Of course, only the **total** charges are conserved. The momentum of a particle can vary during the process as long as the total one does not change.

known that a 1+1 dimensional elastic scattering process is integrable if and only if it satisfies certain conditions. Firstly it must be *completely elastic*. A scattering process is completely elastic if the final state is kinematically identical to the initial state: while the mass and the momenta of each particle do not change during the process<sup>9</sup>, other charges can be reassigned. Additionally, the scattering process must be *factorisable*. The scattering matrix of an  $\ell \rightarrow \ell$  scattering process factorises into  $\ell(\ell - 1)/2$  two-particle matrices. In particular, there are two ways to factorise a three-particle scattering, as it is possible to choose two different orders for the individual two-particle processes (see Figure 3.1).

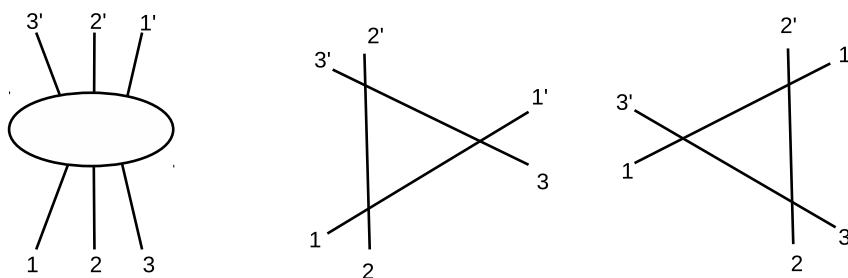


Figure 3.1: The three-particle scattering (first diagram) can be factorised into three two-particle processes (second and third diagrams). The only difference between the two factorisations is the order of the individual scattering processes.

Since the amplitude of the three-particle scattering has to be the same regardless of the order of the individual processes, the two-particle S-matrix is constrained by the *Yang-Baxter* equation [60, 61, 11]

$$S_{12}S_{13}S_{23} = S_{23}S_{13}S_{12} \tag{3.50}$$

In addition to these properties, S-matrices satisfy several general physical constraint. Every physical scattering process must be *unitary*<sup>10</sup> and it must satisfy *crossing symmetry*. While unitarity is associated with the conservation of probability in the scattering, crossing symmetry implies that the process is the same in the three channels  $s$ ,  $t$  and  $u$ . In the 1+1 dimensional case it is useful to introduce new variables in order to represent the energy and the momentum of the various particles. Relativistic invariance  $m^2 = E^2 - p^2$

---

<sup>9</sup>The individual linear momenta can be inverted.

<sup>10</sup>Notice that the unitarity of a scattering processes of a massive IQFT and of a CFT are two distinct properties. In the context of scattering unitarity is associated with invariance under time reversal and conservation of probability through the process. On the other hand, unitarity in CFT is associated with the absence of states of negative norm.

suggests a new parametrisation of the energy and momentum of a particle:

$$\begin{aligned} E &= p^0 = m \cosh \beta \\ p &= p^1 = m \sinh \beta \end{aligned} \tag{3.51}$$

The momentum  $\mathbf{p} = (E, p)$  can then be expressed using a single coordinate  $\beta$ , called *rapidity*.

Let us then denote the two-particle S-matrix as

$$S_{ab}^{cd}(\beta) \tag{3.52}$$

where  $a$  and  $b$  denote the incoming and  $c$  and  $d$  the outgoing particles. Notice that, since we are considering elastic scattering, the final particles must be equal to the initial ones (up to a reassignment of the charges).

In the new variables it is easy to write down the explicit constraints given by unitarity and crossing invariance. The unitarity condition translates to:

$$\sum_{ef} S_{ab}^{ef}(\beta) S_{ef}^{cd}(-\beta) = \delta_{ac} \delta_{bd} \tag{3.53}$$

On the other hand, crossing invariance imposes the following constraint to the S-matrix:

$$S_{ab}^{cd}(\beta) = S_{\bar{d}a}^{\bar{b}c}(i\pi - \beta) \tag{3.54}$$

where  $\bar{a}$  denotes the antiparticle of  $a$ .

From a diagrammatic point of view, the above equation implies that the scattering does not change when rotating the space-time frame.

### Bound states and pole structure

In some theories, the scattering S-matrix presents some purely imaginary poles. If the two-particle S-matrix  $S_{ab}(\beta)$  has a pole in  $iu_{ab}^c$  (with  $u_{ab}^c \in ]0, \pi[$ ) such a pole is called *bound state pole* and it is associated to the creation of a bound state. By a bound state we mean a one-particle state  $c$  that can be created by the scattering of two other particles  $a$  and  $b$ . In particular, if two particles  $a$  and  $b$  create a bound state  $c$ , the S-matrix  $S_{ab}$  has a simple pole at  $iu_{ab}^c$ :

$$\text{Res}_{\beta=iu_{ab}^c} S_{ab}(\beta) = (\Gamma_{ab}^c)^2 \tag{3.55}$$

where  $\Gamma^2$  is the relative residue, or three point coupling.

Once we have briefly reviewed the properties of the S-matrix in integrable systems, we can address the study of the form factor program, which will be largely used in the following chapters.

### 3.2.2 Form factors

Before addressing the actual study of form factors, it is useful to shortly discuss the structure of the Hilbert space. For simplicity we focus on diagonal scattering processes with non-degenerate mass spectrum.

#### Faddeev-Zamolodchikov operators

In order to describe the operators responsible for the creation of particles, it is useful to compare these operators with the familiar creation/annihilation operators of fermionic and bosonic systems:

$$\begin{aligned} \left[ c(\beta_1), c(\beta_2)^\dagger \right]_{\mp} &= 2\pi\delta(\beta_1 - \beta_2) \\ \left[ c(\beta_1), c(\beta_2) \right]_{\mp} &= \left[ c^\dagger(\beta_1), c^\dagger(\beta_2) \right]_{\mp} = 0 \end{aligned} \quad (3.56)$$

where the sign  $\mp$  refers to either boson (-) or fermion operators (+)<sup>11</sup>.

These operators can be used to explore the Hilbert space of particles obeying the Bose-Einstein or the Fermi-Dirac statistics. In practice, the two statistics differ only by the parity of the commutator. In order to describe more complicate statistics (also-called *anyonic* statistics) the above relations should be generalised.

We can then introduce the so-called *Faddeev-Zamolodchikov (FZ) operators*, a generalisation of the usual creation/annihilation operators. In particular the operator  $V_\alpha(\beta)$  annihilates a particle of type  $\alpha$  with rapidity  $\beta$ , while  $V_\alpha^\dagger(\beta)$  creates the same particle. The exchange relations of these operators are given by the so-called *Faddeev-Zamolodchikov algebra*:

$$\begin{aligned} V_{\alpha_i}(\beta_i) V_{\alpha_j}(\beta_j) &= S_{\alpha_i\alpha_j}(\beta_{ij}) V_{\alpha_j}(\beta_j) V_{\alpha_i}(\beta_i) \\ V_{\alpha_i}^\dagger(\beta_i) V_{\alpha_j}^\dagger(\beta_j) &= S_{\alpha_i\alpha_j}(\beta_{ij}) V_{\alpha_j}^\dagger(\beta_j) V_{\alpha_i}^\dagger(\beta_i) \\ V_{\alpha_i}(\beta_i) V_{\alpha_j}^\dagger(\beta_j) &= S_{\alpha_i\alpha_j}(\beta_{ij}) V_{\alpha_j}^\dagger(\beta_j) V_{\alpha_i}(\beta_i) + 2\pi\delta_{\alpha_i\alpha_j}\delta(\beta_{ij}) \end{aligned} \quad (3.57)$$

In particular, it is clear that the boson/fermion commutations relations are recovered from the Faddeev-Zamolodchikov algebra once their S-matrices have been taken into account,

---

<sup>11</sup> $[a, b]_- \equiv [a, b] = ab - ba$ ;  $[a, b]_+ \equiv \{a, b\} = ab + ba$ .

since the S-matrix of free bosonic(fermionic) system is equal to (minus) one.

Quantum states can then be described as the action of  $V$  operators on the vacuum:

$$V_{\alpha_1}^\dagger(\beta_1) V_{\alpha_2}^\dagger(\beta_2) \cdots V_{\alpha_\ell}^\dagger(\beta_\ell) |\emptyset\rangle = |\beta_1, \beta_2, \dots, \beta_\ell\rangle_{\alpha_1 \alpha_2 \cdots \alpha_\ell} \quad (3.58)$$

while  $V_\alpha(\beta)$  acts as annihilator:

$$V_\alpha(\beta) |\emptyset\rangle = 0 \quad (3.59)$$

Since the FZ operators depend explicitly on the rapidities, Poincaré transformations act in a very simple way:

$$\begin{aligned} V_\alpha(\beta) &\rightarrow V_\alpha(\beta + \epsilon) && \text{Lorentz boost} \\ V_\alpha(\beta) &\rightarrow e^{ip_\mu y^\mu} V_\alpha(\beta) && \text{Translations} \end{aligned} \quad (3.60)$$

Of course, these simple properties are reflected on the states created by FZ operators.

The last equation of (3.57) gives also an explicit expression for the inner product between states. For example:

$${}_{\alpha_1} \langle \beta_1 | \beta_2 \rangle_{\alpha_2} = 2\pi \delta_{\alpha_1 \alpha_2} \delta(\beta_{12}) \quad (3.61)$$

where  $\beta_{ij} \equiv \beta_i - \beta_j$ .

We can now try to assemble a vector basis for the Hilbert space. Let us consider the following two-particle state:

$$|\beta_1, \beta_2\rangle_{\alpha_1 \alpha_2} = V_{\alpha_1}^\dagger(\beta_1) V_{\alpha_2}^\dagger(\beta_2) |\emptyset\rangle \quad (3.62)$$

Using the second relation of (3.57) it is equal to

$$S_{\alpha_1 \alpha_2}(\beta_{12}) V_{\alpha_2}^\dagger(\beta_2) V_{\alpha_1}^\dagger(\beta_1) |\emptyset\rangle = S_{\alpha_1 \alpha_2}(\beta_{12}) |\beta_2, \beta_1\rangle_{\alpha_2 \alpha_1} \quad (3.63)$$

$|\beta_1, \beta_2\rangle_{\alpha_1 \alpha_2}$  and  $|\beta_2, \beta_1\rangle_{\alpha_2 \alpha_1}$  are then clearly linearly dependent. In order to select a basis of linearly independent vectors, we add an additional requirement on the basis vectors: by convention, we arrange rapidities in decreasing order for incoming states and in increasing order for outgoing states:

$$\begin{aligned} \beta_1 > \beta_2 > \cdots > \beta_\ell & \text{ incoming state} \\ \beta_1 < \beta_2 < \cdots < \beta_\ell & \text{ outgoing state} \end{aligned} \quad (3.64)$$

Selecting this order for incoming (outgoing) states, we can build up a basis for the Hilbert space of incoming (outgoing) particles.

We can now address the definition and the properties of form factors.

### Form factors

Let us consider the following matrix element<sup>12</sup> of an operator  $\mathcal{O}$  between an  $\ell$ -particle (incoming) and a  $k$ -particle (outgoing) state:

$$\alpha_{\ell+1}\dots\alpha_k \langle \beta_{\ell+1}, \dots, \beta_{\ell+k} | \mathcal{O}(\mathbf{x}) | \beta_1, \dots, \beta_\ell \rangle_{\alpha_1 \dots \alpha_\ell} \quad (3.65)$$

The operator  $\mathcal{O}$  can be translated to  $\mathbf{x} = 0$  via

$$\mathcal{O}(\mathbf{x}) = e^{i\hat{p}_\mu x^\mu} \mathcal{O}(0) e^{-i\hat{p}_\mu x^\mu} \quad (3.66)$$

The action of  $\hat{p}$  onto states is simply given by:

$$\hat{p}_\mu | \beta_1, \dots, \beta_\ell \rangle_{\alpha_1 \dots \alpha_\ell} = \left( \sum_{i=1}^{\ell} p_\mu(\beta_i) \right) | \beta_1, \dots, \beta_\ell \rangle_{\alpha_1 \dots \alpha_\ell} \quad (3.67)$$

Equation (3.65) can be then written as

$$e^{i \left( \sum_{i=\ell+1}^k p_\mu(\beta_i) - \sum_{j=1}^{\ell} p_\mu(\beta_j) \right) x^\mu} \alpha_{\ell+1}\dots\alpha_k \langle \beta_{\ell+1}, \dots, \beta_{\ell+k} | \mathcal{O}(0) | \beta_1, \dots, \beta_\ell \rangle_{\alpha_1 \dots \alpha_\ell} \quad (3.68)$$

Let us now define the  $\ell$ -particle *form factor* FF of the operator  $\mathcal{O}$  as

$$F_\ell^{\mathcal{O}|\alpha_1 \dots \alpha_\ell}(\beta_1, \dots, \beta_\ell) = \langle \emptyset | \mathcal{O}(0) | \beta_1, \dots, \beta_\ell \rangle_{\alpha_1 \dots \alpha_\ell} \quad (3.69)$$

If the theory is local and Poincaré invariant, form factors of scalar fields will depend only on the differences of rapidities:

$$F_\ell^{\mathcal{O}|\alpha_1 \dots \alpha_\ell}(\beta_1, \dots, \beta_\ell) = F_\ell^{\mathcal{O}|\alpha_1 \dots \alpha_\ell}(\beta_{12}, \beta_{13}, \dots, \beta_{jk}, \dots) \text{ for } j < k \quad (3.70)$$

A graphical representation of a form factor can be found in Figure 3.3.

---

<sup>12</sup>In the following, we will consider all matrix elements between out (left) and in (right) states.

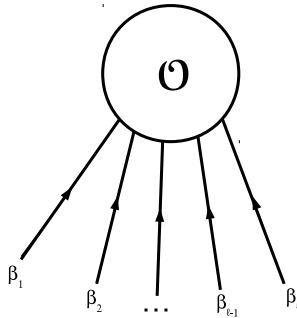


Figure 3.2: Form factors of the operator  $\mathcal{O}$  with  $\ell$  incoming particles

### 3.3 Form Factor Equations

Similarly to the S-matrix, form factors must satisfy some constraints based on physical requirements. For simplicity, we consider theories with diagonal scattering only.

#### Watson equations

From the definitions (3.58) and (3.69) and the Faddeev-Zamolodchikov algebra (3.57) form factors must satisfy two conditions, known as *Watson Equations*:<sup>13</sup>

$$F_\ell^{\alpha_1 \dots \alpha_i \alpha_{i+1} \dots \alpha_\ell}(\beta_1, \dots, \beta_i, \beta_{i+1}, \dots, \beta_\ell) = S_{\alpha_i \alpha_{i+1}}(\beta_{i,i+1}) F_\ell^{\alpha_1 \dots \alpha_{i+1} \alpha_i \dots \alpha_\ell}(\beta_1, \dots, \beta_{i+1}, \beta_i, \dots, \beta_\ell) \quad (3.71)$$

$$\begin{aligned} F_\ell^{\alpha_1 \alpha_2 \dots \alpha_\ell}(\beta_1 + 2\pi i, \beta_2, \dots, \beta_\ell) &= F_\ell^{\alpha_2 \dots \alpha_\ell \alpha_1}(\beta_2, \dots, \beta_\ell, \beta_1) \\ &= \left( \prod_{i=2}^{\ell} S_{\alpha_i \alpha_1}(\beta_{i,1}) \right) F_\ell^{\alpha_1 \dots \alpha_\ell}(\beta_1, \dots, \beta_\ell) \end{aligned} \quad (3.72)$$

The first equation simply follows from the second identity of (3.57) and can be interpreted with the help of the graphical representation:

<sup>13</sup>In the following, we will omit the operator  $\mathcal{O}$  in the form factor in order to have a more compact notation.

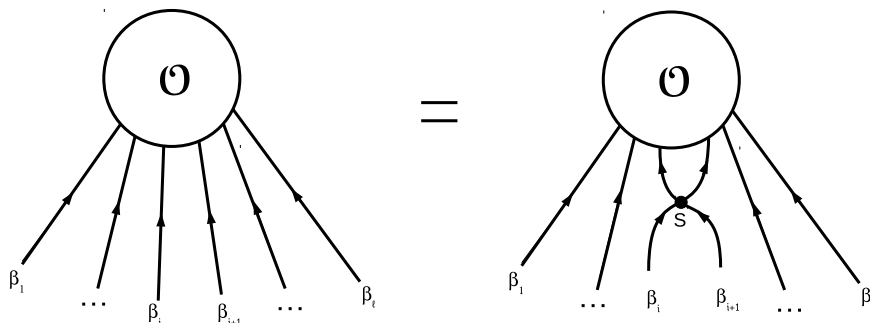


Figure 3.3: Graphical representation of the first Watson equation. In the form factor on the right the two particles  $i$  and  $i + 1$  have been exchanged. Since these particles live in a two-dimensional space-time, the scattering is unavoidable.

The first Watson equation simply describes the exchange of two particles. To restore the original order, the two particles exchanged must scatter and this process is represented by the S-matrix. If the particles were in a higher dimensional space, they could have been exchanged without any scattering. The second Watson equation (3.72) is given by the fact that the first particle becomes the last when rotated around the operator  $\mathcal{O}$ . The second equality is a simple consequence of the first Watson equation (3.71).

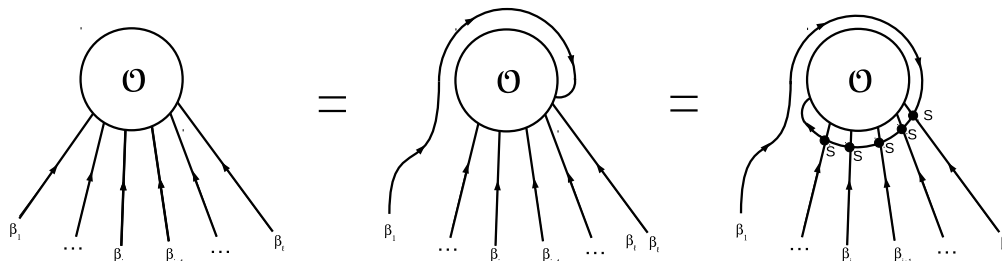


Figure 3.4: Graphical representation of the second Watson equation. A shift by  $2\pi i$  in the first rapidity implies a complete rotation of the particle around the operator  $\mathcal{O}$ . The initial order of particles can be restored by making the first particle scatter with all others.

Watson equations are not sufficient to entirely determine the form factors expressions. However, additional constraints exist which follow from the pole structure of the form factors.

### Poles structure

There can only be two kinds of poles appearing in the form factors' expressions: the *kinematic* and the *bound state* poles. Each pole gives rise to an associated residue equation.

The kinematic residue equation is given by:

$$\text{Res}_{\bar{\beta}_0=\beta_0} F_{\ell+2}^{\bar{\alpha}_0\alpha_0\alpha_1\cdots\alpha_\ell}(\bar{\beta}_0 + i\pi, \beta_0, \beta_1, \dots, \beta_\ell) = i \left( 1 - \prod_{i=1}^{\ell} S_{\alpha_0\alpha_i}(\beta_{1\ell}) \right) F_{\ell}^{\alpha_1\cdots\alpha_\ell}(\beta_1, \dots, \beta_\ell) \quad (3.73)$$

where  $\bar{\alpha}_0$  denotes the antiparticle of  $\alpha_0$ .

Shifting a rapidity of a particle by  $i\pi$  is equivalent to inverting the direction of the motion<sup>14</sup>, transforming the particle from incoming to outgoing. Since the scattering amplitude diverges when an incoming and an outgoing particle have the same rapidity<sup>15</sup>, form factors preserve these poles at  $\beta_{ij} = i\pi$  (kinematic poles).

Moreover, when the scattering matrix has a pole itself, the corresponding form factor preserves the same pole (bound state pole):

$$\text{Res}_{\beta_0=\beta_1} F_{\ell+1}^{\alpha_0\alpha_1\alpha_2\cdots\alpha_\ell}(\beta_0 + iu_{\alpha_0\alpha_1}^\alpha, \beta_1, \dots, \beta_\ell) = \Gamma_{\alpha_0\alpha_1}^\alpha F_{\ell}^{\alpha_2\cdots\alpha_\ell}(\beta_1, \dots, \beta_\ell) \quad (3.74)$$

where  $iu_{\alpha_0\alpha_1}^\alpha$  and  $\Gamma_{\alpha_0\alpha_1}^\alpha$  are one pole of the S-matrix and its residue.

Once we have introduced all the relevant physical properties of form factors, we can describe the tool to compute their explicit expressions. Firstly, we will define minimal form factors, which are the building blocks of form factors with any number of particles. The second step will be the implementation of recursive equations to build up high particle form factors using Watson equations and the knowledge of their pole structure.

### Minimal form factors

In order to construct high particle form factors (i.e. with more than two particles) we start from the so-called *minimal form factors*, denoted by  $F_{\min}$ , which satisfy Watson equations (3.71) for  $\ell = 2$  but are free from kinematic poles

$$F_{\min}^{\alpha_1\alpha_2}(\beta) = S_{\alpha_1\alpha_2}(\beta) F_{\min}^{\alpha_2\alpha_1}(-\beta) \quad (3.75)$$

$$F_{\min}^{\alpha_1\alpha_2}(\beta) = F_{\min}^{\alpha_1\alpha_2}(2\pi i - \beta) \quad (3.76)$$

While minimal form factors have no kinematic poles, they may have bound state poles if the S-matrix has any. For instance, form factors used in Chapter 6 have bound state poles while the ones of Chapter 8 do not.

The minimal form factors can be derived using an integral representation of the S-matrix.

---

<sup>14</sup>Since  $p_\mu(\beta + i\pi) = -p_\mu(\beta)$ , the particle becomes an anti-particle travelling backwards in time.

<sup>15</sup>The scattering amplitude depends explicitly on a delta function  $\delta^{(2)}(\mathbf{p}_1 - \mathbf{p}_2)$ .

Representing the S-matrix as:

$$S_{\alpha_1\alpha_2}(\beta) = \exp \left[ \int_0^\infty \frac{dt}{t} s_{\alpha_1\alpha_2}(t) \sinh \frac{t\beta}{i\pi} \right] \quad (3.77)$$

the minimal form factor is then given by

$$F_{\min}^{\alpha_1\alpha_2}(\beta) = \mathcal{N} \exp \left[ \int_0^\infty \frac{dt}{t} \frac{s_{\alpha_1\alpha_2}(t)}{\sinh t} \sin^2 \left( \frac{t\pi(i\pi - \beta)}{2\pi} \right) \right] \quad (3.78)$$

where the normalisation factor  $\mathcal{N}$  includes also the bound state poles (if any).

Once the explicit expressions of minimal form factors have been derived, higher particle form factors can be written as:

$$F_{\ell}^{\alpha_1 \dots \alpha_{\ell}}(\beta_1, \dots, \beta_{\ell}) = Q_{\ell}^{\alpha_1 \dots \alpha_{\ell}}(x_1, \dots, x_{\ell}) \prod_{i < j} \frac{F_{\min}^{\alpha_i \alpha_j}(\beta_{ij})}{x_i + x_j} \quad (3.79)$$

where  $x_i = e^{\beta_i}$ . Kinematic poles are encapsulated in the denominator  $1/(x_i + x_j)$ <sup>16</sup>. The function  $Q$  is a pole free, completely symmetric function on the physical sheet  $\text{Im}\beta_{ij} \in ]0, 2\pi[$ . This is because all the physical features of form factors (poles and Watson conditions) are satisfied by  $F_{\min}/(x_i + x_j)$ . The explicit expressions of the polynomial  $Q$  can be derived recursively exploiting the pole structure of form factors.

Using the tool we have just introduced it is then possible to construct all possible form factors with arbitrary number of particles. Of course, even though there is no upper limit in the number of particles in a form factor, in an actual computation usually the expressions of many particles form factors become too complicated to be handled. Fortunately, in the majority of cases few particles are enough to describe faithfully a correlation function (see, for instance, [62, 63, 64]).

### Kernel solutions

If we have a closer look at the procedure to construct the explicit expressions of form factors, we should notice that it does not depend explicitly on the field  $\mathcal{O}$ . Additionally, when we compute the  $\ell + 2$ -th form factor from the  $\ell$ -th and the  $\ell + 1$ -th ones, there is no guarantee that the solution is unique. In general, all local operators have form factors that satisfy the same equations. As we showed before, using the kinematic residue equation, we can relate form factors with  $\ell$  and  $\ell + 2$  particles:

$$F_{\ell}^{\mathcal{O}} = \mathfrak{c} [F_{\ell+2}^{\mathcal{O}}] \quad (3.80)$$

---

<sup>16</sup>  $e^{\beta_i+i\pi} + e^{\beta_j} = -e^{\beta_i} + e^{\beta_j} = 0$  for  $\beta_i = \beta_j$ .

On the other hand, bound state poles connect the  $\ell$ -th and the  $\ell+1$ -th form factors:

$$F_\ell^\mathcal{O} = \mathfrak{B} [F_{\ell+1}^\mathcal{O}] \quad (3.81)$$

The functions  $\mathfrak{C}$  and  $\mathfrak{B}$  simply indicate the residue operation relative to, respectively, the kinematic and the bound state poles.

Since we do not know a priori if  $\mathfrak{C}$  and  $\mathfrak{B}$  are injective, it is possible to generate different solutions every time we increase  $\ell$  [65]. In particular, the above equations have some *kernel solutions*  $\mathfrak{K}$ :

$$\begin{aligned} \mathfrak{C}[\mathfrak{K}_C] &= 0 \\ \mathfrak{B}[\mathfrak{K}_B] &= 0 \end{aligned} \quad (3.82)$$

1 These kernel solutions give no contributions to the residue equations because they do not have any poles. Since higher particle form factors can be obtained by inverting the residue equations, kernel solutions must be taken into account. A solution of the above kinematic residue equation will then have the generic form:

$$F_{\ell+2}^\mathcal{O} = \tilde{F}_{\ell+2}^\mathcal{O} + \mathfrak{K}_C \quad (3.83)$$

where  $\tilde{F}_{\ell+2}^\mathcal{O}$  is a *particular* solution of equation (3.80).

The richness of the space of form factors can be associated with the multitude of local fields they are associated with (see e.g. [66, 65, 67, 68]). Moreover, it has been noticed in [69], that the two-particle form factor of a modified twist field (see Chapter 6) arises naturally from a kernel solution. For this reason, every time the form factor program is used to evaluate a correlator (see next section), it is important to check that the series of form factors is the right one for the correlation function under consideration.

### 3.3.1 Correlation functions

Once the explicit expressions of form factors have been computed, they can be used to evaluate correlation functions.

Consider the following correlator:

$$G_2(\mathbf{x}) = \langle \emptyset | \mathcal{O}(\mathbf{x}) \mathcal{O}^\dagger(0) | \emptyset \rangle \quad (3.84)$$

The complete resolution of the identity can be written in terms of the states defined earlier (3.58):

$$\mathbf{1} = \sum_{\ell=0}^{\infty} \frac{1}{\ell!} \sum_{\alpha_1 \dots \alpha_\ell} \int \frac{d^\ell \beta}{(2\pi)^\ell} |\beta_1, \dots, \beta_\ell\rangle_{\alpha_1 \dots \alpha_\ell} {}_{\alpha_1 \dots \alpha_\ell} \langle \beta_1, \dots, \beta_\ell| \quad (3.85)$$

Each term of this resolution is nothing but a projector onto the space spanned by an element of the basis of the Hilbert space. Since the basis chosen is orthogonal, the identity operator of the relative Hilbert space can be constructed by the sum of such projectors<sup>17</sup>. We can then insert the above resolution of the identity between the two fields  $\mathcal{O}$  and  $\mathcal{O}^\dagger$ :

$$\begin{aligned} G_2(\mathbf{x}) &= \sum_{\ell=0}^{\infty} \frac{1}{\ell!} \sum_{\alpha_1 \dots \alpha_\ell} \int \frac{d^\ell \beta}{(2\pi)^\ell} \langle \emptyset | \mathcal{O}(\mathbf{x}) | \beta_1, \dots, \beta_\ell \rangle_{\alpha_1 \dots \alpha_\ell} {}_{\alpha_1 \dots \alpha_\ell} \langle \beta_1, \dots, \beta_\ell | \mathcal{O}(0) | \emptyset \rangle \\ &= \sum_{\ell=0}^{\infty} \frac{1}{\ell!} \sum_{\alpha_1 \dots \alpha_\ell} \int \frac{d^\ell \beta}{(2\pi)^\ell} |\langle \emptyset | \mathcal{O}(0) | \beta_1, \dots, \beta_\ell \rangle_{\alpha_1 \dots \alpha_\ell}|^2 e^{-im \sum_{j=1}^{\ell} (\cosh \beta_j x^0 + \sinh \beta_j x^1)} \end{aligned} \quad (3.86)$$

In the last step we have used (3.68) and, for simplicity, we assumed that all the particles have the same mass  $m_i = m$ . Thanks to Lorentz invariance, whenever the two points  $\mathbf{x}$  and  $\mathbf{0}$  are separated by a time-like interval, we can rotate the frame of reference in order to make the spatial distance  $x^1$  vanish. After a Wick rotation  $ix^0 \rightarrow r$ , the correlation function becomes

$$G_2(\mathbf{x}) = \sum_{\ell=0}^{\infty} \frac{1}{\ell!} \sum_{\alpha_1 \dots \alpha_\ell} \int \frac{d^\ell \beta}{(2\pi)^\ell} |F_\ell^{\alpha_1 \dots \alpha_\ell}(\beta_1, \dots, \beta_\ell)|^2 e^{-mr \sum_{j=1}^{\ell} \cosh \beta_j} \quad (3.87)$$

where  $r$  is the Lorentz invariant distance  $(x^1)^2 - (x^0)^2$  between the two points  $\mathbf{x}$  and  $\mathbf{0}$ . Thanks to the above equation we can express every correlation function as an infinite sum of form factor contributions. If the theory is also integrable, we can, in principle, construct the entire infinite series of form factors and evaluate the correlator exactly.

It has to be noticed that it is generally very difficult to resum the complete series of form factors, apart from some simple cases, like the twist fields [70] or energy-energy

---

<sup>17</sup>In our notation, each term has integration domain  $\mathbb{R}^\ell$ . It should be noticed that it is in contrast with the convention used to define basis vectors. To take into account this discrepancy, we divided each term by  $\ell!$ . In other words, we divide by  $\ell!$  in order to avoid overcounting states. Such a coefficient is simply the ratio between the volume of the box  $[-L, L]^\ell$  and the volume of the domain  $\{\mathbf{x} \in [-L, L]^\ell \text{ s.t. } x_1 < x_2 < \dots < x_\ell\}$ .

[64] correlation functions of the Ising model. Even though the form factor expressions themselves are known in many theories<sup>18</sup>, the main difficulty is usually the (numerical) integration of all the terms of the series.

### 3.3.2 Ultraviolet limit

The form factor expansion can be used not only to compute the actual values of correlation functions, but also some physical constants involved in the scaling of correlators. Since the term  $\exp\left(-mr \sum_{j=1}^{\ell} \cosh \beta_j\right)$  decays very quickly for large  $mr$ , the form factor expansion is very precise in the far-from-criticality region. On the other hand, it would be useful to extract some short distance scaling information. In order to probe this regime, we can rearrange the expansion in a more convenient way to study the ultraviolet scaling [74, 75]. Instead of computing the form factor expansion of a correlation function, we can compute its logarithm, using a different series:

$$\log \frac{\langle \mathcal{O}(\mathbf{x}) \mathcal{O}^\dagger(0) \rangle}{\langle \mathcal{O} \rangle^2} = \sum_{\ell=0}^{\infty} \frac{1}{\ell!} \sum_{\alpha_1 \dots \alpha_\ell} \int \frac{d^\ell \beta}{(2\pi)^\ell} H_\ell^{\alpha_1 \dots \alpha_\ell}(\beta_1, \dots, \beta_\ell) e^{-mr \sum_{j=1}^{\ell} \cosh \beta_j} \quad (3.88)$$

where the new functions  $H_\ell$  must be chosen in order to match the two expansions (3.88) and  $\log$  of (3.87). For instance, the first three  $H$ s are given by

$$H_1^{\alpha_1}(\beta_1) = \frac{|F_1^{\alpha_1}(\beta_1)|}{\langle \mathcal{O} \rangle^2} \quad (3.89)$$

$$H_2^{\alpha_1 \alpha_2}(\beta_1, \beta_2) = \frac{|F_2^{\alpha_1 \alpha_2}(\beta_1, \beta_2)|}{\langle \mathcal{O} \rangle^2} - H_1^{\alpha_1}(\beta_1) H_1^{\alpha_2}(\beta_2) \quad (3.90)$$

$$\begin{aligned} H_3^{\alpha_1 \alpha_2 \alpha_3}(\beta_1, \beta_2, \beta_3) &= \frac{|F_3^{\alpha_1 \alpha_2 \alpha_3}(\beta_1, \beta_2, \beta_3)|}{\langle \mathcal{O} \rangle^2} - H_1^{\alpha_1}(\beta_1) H_1^{\alpha_2}(\beta_2) H_1^{\alpha_3}(\beta_3) \\ &- H_2^{\alpha_1 \alpha_2}(\beta_1, \beta_2) H_1^{\alpha_3}(\beta_3) \\ &- H_2^{\alpha_1 \alpha_3}(\beta_1, \beta_3) H_1^{\alpha_2}(\beta_2) \\ &- H_2^{\alpha_2 \alpha_3}(\beta_2, \beta_3) H_1^{\alpha_1}(\beta_1) \end{aligned} \quad (3.91)$$

The  $H_\ell$  terms can be seen as the connected part of the  $|F_\ell|^2$  terms. From an intuitive QFT point of view,  $|F_\ell|^2$  is to the partition function as  $H_\ell$  is to the free energy.

The short distance scaling is given by

$$\frac{\langle \mathcal{O}(r) \mathcal{O}^\dagger(0) \rangle}{\langle \mathcal{O} \rangle^2} \sim K_{\mathcal{O}} \times r^{-4x_{\mathcal{O}}} \quad (3.92)$$

<sup>18</sup>Like, for instance, the sinh-Gordon model [63], the Lee-Yang model [62] or the Ising model in a magnetic field [71, 72, 73].

where the coefficients  $K_{\mathcal{O}}$  and  $x_{\mathcal{O}}$  are constants depending on the particular field  $\mathcal{O}$ . Comparing such short distance scaling with (3.88) we can extract  $K_{\mathcal{O}}$  and  $x_{\mathcal{O}}$  from the form factor expansion. In other words, we can write an explicit form factor expansion for the two constants.

Thanks to Poincaré invariance, we can shift all the rapidities by  $\beta_1$ :

$$\log \frac{\langle \mathcal{O}(\mathbf{x}) \mathcal{O}^\dagger(0) \rangle}{\langle \mathcal{O} \rangle^2} = \sum_{\ell=0}^{\infty} \frac{1}{\ell!} \sum_{\alpha_1 \dots \alpha_\ell} \int \frac{d^\ell \beta}{(2\pi)^\ell} H_\ell^{\alpha_1 \dots \alpha_\ell} (0, \beta_2 - \beta_1, \dots, \beta_\ell - \beta_1) e^{-mr \sum_{j=1}^{\ell} \cosh \beta_j} \quad (3.93)$$

Performing a change of variables

$$\begin{aligned} \beta_1 &\rightarrow t_1 \\ \beta_j &\rightarrow t_j + t_1 \end{aligned} \quad (3.94)$$

the integral becomes

$$\begin{aligned} &\int \frac{d^\ell t}{(2\pi)^\ell} H_\ell^{\alpha_1 \dots \alpha_\ell} (0, t_2, \dots, t_\ell) e^{-mr[\cosh t_1 + \cosh(t_1+t_2) + \dots + \cosh(t_1+t_\ell)]} \quad (3.95) \\ &= \int \frac{dt_2 \dots dt_\ell}{(2\pi)^\ell} H_\ell^{\alpha_1 \dots \alpha_\ell} (0, t_2, \dots, t_\ell) \int dt_1 e^{-mr[\cosh t_1 + \cosh(t_1+t_2) + \dots + \cosh(t_1+t_\ell)]} \end{aligned} \quad (3.96)$$

The exponent can be rearranged in the following way:

$$\begin{aligned} &\cosh t_1 + \cosh(t_1 + t_2) + \dots + \cosh(t_1 + t_\ell) \\ &= \cosh t_1 + \cosh t_1 \cosh t_2 + \sinh t_1 \sinh t_2 + \dots + \cosh t_1 \cosh t_\ell + \sinh t_1 \sinh t_\ell \\ &= \cosh t_1 (1 + \cosh t_2 + \dots + \cosh t_\ell) + \sinh t_1 (\sinh t_2 + \dots + \sinh t_\ell) \end{aligned} \quad (3.97)$$

Then, the last integral of (3.95) can be performed exactly:

$$\begin{aligned} &\int_{-\infty}^{\infty} dt_1 e^{-mr[\cosh t_1 + \cosh(t_1+t_2) + \dots + \cosh(t_1+t_\ell)]} \\ &= \int_{-\infty}^{\infty} dt_1 e^{-mr[\cosh t_1 (1 + \cosh t_2 + \dots + \cosh t_\ell) + \sinh t_1 (\sinh t_2 + \dots + \sinh t_\ell)]} \\ &= 2K_0(mrd_\ell) \end{aligned} \quad (3.98)$$

where  $K_0$  is the modified Bessel function of the second kind [49] and  $d_\ell$  is given by

$$d_\ell^2 = (1 + \cosh t_2 + \cdots + \cosh t_\ell)^2 - (\sinh t_2 + \cdots + \sinh t_\ell)^2 \quad (3.99)$$

Putting everything together, (3.88) becomes

$$\log \frac{\langle \mathcal{O}(r) \mathcal{O}^\dagger(0) \rangle}{\langle \mathcal{O} \rangle^2} = 2 \sum_{\ell=0}^{\infty} \frac{1}{\ell!} \sum_{\alpha_1 \cdots \alpha_\ell} \int \frac{d^{\ell-1}t}{(2\pi)^\ell} H_\ell^{\alpha_1 \cdots \alpha_\ell}(0, t_1, \dots, t_{\ell-1}) K_0(mrd_\ell) \quad (3.100)$$

In order to study the short-distance scaling, we can expand the Bessel function around  $mr = 0$ :

$$K_0(mrd_\ell) = (\log 2 - \gamma_E - \log r - \log(md_\ell)) + O((mrd_\ell)^2) \quad (3.101)$$

where  $\gamma_E = \lim_{n \rightarrow \infty} \left( \sum_{k=1}^n -\log n \right) = 0.5772156649 \dots$  is the Euler-Mascheroni constant.

Collecting all the  $\log r$  and the  $r$ -independent contributions from (3.100) we have

$$\begin{aligned} \log \frac{\langle \mathcal{O}(r) \mathcal{O}^\dagger(0) \rangle}{\langle \mathcal{O} \rangle^2} &= -\log r \left[ 2 \sum_{\ell=0}^{\infty} \frac{1}{\ell!} \sum_{\alpha_1 \cdots \alpha_\ell} \int \frac{d^{\ell-1}t}{(2\pi)^\ell} H_\ell^{\alpha_1 \cdots \alpha_\ell}(0, t_1, \dots, t_{\ell-1}) \right] \\ &\quad - \left[ 2 \sum_{\ell=0}^{\infty} \frac{1}{\ell!} \sum_{\alpha_1 \cdots \alpha_\ell} \int \frac{d^{\ell-1}t}{(2\pi)^\ell} H_\ell^{\alpha_1 \cdots \alpha_\ell}(0, t_1, \dots, t_{\ell-1}) \left( \log \frac{md_\ell}{2} - \gamma_E \right) \right] \end{aligned} \quad (3.102)$$

Comparing the above expansion with (3.92) we obtain a form factor expansion for  $x_{\mathcal{O}}$  and  $K_{\mathcal{O}}$ :

$$x_{\mathcal{O}} = \frac{1}{4\pi} \sum_{\ell=0}^{\infty} \frac{1}{\ell!} \sum_{\alpha_1 \cdots \alpha_\ell} \int \frac{d^{\ell-1}t}{(2\pi)^{\ell-1}} H_\ell^{\alpha_1 \cdots \alpha_\ell}(0, t_1, \dots, t_{\ell-1}) \quad (3.103)$$

$$K_{\mathcal{O}} = \exp \left[ -\frac{1}{\pi} \sum_{\ell=0}^{\infty} \frac{1}{\ell!} \sum_{\alpha_1 \cdots \alpha_\ell} \int \frac{d^{\ell-1}t}{(2\pi)^{\ell-1}} H_\ell^{\alpha_1 \cdots \alpha_\ell}(0, t_1, \dots, t_{\ell-1}) \left( \log \frac{md_\ell}{2} - \gamma_E \right) \right] \quad (3.104)$$

This ultraviolet scaling can be compared with the conformal scaling, since (at short distance)

$$\langle \mathcal{O}(r) \mathcal{O}^\dagger(0) \rangle \sim C_{\mathcal{O}\mathcal{O}}^{A_k} r^{-2(\Delta_{\mathcal{O}} - \Delta_k)} \langle A_k \rangle \quad (3.105)$$

where  $A_k$  is the field with the smallest conformal dimension arising from the OPE between  $\mathcal{O}$  and  $\mathcal{O}^\dagger$  (see the end of this chapter). Since in ordinary unitary theories  $A_k = \mathbf{1}$  and  $C_{\mathcal{O}\mathcal{O}}^1 = 1$ , we can use the form factor expansion of  $K_{\mathcal{O}}$  to compute the vacuum expectation value of  $\mathcal{O}$ . Combining (3.92) and (3.105) we obtain

$$\langle \mathcal{O} \rangle = \frac{1}{\sqrt{K_{\mathcal{O}}}} \quad (3.106)$$

Notice that the vacuum expectation value of a field in the massive regime is not always easy to evaluate. The form factor programme gives a powerful tool which can be applied in a multitude of cases.

The study of the ultraviolet regime can also be used to test (or identify) the form factors. A direct comparison between  $x_{\mathcal{O}}$  and  $\Delta_{\mathcal{O}}$  (or something slightly more complicated for the non unitary cases) is a strong check and can be used to test whether the right form factors have been used.

### 3.3.3 Non unitary case

The form factor program can be used also when studying non unitary systems, even if some modifications need to be put in place. Since form factors can be derived directly from the S-matrix<sup>19</sup> and from its pole structure, the procedure is similar to the one for unitary systems. The main difference appears when evaluating correlation functions using form factors. The formula (3.87) has been derived from the tacit assumption that bra states can be mapped onto ket states by a simple Hermitian conjugation:

$$\langle \beta_1, \dots, \beta_\ell | \mathcal{O}^\dagger | \emptyset \rangle = \langle \emptyset | \mathcal{O} | \beta_1, \dots, \beta_\ell \rangle^* \quad (3.107)$$

While this relation holds for unitary theories, it is no more valid in non unitary models. In the Lee-Yang model it is possible to show explicitly that bra and ket states are connected via a slightly different relation ( $\phi$  is the fundamental Lee-Yang field):

$$\frac{\langle \beta_1, \dots, \beta_\ell | \phi(0) | \emptyset \rangle}{\langle \phi \rangle} = (-1)^\ell \left( \frac{\langle \emptyset | \phi(0) | \beta_1, \dots, \beta_\ell \rangle}{\langle \phi \rangle} \right)^* \quad (3.108)$$

In unitary theories, the bound state residue  $\Gamma^2$  is always positive. On the other hand, a signal of non unitarity of a theory is the wrong sign of the residue  $\Gamma^2 < 0$ , even though the associate S-matrix satisfies the unitarity condition  $S(\beta)S(-\beta) = 1$ . For instance, in the Lee-Yang theory (see Chapter 6), the residue is  $-2\sqrt{3}$ . When a theory is non unitary,

---

<sup>19</sup>Note that even though the theory is called non unitary, the S-matrix describing the process satisfies the unitarity condition.

it is possible to define a charge conjugate operator  $\mathbf{C}$  [76]:

$$\mathbf{C}\phi\mathbf{C} = -\phi \quad (3.109)$$

Moreover, the associate quantum Hamiltonians  $H$  (see [77] and Chapter 7) is not hermitian, even though has real eigenvalues and satisfies a “relaxed” hermiticity condition:

$$\mathbf{C}H\mathbf{C} = H^\dagger \quad (3.110)$$

Since the Hamiltonian is not hermitian, left and right eigenvectors are not related by a simple hermitian conjugation. The operator  $\mathbf{C}$  provides a “generalised hermitian conjugation”, i.e. it maps asymptotic past states into asymptotic future states. Since a generic state is generated by the iterate action of the field  $\phi$  on the vacuum state, using (3.109) it is possible to show that asymptotic states are eigenvectors of the operator  $\mathbf{C}$  with eigenvalues  $(-1)^\ell$  (with  $\ell$  being the number of particles). Since the two matrix elements of (3.108) are related one to the other by a “generalised hermitian conjugation” the  $(-1)^\ell$  appears.

For non unitary models, the formula (3.87) is then modified to

$$\frac{\langle \mathcal{O}(r)\mathcal{O}^\dagger(0) \rangle}{\langle \mathcal{O} \rangle^2} = \sum_{\ell=0}^{\infty} \frac{(-1)^\ell}{\ell!} \sum_{\alpha_1 \dots \alpha_\ell} \int \frac{d^\ell \beta}{(2\pi)^\ell} \left| \frac{F_\ell^{\alpha_1 \dots \alpha_\ell}(\beta_1, \dots, \beta_\ell)}{\langle \mathcal{O} \rangle} \right|^2 e^{-mr \sum_{j=1}^{\ell} \cosh \beta_j} \quad (3.111)$$

For the very same reason, formulas (3.88), (3.103) and (3.104) will be affected in a similar way:

$$\log \frac{\langle \mathcal{O}(\mathbf{x})\mathcal{O}^\dagger(0) \rangle}{\langle \mathcal{O} \rangle^2} = \sum_{\ell=0}^{\infty} \frac{(-1)^\ell}{\ell!} \sum_{\alpha_1 \dots \alpha_\ell} \int \frac{d^\ell \beta}{(2\pi)^\ell} H_\ell^{\alpha_1 \dots \alpha_\ell}(\beta_1, \dots, \beta_\ell) e^{-mr \sum_{j=1}^{\ell} \cosh \beta_j} \quad (3.112)$$

$$x_{\mathcal{O}} = \frac{1}{4\pi} \sum_{\ell=0}^{\infty} \frac{(-1)^\ell}{\ell!} \sum_{\alpha_1 \dots \alpha_\ell} \int \frac{d^{\ell-1} t}{(2\pi)^{\ell-1}} H_\ell^{\alpha_1 \dots \alpha_\ell}(0, t_1, \dots, t_{\ell-1}) \quad (3.113)$$

$$K_{\mathcal{O}} = \log \left[ -\frac{1}{\pi} \sum_{\ell=0}^{\infty} \frac{(-1)^\ell}{\ell!} \sum_{\alpha_1 \dots \alpha_\ell} \int \frac{d^{\ell-1} t}{(2\pi)^{\ell-1}} H_\ell^{\alpha_1 \dots \alpha_\ell}(0, t_1, \dots, t_{\ell-1}) \left( \log \frac{\xi}{2} - \gamma_E \right) \right] \quad (3.114)$$

Since the model studied in Chapter 6 will be non unitary, we will use these last formulæ, which include the  $(-1)^\ell$  factor. On the other hand, the analysis performed in Chapter 8 will look at unitary theories and we will then refer to the unitary expansion (3.87).

Even though the nature of the  $(-1)^\ell$  sign is quite strange, this factor gives a strong benefit to numerical computations: alternate series usually converge at a much faster rate than series with elements all of the same sign.

### 3.4 Operator Product Expansion

In Quantum Field Theory the Operator Product Expansion (OPE) define the product of two fields as a sum of all possible fields in the theory. Consider the product of two operators  $\mathcal{O}_A$  and  $\mathcal{O}_B$  at two different points  $x$  and  $y$ . The OPE between the two operators gives rise to a (possibly infinite) sum of all the operators in the theory:

$$\mathcal{O}_A(x)\mathcal{O}_B(y) = \sum_k C_{AB}^k(|x-y|)\mathcal{O}_k(y) \quad (3.115)$$

where  $\mathcal{O}_k$  are the various fields in the theory.

The main idea is to express the product of the two operators at different points as a sum of other operators in one of the two points. Once the operator content  $\{\mathcal{O}_k\}_k$  of the theory is known, the OPE can be performed between any two fields once the coefficients  $C_{AB}^k(|x-y|)$  are known. While OPE is a tool available in any QFT, the form of the coefficients  $C$  is very simple in CFT. In particular these coefficients become:

$$C_{AB}^k(|x-y|) = C_{AB}^k \cdot |x-y|^{-2(\Delta_A+\Delta_B-\Delta_k)} \quad (3.116)$$

where  $C_{AB}^k$  are constants (called *OPE structure constants*) and  $\Delta_k$  are the conformal dimensions of the theory. Notice that the OPE structure constants are the same constants appearing in the scaling of three-point conformal correlation functions. On the other hand, when considering a perturbed CFT (i.e. a system just outside its critical phase) the coefficients  $C$  can be expanded as a power series in the distance and the coupling constant of the field responsible for the off-critical perturbation. An actual example of OPE in the two regimes (critical and off critical) can be found in Section 6.2.

### 3.5 Conclusions

In this chapter we reviewed very briefly some fundamental concepts of integrable field theories. In particular we focused on the case when the system is critical and can be described

by conformal field theory and on massive theories with infinitely many conservation laws. Moreover, we introduced the form factor programme for the study of correlation functions in massive QFT. In the next chapters we will largely make use of all the tools we have just presented in order to evaluate the amount of entanglement in integrable quantum field theories.

## Chapter 4

# Entanglement in Quantum Field Theory

In previous chapters we discussed quantum entanglement and some of its measures. In this chapter we will address the evaluation of the entanglement entropy in systems whose properties can be described by a quantum field theory.

In particular we will focus on one-dimensional systems, such as spin chains. We will introduce the so-called replica-trick and its application to conformal field theories and integrable systems [7, 8, 14]. After having explained in some detail the replica trick and its applications in computing entanglement entropy in CFT, we will discuss some known generalisations to the massive case.

The main idea behind the replica trick is to compute the trace  $\text{tr}\rho_A^n$  as a partition function of  $n$  copies (or replicas) of our original theory. The interaction between these copies depends on the shape of the subsystem  $A$  and it affects the scaling of entanglement. Once the trace has been computed, it can be used to compute the Rényi entropy:

$$S_n = \frac{1}{1-n} \log \text{tr}\rho_A^n \quad (4.1)$$

Even though the number  $n$  of copies is integer, in some cases it is possible to perform an analytic continuation of the Rényi entropy to compute the actual entanglement entropy:

$$S = -\text{tr}(\rho_A \log \rho_A) = \lim_{n \rightarrow 1} S_n \quad (4.2)$$

In this chapter we will focus on the evaluation of the trace  $\text{tr}\rho_A^n$ . While the leading logarithmic term of the scaling of the entropy usually can be easily analytically continued, the various corrections to such scaling sometimes require some additional effort to be

computed at  $n = 1$ .

## 4.1 Entanglement Entropy and Partition Functions

As we said, the scope of this chapter is the study of the scaling of entanglement entropy in one dimensional systems. In our considerations the physical dimension of the system is represented by the real axis of a complex plane  $\mathbb{C}$ . On the other hand, the imaginary axis plays the role of the euclidean time. For simplicity, we consider a finite system  $[x_1, x_2]$  and we are interested in the entanglement between its subsystems  $A = [a, b]$  and the rest of the system  $B = [x_1, a] \cup [b, x_2]$ . Following [8], we consider a discrete system in order to give sense to some notations otherwise ambiguous in a continuum framework. However many of the definitions and tools we will use in this section are more suitable in a continuum description of such models. The main idea is to consider a case such that a continuum limit can be performed. Even though the system is discrete, the number of sites is large enough (and the lattice spacing is small enough) to let the the system “look” continuous. In such a limit a field theory description is perfectly suitable to investigate the properties of the system.

To describe faithfully the system we consider a complete set of commuting local observables, denoted by  $\{\hat{\phi}(x)\}$  with  $|\{\phi(x)\}\rangle$  and  $\{\phi(x)\}$  being the respective eigenvectors and eigenvalues. For instance, when considering a spin system, the local observables could be the spin operators at each site. Let  $\hat{H}$  be the Hamiltonian underlying the time evolution of the system. The density matrix  $\rho$  at inverse temperature  $\beta$  is given by

$$\rho = \frac{1}{Z(\beta)} e^{-\beta \hat{H}} \quad (4.3)$$

where  $Z(\beta) = \text{tr} e^{-\beta \hat{H}}$  is the partition function.

The matrix elements of the propagator  $\langle \{\phi''\} | e^{-\beta \hat{H}} | \{\phi'\} \rangle$  can be evaluated using an euclidean path integral formulation ( $S_E = \int_{\square} d^2x \mathcal{L}[\phi](x, t)$  euclidean action):

$$\langle \{\phi''\} | e^{-\beta \hat{H}} | \{\phi'\} \rangle = \int_{\square} \mathcal{D}\phi(x, \tau) e^{-S_E} \prod_{x \in \text{system}} \delta(\phi(x, 0) - \phi'(x)) \delta(\phi(x, \beta) - \phi''(x)) \quad (4.4)$$

which is a path integral<sup>1</sup> from the state  $\phi'$  at euclidean time  $\tau = 0$  to  $\phi''$  at  $\tau = \beta$ . The role of the  $\delta$  function inside the integral is to identify the states at the bottom and at the

---

<sup>1</sup>The symbol  $\square = [x_1, x_2] \times [0, \beta]$  represents the rectangular domain of the path integral. It will be used to represent both the integration domain  $[x_1, x_2] \times [0, \beta]$  in normal integrals and the domain of fields on  $[x_1, x_2] \times [0, \beta]$  when path integrals are taken into account.

top with the given initial and the final states.

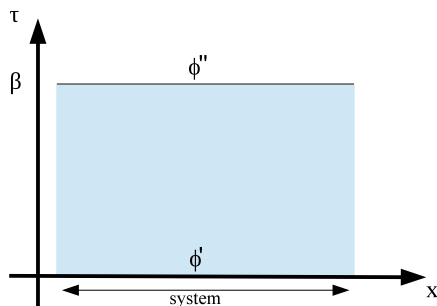


Figure 4.1: Propagator using path integrals.

The partition function can be obtained in a very similar way. Since  $Z(\beta) = \text{tr} e^{-\beta \hat{H}}$ , the partition function is given by:

$$Z(\beta) = \int_{\square} \mathcal{D}\phi(x, \tau) e^{-S_E} \prod_{x \in \text{system}} \delta(\phi(x, 0) - \phi(x, \beta)) \quad (4.5)$$

This main difference between these two path integrals is given by the boundary conditions: while in the propagator they are fixed and equal to given configurations  $\phi'$  and  $\phi''$ , in the partition function they have been identified ( $\phi' = \phi = \phi''$ ) Let us now focus on the

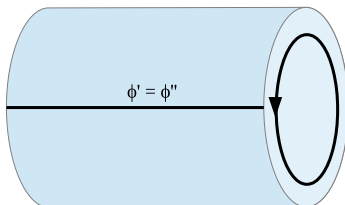


Figure 4.2: Partition function

evaluation of the reduced density matrix  $\rho_A$ . Also in this case we have to “bend” the propagator (fig. 4.1) into a cylinder, but, if we identify the two edges only for  $x \in B$ , the degrees of freedom of  $A$  remain free. This process is indeed equivalent to tracing over  $B$ ’s degrees of freedom or, in other words, to compute the reduced density matrix  $\rho_A$ . Its path

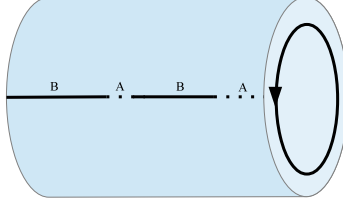


Figure 4.3: Reduced density matrix.

integral representation is given by:

$$\begin{aligned}
 \langle \{\phi''_A\} | \rho_A | \{\phi'_A\} \rangle &= \frac{1}{Z(\beta)} \int_{\square} \mathcal{D}\phi(x, \tau) e^{-S_E} \\
 &\times \prod_{x \in A} \delta(\phi(x, 0) - \phi'_A(x)) \delta(\phi(x, \beta) - \phi''_A(x)) \\
 &\times \prod_{x \notin A} \delta(\phi(x, 0) - \phi(x, \beta))
 \end{aligned} \tag{4.6}$$

Once we have computed the reduced density matrix, we can address the evaluation of the Rényi Entropy using this path integral formulation.

Let us suppose we are interested in evaluating  $\rho_A^2$ . Its path integral representation can be given by two copies of the propagator (4.4), i.e. by two rectangles. For each rectangle, all the points outside  $A$  on the top and the bottom edge are identified. Moreover, the points inside  $A$  on the top edge of the first rectangle are identified with the respective points inside  $A$  on the bottom edge of the second rectangle.

In the path-integral formulation these conditions become:

$$\begin{aligned}
 \langle \{\phi''_A\} | \rho_A^2 | \{\phi'_A\} \rangle &= \frac{1}{Z(\beta)^2} \int_{\square^2} \mathcal{D}\phi_1(x, \tau) \mathcal{D}\phi_2(x, \tau) e^{-\int d^2x (\mathcal{L}[\phi_1](x, \tau) + \mathcal{L}[\phi_2](x, \tau))} \\
 &\times \prod_{i=1}^2 \prod_{x \notin A} \delta(\phi_i(x, 0) - \phi_i(x, \beta)) \\
 &\times \prod_{x \in A} \delta(\phi_1(x, \beta) - \phi_2(x, 0)) \\
 &\times \prod_{x \in A} \delta(\phi_1(x, 0) - \phi'_A(x)) \\
 &\times \prod_{x \in A} \delta(\phi_2(x, \beta) - \phi''_A(x))
 \end{aligned} \tag{4.7}$$

The first set of deltas (2nd line) represent the identification of the points outside  $A$  on

the upper and lower edges of the two rectangles. The following deltas (3rd line) connect the points inside  $A$  on the top edge of the first rectangle with the respective ones on the bottom edge of the second rectangle. The last two lines identify the lowermost and the uppermost edges with the states assigned  $\phi'_A$  and  $\phi''_A$ . When taking the trace, the last two lines of the above equations change accordingly: the points inside  $A$  on the top edge of the second rectangle are identified with the respective points on the bottom edge of the first rectangle:

$$\begin{aligned}
 \text{tr}\rho_A^2 &= \frac{1}{Z(\beta)^2} \int_{\square^2} \mathcal{D}\phi_1(x, \tau) \mathcal{D}\phi_2(x, \tau) e^{-S_E} \\
 &\times \prod_{i=1}^2 \prod_{x \notin A} \delta(\phi_i(x, 0) - \phi_i(x, \beta)) \\
 &\times \prod_{x \in A} \delta(\phi_1(x, \beta) - \phi_2(x, 0)) \\
 &\times \prod_{x \in A} \delta(\phi_1(x, 0) - \phi_2(x, \beta))
 \end{aligned} \tag{4.8}$$

Of course, this construction can be extended to arbitrary  $n \in \mathbb{N}$ :

$$\begin{aligned}
 \text{tr}\rho_A^n &= \frac{1}{Z(\beta)^n} \int_{\square^n} \left( \prod_{i=1}^n \mathcal{D}\phi_i(x, \tau) \right) e^{-\int d^2x \sum_{i=1}^n \mathcal{L}[\phi_i](x, \tau)} \\
 &\times \prod_{i=1}^n \prod_{x \notin A} \delta(\phi_i(x, 0) - \phi_i(x, \beta)) \\
 &\times \prod_{i=1}^n \prod_{x \in A} \delta(\phi_i(x, \beta) - \phi_{i+1}(x, 0)) \\
 &\times \prod_{x \in A} \delta(\phi_1(x, 0) - \phi_n(x, \beta))
 \end{aligned} \tag{4.9}$$

where we have made the identification  $n + 1 \equiv 1$ .

From a field theoretical point of view, the evaluation of the trace  $\text{tr}\rho_A^n$  can be performed by computing the partition function of  $n$  copies of the original theory. These copies are “almost” independent of one another but for the points around the subsystem  $A$ . Such a construction, which has been developed for the first time by P Calabrese and J Cardy [8], provides a very good operative tool to evaluate the Rényi entropy using QFT partition

functions<sup>2</sup>.

The complicated integration region and the intricate set of delta functions can be encapsulated in the definition of a particular surface  $\mathcal{M}_n$  (a *Riemann surface*) whose geometry is given by the aforementioned constraints. In this notation, the collection of different fields  $\{\phi_i\}_{i=1}^n$  living on the different copies of  $\square$  is replaced by a single field  $\phi$  which is defined on the whole surface  $\mathcal{M}_n$ . The two segments  $A$  on the top and the bottom of each sheet  $\square$  become *branch cuts*. This is because of the gluing conditions between sheets described before. These cuts are analogous to the branch cuts commonly encountered in the study of complex multivalued functions. For instance, the function  $f(z)=z^{1/n}$  has a branch cut in  $[0, +\infty[$  and a branch point at  $z=0$ . When considering a particular value of such function, say at  $z=2 + i\epsilon$  ( $\epsilon > 0$ ), this value changes when performing a rotation around the origin:  $f(ze^{2\pi i}) \neq f(z)$ . Such an inequality is given by the branch cut, which affects the value of a function every time it is crossed. The branch cut makes the function single-valued and analytic. This example is particularly suitable for the description of the surface  $\mathcal{M}_n$  not only because it represent  $n$  sheets sequentially connected, but also because the branch cut of  $z^{1/n}$  is “periodic”: when it is crossed  $n$  times the value of the function comes back to its original value  $f(ze^{2\pi in})=f(z)$ . In the same way, each time a particle in the sheet  $i$  crosses the cut  $A$  it ends up in the sheet  $i + 1$ , but it comes back to the original place after crossing the cut  $n$  times.

From a mathematical point of view, such a surface cannot be a manifold, since the points around  $a$  and  $b$  cannot be mapped to some  $\mathbb{R}^m$  smoothly. The mathematical object suitable to describe such a surface is the *orbifold*. From an intuitive point of view, an orbifold is a manifold quotient by some symmetry group. In particular, the surface  $\mathcal{M}_n$  is equivalent to  $\mathbb{R}^{2n}$  where some points are identified between the copies thanks to the connections of the sheets  $\square^n$  through the points in  $A$ .

For instance, the  $n = 3$  equivalent surface can be represented as

For generic  $n$  the path integrals takes the form

$$\mathrm{tr}\rho_A^n = \frac{1}{Z(\beta)^n} \int_{\mathcal{M}_n} \mathcal{D}\phi(x, \tau) e^{-\int d^2x \mathcal{L}[\phi](x, \tau)} \quad (4.10)$$

The lagrangian density  $\mathcal{L}$  depends only on one single field  $\phi$  which “lives” on the entire surface  $\mathcal{M}_n$ .

In the zero temperature case ( $\beta \rightarrow \infty$ ) the cylinders of Figure 4.1 become complex planes. For instance, the graphical representation of the  $n = 3$  case is given by: As we have just seen, the computation of the Rényi entropy (and the entanglement entropy) involves the

---

<sup>2</sup>Different geometrical arguments had already been used [7] to compute the Rényi and von Neumann entropy in CFT.

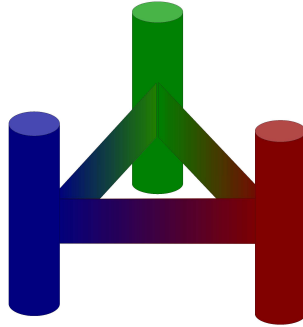


Figure 4.4: Surface  $\mathcal{M}_3$  for  $n = 3$ .

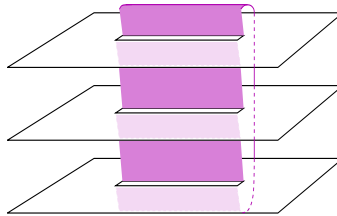


Figure 4.5: Surface  $\mathcal{M}_3$  for  $n = 3$  and  $\beta = \infty$ . Picture taken from [14] with permission from authors.

evaluation of complicated path integrals, which can be interpreted as partition functions on particular geometries (4.10). Alternatively, we can simplify the integration domain by introducing some special operator to guarantee the equivalence between path integrals.

## 4.2 Branch Point Twist Fields

Consider the partition function (4.9), which is defined on a collection of  $n$  rectangular sheets. The  $\delta$ -functions inside the path integral constraint the values of the fields at some particular points. In order to get rid of the  $\delta$ -functions, we can restrict the integration domain from  $\square^n$  to  $\mathcal{C}$ , which is equivalent to  $\square^n$  once removed all the configurations not allowed by the  $\delta$ s.

$$\text{tr} \rho_A^n = \frac{1}{Z(\beta)^n} \int_{\mathcal{C}} \left( \prod_{i=1}^n \mathcal{D}\phi_i(x, \tau) \right) e^{-\int d^2x \sum_{i=1}^n \mathcal{L}[\phi_i](x, \tau)} \quad (4.11)$$

The main idea is to relax the conditions of the domain  $\mathcal{C}$  to the much simpler domain  $\square^n$ . If we do so, the various fields  $\phi_i$ s are now completely free and can take different

values around the subsystem  $A$ . Since  $\phi_i$  (“just below  $A$ ”) =  $\phi_{i+1}$  (“just above  $A$ ”) in the definition of the trace  $\text{tr}\rho_A^n$ , we need to restore this constraint. To do so we introduce two fields, called *branch point twist fields*  $\mathcal{T}$  and  $\tilde{\mathcal{T}}$ , whose role is to implement the above constraint on the fields  $\phi_i$ s.

$$\text{tr}\rho_A^n = \frac{1}{Z(\beta)^n} \int_{\square^n} \left( \prod_{i=1}^n \mathcal{D}\phi_i(x, \tau) \right) \mathcal{T}(a)\tilde{\mathcal{T}}(b) e^{-\int d^2x \sum_{i=1}^n \mathcal{L}[\phi_i](x, \tau)} \quad (4.12)$$

Even though twist fields have been known for a long time in the literature [78, 79], in [8] the authors associated the branch points of Riemann surfaces to some quantum fields. Subsequently, [14] such quantum fields were interpreted as twist fields.

The action of the twist fields is to actually create the branch cut. In particular, the field  $\mathcal{T}(a)$  creates a cut from  $a$  to  $+\infty$ , while  $\tilde{\mathcal{T}}(b)$  creates a “reversed” cut from  $b$  to  $+\infty$ . For reverse cut we mean a cut which works like a normal branch cut, but with opposite orientation. If  $\mathcal{T}$  creates a cut which maps the sheet  $i$  to  $i+1$  when a particle crosses it from below, the reverse field  $\tilde{\mathcal{T}}$  performs a mapping from  $i$  to  $i-1$ . The combined action of the two fields creates a finite branch  $A$ . In particular, while  $\mathcal{T}(a)$  creates an infinite cut from  $a$  to infinity,  $\tilde{\mathcal{T}}(b)$  annihilates the effect of  $\mathcal{T}(a)$  from  $b$  onwards.

From the operators point of view, the action of these fields on an operator  $\Psi_i$  (the  $i$ th copy of some operator  $\Psi$  of the original theory) is given by:

$$\begin{aligned} \Psi_i(y)\mathcal{T}(x) &= \mathcal{T}(x)\Psi_{i+1}(y) & \text{for } x^1 > y^1 \\ \Psi_i(y)\mathcal{T}(x) &= \mathcal{T}(x)\Psi_i(y) & \text{for } x^1 < y^1 \end{aligned} \quad (4.13)$$

where  $x = (x^0, x^1)$  and the above relations hold at “equal time”<sup>3</sup>  $x^0 = y^0$ .

Similar relations hold also for the the conjugate field  $\tilde{\mathcal{T}}$ :

$$\begin{aligned} \Psi_i(y)\tilde{\mathcal{T}}(x) &= \tilde{\mathcal{T}}(x)\Psi_{i-1}(y) & \text{for } x^1 > y^1 \\ \Psi_i(y)\tilde{\mathcal{T}}(x) &= \tilde{\mathcal{T}}(x)\Psi_i(y) & \text{for } x^1 < y^1 \end{aligned} \quad (4.14)$$

The equation 4.12 does not seem a particular improvement to the previous partition functions. The tremendous advantage that such a formulation gives is the fact that it is the actual definition of the correlation function between the two twist fields  $\mathcal{T}$  and  $\tilde{\mathcal{T}}$ !

$$\text{tr}\rho_A^n \propto \left\langle \mathcal{T}(a)\tilde{\mathcal{T}}(b) \right\rangle_{\square, \mathcal{L}^n} \quad (4.15)$$

<sup>3</sup>The action of twist fields is defined at equal time since they create horizontal branch cuts.

where  $\langle \cdot \rangle_{\square, \mathcal{L}^{(n)}}$  is the expectation value taken on  $\square$  with  $n$  copies of the original theory (with lagrangian  $\mathcal{L}^{(n)}[\phi_1, \dots, \phi_n] = \sum_{i=1}^n \mathcal{L}[\phi_i]$ ). As we will see in the next sections, it is worth stressing which theory we are referring to when computing correlation functions. The action of twist fields inside correlation functions can be better understood by looking at its operative definition [14]:

$$\frac{\langle \mathcal{T}(a) \tilde{\mathcal{T}}(b) \Psi_i(x) \rangle_{\square, \mathcal{L}^{(n)}}}{\langle \mathcal{T}(a) \tilde{\mathcal{T}}(b) \rangle_{\square, \mathcal{L}^{(n)}}} = \langle \Psi(x; \text{sheet } i) \rangle_{\mathcal{M}_n, \mathcal{L}} \quad (4.16)$$

On both sides of the above definition the operator  $\Psi$  appears. On the left hand side  $\Psi_i$  is the  $i$ th copy of the original field living on  $\square$ . On the other side it is the same operator  $\Psi$ , but in this case its domain is given by  $\mathcal{M}_n$ . Since  $\Psi$  is multivalued on  $\mathcal{M}_n$ , it is important to indicate which sheet we are referring to. Apart from the actual domain of fields, there is a substantial difference also concerning the operator content between the two sides. Consider, for instance, a simple theory with a single field  $\Psi$  living on  $\square$  and a lagrangian  $\mathcal{L}$ , to obtain the left hand side of (4.16) we copy the original theory  $n$  times and we add the twist fields. On the right hand side the theory remains the same (from the lagrangian point of view) but the domain of  $\Psi$  becomes  $\mathcal{M}_n$ .

Since we are interested in the ground state properties of very large systems, the integration rectangle  $\square$  will be extended to the whole plane  $\mathbb{C}$ . A particular case when the scaling of entanglement entropy can be computed is when a method for the evaluation of the correlation function (4.15) is available. In the next sections we will discuss the scaling of this correlator in some known cases. In particular we will focus on critical and off critical unitary systems. In the following chapters we will extend these results to some non unitary cases.

### 4.3 Entropy in Conformal Field Theory

In the specific case of critical systems enjoying conformal invariance, two-point correlation functions like (4.15) have a very simple power law scaling (see Chapter 3):

$$\langle \mathcal{T}(a) \tilde{\mathcal{T}}(b) \rangle_{\mathbb{C}, \mathcal{L}^{(n)}} = |a - b|^{-4\Delta_{\mathcal{T}}} \quad (4.17)$$

where  $\Delta_{\mathcal{T}}$  is the conformal dimension of the field  $\mathcal{T}$ .

The study of the scaling of entanglement entropy in one-dimensional conformal systems is then reduced to the evaluation of the conformal dimension  $\Delta_{\mathcal{T}}$  of twist fields. Such a quantity can be easily computed by implementing the working definition (4.16). In

this section we briefly review the procedure proposed in [14] to compute the conformal dimension  $\Delta_{\mathcal{T}}$ .

Consider a certain CFT with lagrangian  $\mathcal{L}$  and central charge  $c$  defined on the whole complex plane  $\mathbb{C}$ . Its multicopied version  $\mathcal{L}^{(n)}$  is still a CFT and the new central charge is given by  $nc$ . In particular, the total stress energy  $T^{(n)}$  can be simply obtained by combining the stress energy tensors of the various copies:

$$T^{(n)}(z) = \sum_{j=1}^n T_j(z) \quad z \in \mathbb{C} \quad (4.18)$$

where  $T_j$  is the stress energy tensor of a single copy.

On the other hand, let  $T(w)$  be the stress energy tensor of the same CFT defined on  $\mathcal{M}_n$ . The CFT on  $\mathcal{M}_n$  has central charge  $c$ . In order to compare the two sides of equation (4.16) we can map  $\mathcal{M}_n$  to  $\mathbb{C}$  by performing the conformal transformation:

$$z = \left( \frac{w-a}{w-b} \right)^{\frac{1}{n}} \quad (4.19)$$

The stress energy tensor  $T(w)$  transforms according to (3.8):

$$\langle T(w) \rangle_{\mathcal{M}_n, \mathcal{L}} = \left( \frac{\partial z}{\partial w} \right)^2 \langle T(z) \rangle_{\mathbb{C}, \mathcal{L}} + \frac{c}{12} \{z; w\} \quad (4.20)$$

where  $\{\cdot; \cdot\}$  is the Schwarzian derivative:

$$\{z; w\} = \left( \frac{\partial z}{\partial w} \right)^{-2} \left[ \frac{\partial^3 z}{\partial w^3} \frac{\partial z}{\partial w} - \frac{3}{2} \left( \frac{\partial z}{\partial w} \right)^2 \right] \quad (4.21)$$

Since  $\langle T(z) \rangle_{\mathbb{C}, \mathcal{L}}$  vanishes (see equation 3.19) the above one-point function becomes:

$$\langle T(w) \rangle_{\mathcal{M}_n, \mathcal{L}} = \frac{c(n^2 - 1)}{24n^2} \frac{(a-b)^2}{(w-a)^2(w-b)^2} \quad (4.22)$$

On the other hand, applying (4.16),  $\langle T(w) \rangle$  becomes:

$$\frac{\left\langle \mathcal{T}(a) \tilde{\mathcal{T}}(b) T_j(w) \right\rangle_{\mathbb{C}, \mathcal{L}^{(n)}}}{\left\langle \mathcal{T}(a) \tilde{\mathcal{T}}(b) \right\rangle_{\mathbb{C}, \mathcal{L}^{(n)}}} = \langle T(w) \rangle_{\mathcal{M}_n, \mathcal{L}} \quad \text{for any value of } j \quad (4.23)$$

Combining (4.22), (4.23) with the definition (4.18) of the stress energy tensor of  $\mathcal{L}^{(n)}$  we have:

$$\frac{\langle \mathcal{T}(a)\tilde{\mathcal{T}}(b)T^{(n)}(w) \rangle_{\mathbb{C},\mathcal{L}^{(n)}}}{\langle \mathcal{T}(a)\tilde{\mathcal{T}}(b) \rangle_{\mathbb{C},\mathcal{L}^{(n)}}} = \frac{c(n^2-1)}{24n} \frac{(a-b)^2}{(w-a)^2(w-b)^2} \quad (4.24)$$

Since  $T^{(n)}(z)$  is the stress energy tensor, we can apply conformal Ward's identity (3.11) on the left hand side of (4.24):

$$\langle \mathcal{T}(a)\tilde{\mathcal{T}}(b)T^{(n)}(w) \rangle = \left( \frac{1}{w-a} \frac{\partial}{\partial a} + \frac{1}{w-b} \frac{\partial}{\partial b} + \frac{\Delta_{\mathcal{T}}}{(w-a)^2} + \frac{\Delta_{\tilde{\mathcal{T}}}}{(w-b)^2} \right) \langle \mathcal{T}(a)\tilde{\mathcal{T}}(b) \rangle \quad (4.25)$$

Since  $\mathcal{T}$  and  $\tilde{\mathcal{T}}$  are conjugate to each other ( $\mathcal{T}^\dagger = \tilde{\mathcal{T}}$ ), they should have the same conformal dimension.

Inserting the scaling (4.17) in equations (4.24) and (4.25) we can extract the conformal dimension  $\Delta_{\mathcal{T}}$  of twist fields [8, 14, 80]

$$\Delta_{\mathcal{T}} = \frac{c}{24} \left( n - \frac{1}{n} \right) = \Delta_{\tilde{\mathcal{T}}} \quad (4.26)$$

The scaling dimension of twist fields then depends on two parameters: the central charge  $c$  of the underlying system and the number  $n$  of copies involved.

In the single copy case ( $n = 1$ ), the conformal dimension of the twist field vanishes. Of course, this fact should not surprise, since in the  $n = 1$  case the twist field acts trivially and then it is equal to the identity.

### 4.3.1 Entanglement entropy

Once we have computed the conformal dimension of twist fields, we can immediately study the scaling of entanglement. From equation (4.15) we can directly estimate the Rényi entropy:

$$\begin{aligned} S_n(|b-a|) &= \frac{1}{1-n} \log \text{tr} \rho_A^n \sim \frac{1}{1-n} \log \langle \mathcal{T}(a)\tilde{\mathcal{T}}(b) \rangle_{\mathbb{C},\mathcal{L}^{(n)}} \\ &= \frac{cn+1}{6n} \log \frac{|b-a|}{\epsilon} \end{aligned} \quad (4.27)$$

where  $\epsilon$  is some ultraviolet cut-off which restores the correct dimensionality of the scaling. Of course this simple logarithmic scaling is perfectly suitable for an  $n \rightarrow 1$  limit. The

entanglement entropy is then given by:

$$S(|b-a|) \sim \frac{c}{3} \log \frac{|b-a|}{\epsilon} \quad (4.28)$$

which is the celebrated result of Holzhey, Larsen and Wilczek [7].

Thanks to the twist field interpretation, it is very easy to study also the scaling of entanglement in different geometries. The above result has been derived for a very large system, represented by a complex plane, without taking into account boundary conditions. In order to study a finite system with periodic boundary conditions, we can simply map the plane into a cylinder:

$$\begin{aligned} f : \mathbb{C} &\rightarrow S^1 \times \mathbb{R} \\ w &\mapsto w' = \frac{R}{2\pi} \log w \end{aligned} \quad (4.29)$$

where  $R$  denotes the size of the system.

Inverting the above map and using the transformation law (3.3), it is possible to compute the twist field correlation function in a cylindrical geometry:

$$\langle \mathcal{T}(a) \tilde{\mathcal{T}}(b) \rangle_{\text{cyl}} \sim \left( \sin \frac{\pi|b-a|}{R} \right)^{-4\Delta\tau} \quad (4.30)$$

Such a correlator can be used to compute directly the Rényi and von Neumann entanglement entropy a periodic system [8]:

$$S(|b-a|) \sim \frac{c}{3} \log \left[ \frac{R}{\pi\epsilon} \sin \frac{\pi|b-a|}{R} \right] \quad (4.31)$$

Such results have been derived for *unitary* systems at the *critical* points. In Chapter 5 we will study how the scaling is affected when the system becomes non unitary and (Chapter 6) when the conformal invariance is broken. Before addressing these problems, it is useful to recap some known results about entanglement in systems outside their critical points.

### 4.3.2 Beyond criticality

From the physical point of view, the massive regime and the conformal case are qualitatively similar. It is known that when the system is far enough from its critical point, i.e. its correlation lengths  $\xi = m^{-1}$  is smaller than the size  $r = |b-a|$  of the subsystem studied, entanglement scales like (4.28) with  $r$  replaced by  $\xi$  [8, 81]

$$S(\xi) \sim \frac{c}{3} \log \frac{\xi}{\epsilon} \quad \text{for } r \gg \xi \quad (4.32)$$

The physical interpretation of this scaling is very intuitive. The correlation length (which diverges at the critical point) is the actual size a system can physically “see”. In other words, when the correlation length is finite, the interaction is no more long range and two points of the system affect each other if their distance is comparable to the correlation length.

The formulation of the entropy using correlators of twist fields makes also possible the study of entanglement in an intermediate regime  $r \sim \xi$ . Such a situation, which lies between the ultraviolet conformal scale and the “highly massive” infrared regime, can be probed by expanding the correlator using the so-called form factors program (see Chapter 3). While this approach will be explained in detail in Chapter 6 (for non unitary theories), here we can simply summarise some of the results already known in the literature [14]. In this intermediate regime, entanglement scales in the following way:

$$S(r, \xi) = \frac{c}{3} \log \frac{\xi_1}{3} + U - \frac{1}{8} \sum_{\alpha=1}^{N_p} K_0 \left( \frac{2r}{\xi_\alpha} \right) + O \left( e^{-\frac{3r}{\xi_1}} \right) \quad (4.33)$$

where  $K_0$  is the modified Bessel’s function of second kind [49] and  $U$  is a numerical constant which depends on the system.

The above equation describes the entanglement in a theory with  $N_p$  particles types. While there is a  $K_0$  contribution for each particle type, the logarithmic term depends only on the lightest mass  $m_1 = \xi_1^{-1}$ . While the logarithmic term and the constant  $U$  depend on the theory studied, the  $K_0$  corrections are universal. No matter what kind of theory is taken into account (as long as it is unitary) the  $K_0$  corrections have always the same form and the coefficient is always equal to  $1/8$ .

## 4.4 Conclusions

In this chapter we quickly reviewed the main known results about the scaling of entanglement entropy of one-dimensional quantum systems. We introduced the replica trick for the computation of the entropy and how to represent the trace of reduced density matrix using partition functions on Riemann surfaces. Additionally, we reviewed the role of twist field correlation functions in the evaluation of such partition functions. We showed how the central charge  $c$  affects the scaling of entropy in various (conformal and not) regimes. Moreover we reported some known results about the saturation of entanglement in the massive regime. In particular, we showed that entanglement tends to its saturation value as a Bessel function and that this behaviour is universal and does not depend on the particular features of the (unitary) theory taken into account. In the next chapters (5, 6 and

7) we generalise these results to non unitary systems. We will see how the non unitary features of these systems will affect the scaling of the entanglement entropy.

## Chapter 5

# Entanglement in Non Unitary Conformal Field Theory

Even though entanglement has been widely studied in unitary models, less is known about the non unitary case. While such models have always been branded as non physical, they can be used to describe particular systems, like the fractional quantum Hall effect in some configurations [51]. In the context of quantum mechanics, these models have given rise to active areas of research [82, 83, 84, 85, 86]. In this chapter we will discuss the scaling of entanglement of non unitary critical systems through the development of a CFT tool to study such a quantity in systems without a mass gap. In Chapter 6 we will extend the critical results to the massive, non critical regime. Examples of lattice systems enjoying such a non-unitary behaviour will be introduced in Section 5.3 and Chapter 7.

As we have seen in Chapter 3, in non unitary CFT the physical ground state and the conformal vacuum are not the same state. As the most important physical information comes from the ground state structure, such systems behave quite differently from their unitary counterpart. In unitary systems, the conformal vacuum  $|\emptyset\rangle$  (i.e. the state annihilated by all  $L_n$  with  $n \geq -1$ ) is also the ground state  $|gs\rangle$  (i.e. the eigenstate of the Hamiltonian with the smallest eigenvalue). In the non unitary regime these two states are different: since there exist a primary field  $\phi$  with negative (and smallest) conformal dimension  $\Delta < 0$ , the relative primary state is the ground state

$$|gs\rangle = \phi(0)|\emptyset\rangle \tag{5.1}$$

In this chapter we will show how non unitarity affects the scaling of entanglement entropy.

In the following, all the expectation values  $\langle \cdot \rangle$  will be taken with respect to the con-

formal vacuum  $|\emptyset\rangle$ .

## 5.1 Entanglement Entropy in Non Unitary CFT

In this section we will discuss a new method for the evaluation of the bipartite entanglement entropy in non unitary CFT.

Let us then consider an infinite system and suppose we would like to evaluate the entanglement between the subsystem  $A = [a, b]$  and the rest of the system ( $B = [-\infty, a] \cup [b, \infty]$ ). In the following we will use  $r$  to denote the length of the interval  $[a, b]$ :

$$r = |b - a| \tag{5.2}$$

In the same spirit of Chapter 4, when evaluating  $Z_n$  we have to consider  $n$  different fields

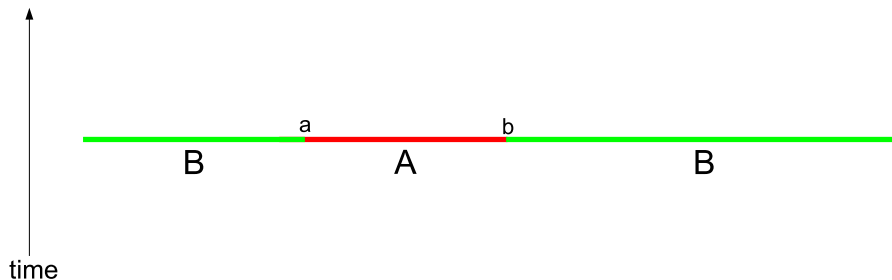


Figure 5.1: Space-time representation of the system.

living on  $\mathbb{R} \times \mathbb{R} \simeq \mathbb{C}$ . Such fields interact only around the branch cut: a particle  $i$  becomes the particle  $i + 1$  when it crosses  $[a, b]$  from below (or  $i - 1$  if it is approaching from above) while it remains unaffected if it crosses at any point  $x \notin [a, b]$ . In the following we will refer to this situation as *orbifold*.<sup>1</sup>

Since in the unitary case the ground state is an excitation-free state, the reduced density matrix obtained as a partition function on the manifold  $\mathcal{M}_n$  is automatically normalised (up to the expectation value of the vacuum  $\langle \emptyset | \emptyset \rangle$  - which can be set to one). On the other hand, in non unitary system the ground state is an excited state. For this reason, in order to have a normalised reduced density matrix, we should take care of the normalisation of the ground state. Such a normalisation can be obtained by dividing the partition function  $Z_n$  on the manifold  $\mathcal{M}_n$  by the partition function of  $n$  disconnected theories  $Z_1^n$ . The trace of the  $n$ -th power of the reduced density matrix is then given by

$$\text{tr} \rho_A^n = \frac{Z_n}{Z_1^n} \tag{5.3}$$

---

<sup>1</sup>Roughly speaking, an orbifold is a manifold - in this case  $\mathbb{C}^n$  - modulo some symmetry group.

The  $Z_1^n$  partition function - called *replica* case in the following - is calculated on  $\mathbb{C}$  (as  $Z_n$ ) without any branch cut.

In other words, both  $Z_n$  and  $Z_1^n$  are partition functions of  $n$  fields on  $\mathbb{C}$ . The only difference is that in the former there is a branch cut between  $a$  and  $b$ .

We can map the complex plane to a cylinder using the map

$$z \mapsto w = i \log \frac{z-a}{z-b} \tag{5.4}$$

Around the singularities  $z = a$  and  $z = b$  the system is no more scale invariant and then we introduce an ultraviolet cut-off  $0 < \epsilon \ll r$  to take care of possible divergences. After the conformal transformation, the plane with the cut becomes a cylinder with the cut running from  $\text{Im } w = \log \frac{\epsilon}{r}$  to  $\text{Im } w = -\log \frac{\epsilon}{r}$  (the length of the cylinder is then  $2 \log \frac{r}{\epsilon}$ ). Thanks to modular invariance, we can choose to quantise with the time running along the

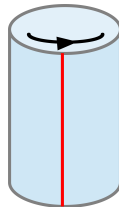


Figure 5.2: The system mapped to a cylinder

cut. The two partition functions will then be given by

$$\begin{aligned} Z_n &= \left\langle e^{-2 \log \frac{r}{\epsilon} H_{orb}} \right\rangle \\ Z_1^n &= \left\langle e^{-2 \log \frac{r}{\epsilon} H_{rep}} \right\rangle \end{aligned} \tag{5.5}$$

The continuity boundary conditions in the replica and the orbifold cases are different. In the replica case, when a particle  $i$  performs a complete rotation of  $2\pi$  around the cylinder it will remain the particle  $i$ . In the orbifold case, if a particle  $i$  performs a complete rotation, it will become the particle  $i \pm 1$  (the sign depends on the orientation of the rotation). In order to extrapolate the scaling of the partition functions (5.5), we need to investigate the ground state structure of the two Hamiltonians  $H_{orb}$  and  $H_{rep}$ . Since the Hamiltonian of a critical conformal system can be written in terms of Virasoro modes, we can derive the energy spectrum from the property of the stress-energy tensor in these theories.

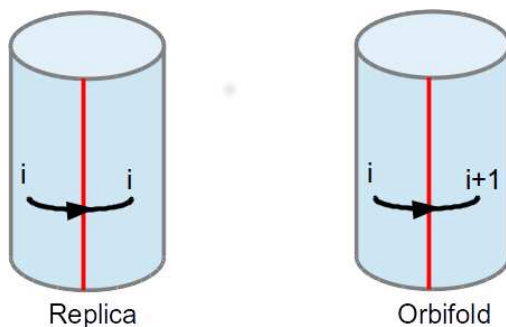


Figure 5.3: Different cylinders.

### 5.1.1 Two Virasoro algebras

The difference in the boundary conditions is reflected also in the continuity conditions of the stress-energy tensor. Let  $T^{(j)}$  be the holomorphic part of the stress-energy tensor of the  $j$ th copy. In the replica case we have

$$T^{(j)}(w + 2\pi) = T^{(j)}(w) \quad (5.6)$$

while in the orbifold case we have

$$T^{(j)}(w + 2\pi) = T^{(j+1)}(w) \quad (5.7)$$

The two different stress energy tensors give rise to two different Virasoro Algebras. In the two cases the total stress-energy tensor is given by the sum of the single components:

$$T(w) = \sum_{j=1}^n T^{(j)}(w)$$

#### Replica case

Let us focus first with the replica case (periodic boundary conditions). There are  $n$  completely non-interacting theories giving rise to  $n$  orthogonal Virasoro algebras  $\text{Vir}_j$  with modes  $L_k^{(j)}$ , each of them with central charge  $c$ . The total Virasoro modes are then given by

$$L_k^{rep} = \sum_{j=1}^n L_k^{(j)} \quad (5.8)$$

which give rise to the total Virasoro Algebra  $\text{Vir}_{rep} = \bigoplus_{j=1}^n \text{Vir}_j$  with central charge  $nc$ .

### Orbifold case

The cyclical boundary conditions of the orbifold case make the underlying conformal algebra more complicated. Let us start by constructing a continuous version of the stress energy tensor:

$$T_{orb}(w) \equiv T^{(1 + \lfloor \frac{\text{Re } w}{2\pi} \rfloor)}(w) \quad (5.9)$$

This stress energy tensor is, by construction, continuous around the cylinder and the underlying Virasoro algebra  $\mathfrak{Vir}$  has central charge  $c$  and Virasoro modes  $\mathcal{L}_k$ . The total Virasoro algebra  $\text{Vir}_{orb}$  is a subalgebra of  $\mathfrak{Vir}$ , with central charge  $nc$  and it is generated by  $\mathcal{L}_{nk}$  [80, 87]:

$$L_k^{orb} = \frac{\mathcal{L}_{nk}}{n} + \delta_{k0} \Delta_{\mathcal{T}} \quad (5.10)$$

where  $\Delta_{\mathcal{T}} = \frac{c}{24} (n - \frac{1}{n})$  is the conformal dimension of the twist field  $\mathcal{T}$  introduced in Chapter 4.

#### 5.1.2 Partition functions

Using the explicit expressions for the Virasoro modes (5.8) and (5.10), we can now evaluate the partition functions 5.5.

The Quantum Hamiltonian of a CFT on a cylinder is given by [37]:

$$H_a = L_0^a + \bar{L}_0^a - \frac{c_a}{12} \quad (5.11)$$

where  $a = rep, orb$  refers to the replica or the orbifold case.

Notice that this derivation is completely general and it includes also the unitary case. It provides a slightly more general approach than [7] in order to take into account also the non unitary case.

The leading terms of the partition functions (5.5) are given by the lowest eigenvalues of the Hamiltonians (5.11). If  $\Delta$  is the lowest eigenvalue of  $L_0^{(j)}$  and  $\mathcal{L}_0$ , the smallest and the most relevant eigenvalues of  $L_0^{rep}$  and  $L_0^{orb}$  are respectively  $n\Delta$  and  $\frac{\Delta}{n} + \Delta_{\mathcal{T}}$ . In the limit

$r/\epsilon \rightarrow \infty$  the two partition functions diverge like

$$\begin{aligned} Z_1^n &\sim e^{-4 \log \frac{r}{\epsilon} (n\Delta - \frac{nc}{12})} = \left(\frac{r}{\epsilon}\right)^{4(\frac{nc}{12} - n\Delta)} \\ Z_n &\sim e^{-4 \log \frac{r}{\epsilon} (\frac{\Delta}{n} + \Delta\mathcal{T} - \frac{nc}{12})} = \left(\frac{r}{\epsilon}\right)^{4(\frac{nc}{12} - \frac{\Delta}{n} - \Delta\mathcal{T})} \end{aligned} \quad (5.12)$$

The extra factors 2 in the exponent are due to the contributions of both the holomorphic and antiholomorphic parts of the Hamiltonians.

Putting together the two partition functions 5.12 we have

$$\text{Tr } \rho_A^n = \frac{Z_n}{Z_1^n} \sim \left(\frac{r}{\epsilon}\right)^{4\Delta\mathcal{T} - 4n\Delta + \frac{4\Delta}{n}} \quad (5.13)$$

The exponent can be rearranged in the following way:

$$\begin{aligned} \Delta\mathcal{T} - n\Delta + \frac{\Delta}{n} &= \frac{c}{24} \left(n - \frac{1}{n}\right) - n\Delta + \frac{\Delta}{n} \\ &= \frac{c - 24\Delta}{24} \left(n - \frac{1}{n}\right) = \frac{c_{\text{eff}}}{24} \left(n - \frac{1}{n}\right) \end{aligned} \quad (5.14)$$

and the Rényi Entropy becomes

$$S_n = \frac{1}{1-n} \log \text{Tr } \rho_A^n \sim \frac{c_{\text{eff}}}{6} \frac{n+1}{n} \log \frac{r}{\epsilon} \quad (5.15)$$

From the above expression, we can see that the Rényi entanglement entropy for non unitary CFT diverges logarithmically and the coefficient is given by the *effective central charge* in a similar fashion to the scaling of the ground state energy (3.49).

As we have discussed in Chapter 3, the effective central charge  $c_{\text{eff}} = c - 24\Delta_{\text{min}}$  is the *physical* central charge, i.e. the one which determines the physics of a system.

A similar computation can be performed for a half-infinite system in presence of a boundary [1]. The Entropy between the subsystem  $A = [0, r]$  and the subsystem  $B = [r, \infty[$  (we consider the whole system  $A \cup B$  as a half-infinite line  $[0, \infty[$ ) is given by

$$S_n = \frac{1}{1-n} \log \text{Tr } \rho_A^n \sim \frac{c_{\text{eff}}}{12} \frac{n+1}{n} \log \frac{r}{\epsilon} \quad (5.16)$$

which differs from 5.15 only by a factor two. As in the unitary case [8], the Entropy is proportional to the area of the boundary between the two subsystems.

A more general formula is then given by

$$S_n = \mathcal{A} \frac{1}{1-n} \log \text{Tr } \rho_A^n \sim \mathcal{A} \frac{c_{\text{eff}}}{12} \frac{n+1}{n} \log \frac{r}{\epsilon} \quad (5.17)$$

where  $\mathcal{A} = 1, 2$  is the number of boundary points between  $A$  and  $B$ .

Of course, our results are still valid in the unitary case: if the CFT is unitary, the smallest conformal dimension is zero and the effective central charge is equal to the usual central charge.

### 5.1.3 Interpretation in terms of twist fields

As we have seen in Chapter 4, the partition functions used to evaluate the Rényi Entropy can be interpreted as correlation functions of Twist Fields  $\mathcal{T}$ . This construction “as it is” seems to fail in the non unitary case, since their conformal dimensions involve the central charge  $c$  only and they do not depend on the smallest conformal dimension  $\Delta$ . In order to interpret our results in terms of correlation functions of twist fields, we introduced a modified version of these fields. Let  $\mathcal{T}$  be the standard twist field, as introduced in 4, and let  $\phi_j$  be the  $j$ -th copy of the primary field with the smallest conformal dimension  $\Delta$ . We can then define a *fused* or *composite* field:

$$:\mathcal{T}\phi:(x) \equiv n^{2\Delta-1} \lim_{y \rightarrow x} |x-y|^{2\Delta(1-\frac{1}{n})} \mathcal{T}(x) \sum_{j=1}^n \phi_j(y) \quad (5.18)$$

This field has already been introduced in a different context [88] and its conformal dimension is given by:

$$\Delta_{:\mathcal{T}\phi:} = \Delta_{\mathcal{T}} + \frac{\Delta}{n} \quad (5.19)$$

By a simple comparison between the scaling of (5.15) and the conformal dimension of the modified twist field  $:\mathcal{T}\phi:$ , we can interpret the two partition functions as

$$\frac{Z_n}{Z_1^n} \propto \frac{\langle :\mathcal{T}\phi:(a) : \tilde{\mathcal{T}}\phi:(b) \rangle}{\langle \phi(a)\phi(b) \rangle^n} \quad (5.20)$$

These correlation functions are taken with respect to the conformal vacuum  $|\emptyset\rangle$ . The presence of the field  $\phi$  in the correlation function in the numerator comes naturally, since this field creates the physical ground state  $|gs\rangle = \phi(0)|\emptyset\rangle$  acting on the conformal vacuum. In the case with a boundary, where there is only one boundary point between the two subsystem  $A$  and  $B$  ( $A = [0, r]$  and  $B = [r, +\infty[$ ), dimensional analysis arguments can be used to interpret the partition functions as the ratio:

$$\frac{Z_n}{Z_1^n} \propto \frac{\langle :\mathcal{T}\phi:(r) \rangle}{\langle \phi(r) \rangle^n} \quad (5.21)$$

The equation (5.20) can be very useful also for the study of entanglement outside the critical point. Although it has been derived in CFT, we can assume that it holds also outside the conformal regime. The study of such a correlation function in the massive case will be discussed in Chapter 6.

## 5.2 Entanglement Entropy in Logarithmic CFT

The above formulation can be easily adapted to the study of logarithmic conformal field theory. Logarithmic CFTs are a particular class of CFTs whose  $L_0$  (and thus their Hamiltonians) operators are not fully diagonalisable, but they can be reduced to a Jordan's block form. An example of logarithmic CFT is the  $c = -2$  ghost theory, which can be seen as a particular limit of a certain series of non unitary minimal models [89]. A particular feature of logarithmic CFT is the presence of logarithmic terms alongside the power-law decay in the correlation functions [90].

Let us consider the case when the projection of the operator  $L_0$  onto its lowest eigenstate has triangular form:

$$L_0 = \Delta \mathbf{1} + \mathbf{N} \quad (5.22)$$

where  $\mathbf{1}$  is the identity operator and  $\mathbf{N}$  is some nilpotent operator with  $\mathbf{N}^p = \mathbf{0}$ . Let  $\rho = 1, 2, \dots, p-1$  be the highest number such that  $\langle \mathbf{N}^\rho \rangle \neq \mathbf{0}$ . Then we have

$$\langle e^{-u L_0} \rangle = e^{-u\Delta} \left\langle \sum_{k=0}^{\rho} \frac{(-u\mathbf{N})^k}{k!} \right\rangle \quad (5.23)$$

In the limit  $u = \mathcal{A} \log \frac{r}{\epsilon} \rightarrow \infty$  we can keep just the most relevant term, i.e.  $u^\rho \langle \mathbf{N}^\rho \rangle$ . Applying this argument for the two cases  $L_0^{(j)}$  and  $\mathcal{L}_0$  and putting all contributions together into (5.5), the Rényi Entropy becomes

$$S_n = \mathcal{A} \frac{1}{1-n} \log \text{Tr} \rho_A^n \sim \frac{c_{\text{eff}}}{12} \frac{n+1}{n} \log \frac{r}{\epsilon} + \rho \log \log \frac{r}{\epsilon} \quad (5.24)$$

The presence of the double log term is not completely surprising, since logarithmic CFT present such features. An interpretation in term of modified twist fields :  $\mathcal{T}\phi$  : is still missing, although it is reasonable to expect a mixture of algebraic and logarithmic scaling for the correlation functions of such fields.

### 5.3 Numerical Checks

In this section we will perform a numerical study of a spin chain in order to test our field theory results about the scaling of the entanglement entropy.

Let us consider the following spin chain, introduced and studied for the first time by Von Gehlen [77]:

$$H(\lambda, \kappa) = - \sum_{j=1}^N [\sigma_j^z + \lambda \sigma_j^x \sigma_{j+1}^x + i\kappa \sigma_j^x] \quad (5.25)$$

In the thermodynamic limit  $N \rightarrow \infty$ , the above Hamiltonian has a critical line in the plane  $\lambda - \kappa$  which is described by the Lee-Yang universality class ( $c = -22/5$ ,  $\Delta_{min} = -1/5$  and  $c_{\text{eff}} = 2/5$ ).

Whilst there is no mathematical proof about the universality class of the aforementioned critical line, it can be easily identified by numerical exact diagonalisation of the above Hamiltonian and by studying the scaling of the gap between the two lowest eigenenergies. Such an exact diagonalisation can also be implemented to study the scaling of the entanglement entropy. An example of this behaviour is provided the massless free boson theory (see Chapter 8). In particular, we have considered the case  $\lambda = 0.90$  and  $\kappa = 0.0065$  with

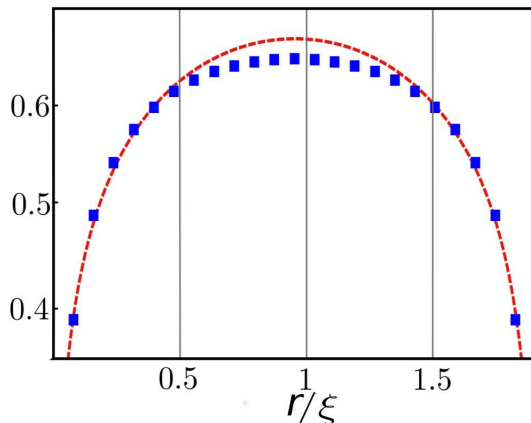


Figure 5.4: Scaling of entanglement entropy in the Lee-Yang chain with  $N = 24$  sites against the length  $r$  of the subsystem  $A$  (normalised by the correlation length  $\xi$  - see text). The blue squares represent the numerical data, while the red dashed line corresponds to the fit (5.26).

$N = 24$  sites with periodic boundary conditions. Then we computed the entanglement entropy for different sizes of the subsystem  $A$ . Once interpolated, it can be shown that

the entropy scales as

$$S = \frac{\gamma}{3} \log \left( \frac{N}{\pi} \sin \frac{r\pi}{N} \right) + \alpha \quad (5.26)$$

where the interpolating constants  $\gamma$  and  $\alpha$  are respectively given by 0.4056 and 0.3952. The constant  $\gamma$  is in strong agreement with the theoretical prediction  $\gamma = c_{\text{eff}} = 2/5 = 0.4$  and its value confirms the previous results.

From Picture 5.4 it is clear that the interpolating curve (red line) and the actual data (blue squares) do not always agree. In particular, while the squares and the line match perfectly in the small and large  $r$  regimes, the actual data are a bit smaller than the interpolating prediction around  $r = \xi$ . Such a disagreement has actually a very physical interpretation. Since the numerical simulation has been performed with a not so large number of sites ( $N = 24$ ), the system does not exhibit a properly critical behaviour: the gap  $\xi^{-1} \propto E_1 - E_0$  defined as the difference between the lowest eigenenergies vanishes only when considering the limit  $N \rightarrow \infty$ . As long as the subsystem  $A$  is much smaller than the correlation length ( $r \ll \xi$ ), the physical scale of the system is large enough to “look” infinite. In such a regime, the induced correlation length is too large to affect the system and the entanglement scales in a conformal fashion. On the other hand, when the correlation length has almost the same size of the subsystem  $A$ , it plays an important role and bounds the entanglement from above. While at the critical point entanglement always scales logarithmically with the size  $r$  of the subsystem, it saturates around  $r \sim \xi$  as long as the mass gap is non zero. The fact that there is a very good agreement also in the right hand side of Figure 5.4 (even though  $r > \xi$  in that region) is due to the symmetric property of entanglement entropy. The entropy of the subsystem  $A$  with respect to  $B$  has to be the same as the entropy of  $B$  respect with to  $A$ , as long as the entire system is just  $A \cup B$ .

The above picture shows the scaling of entanglement for a specific point of the Lee-Yang critical line ( $\lambda = 0.90$  and  $\kappa = 0.0065$ ). We have studied also other points of the critical line but the larger mass gap of such points makes the system definitely not critical and affects the entropy too much (see Figure 5.5).

## 5.4 Comments about Non Hermiticity

One of the first things one can notice is that the Hamiltonian (5.25) is not hermitian, i.e.  $H^\dagger \neq H$ . Moreover, also the Hamiltonians we will introduce in Chapter 7 are not Hermitian. Nevertheless, all their eigenvalues are real and they *almost* hermitian: the so-called  $\mathbb{P}\mathbb{T}$  *symmetry* [82, 83, 84, 85, 86].

Since these Hamiltonian operators are not hermitian, the left- and right- eigenvalues do

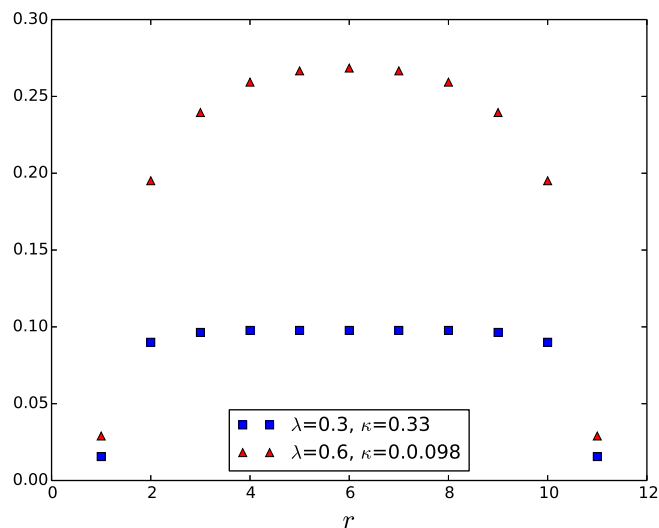


Figure 5.5: Scaling of entanglement entropy in the Lee-Yang chain with  $N = 12$  sites against the length  $r$  of the subsystem. In this case the finite size gap is too large to extract meaningful critical information.

not always coincide. For this reason, the *correct* reduced density matrix should have been

$$\rho_A = \text{tr}_B |\Psi_R\rangle\langle\Psi_L| \quad (5.27)$$

where  $|\Psi_R\rangle$  and  $|\Psi_L\rangle$  represent respectively the right and left ground states (the left and right eigenvectors relative to the lowest eigenenergy). However, at least at the critical point, the conformal invariance and the  $\mathbb{PT}$  symmetry implies the equality between the two eigenvectors:

$$|\Psi_R\rangle = |\Psi_L\rangle \quad (5.28)$$

Consider the conformal field  $\phi$  representing the ground state. Thanks to conformal invariance, it can be factorised into its holomorphic and anti-holomorphic parts:

$$\phi(z, \bar{z}) = \varphi(z)\bar{\varphi}(\bar{z}) \quad (5.29)$$

Once having set the origin of the  $x$ - $y$  axis on the point ( $z = e^{ix+\tau}$ ), the parity transformation  $x \rightarrow -x$  maps  $z$  to  $\bar{z}$ . Such a transformation exchanges the roles of  $\varphi$  and  $\bar{\varphi}$  and preserves  $\phi$ . Thus, the ground state is  $\mathbb{P}$  invariant. Thanks to  $\mathbb{PT}$  symmetry, it has to be  $\mathbb{T}$  invariant as well. Since the  $\mathbb{T}$  transformation ( $t \rightarrow -t$ ) maps left eigenvectors to their

corresponding right versions and vice versa, the two ground states have to coincide.

## 5.5 Conclusions

In this chapter we extended some well known results (Chapter 4) concerning the scaling of entanglement entropy of critical 1+1 dimensional systems. In particular, we discussed the case when the underlying conformal theory is non unitary. The main difference between unitary and non unitary CFT is the fact that the physical ground state and the conformal vacuum coincide in the former while they do not in the latter. One of the most “famous” effect of such a non unitary feature can be seen in the scaling of the ground state energy at various sizes of the systems (also known as Casimir effect). In unitary CFT the numerical multiplicative constant in front of the  $size^{-1}$  correction is given by the central charge, a number associated with the universality class of the underlying conformal field theory. In non unitary theories such a number is replaced by the effective central charge, a combination of the central charge and the conformal dimension of the field creating the ground state from the conformal vacuum.

When studying the scaling of entanglement entropy, we showed that the main difference with the unitary case is the replacement of the central charge with the effective central charge. Of course, this is not surprising, since the effective central charge is (like entanglement) a *physical* quantity.

Since logarithmic CFTs are a further generalisation of non unitary CFT, we could also extend our results for entanglement entropy to such theories. We showed that in logarithmic theories a double logarithmic term is present in the scaling of the entropy. We believe that such a correction can be associated to the logarithmic terms appearing in four-point correlation functions in logarithmic CFT.

In addition to our CFT derivation, we presented an interpretation of entanglement entropy of unitary systems in terms of correlation functions involving modified twist fields. Such an interpretation will be fundamental in the next chapter to study the off-critical scaling of the entanglement entropy in non unitary quantum field theories.

## Chapter 6

# Entanglement in Non Unitary Quantum Field Theory

In Chapter 5 we have discussed the scaling of entanglement entropy in non unitary conformal field theory. The Rényi Entropy between a subsystem  $A = [a, b]$  and the rest of the system can be computed by evaluating partition functions on complicated manifolds and it is given by:

$$S_n = \frac{1}{1-n} \log \text{Tr} \rho_A^n \equiv \frac{1}{1-n} \log \frac{Z_n}{Z_1^n} \propto \frac{c_{\text{eff}}}{6} \frac{n+1}{n} \log \frac{r}{\epsilon} \quad (6.1)$$

where  $r = |b - a|$  is the size of the subsystem  $A$ .

It has also been suggested that the ratio of the two partition functions can be written in terms of correlation functions:

$$\frac{Z_n}{Z_1^n} = \mathcal{Z}_n \epsilon^{4(\Delta; \mathcal{T}\phi; -n\Delta)} \frac{\langle : \mathcal{T}\phi : (a) : \tilde{\mathcal{T}}\phi : (b) \rangle}{\langle \phi(a)\phi(b) \rangle^n} \quad (6.2)$$

where  $\mathcal{Z}_n$  is some normalisation constant such that  $\frac{d\mathcal{Z}_n}{dn} \Big|_{n=1} = 1$  and  $\epsilon$  is an ultraviolet cut-off. It has been shown that this relation reproduces the correct entanglement entropy in non unitary CFT and it is natural to assume that the same expression holds also outside the critical point in the massive regime.

The form factor program (see Chapter 3 ) is a successful tool for studying correlation functions in the massive regime. In this chapter we will study the form factor expansion of the correlation functions 6.2 for the Lee-Yang model, the simplest non unitary integrable quantum field theory in  $1 + 1$  dimensions.

## 6.1 Twist Field Form Factors in the Lee-Yang Model

As we have seen before in Chapter 3, it could happen that different fields' form factors satisfy the same equations. In this specific case, the equations of both the standard ( $\mathcal{T}$ ) and the modified ( $: \mathcal{T}\phi :$ ) twist fields are the same. In this section, we let  $\mathcal{O}$  be either twist field,  $\mathcal{T}$  or  $: \mathcal{T}\phi :$ . If not otherwise stated, all form factors refer to both fields.

The Lee-Yang model is one of the simplest integrable quantum field theories in two dimensions. It can be seen as a thermal perturbation  $\phi_{13}$  of the minimal model  $\mathcal{M}_{25}$  with central charge  $c = -\frac{22}{5}$ . The operator content of this minimal model is very simple: apart from the identity field  $\mathbf{1}$ , there is only one other field  $\phi \equiv \phi_{13} \equiv \phi_{12}$  with conformal dimension  $\Delta = -\frac{1}{5}$ . The two-particle scattering matrix is given by [76]:

$$S(\beta) = \frac{\tan \frac{1}{2} \left( \beta + \frac{2\pi i}{3} \right)}{\tan \frac{1}{2} \left( \beta - \frac{2\pi i}{3} \right)} \quad (6.3)$$

which has a bound state pole in the physical sheet at  $\beta = \frac{2\pi i}{3}$ :

$$-i \operatorname{Res}_{\beta=\frac{2\pi i}{3}} S(\beta) = \Gamma^2 = -2\sqrt{3} \quad (6.4)$$

From the sign of the bound state residue we can immediately infer the non unitarity of the model [76], since  $\Gamma \in \mathbb{R}$  for unitary theories.

In order to construct form factors for the twist fields, we need to define a S-matrix for the  $n$ -copy theory:

$$S_{\mu\nu}(\beta) = \begin{cases} S(\beta) & \mu = \nu \\ 1 & \mu \neq \nu \end{cases} \quad (6.5)$$

where the index  $\mu$  refers to the  $\mu$ -th copy of the theory. With the definition of the S-matrix alone, we simply have  $n$  non-interacting theories: two given particles have a non trivial scattering only if they belong to the same copy. Of course, this set-up is not enough to recreate the complex situation such that particles do interact only around the branch cut. In order to take into account this property, we introduce the Branch Point Twist Fields (see Chapter 4). The peculiar action of twist fields on particles gives rise to a modified version of Watson and kinematic residue equations. In standard theories, when a particle performs a rotation around an operator (with a shift of  $2\pi i$  in its rapidity) the type of particle is not affected. Since a twist field creates a branch cut, when a particle belonging to the copy  $\mu$  rotates clockwise around it, it ends up in the copy  $\mu - 1$ . The second Watson

equation (3.72) now becomes:

$$\begin{aligned}
 F_\ell^{\mu_1 \mu_2 \dots \mu_\ell}(\beta_1 + 2\pi i, \beta_2, \dots, \beta_\ell) &= F_\ell^{\mu_2 \dots \mu_\ell \hat{\mu}_1}(\beta_2, \dots, \beta_\ell, \beta_1) \\
 &= \left( \prod_{i=2}^{\ell} S_{\mu_i \hat{\mu}_1}(\beta_i - \beta_1) \right) F_\ell^{\hat{\mu}_1 \dots \mu_\ell}(\beta_1, \dots, \beta_\ell)
 \end{aligned} \tag{6.6}$$

where  $\hat{\mu} = \mu - 1$ .

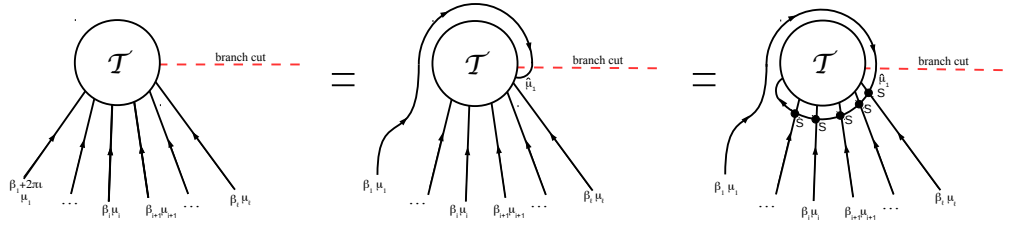


Figure 6.1: Second Watson equation for twist field. The branch cut (red dashed line) modifies particles when they cross it.

The kinematic residue equation becomes:

$$\begin{aligned}
 \text{Res}_{\beta=\beta_0} F_{\ell+2}^{\bar{\mu} \hat{\mu} \mu_1 \dots \mu_\ell}(\beta + i\pi, \beta_0, \beta_1, \dots, \beta_\ell) &= i F_\ell^{\mu_1 \dots \mu_\ell}(\beta_1, \dots, \beta_\ell) \\
 \text{Res}_{\beta=\beta_0} F_{\ell+2}^{\bar{\mu} \hat{\mu} \mu_1 \dots \mu_\ell}(\beta + i\pi, \beta_0, \beta_1, \dots, \beta_\ell) &= -i \left( \prod_{j=1}^k S_{\hat{\mu} \mu_j}(\beta_{0j}) \right) F_\ell^{\mu_1 \dots \mu_\ell}(\beta_1, \dots, \beta_\ell)
 \end{aligned} \tag{6.7}$$

In order to understand the formulation of these residue equations, we should recall which is the action of twist fields on particles. Branch point twist fields can be defined on a system in which each theory is copied  $n$  times and particles interact only if they belong to the same copy. Additionally, when a particle belonging to the copy  $i$  crosses the segment  $[a, b]$  from below it becomes a particle of the  $i + 1$  copy. The role of a twist field  $\mathcal{T}(a)$  is to create a half-infinite branch cut from the point  $a$  onwards (see Figure 6.2). In order to create a finite branch cut, we need also a second kind of twist field, denoted by  $\tilde{\mathcal{T}}$ . The role of  $\tilde{\mathcal{T}}(b)$  is to create another half-infinite branch cut from  $b$  to  $+\infty$  with inverted orientation. If the branch cut of  $\mathcal{T}$  moves particles from a copy to the following one when they approach from below, the branch cut of  $\tilde{\mathcal{T}}$  moves the particles to the previous copy.

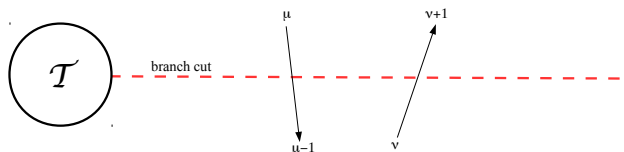


Figure 6.2: The twist field  $\mathcal{T}$  creates a branch cut (red dashed line) which moves particles between adjacent copies.

The second branch cut ( $\tilde{\mathcal{T}}$ ) annihilates the effect of the first cut ( $\mathcal{T}$ ) from  $b$  onwards. The

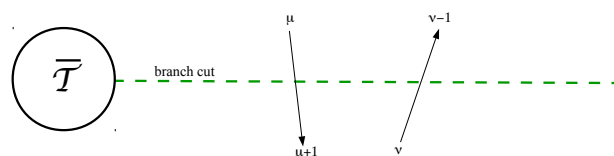


Figure 6.3: The twist field  $\tilde{\mathcal{T}}$  creates a branch cut (green dashed line) which moves particles between adjacent copies. Notice that the orientation of this branch cut is reversed compared to  $\mathcal{T}$  (Figure 6.2).

two twist fields then create a finite branch cut (see Figure 6.4):

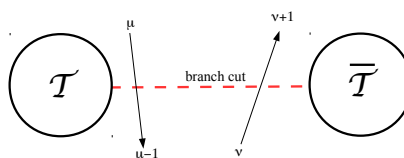


Figure 6.4: When both twist fields are present, a finite branch cut (red dashed line) is created.

Let us consider the scattering of  $\ell$  particles onto a twist field  $\mathcal{T}$  in 0. If the first and the second particle have the same rapidity but shifted by  $i\pi$  (aka two particles with the same momentum, one incoming and the other outgoing), they create a pole in the scattering amplitude if they can interact. Such an interaction can happen only if the two particles share the same copy, say  $\mu$ . There are two ways such that they belong to the same copy when they interact: they can be originally in the same copy  $\mu$  (second equation) or they can belong to neighbour copies (first equation). If they belong to neighbour copies, say  $\mu$  and  $\mu-1$ , the first particle has to perform a circle around the twist field in order to decrease its “copy number” by one. On the other hand, if they are already in the same copy, they can interact (and then create a pole) only if neither of them perform a cycle around the

twist field. For this reason, kinematic residue equations can be of two kinds to include both possibilities of creating a kinematic pole. The main difference from “ordinary” form factor kinematic poles is that in the twist field case particles change their properties when rotating around twist fields. When studying kinematic poles of form factors for other local operators, particles do not change their nature when performing a rotation around the operator, so the same two particles can form a kinematic pole depending on whether one of them rotates or not around the operator.

Of course, since the S-matrix has a pole in the physical strip, there is also a non trivial bound state residue equation:

$$\text{Res}_{\beta_0=\beta} F_{\ell+1}^{\mu\mu\mu_1\cdots\mu_{\ell-1}} \left( \beta + \frac{i\pi}{3}, \beta_0 - \frac{i\pi}{3}, \beta_1, \dots, \beta_{\ell-1} \right) = i\Gamma F_{\ell}^{\mu\mu_1\cdots\mu_{\ell-1}} (\beta, \beta_1, \dots, \beta_{\ell-1}) \quad (6.8)$$

In “usual” form factors problems, the rapidities lie in the strip  $\text{Im}\beta \in [0, 2\pi[$ , since a rotation of  $2\pi i$  has no effect on the rapidity of a particle, due to the periodicity of hyperbolic functions. In this case, when a particle from the copy  $\mu$  rotates by  $2\pi$  around a twist field, it ends up in the  $\mu \pm 1$  copy (depending on the sign of the rotation). From a form factors point of view, such a rotation can be implemented by a  $2\pi i$  shift in the rapidity. For this reason, Twist Fields form factors cannot have periodicity of just  $2\pi i$ . Since the  $n$ -th copy is connected to the first, it is clear that the correct periodicity of such form factors has to be  $2\pi ni$ . The relation between rotations of rapidities and the change of a copy can be exploited to connect form factors of particles belonging to different copies to form factors of particles all from the same copy (say the first one):

$$F_{\ell}^{\mu_1\cdots\mu_{\ell}}(\beta_1, \dots, \beta_{\ell}) = F_{\ell}^{1\cdots 1}(\beta_1 + 2\pi i(\mu_1 - 1), \dots, \beta_{\ell} + 2\pi i(\mu_{\ell} - 1)) \quad (6.9)$$

if  $\mu_1 < \dots < \mu_{\ell}$ .

Thanks to this relation, we can compute form factors of particles belonging to the same copy (say the first) and we can recover all the others using (6.9) together with the S-matrix (6.5).

### 6.1.1 One- and two-particle form factors

Let us start from the  $\ell = 0$  and  $\ell = 1$  form factors. The zero-particle form factor is simply given by the expectation value  $\langle \mathcal{O} \rangle$ . Since we are considering a spinless theory, thanks to relativistic invariance, form factors depend only on the difference between rapidities. Specialising to  $\ell = 1$ , it implies that one-particle form factors have to be rapidity independent.

The bound state residue equation connects the one- and two-particle form factors:

$$\text{Res}_{\beta=\beta_0} F_2^{\mu\mu} \left( \beta - \beta_0 + \frac{2\pi i}{3} \right) = i\Gamma F_1^\mu \quad (6.10)$$

The two-particle form factor must also satisfy:

$$F_2^{\mu\mu}(\beta) = S(\beta)F_2^{\mu\mu}(-\beta) = F_2^{\mu\mu}(2\pi i n - \beta) \quad (6.11)$$

These two equations, together with the kinematic poles in  $\beta = \beta_1 - \beta_2 = \pm i\pi, \pm i\pi(2n - 1)$ , constrain the form of the two-particle form factor to:

$$F_2^{\mu\mu}(\beta_1, \beta_2) = F_2^{\mu\mu}(\beta = \beta_{1,2}) = \frac{\langle \mathcal{O} \rangle \sin \frac{\pi}{n}}{2n \sinh \left( \frac{i\pi - \beta}{2n} \right) \sinh \left( \frac{i\pi + \beta}{2n} \right)} \frac{F_{\min}(\beta)}{F_{\min}(i\pi)} + \mathcal{K}(\beta) \quad (6.12)$$

where  $F_{\min}$  is the solution of (6.11) without kinematic poles and  $\mathcal{K}$  is the kernel solution of the kinematic residue equation, i.e. it has no kinematic poles (see Chapter 3):

$$\text{Res}_{\beta=0} \mathcal{K}(\beta + i\pi) = 0 \quad (6.13)$$

In order to be compatible with the bound state pole, the kernel solution has to be proportional to the minimal form factor:

$$\mathcal{K}(\beta) = \kappa F_{\min}(\beta) \quad (6.14)$$

The minimal form factor  $F_{\min}$  can be split into two components, in a similar fashion to [62]:

$$F_{\min}(\beta) = a(\beta)f_n(\beta) \quad (6.15)$$

where  $a$  encapsulates the bound state pole

$$a(\beta) = \frac{\cosh \frac{\beta}{n} - 1}{\cosh \frac{\beta}{n} - \cos \frac{2\pi}{3n}} \quad (6.16)$$

and  $f_n$  can be computed using the integral representation of the S-matrix [91]:

$$f_n(\beta) = \exp \left( 2 \int_0^\infty dt \frac{\sinh \frac{t}{3} \sinh \frac{t}{6}}{t \cosh \frac{t}{2} \sinh(nt)} \cosh \left[ t \left( n + \frac{i\beta}{\pi} \right) \right] \right) \quad (6.17)$$

The function  $f_n$  can also be computed using an infinite product:

$$\begin{aligned}
& f_n(\beta)^{-1} \\
&= \prod_{k=0}^{\infty} \left[ \frac{\Gamma\left(\frac{2n-2w+\frac{2}{3}+4k}{4n}\right) \Gamma\left(\frac{2n+2w+\frac{2}{3}+4k}{4n}\right) \Gamma\left(\frac{2n-2w+\frac{4}{3}+4k}{4n}\right) \Gamma\left(\frac{2n+2w+\frac{4}{3}+4k}{4n}\right)}{\Gamma\left(\frac{n-w+2k}{2n}\right) \Gamma\left(\frac{n+w+2k}{2n}\right)} \right. \\
&\quad \times \left. \frac{\Gamma\left(\frac{n-w+2k+2}{2n}\right) \Gamma\left(\frac{n+w+2k+2}{2n}\right)}{\Gamma\left(\frac{2n-2w+\frac{8}{3}+4k}{4n}\right) \Gamma\left(\frac{2n+2w+\frac{8}{3}+4k}{4n}\right) \Gamma\left(\frac{2n-2w+\frac{10}{3}+4k}{4n}\right) \Gamma\left(\frac{2n+2w-\frac{14}{3}+4k}{4n}\right)} \right]
\end{aligned} \tag{6.18}$$

with  $w = n + i\beta/n$ .

The function  $f_n$  enjoys the following property, which can be proved using either the integral or the infinite product representation:

$$\frac{f_n(i\pi)}{f_n\left(\frac{2\pi i}{3}\right)} = \frac{n}{\sqrt{3}} \frac{\sin^3 \frac{\pi}{3n}}{\sin \frac{\pi}{6n} \sin \frac{\pi}{2n}} \tag{6.19}$$

Moreover, it can be shown that the following relations hold for minimal form factors:

$$F_{\min}\left(\beta + \frac{i\pi}{3}\right) F_{\min}\left(\beta - \frac{i\pi}{3}\right) = \frac{\cosh \frac{\beta}{n} - \cos \frac{2\pi}{3n}}{\cosh \frac{\beta}{n} - \cos \frac{\pi}{n}} F_{\min}(\beta) \tag{6.20}$$

$$F_{\min}(\beta + i\pi) F_{\min}(\beta) = \frac{\sinh \frac{\beta}{2n} \sinh\left(\frac{\beta}{2n} + \frac{i\pi}{2n}\right)}{\sinh\left(\frac{\beta}{2n} - \frac{i\pi}{3n}\right) \sinh\left(\frac{\beta}{2n} + \frac{5i\pi}{6n}\right)} \tag{6.21}$$

which will be used to compute the higher particle form factors.

The two functions  $a$  and  $f_n$  all together satisfy the equation (6.11) and they have no pole in the physical sheet but the bound state pole at  $\beta = \frac{2\pi i}{3}$ . Even if  $f_n$  has a simple pole at  $\beta = 0$ , the function  $F_{\min}$  as a whole is regular at this point thanks to the choice of the function  $a$ . Furthermore, it can be shown that the minimal form factor tends to one for  $|\beta| \rightarrow \infty$ .

**Fixing the parameter  $\kappa$**

The parameter  $\kappa$  can be fixed using the cluster decomposition property of form factors [92]:

$$\lim_{\lambda \rightarrow \infty} F_{k+\ell}(\beta_1, \dots, \beta_k, \theta_1 + \lambda, \dots, \theta_\ell + \lambda) = \frac{1}{\langle \mathcal{O} \rangle} F_k(\beta_1, \dots, \beta_k) F_\ell(\theta_1, \dots, \theta_\ell) \quad (6.22)$$

Specialising the above equation to  $k = \ell = 1$  and we have

$$\lim_{\lambda \rightarrow \infty} F_2^{\mu\mu}(\beta, \theta + \lambda) = \frac{1}{\langle \mathcal{O} \rangle} F_1^\mu(\beta) F_1^\mu(\theta) = \frac{(F_1^\mu)^2}{\langle \mathcal{O} \rangle} \quad (6.23)$$

Since  $F_{\min}(\beta) \rightarrow 1$  for  $|\beta| \rightarrow \infty$ , when taking such a limit of (6.12), the first term vanishes and the second tends to  $\kappa$ . Thanks to the above equation we can now fix  $\kappa = (F_1^\mu)^2 / \langle \mathcal{O} \rangle$ .

**Fixing  $F_1$  and distinguish  $\mathcal{T}$  from  $\mathcal{T}\phi$ :**

When applying the bound state residue equation to the two-particle form factors, a constraint on  $F_1$  emerges:

$$\begin{aligned} F_1^\mu &= \frac{1}{i\Gamma} \operatorname{Res}_{\beta=\beta_0} F_2^{\mu\mu} \left( \beta - \beta_0 + \frac{2\pi i}{3} \right) \\ &= \frac{1}{\Gamma} \left[ n \tan \frac{\pi}{3n} f \left( \frac{2\pi i}{3} \right) \frac{(F_1^\mu)^2}{\langle \mathcal{O} \rangle} - \frac{\tan \frac{\pi}{3n} f_n \left( \frac{2\pi i}{3} \right)}{\tan \frac{\pi}{2n} f_n(i\pi)} \right] \end{aligned} \quad (6.24)$$

The above second order equation has two different solutions:

$$F_1^\mu = -\langle \mathcal{O} \rangle \Gamma \frac{\cos \frac{\pi}{3n} \pm 2 \sin^2 \frac{\pi}{6n}}{2n \sin \frac{\pi}{3n} f_n \left( \frac{2\pi i}{3} \right)} \quad (6.25)$$

The presence of two distinguishable solutions should not be a surprise, since the “normal” twist field  $\mathcal{T}$  is not the only one we are looking for. The modified twist field  $\mathcal{T}\phi$  has the very same property of  $\mathcal{T}$ , as both of them have the same action on particles. The two solutions should then correspond to the two different twist fields. In order to identify correctly the right form factor solution for the right field, we can specialise  $F_1$  to  $n = 1$ :

$$F_1^\mu \stackrel{n=1}{=} \begin{cases} F_1^\phi & \text{(solution with +)} \\ 0 & \text{(solution with -)} \end{cases} \quad (6.26)$$

where  $F_1^\phi$  is the one-particle form factor for the field  $\phi$  as derived in [62]. Since when  $n = 1 : \mathcal{T}\phi :$  coincides with  $\phi$  itself and  $\mathcal{T}$  becomes the identity  $\mathbf{1}$ , the solution with the plus sign should correspond to the composite twist field  $: \mathcal{T}\phi :$  while the other is the form factor of the twist field  $\mathcal{T}$ :<sup>1</sup>

$$\frac{F_1^{\mathcal{T}|\mu}}{\langle \mathcal{T} \rangle} = -\Gamma \frac{2 \cos \frac{\pi}{3n} - 1}{2n \sin \frac{\pi}{3n} f_n \left( \frac{2\pi i}{3} \right)} \quad (6.27)$$

$$\frac{F_1^{:\mathcal{T}\phi| \mu}}{\langle : \mathcal{T}\phi : \rangle} = -\frac{\Gamma}{2n \sin \frac{\pi}{3n} f_n \left( \frac{2\pi i}{3} \right)} \quad (6.28)$$

This identification will be confirmed in the following section 6.3 checking the short-distance scaling of the form factor expansion against perturbative CFT.

### 6.1.2 Higher particle form factors

Using bound state and kinematic pole recursive equations, we can construct higher particle form factors from the zero-, one- and two-particle ones. Thanks to the special relations between form factors of particles belonging to different copies (Equation 6.9), we can focus on computing form factors of particles all belonging to the first copy. We can construct a generic form factor using the following ansatz:

$$F_\ell(x_1, \dots, x_\ell) = Q_\ell(x_1, \dots, x_\ell) \prod_{i < j}^k \frac{F_{\min} \left( \frac{x_i}{x_j} \right)}{(x_i - \alpha x_j)(x_j - \alpha x_i)} \quad (6.29)$$

where new variables  $x_i = e^{\frac{\beta_i}{n}}$  and  $\alpha = e^{\frac{i\pi}{n}}$  have been introduced for convenience. In the above equation,  $Q_\ell$  is a completely symmetric polynomial. This ansatz, used for the first time in [93], resembles the usual ansatz used for the evaluation of form factors of local operators [62, 63]. In the above equations, all the kinematic poles have been made explicit in the denominator.

#### Kinematic poles

The kinematic pole residue equation applied to (6.29) gives the first constraint on the polynomials  $Q_\ell$ :

$$Q_{\ell+2}(\alpha x_0, x_0, x_1, \dots, x_\ell) = x_0^2 P_\ell(x_0, x_1, \dots, x_\ell) Q_\ell(x_1, \dots, x_\ell) \quad (6.30)$$

---

<sup>1</sup>Since  $\langle \emptyset | \mathbf{1} | \psi \rangle \neq 0$  iff  $|\psi\rangle = |\emptyset\rangle$ , all form factors of the identity but the zero-particle form factor vanish.

The polynomial  $P_\ell$  is given by

$$P_\ell(x_0, x_1, \dots, x_\ell) = C_\ell(n) \prod_{b=1}^{\ell} [(x_b - \alpha^2 x_0)(x_b - \alpha^{-1} x_0)(x_b - \gamma x_0)(x_b - \alpha \gamma^{-1} x_0)] \quad (6.31)$$

where  $\gamma = e^{-\frac{2\pi i}{3n}}$  and

$$C_\ell(n) = \frac{2 \sin \frac{\pi}{n}}{n F_{\min}(i\pi)} \alpha^{2(\ell+1)} = C_0(n) \alpha^{2\ell} \quad (6.32)$$

Since, by definition, the polynomials  $Q_\ell$  are completely symmetric, the above constraint (6.30) can be solved using *elementary symmetric polynomials*  $\sigma_i^{(\ell)}$ , which can be generated by the following implicit definition:

$$\sum_{i=0}^{\sigma} x^{\ell-i} \sigma_i^{(\ell)}(x_1, \dots, x_\ell) = \prod_{j=1}^{\ell} (x_j + x) \quad (6.33)$$

In other words,  $\sigma_i^{(\ell)}(x_1, \dots, x_\ell)$  is *the* completely symmetric homogeneous polynomial of degree  $i$  of  $\ell$  variables. For instance: <sup>2</sup>

$$\sigma_0^{(\ell)} = 1 \quad (6.34)$$

$$\sigma_1^{(\ell)} = \sum_{i=1}^{\ell} x_i \quad (6.35)$$

$$\sigma_2^{(3)} = x_1 x_2 + x_1 x_3 + x_2 x_3 \quad (6.36)$$

$$\dots \quad (6.37)$$

The polynomial  $P_\ell$  can be expressed in terms of elementary symmetric polynomials:

$$P_\ell = C_\ell(n) \sum_{a,b,c,d=0}^{\ell} (-\alpha^2 x_0)^{\ell-a} (-\alpha^{-1} x_0)^{\ell-b} (-\alpha \gamma^{-1} x_0)^{\ell-c} (-\gamma x_0)^{\ell-d} \sigma_a^{(\ell)} \sigma_b^{(\ell)} \sigma_c^{(\ell)} \sigma_d^{(\ell)} \quad (6.38)$$

The kinematic pole residue equation gives already a strong constraint on the polynomials  $Q_\ell$ , constraints which can be further strengthened using bound state residue equations.

---

<sup>2</sup>In the following, we will drop the arguments  $x_1, \dots, x_\ell$  when no confusion is possible.

### Bound state poles

Applying the bound state residue equation to (6.29) we obtain:

$$Q_{\ell+1} \left( x_0 \gamma^{-\frac{1}{2}}, x_0 \gamma^{\frac{1}{2}}, x_1, \dots, x_{\ell-1} \right) = x_0^2 U_\ell(x_0, x_1, \dots, x_{\ell-1}) Q_\ell(x_0, x_1, \dots, x_{\ell-1}) \quad (6.39)$$

where  $U_\ell$  is given by:

$$U_\ell(x_0, x_1, \dots, x_{\ell-1}) = H_\ell(n) \prod_{i=1}^{\ell-1} (x_i - \gamma^{-2} x_0)(x_i - \gamma^2 x_0) \quad (6.40)$$

and the constant  $H_\ell$  is given by

$$H_\ell(n) = \frac{4\Gamma \sin^2 \left( \frac{\pi}{2n} \right)}{n \tan \left( \frac{\pi}{3n} \right) a(i\pi) f \left( \frac{2\pi i}{3} \right)} (-\alpha)^\ell = H_1(n) (-\alpha)^{\ell-1} \quad (6.41)$$

As before, the polynomial  $U_\ell$  can be expressed in terms of elementary symmetric polynomials:

$$U_\ell = H_k(n) \sum_{a,b=0}^{\ell-1} (-\gamma^{-2} x_0)^{\ell-1-a} (-\gamma^2 x_0)^{\ell-1-b} \sigma_a^{(\ell-1)} \sigma_b^{(\ell-1)} \quad (6.42)$$

Using the kinematic and the bound state pole residue equations we then compute the  $Q_{\ell+2}$  polynomial starting from  $Q_{\ell+1}$  and  $Q_\ell$ .

### Three-particle form factors

In order to construct the polynomial  $Q_3$  (and thus the three particle form factor), we need to know  $Q_1$  and  $Q_2$ . They can be simply inferred from the explicit expressions of the relative form factors:

$$Q_1 = F_1^{\mathcal{O}|1} \quad (6.43)$$

$$Q_2 = \langle \mathcal{O} \rangle C_0(n) \alpha^{-1} \sigma_2 + \frac{\left( F_1^{\mathcal{O}|1} \right)^2}{\langle \mathcal{O} \rangle} \left( (1 + \alpha)^2 \sigma_2 - \alpha \sigma_1^2 \right). \quad (6.44)$$

One can immediately check that  $Q_2$  satisfies the kinematic residue equation (with  $Q_0 = F_0^{\mathcal{O}} = \langle \mathcal{O} \rangle$ ) and the bound state equation.  $Q_2$  is in fact the *unique* solution of the two residue equations, once  $Q_0$  and  $Q_1$  are given. This couple of residue equations fix uniquely also higher particle form factors, without any ambiguity regarding possible kernel solutions. In different theories, when there is no bound state residue equations, higher particle form

factors are defined up to kernel solutions, as happens in [93].

We can now write down the most general expression for the polynomial  $Q_3$ :

$$Q_3 = A_1\sigma_1^3\sigma_3 + A_2\sigma_1^2\sigma_2^2 + A_3\sigma_1\sigma_2\sigma_3 + A_4\sigma_2^3 + A_5\sigma_3^2 + A_6\sigma_1^4\sigma_2 + A_7\sigma_1^6 \quad (6.45)$$

The coefficients  $A_i$  can be computed exactly using the kinematic and bound state residue equations. Their values are reported in appendix A. It can be noted that the  $n \rightarrow 1$  correspondence of  $:\mathcal{T}\phi:$  and  $\mathcal{T}$  with respectively  $\phi$  and  $\mathbf{1}$  holds also at three-particle level. All the  $A_i$ s vanish for  $n = 1$  and  $\mathcal{O} = \mathcal{T}$ , while for  $\mathcal{O} = :\mathcal{T}\phi:$  the  $A_i$ s are given by:

$$A_1 = A_4 = A_5 = A_6 = A_7 = 0, \quad A_2 = -A_3 = \frac{(F_1^\phi)^2 H_1(1)}{\langle \phi \rangle} = \frac{i\pi m^2 \mathfrak{z}^{1/4}}{2^{7/2} f_1(i\pi)^{3/2}} \quad (6.46)$$

reproducing exactly the three-particle form factor for the field  $\phi$  as computed in [62]. Moreover, the clustering property is automatically satisfied, since the identities

$$\lim_{\lambda \rightarrow \infty} F_3^{\mathcal{O}|111}(\beta_1, \beta_2, \beta_3 + \lambda) = \frac{1}{\langle \mathcal{O} \rangle} F_2^{\mathcal{O}|11}(\beta_1, \beta_2) F_1^{\mathcal{O}|1}(\beta_3) \quad (6.47)$$

$$\lim_{\lambda \rightarrow \infty} F_3^{\mathcal{O}|111}(\beta_1, \beta_2 + \lambda, \beta_3 + \lambda) = \frac{1}{\langle \mathcal{O} \rangle} F_1^{\mathcal{O}|1}(\beta_1) F_2^{\mathcal{O}|11}(\beta_2, \beta_3) \quad (6.48)$$

can be checked analytically. In this case, clustering properties produce just identities, while in other cases, like [93], these properties have been used to fix the form factors expressions to remove the kernel ambiguity.

The agreement in the  $n = 1$  case and the validity of the clustering properties are a strong hint that these form factor expressions are correct.

In the work [62], Zamolodchikov managed to make an ansatz for generic  $\ell$ -particle form factors. Such a generalisation cannot be done at this point when computing twist field form factors. This is mainly due to the fact that the number of kinematic poles ( $x_i = \alpha^{\pm 1} x_j$ ) doubles the number of poles in the standard theory ( $x_i + x_j = 0$ ). For this reason the degree of the polynomials  $Q_\ell$  in the twist field case grows at a much greater rate than the usual case, leading to much more intricate recursive equations.

### Form factor of the fields $\tilde{\mathcal{T}}$ and $:\tilde{\mathcal{T}}\phi:$

In the previous sections we focused on the computation of form factors for the twist fields  $\mathcal{T}$  and  $:\mathcal{T}\phi:$ . These fields are not the only ones that enter the correlation functions for the evaluation of Rényi entanglement entropy: the field  $\tilde{\mathcal{T}}$  and  $:\tilde{\mathcal{T}}\phi:$  play a role too. As we have seen in Chapter 4, the field  $\tilde{\mathcal{T}}$  acts as the field  $\mathcal{T}$  but it creates a different branch

cut. If a particle belonging to the copy  $\mu$  performs an anticlockwise rotation around  $\mathcal{T}$ , it will end up in the copy  $\mu + 1$ . On the other hand, if this circle is performed around  $\tilde{\mathcal{T}}$ , the particle will belong to the copy  $\mu - 1$ . In other words, if  $\mathcal{T}$  is associated to the cyclic permutation symmetry  $i \mapsto i + 1$ ,  $\tilde{\mathcal{T}}$  implements the opposite symmetry  $i \mapsto i - 1$ . Similarly,  $:\tilde{\mathcal{T}}\phi:$  acts in the same way as  $:\mathcal{T}\phi:$  but with opposite orientation. Thanks to this particular relation, the two fields  $\mathcal{T}$  and  $\tilde{\mathcal{T}}$  can be considered one the conjugate of the other:  $\mathcal{T}$  transforms to  $\tilde{\mathcal{T}}$  once the direction of time has been inverted (as it could be easily inferred by comparing Figures and 6.3).

The relationship between the two twist fields imposes then the following equality:

$$F_\ell^{\mathcal{T}|\mu_1 \dots \mu_\ell}(\beta_1, \dots, \beta_\ell) = F_\ell^{\tilde{\mathcal{T}}|(n-\mu_1) \dots (n-\mu_\ell)}(\beta_1, \dots, \beta_\ell) \quad (6.49)$$

In other words, the conjugate twist field  $\tilde{\mathcal{T}}$  “counts” the copies with reversed order.

Moreover, since the theory is non unitary, we would expect the following identity to hold: [62, 74]

$$\left[ \frac{1}{\langle \tilde{\mathcal{T}} \rangle} \langle \emptyset | \tilde{\mathcal{T}}(0) | \beta_1, \dots, \beta_\ell \rangle_{\mu_1 \dots \mu_\ell} \right]^* = (-1)^\ell \frac{1}{\langle \mathcal{T} \rangle} {}_{\mu_1 \dots \mu_\ell} \langle \beta_1, \dots, \beta_\ell | \mathcal{T} | \emptyset \rangle \quad (6.50)$$

The generic matrix element of the form factor expansion of the correlation function  $\langle \mathcal{T}(0) \tilde{\mathcal{T}}(r) \rangle$  is then given by

$$\begin{aligned} & \frac{\langle \emptyset | \mathcal{T}(0) | \beta_1, \dots, \beta_\ell \rangle_{\mu_1 \dots \mu_\ell} {}_{\mu_1 \dots \mu_\ell} \langle \beta_1, \dots, \beta_\ell | \tilde{\mathcal{T}}(0) | \emptyset \rangle}{\langle \mathcal{T} \rangle \langle \tilde{\mathcal{T}} \rangle} \\ &= (-1)^\ell \left| \frac{F_\ell^{\mathcal{T}|\mu_1 \dots \mu_\ell}(\beta_1, \dots, \beta_\ell)}{\langle \mathcal{T} \rangle^2} \right|^2 \end{aligned} \quad (6.51)$$

The same equality holds also for  $:\mathcal{T}\phi:$ , i.e.

$$\begin{aligned} & \frac{\langle \emptyset | : \mathcal{T}\phi : (0) | \beta_1, \dots, \beta_\ell \rangle_{\mu_1 \dots \mu_\ell} {}_{\mu_1 \dots \mu_\ell} \langle \beta_1, \dots, \beta_\ell | : \tilde{\mathcal{T}}\phi : (0) | \emptyset \rangle}{\langle : \mathcal{T}\phi : \rangle \langle : \tilde{\mathcal{T}}\phi : \rangle} \\ &= (-1)^\ell \left| \frac{F_\ell^{:\mathcal{T}\phi:|\mu_1 \dots \mu_\ell}(\beta_1, \dots, \beta_\ell)}{\langle : \mathcal{T}\phi : \rangle^2} \right|^2 \end{aligned} \quad (6.52)$$

Now we have the complete explicit expressions of the form factors of  $\mathcal{T}$  and  $:\mathcal{T}\phi:$  (and their conjugates) up to the three particle level. We can then study numerically the correlation functions  $\langle \mathcal{T}(0)\tilde{\mathcal{T}}(r) \rangle$  and  $\langle : \mathcal{T}\phi : (0) : \tilde{\mathcal{T}}\phi : (r) \rangle$ : not only we can evaluate these correlators at different values of the distance  $r$ , but we can also extract structural informations (like the short-distance scaling and the vacuum expectation value of these fields) using the method illustrated in Section 3.3.2.

## 6.2 Conformal Perturbation Theory

Before addressing the numerical evaluation of the correlation functions, we should analyse the expected short distance behaviour. Even though the form factor program is expected to work very well for large  $mr$ , it can also be used to probe the short-distance behaviour once enough particles have been taken into account. The ultraviolet behaviour can also be studied by another approach: the *conformal perturbation theory*.

### Massive integrable quantum field theory as perturbed conformal field theory

Let us start with the Lee-Yang model, as studied in [62]. The massive theory can be seen as the Lee-Yang minimal model  $\mathcal{M}(2,5)$  perturbed by the only non trivial field of the theory  $\phi \equiv \phi_{13} \equiv \phi_{12}$  with dimension  $\Delta = -\frac{1}{5}$ . The action of the perturbed theory can be written as

$$S = S_{CFT} + ih \int d^2x \phi(x) \quad (6.53)$$

where  $S_{CFT}$  is the unperturbed CFT action and  $h$  is some coupling constant, which is proportional to the mass gap ( $h \propto m^{2-\Delta}$ ).

A correlation function in the massive regime can be computed as an expansion involving conformal correlators [94, 95]<sup>3</sup>

$$\begin{aligned} \langle \mathcal{O}_A(0)\mathcal{O}_B(x) \rangle &= \sum_P \sum_{k=0}^{\infty} \frac{(-ih)^k}{k!} \langle \Phi_P \rangle \\ &\times \int_{reg} d^2y_1 \cdots d^2y_k \langle \mathcal{O}_A(0)\mathcal{O}_B(x)\phi(y_1) \cdots \phi(y_k)\Phi_P(\infty) \rangle_{CFT} \end{aligned} \quad (6.54)$$

where the first summation is over all fields  $\Phi_P$  appearing in the conformal Operator Product Expansion (OPE) between  $\mathcal{O}_A$  and  $\mathcal{O}_B$ . The objects appearing in the above integrals

---

<sup>3</sup>In the following integral all the infrared divergences have to be properly regularised.

are defined as

$$\langle X\Phi_P(\infty)\rangle_{CFT} \equiv \lim_{w\rightarrow\infty} \frac{\langle X\Phi_P(w)\rangle_{CFT}}{\langle \Phi_P(w)\Phi_P(0)\rangle_{CFT}} \quad (6.55)$$

and  $\langle X\Phi_P(\infty)\rangle_{CFT}$  can be (in principle) computed using conformal OPEs. Equivalently, correlation functions can be evaluated using perturbed OPEs, where the conformal structure constants are now functions of  $mr$  that can be evaluated perturbatively in series of  $h$ :

$$C_{\mathcal{O}_A\mathcal{O}_B}^{\Phi_P}(mr) = C_{\mathcal{O}_A\mathcal{O}_B}^{\Phi_P} + O(h) \quad (6.56)$$

This second approach is a consequence of (6.54), and the actual perturbative expansion of the structure constants can be recovered by comparing the two approaches.

Moreover, while vacuum expectation values vanish at the critical point ( $\langle\phi\rangle_{CFT} = 0$ ), they are finite outside the critical regime and they play a non trivial role in off-critical OPEs. A detailed and rigorous derivation of 6.54 can be found in [96]. Intuitively, it can be justified by considering the following argument. Consider the conformal OPE:

$$\mathcal{O}_A(0)\mathcal{O}_B(x) = \sum_P C_{AB}^P(x)\Phi_P(x) \quad (6.57)$$

Multiplying both sides by  $\Phi_Q(w)$  and taking the expectation value we have:

$$\langle \Phi_Q(x)\Phi_Q(w)\rangle C_{AB}^Q(x) = \langle \mathcal{O}_A(0)\mathcal{O}_B(x)\Phi_Q(w)\rangle \quad (6.58)$$

since  $\langle \Phi_P(x)\Phi_Q(w)\rangle = 0$  if  $P \neq Q$ . Such an argument can be used to compute two-point correlation functions:

$$\langle \mathcal{O}_A(0)\mathcal{O}_B(x)\rangle = \sum_P C_{AB}^P(x) \langle \Phi_P\rangle \quad (6.59)$$

Of course, since the theory is critical, the above sum is non trivial only for  $P = 1$  ( $\Phi_1 = \mathbf{1}$ ). Such an argument can then be extended to the massive regime by expanding the path integral correlation function

$$\langle X\rangle \propto \int \mathcal{D}\phi X e^{-S_{CFT} - ih \int d^2x \phi(x)}$$

around  $h = 0$ :

$$\langle X\rangle = \sum_{k=0}^{\infty} \frac{(-ih)^k}{k!} \int_{reg} d^2y_1 \cdots d^2y_k \langle X\phi(y_1)\cdots\phi(y_k)\rangle_{CFT} \quad (6.60)$$

**Example** In the Lee-Yang case, the correlation function of the field  $\phi$  is given by (at the critical point):

$$\langle \phi(0)\phi(r) \rangle_{CFT} = r^{\frac{4}{5}} (\langle \mathbf{1} \rangle_{CFT} + \dots) + C_{\phi\phi}^{\phi} r^{\frac{2}{5}} (\langle \phi \rangle_{CFT} + \dots) \quad (6.61)$$

where the structure constant is

$$C_{\phi\phi}^{\phi} = \frac{i \Gamma\left(\frac{1}{5}\right)^{\frac{3}{2}} \Gamma\left(\frac{2}{5}\right)^{\frac{1}{2}}}{5 \Gamma\left(\frac{4}{5}\right)^{\frac{3}{2}} \Gamma\left(\frac{3}{5}\right)^{\frac{1}{2}}} = i1.91131\dots \quad (6.62)$$

The expansion of the correlator in the massive theory is given by [62]

$$\langle \phi(0)\phi(r) \rangle = C_{\phi\phi}^{\mathbf{1}}(r) \langle \mathbf{1} \rangle + C_{\phi\phi}^{\phi}(r) \langle \phi \rangle + \dots \quad (6.63)$$

alternatively, can also be estimated using (6.54):

$$\langle \phi(0)\phi(r) \rangle = \langle \phi(0)\phi(r)\mathbf{1}(\infty) \rangle_{CFT} \langle \mathbf{1} \rangle + \langle \phi(0)\phi(r)\phi(\infty) \rangle_{CFT} \langle \phi \rangle + \dots \quad (6.64)$$

after having performed the limit, we have

$$\langle \phi(0)\phi(r)\mathbf{1}(\infty) \rangle_{CFT} = r^{\frac{4}{5}} \quad (6.65)$$

$$\langle \phi(0)\phi(r)\phi(\infty) \rangle_{CFT} = C_{\phi\phi}^{\phi} r^{\frac{2}{5}} \quad (6.66)$$

Comparing (6.63) and (6.64) we notice that the first terms of the expansion of the massive structure constant correspond to their conformal counterparts:

$$C_{\phi\phi}^{\mathbf{1}}(r) = 1 \times r^{\frac{4}{5}} + \dots \quad (6.67)$$

$$C_{\phi\phi}^{\phi}(r) = C_{\phi\phi}^{\phi} \times r^{\frac{2}{5}} + \dots \quad (6.68)$$

Of course, through a complete perturbative expansion further terms can be computed (see [62]) for more details).

The massive expansion can now be written as

$$\langle \phi(0)\phi(r) \rangle = r^{\frac{4}{5}} + r^{\frac{2}{5}} \langle \phi \rangle C_{\phi\phi}^{\phi} + \dots \quad (6.69)$$

It has been noticed [62] that the massive expansion *does not* tend to the ultraviolet scaling at short-distance! Since  $\langle \phi \rangle \neq 0$  outside the critical point, the  $r^{\frac{2}{5}}$  term is more relevant than  $r^{\frac{4}{5}}$  for small  $r$ , thus  $\langle \phi(0)\phi(r) \rangle \sim r^{\frac{2}{5}}$  at small distance. On the other hand, at the critical point  $\langle \phi(0)\phi(r) \rangle_{CFT} = r^{\frac{4}{5}}$  at any scale. This peculiar feature is due to the

non-unitary nature of the Lee-Yang model, which allows primary fields to have negative conformal dimensions.

We have just shown that the Lee-Yang model behaves in a quite surprising way in the short distance regime. We should then expect something similar also for the twist field case.

### 6.2.1 Twist field OPEs

In order to address the perturbative expansion of correlators involving twist fields, we should study their OPEs. When the fields  $\mathcal{T}$  and  $\tilde{\mathcal{T}}$  come close to each other, we would expect that only non-twist operators arise in the OPE. Non-twisted operators are simple combinations of fields belonging to different non-interacting copies of the theory which preserve cyclic symmetry of the model. We would not expect any twist fields arising from the OPE since the geometric structure will not be globally affected. Even though the field  $\mathcal{T}$  creates a branch cut, the geometry is “immediately” restored by  $\tilde{\mathcal{T}}$ . Thanks to the intrinsic permutation symmetry of twist fields, the collection of fields arising from their OPE has to be symmetric under permutation by construction. A generic field involved in the OPE has the following form ( $J = 1, 2, \dots, n$ ):

$$\Phi_{k_1 \dots k_J} = \frac{\phi_{k_1} \cdots \phi_{k_J} + \text{cyclic permutations}}{\#_{k_1 \dots k_J}} \quad (6.70)$$

where the symbol  $\#_{k_1 \dots k_J}$  counts the number of identical permutations and it is needed to avoid overcounting (each term of (6.70) then appears with coefficient one). In order to have a more consistent notation, we consider  $k_1 = 1 < k_2 < \dots < k_J$ . Consider, for instance, the case  $n = 4$ . The permutation

$$\phi_1 \phi_2 + \text{cyclic permutations} = \phi_1 \phi_2 + \phi_2 \phi_3 + \phi_3 \phi_4 + \phi_4 \phi_1 \quad (6.71)$$

does not require any adjustment, since all terms are different and they appear just once each. On the other hand, the term

$$\phi_1 \phi_3 + \text{cyclic permutations} = \phi_1 \phi_2 + \phi_2 \phi_3 + \phi_3 \phi_1 + \phi_4 \phi_2 = 2\phi_1 \phi_3 + 2\phi_2 \phi_4 \quad (6.72)$$

presents a double degeneracy and the coefficient  $\#_{13} = 2$  has a non trivial normalisation role. The general expressions for  $\#$  at  $J = 1, 2$  or  $3$  is given by:

$$\begin{aligned}
 \#_{1k} &= \begin{cases} 2 & n \text{ even} \wedge k = \frac{n}{2} + 1 \\ 1 & \text{otherwise} \end{cases} \\
 \#_{1kj} &= \begin{cases} 3 & k - 1 = j - k = n + 1 - j \\ 1 & \text{otherwise} \end{cases} \\
 \#_{1kjp} &= \begin{cases} 4 & k - 1 = j - k = p - j = n + 1 - p \\ 2 & k - 1 = p - j \neq j - k = n + 1 - p \\ 1 & \text{otherwise} \end{cases}
 \end{aligned} \tag{6.73}$$

By construction, the field  $\Phi_{k_1 \dots k_J}$  has conformal dimension  $J\Delta$ :

$$\begin{aligned}
 \langle \Phi_{k_1 \dots k_J}(0) \Phi_{k_1 \dots k_J}(0r) \rangle &= \frac{\langle \phi_{k_1}(0) \dots \phi_{k_J}(0) \phi_{k_1}(r) \dots \phi_{k_J}(r) \rangle + \text{other combinations}}{\#_{k_1 \dots k_J}^2} \\
 &= \frac{\langle \phi_{k_1}(0) \phi_{k_1}(r) \rangle \dots \langle \phi_{k_J}(0) \phi_{k_J}(r) \rangle + \text{other combinations}}{\#_{k_1 \dots k_J}^2} \\
 &= \frac{r^{-4\Delta} \dots r^{-4\Delta} + \text{other combinations}}{\#_{k_1 \dots k_J}^2} \\
 &= \frac{r^{-4J\Delta} + \text{other combinations}}{\#_{k_1 \dots k_J}^2}
 \end{aligned} \tag{6.74}$$

We can now write down the OPE of a twist field  $\mathcal{O} = \mathcal{T}, : \mathcal{T}\phi$ :

$$\begin{aligned}
 \mathcal{O}(x_1) \tilde{\mathcal{O}}(x_2) &\sim r^{-4\Delta_{\mathcal{O}}} \left( C_{\mathcal{O}\tilde{\mathcal{O}}}^{\mathbf{1}}(mr) \mathbf{1} + C_{\mathcal{O}\tilde{\mathcal{O}}}^{\Phi_1}(mr) r^{2\Delta} \Phi_1(x_2) \right. \\
 &\quad \left. + \sum_{k=2}^{\lfloor \frac{n}{2} \rfloor + 1} C_{\mathcal{O}\tilde{\mathcal{O}}}^{\Phi_{1k}}(mr) r^{4\Delta} \Phi_{1k}(x_2) + \dots + C_{\mathcal{O}\tilde{\mathcal{O}}}^{\Phi_{1 \dots n}}(mr) r^{2n\Delta} \Phi_{1 \dots n}(x_2) \right) \\
 &\quad + \text{Virasoro descendants}
 \end{aligned} \tag{6.75}$$

Since the various fields  $\phi_k$  are independent, their two-point functions vanish if the two indices  $k$  are different. Above  $r = |x_1 - x_2|$  and  $m$  is the mass of the Lee-Yang model. The first summation stops at  $\lfloor \frac{n}{2} \rfloor + 1$  in order to avoid repetitions in the  $\Phi_{1k}$  fields.

### Short-distance scaling

The first information that can be extracted from (6.75) is its short-distance scaling: at small  $mr$  correlation functions scale as

$$\langle \mathcal{O}(x_1) \tilde{\mathcal{O}}(x_2) \rangle \sim r^{-4\Delta_{\mathcal{O}} + 2n\Delta} \quad (6.76)$$

Like in the  $\langle \phi(x_1) \phi(x_2) \rangle$  case, the leading term does not scale as  $r^{-4\Delta_{\mathcal{O}}}$ .

This exponent can be easily checked numerically using form factors and it will be the first numerical check of the form factor program.

### Vacuum expectation value

Moreover, it is also possible to estimate the vacuum expectation value (VEV) of twist fields by comparing the form factor expansion with the short distance perturbative expansion. Typically, the form factor program is able to compute the coefficient  $\mathcal{K}_{\mathcal{O}}$  in the short distance expansion of local operators (3.114):

$$\frac{\langle \mathcal{O}(x_1) \tilde{\mathcal{O}}(x_2) \rangle}{\langle \mathcal{O} \rangle^2} = \mathcal{K}_{\mathcal{O}} r^{-4x_{\mathcal{O}}} + \dots \quad (6.77)$$

which, compared with (6.75) can be used to estimate the vacuum expectation value of the twist field. In order to do so, we have to compare the above equation with the short-distance limit of (6.75):

$$\langle \mathcal{O}(x_1) \tilde{\mathcal{O}}(x_2) \rangle \sim C_{\mathcal{O}\tilde{\mathcal{O}}}^{\Phi_{1\dots n}}(mr) r^{-4\Delta_{\mathcal{O}} + 2n\Delta} \langle \Phi_{1,\dots,n}(x_2) \rangle \quad (6.78)$$

Before extracting the VEV of the twist field, the values of  $C_{\mathcal{O}\tilde{\mathcal{O}}}^{\Phi_{1\dots n}}(mr)$  and  $\langle \Phi_{1,\dots,n}(x_2) \rangle$  have to be computed. The latter can be easily evaluated, since it is just a collection of independent fields and it is completely factorisable:

$$\langle \Phi_{1\dots n} \rangle = \frac{\langle \phi_1 \cdots \phi_n \rangle}{\#_{1\dots n}} = \frac{\langle \phi_1 \rangle \cdots \langle \phi_n \rangle}{\#_{1\dots n}} = \frac{\langle \phi \rangle^n}{\#_{1\dots n}} \quad (6.79)$$

The VEV of the field  $\phi$  can be computed exactly using the Thermodynamic Bethe Ansatz (TBA) and by solving numerically the thermodynamic Yang-Yang equation for the massive Lee-Yang model [62, 97]:

$$\langle \phi \rangle = \frac{5im^{-2/5}}{24\mathfrak{h}\sqrt{3}} \quad (6.80)$$

with  $\mathfrak{h} = 0.09704845636\dots$ .

The solution of the thermodynamic Yang-Yang equation [97] provides also a precise link between the mass  $m$  and the perturbative parameter  $h$ :

$$h = \mathfrak{h} m \tag{6.81}$$

The computation of structure constants is more complicated and it requires a deep analysis of the action of twist fields.

Since we are interested in the short distance behaviour we can consider the leading term of the expansion of the structure constants, which coincide with the respective conformal value:

$$C_{ab}^c(r) \sim C_{ab}^c + \dots \tag{6.82}$$

The conformal structure constant involving twist fields  $C_{\mathcal{O}\tilde{\mathcal{O}}}^a$  can be computed by comparing the twist field OPE expansion of correlators like  $\langle \mathcal{O}(x_1)\tilde{\mathcal{O}}(x_2)X \rangle$  with the equation 4.16 of Chapter 4. Using the OPE we have:

$$\frac{\langle \mathcal{T}(x_1)\tilde{\mathcal{T}}(x_2)X \rangle}{\langle \mathcal{T}(x_1)\tilde{\mathcal{T}}(x_2) \rangle} \sim r^{2\Delta_X} C_{\mathcal{T}\tilde{\mathcal{T}}}^X \langle X \rangle \tag{6.83}$$

The LHS of (6.83) is also the definition of the correlation function of the string of fields  $X$  on the Riemann manifold  $\mathcal{M}_n$ , i.e. it is equal to  $\langle X \rangle_{\mathcal{M}_n}$ . By direct comparison of this correlator with the RHS of (6.83), we can evaluate directly some structure constants. Unfortunately this method has some limitations, since the direct evaluation of  $\langle X \rangle_{\mathcal{M}_n}$  is not always straightforward and can be performed exactly only when  $X$  is a product of four or less fields. In these cases the value of the structure constants are given by:

$$\begin{aligned} C_{\mathcal{T}\tilde{\mathcal{T}}}^{\Phi_1} &= 0, \quad C_{\mathcal{T}\tilde{\mathcal{T}}}^{\Phi_{1,k}} = n^{-4\Delta} \left| 1 - e^{\frac{2\pi i(k-1)}{n}} \right|^{-4\Delta} \quad \text{for } k > 1, \\ C_{\mathcal{T}\tilde{\mathcal{T}}}^{\Phi_{1,k,j}} &= n^{-6\Delta} C_{\phi\phi}^\phi \left| \left( 1 - e^{\frac{2\pi i(k-1)}{n}} \right) \left( 1 - e^{\frac{2\pi i(j-1)}{n}} \right) \left( 1 - e^{\frac{2\pi i(j-k)}{n}} \right) \right|^{-2\Delta} \quad \text{for } j > k > 1, \\ C_{\mathcal{T}\tilde{\mathcal{T}}}^{\Phi_{1,k,j,p}} &= n^{-8\Delta} \left\langle \phi \left( e^{\frac{2\pi i}{n}} \right) \phi \left( e^{\frac{2\pi ik}{n}} \right) \phi \left( e^{\frac{2\pi ij}{n}} \right) \phi \left( e^{\frac{2\pi ip}{n}} \right) \right\rangle \quad \text{for } p > j > k > 1, \\ C_{\mathcal{T}\tilde{\mathcal{T}}}^{\Phi_1} &= n^{-2\Delta} C_{\phi\phi}^\phi, \quad C_{\mathcal{T}\tilde{\mathcal{T}}}^{\Phi_{1,k}} = n^{-4\Delta} \mathcal{F} \left( 1 - e^{\frac{2\pi i(k-1)}{n}} \right) \quad \text{for } k > 1 \end{aligned} \tag{6.84}$$

A detailed derivation of these constants can be found in Appendix B. The structure constants of the  $\mathcal{T}$  fields have been computed for the first time in [98].

For generic  $\Phi_{1k_2\dots k_J}$  fields, structure constants are given by:

$$C_{\mathcal{T}\tilde{\mathcal{T}}}^{\Phi_{1k_1\dots k_J}} = n^{-2J\Delta} \left\langle \phi \left( e^{\frac{2\pi i}{n}} \right) \phi \left( e^{\frac{2\pi i k_2}{n}} \right) \dots \phi \left( e^{\frac{2\pi i k_J}{n}} \right) \right\rangle \quad (6.85)$$

$$C_{\mathcal{T}\phi:\tilde{\mathcal{T}}\phi}^{\Phi_{1k_1\dots k_J}} = n^{-2J\Delta} \mathcal{F} \left( e^{\frac{2\pi i}{n}}, e^{\frac{2\pi i k_1}{n}}, \dots, e^{\frac{2\pi i k_J}{n}} \right) \quad (6.86)$$

where the function  $\mathcal{F}$  is a non universal, model-dependent building block of correlation functions:

$$\mathcal{F}(x_1, x_2, \dots) = \lim_{y \rightarrow \infty} |y|^{4\Delta} \langle \phi(0)\phi(1)\phi(y)\phi(x_1)\phi(x_2)\dots \rangle \quad (6.87)$$

Even though in principle all structure constants can be computed, only few can be actually evaluated. The main obstacle is the evaluation of many-point correlation functions. Note that in the case of composite twist field  $:\mathcal{T}\phi:$ , we can compute less structure constants than for  $\mathcal{T}$ . This difference is due to the fact that when computing correlation functions involving the composite twist field, two extra fields  $\phi$  appear in the correlation function, increasing the number of points by two.

Using conformal perturbation theory we managed to have a better understanding of the short distance behaviour of correlation functions of twist fields. We can use this knowledge for two purposes. We can check the accuracy of our form factor program, comparing the scaling dimension computed numerically against the theoretical value. Moreover, we can compute the vacuum expectation values of the twist fields, once we know the value of the structure constants, which can be computed in some cases.

## 6.3 Numerics

In this section we will firstly check the scaling obtained using the form factor program against that predicted by perturbative CFT in order to assess the accuracy of form factor expressions. Moreover such a program can also be used to compute the vacuum expectation values of twist fields as a form factor expansion.

From the form factor point of view, we will use equations (3.113) and (3.114) to compute the coefficients  $K_{\mathcal{O}}$  and  $x_{\mathcal{O}}$  of the correlator:

$$\frac{\langle \mathcal{O}(0)\tilde{\mathcal{O}}(0) \rangle}{\langle \mathcal{O} \rangle^2} = K_{\mathcal{O}} r^{-4x_{\mathcal{O}}} + \dots \quad \text{for } mr \rightarrow 0 \quad (6.88)$$

All the integrals appearing in this section have been computed using the Monte-Carlo integration algorithm. A short introduction to this method can be found in Appendix C.

### 6.3.1 Short distance scaling

Using (3.113) we can compute the scaling factor  $-4x_{\mathcal{O}}$  for the twist fields  $\mathcal{T}$  and  $:\mathcal{T}\phi:$  for some values of  $n$ :

$$\frac{\langle \mathcal{O}(0)\tilde{\mathcal{O}}(r) \rangle}{\langle \mathcal{O} \rangle^2} = K_{\mathcal{O}} r^{-4x_{\mathcal{O}}} + \dots \text{ for } mr \rightarrow 0 \quad (6.89)$$

which can be compared with the expected perturbative CFT scaling<sup>4</sup>

$$\langle \mathcal{O}(0)\tilde{\mathcal{O}}(r) \rangle_{CFT} = r^{-4d_{\mathcal{O}}} \quad (6.90)$$

The scaling factor  $d_{\mathcal{O}}$  has different values for the two twist fields:

$$\begin{aligned} 4d_{\mathcal{T}} &= 4\Delta_{\mathcal{T}} - 2n\Delta \\ 4d_{:\mathcal{T}\phi:} &= 4\Delta_{:\mathcal{T}\phi:} - 2n\Delta \end{aligned} \quad (6.91)$$

In the following sections we will compare the form factor expansion for  $x_{\mathcal{O}}$  against the perturbative prediction  $d_{\mathcal{O}}$ .

#### Simple twist field $\mathcal{T}$

The perturbative prediction for the short distance scaling of the correlator  $\langle \mathcal{T}(0)\tilde{\mathcal{T}}(r) \rangle$  is given by

$$-4d_{\mathcal{T}} = -4\Delta_{\mathcal{T}} + 2n\Delta \quad (6.92)$$

In the following table we compare this quantity against the form factor expansion (up to the three-particle level) for some values of  $n$ :

The form factor extrapolation of the scaling is compatible with the perturbative predictions and it is clear that the agreement improves adding more particles. Plotting the scaling obtained from the form factor expansion makes it clear that each time a particle is added to the expansion the prediction is more precise and closer to the perturbative CFT prediction (Figure 6.5).

---

<sup>4</sup>In the following we denote with  $-4d_{\mathcal{O}}$  the perturbative CFT scaling factor and with  $-4x_{\mathcal{O}}$  the form factor expansion of such a quantity. Of course we expect that these two quantities coincide when infinite form factor contributions are taken into account.

n	2	3	5	8	10
1-particle	0.209643	0.442562	0.861066	1.44896	1.83206
1+2-particles	0.259028	0.564549	1.10754	1.86697	2.3611
1+2+3-particles	0.279487	0.625075	1.23376	2.13554	2.70666
CFT ( $-4d_{\mathcal{T}}$ )	$\frac{3}{10} = 0.3$	$\frac{34}{45} = 0.756$	$\frac{38}{25} = 1.52$	$\frac{103}{40} = 2.575$	$\frac{163}{50} = 3.26$

Table 6.1: Scaling of the  $\langle \mathcal{T}(0)\tilde{\mathcal{T}}(r) \rangle$  correlation function. The perturbative CFT prediction is presented together with the one-, two- and three-particle form factor computation. Clearly, adding more particles, the form factors expansion approaches the perturbative prediction.

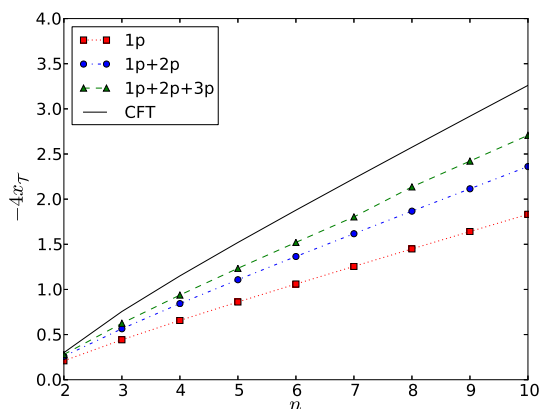


Figure 6.5: Scaling of the correlator  $\langle \mathcal{T}(0)\tilde{\mathcal{T}}(r) \rangle$ . The CFT prediction is given by the black solid line, while the one-, two- and three- particle form factor expansion are given respectively by the red squares, blue circles and green triangles.

### Composite twist field : $\mathcal{T}\phi$ :

As in the previous case, the short distance scaling of the composite twist field :  $\mathcal{T}\phi$  : can be computed using perturbative CFT and form factor expansion. The CFT approach gives:

$$-4d_{\mathcal{T}\phi} = -4\Delta_{\mathcal{T}\phi} + 2n\Delta \quad (6.93)$$

which can be checked against the form factors expansion:

Also in this case, the form factor extrapolation of the scaling is compatible with the perturbative predictions and it is clear that the agreement improves adding more particles. Plotting the scaling obtained from the form factors expansion makes clear that each time a particle is added to the expansion the prediction is more precise and closer to the perturbative CFT prediction (Figure 6.6).

n	2	3	5	8	10
1-particle	0.391185	0.572281	0.941564	1.499823	1.87287
1+2-particles	0.505165	0.737822	1.213628	1.931704	2.41539
1+2+3-particles	0.575841	0.843472	1.38907	2.21646	2.77169
CFT ( $-4d_{:\mathcal{T}\phi:}$ )	$\frac{7}{10} = 0.7$	$\frac{46}{45} = 1.022$	$\frac{42}{25} = 1.68$	$\frac{107}{40} = 2.675$	$\frac{167}{50} = 3.34$

Table 6.2: Scaling of the  $\langle : \mathcal{T}\phi : (0) : \tilde{\mathcal{T}}\phi : (r) \rangle$  correlation function. The perturbative CFT prediction is presented together with the one-, two- and three-particle form factor computation. Clearly, adding more particles, the form factors expansion approaches the perturbative prediction.

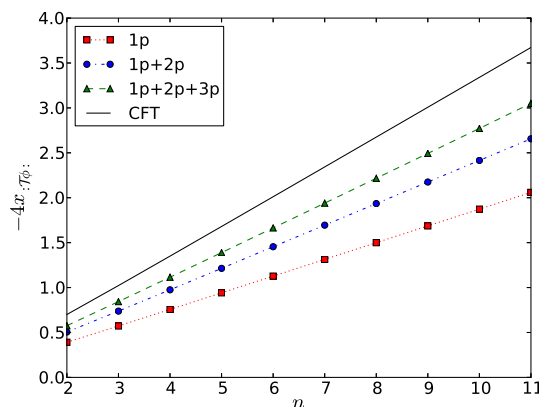


Figure 6.6: Scaling of the correlator  $\langle : \mathcal{T}\phi : (r) : \tilde{\mathcal{T}}\phi : (0) \rangle$ . The CFT prediction is given by the black solid line, while the one-, two- and three- particle form factor expansion are given respectively by the red squares, blue circles and green triangles.

In both cases ( $\mathcal{T}$  and  $:\mathcal{T}\phi:$ ) the form factors expansion recovers the relative perturbative CFT prediction of the scaling. This is not only a good test of the integration routines on their own, but it confirms also the identification of the two form factor series relative to the two twist fields (6.27).

### One-particle form factor contribution

Even though an infinite amount of form factor contributions are required to produce a perfect 100% agreement with the short distance perturbative approach, the most important contribution is given by the first few particles. The complicated expressions of the form factor contributions with two or more particles makes it very hard to estimate their contribution from the analytical point of view. On the other hand, the one-particle form

factor is simple enough to attempt an analytical study of its contribution, at least in the large  $n$  regime. Of course, we cannot directly compare the intricate one-particle form factor (6.27) with a perturbative conformal prediction of the scaling

$$-4d_{\mathcal{O}} = -4\Delta_{\mathcal{O}} + 2n\Delta = \left(2\Delta - \frac{c}{6}\right)n - \frac{\tilde{c}}{6}n^{-1}, \quad (6.94)$$

where  $\tilde{c}$  is equal to  $c$  or  $c_{\text{eff}}$  according to the choice of  $\mathcal{O} = \mathcal{T}, : \mathcal{T}\phi :$ .

The implicit  $n$  dependence of the one-particle form factor has to be extracted in order to do a direct comparison with the above equation.

This can be done in the large  $n$  limit, when a Laurent expansion of the form factor can be performed.

Isolating the first contribution of equation (3.113), it is clear that the one particle contribution is given by<sup>5</sup>

$$-4x_{\mathcal{O}}^{(1)} = \frac{n}{\pi} \left| \frac{F_1^{\mathcal{O}|1}}{\langle \mathcal{O} \rangle} \right|^2 \quad (6.95)$$

whose explicit expression is given by

$$\frac{n}{\pi} \left| \frac{F_1^{\mathcal{O}|1}}{\langle \mathcal{O} \rangle} \right|^2 = \frac{\sin \frac{\pi}{3n}}{2\pi \sin \frac{\pi}{6n} \sin \frac{\pi}{2n} f_n(i\pi)} \left( \cos \left( \frac{\pi}{3n} \right) \pm 2 \sin^2 \left( \frac{\pi}{6n} \right) \right)^2 \quad (6.96)$$

Apart from the  $f_n(i\pi)^{-1}$  contribution, all the other terms can be easily expanded for large  $n$ :

$$\begin{aligned} \frac{\sin \frac{\pi}{3n}}{2\pi \sin \frac{\pi}{6n} \sin \frac{\pi}{2n}} \left( \cos \left( \frac{\pi}{3n} \right) + 2 \sin^2 \left( \frac{\pi}{6n} \right) \right)^2 &= \frac{2n}{\pi^2} + \frac{1}{18n} + \frac{13\pi^2}{9720n^3} + O(n^{-5}) \\ \frac{\sin \frac{\pi}{3n}}{2\pi \sin \frac{\pi}{6n} \sin \frac{\pi}{2n}} \left( \cos \left( \frac{\pi}{3n} \right) - 2 \sin^2 \left( \frac{\pi}{6n} \right) \right)^2 &= \frac{2n}{\pi^2} - \frac{7}{18n} + \frac{173\pi^2}{9720n^3} + O(n^{-5}) \end{aligned} \quad (6.97)$$

---

<sup>5</sup>Here we denote with  $x_{\mathcal{O}}^{(1)}$  the one particle contribution of the scaling factor  $x_{\mathcal{O}}$ .

The expansion of the coefficient  $f_n(i\pi)^{-1}$  can be performed by expanding all terms of its infinite product representation:

$$\begin{aligned}
 f_n(i\pi)^{-1} &= \prod_{k=1}^{\infty} a_k(n) \\
 &= \prod_{k=1}^{\infty} \frac{\Gamma(kn + \frac{1}{2}) \Gamma(kn + \frac{7}{6}) \Gamma(kn + \frac{4}{3})}{\Gamma(kn + \frac{2}{3}) \Gamma(kn + \frac{5}{6}) \Gamma(kn + \frac{3}{2})} \\
 &\times \frac{\Gamma((k+1)n - \frac{1}{2}) \Gamma((k+1)n + \frac{1}{6}) \Gamma((k+1)n + \frac{1}{3})}{\Gamma((k+1)n - \frac{1}{3}) \Gamma((k+1)n - \frac{1}{6}) \Gamma((k+1)n + \frac{1}{2})}
 \end{aligned} \tag{6.98}$$

The large  $n$  scaling of the first  $a_k$  terms is given by

$$\begin{aligned}
 a_0(n) &= \frac{1}{2} \frac{\Gamma(\frac{5}{6})\Gamma(\frac{2}{3})}{\Gamma(\frac{4}{3})\Gamma(\frac{7}{6})} \left( 1 - \frac{1}{36n^2} - \frac{1}{36n^3} + O(n^{-4}) \right) \\
 a_1(n) &= 1 - \frac{5}{144n^2} + \frac{7}{288n^3} + O(n^{-4}) \\
 a_2(n) &= 1 - \frac{13}{1296n^2} + \frac{19}{7776n^3} + O(n^{-4}) \\
 a_3(n) &= 1 - \frac{25}{5184n^2} + \frac{37}{62208n^3} + O(n^{-4}) \\
 a_4(n) &= 1 - \frac{41}{14400n^2} + \frac{61}{288000n^3} + O(n^{-4}) \\
 a_5(n) &= 1 - \frac{61}{32400n^2} + \frac{91}{972000n^3} + O(n^{-4})
 \end{aligned} \tag{6.99}$$

Collecting all expansions together we can study the large  $n$  behaviour of the scaling dimension of the twist fields:

$$\begin{aligned}
 -4x_{\mathcal{I}\phi}^{(1)} &\approx \frac{1}{2} \frac{\Gamma(\frac{5}{6})\Gamma(\frac{2}{3})}{\Gamma(\frac{4}{3})\Gamma(\frac{7}{6})} \left( \frac{2n}{\pi^2} + \frac{1}{n} \left( -\frac{197}{2400\pi^2} + \frac{1}{18} \right) + O(n^{-3}) \right) \\
 &= (0.186944\dots)n - \frac{(0.0435792\dots)}{n} + O(n^{-3})
 \end{aligned} \tag{6.100}$$

$$\begin{aligned}
 -4x_{\mathcal{I}\mathcal{F}}^{(1)} &\approx \frac{1}{2} \frac{\Gamma(\frac{5}{6})\Gamma(\frac{2}{3})}{\Gamma(\frac{4}{3})\Gamma(\frac{7}{6})} \left( \frac{2n}{\pi^2} - \frac{1}{n} \left( \frac{197}{2400\pi^2} + \frac{7}{18} \right) + O(n^{-3}) \right) \\
 &= (0.186944\dots)n - \frac{(0.366434\dots)}{n} + O(n^{-3})
 \end{aligned} \tag{6.101}$$

where the  $n^{-1}$  term has been computed using up to  $k = 5$  contributions. The subsequent contributions can be safely dropped since the  $a_6$  term would have had a negligible contribution of magnitude 0.001.

This one-particle approximation can be compared with the expected CFT prediction of:

$$\begin{aligned} -4d:\mathcal{T}\phi &= (0.33333\dots)n + \frac{(0.06666\dots)}{n} \\ -4d\mathcal{T} &= (0.33333\dots)n - \frac{(0.73333\dots)}{n} \end{aligned} \quad (6.102)$$

A direct comparison immediately shows that the one-particle term contributes for about 50% of the scaling dimension's value. In particular, it provides 56% of the  $n$  coefficient and 65% (49%) of the  $n^{-1}$  coefficient for the  $:\mathcal{T}\phi:(\mathcal{T})$  case.

We can now use the form factor expansion to address a much more complicated problem, the evaluation of the vacuum expectation values of these fields, which cannot be computed using a perturbative CFT approach.<sup>6</sup>

### 6.3.2 Vacuum expectation values $\langle\mathcal{T}\rangle$ and $\langle:\mathcal{T}\phi:\rangle$

The short-distance form factor expansion can be used not only to extrapolate the ultraviolet scaling of correlation functions, but it also reveals precious information concerning other numerical constants:

$$\frac{\langle\mathcal{O}(r)\tilde{\mathcal{O}}(0)\rangle}{\langle\mathcal{O}\rangle^2} = K_{\mathcal{O}} r^{-4x_{\mathcal{O}}} + \dots \text{ for } mr \rightarrow 0 \quad (6.103)$$

Since the value of the constant  $K_{\mathcal{O}}$  can be computed as a form factor expansion, the above equation can be compared with its perturbative CFT equivalent in order to estimate the vacuum expectation value (VEV) of the operator  $\mathcal{O}$ .

As shown in Section 6.2, at short distances the leading term of the perturbative expansion is given by

$$\langle\mathcal{O}(r)\tilde{\mathcal{O}}(0)\rangle \sim C_{\mathcal{O}\tilde{\mathcal{O}}}^{\Phi_{1\dots n}} \langle\phi\rangle^n r^{-4d_{\mathcal{O}}} \quad (6.104)$$

Comparing the two expansions, the VEV of the operator  $\mathcal{O}$  is given by

$$\langle\mathcal{O}\rangle = \sqrt{\frac{C_{\mathcal{O}\tilde{\mathcal{O}}}^{\Phi_{1\dots n}} \langle\phi\rangle^n}{K_{\mathcal{O}}}} \quad (6.105)$$

while there is no theoretical upper limit on the value of  $n$  for the computation of  $K_{\mathcal{O}}$ , the conformal structure constant  $C$  depends on  $n$ -point correlation functions (or  $n+2$ -point for composite twist fields). For this reason, this method can be used to compute the VEV

<sup>6</sup>In some other cases, e.g. Free Fermions, the VEV  $\langle\mathcal{T}\rangle$  of the twist field can be computed using alternative approaches [14].

of a twist fields only for  $n$  up to 4 (or up to 2 in the composite case).

**The  $n = 2$  case**

In the  $n = 2$  case, the CFT structure constant can be computed for both twist fields  $\mathcal{T}$  and  $:\mathcal{T}\phi:$ . Using the results obtained in Section 6.2, we have:

$$\begin{aligned} C_{\mathcal{T}\tilde{\mathcal{T}}}^{\Phi_{12}} &= 2^{-8\Delta} = 4.6566\dots \\ C_{:\mathcal{T}\phi:;\tilde{\mathcal{T}}\phi}^{\Phi_{12}} &= 2^{-4\Delta}\mathcal{F}(2) = -5.5370\dots \end{aligned} \tag{6.106}$$

Using the form factor program, the constants  $K_{\mathcal{O}}$  can be computed (at three-particle level):

$$\begin{aligned} K_{\mathcal{T}} &\sim 1.35236\dots \\ K_{:\mathcal{T}\phi:} &\sim 1.95908\dots \end{aligned} \tag{6.107}$$

Using these results we can estimate the VEVs of  $\mathcal{T}$  and  $:\mathcal{T}\phi:$  as a function of the mass gap  $m$ :

$$\begin{aligned} \langle \mathcal{T} \rangle &\sim i1.8555 m^{-\frac{11}{20}} \\ \langle : \mathcal{T}\phi : \rangle &\sim 2.0837 m^{-\frac{3}{4}} \end{aligned} \tag{6.108}$$

The imaginary nature of the  $n = 2$  VEV of  $\mathcal{T}$  should not surprise: the VEV of the Lee Yang field itself is purely imaginary [97]. We believe that the VEV of the composite field is real because of the two purely imaginary contributions ( $\mathcal{T}$  and  $\phi$ ).

**6.3.3 The  $n = 3, 4$  cases**

As we said before, the most relevant conformal structure constant in the short-distance OPE of two fused twist fields  $:\mathcal{T}\phi:$  is given by  $n+2$ -point correlation functions. For this reason the  $n = 3$  and  $n = 4$  cases can be addressed only for the field  $\mathcal{T}$ . The most relevant structure constants involving twist fields  $\mathcal{T}$  for  $n = 3, 4$  are given by:

$$\begin{aligned} C_{\mathcal{T}\tilde{\mathcal{T}}}^{\Phi_{123}} &= 3^{-9\Delta}C_{\phi\phi}^{\phi} = i13.8086\dots && \text{for } n = 3 \\ C_{\mathcal{T}\tilde{\mathcal{T}}}^{\Phi_{1234}} &= 4^{-8\Delta}\langle \phi(i)\phi(-1)\phi(-i)\phi(1) \rangle = -50.8836\dots && \text{for } n = 4 \end{aligned} \tag{6.109}$$

These values, together with three-particle level form factor expansion for the constants  $K_{\mathcal{T}}$ :

$$\begin{aligned} K_{\mathcal{T}} &= 2.02966\dots & \text{for } n &= 3 \\ K_{\mathcal{T}} &= 3.48758\dots & \text{for } n &= 4 \end{aligned} \tag{6.110}$$

give the estimate of the VEV of  $\mathcal{T}$  for  $n = 2$  and  $n = 4$ :

$$\begin{aligned} \langle \mathcal{T} \rangle &= 3.59903m^{-\frac{44}{45}} & \text{for } n &= 3 \\ \langle \mathcal{T} \rangle &= i6.44411m^{-\frac{11}{8}} & \text{for } n &= 4 \end{aligned} \tag{6.111}$$

As before, the imaginary VEV is not a surprise and it is due to the non unitary nature of the model.

The knowledge of the VEV plays a central role also in the actual evaluation of correlation functions  $\langle \mathcal{O}(0)\tilde{\mathcal{O}}(r) \rangle$  at different values of  $r$ , since all form factors are proportional to the VEV itself. The estimations of the constants  $K_{\mathcal{O}}$  and  $x_{\mathcal{O}}$  require only “rescaled” form factors  $|F_k^{\mathcal{O}}|^2 / \langle \mathcal{O} \rangle^2$  and they can be computed without knowing the actual value of the VEV  $\langle \mathcal{O} \rangle$  a priori. On the other hand, the form factor expansion of correlation functions  $\langle \mathcal{O}(0)\tilde{\mathcal{O}}(r) \rangle$  involves “non rescaled” form factors  $|F_k^{\mathcal{O}}|^2$ , which depend on the VEV  $\langle \mathcal{O} \rangle$  explicitly.

The short distance form factor expansion of the constant  $K_{\mathcal{O}}$  gives then vital information about the VEV. Such values can now be used to compare directly the perturbative CFT approach and the form factor expansion at different values of the distance  $r$ .

### 6.3.4 Perturbative CFT vs form factor expansion

Once we have estimated the vacuum expectation values of twist fields in some cases, we can compare the form factor expansion with the perturbative CFT prediction at different values of the distance  $r$ .

While in the previous section we checked the short-distance form factor expansion only against the most relevant perturbative CFT contribution, here we take into account all the possible contributions of the zeroth order perturbative approach<sup>7</sup>. Since we will compare the two approaches at different values of  $r$ , we include the extra terms in order to have a more genuine prediction of the scaling of the correlation function.

<sup>7</sup>The complete perturbative series will include contributions not only from primary states, but also from their descendants. The zeroth order expansion takes into account only the primary fields’ contributions and it does not consider all the descendants’ contributions. For instance, equation (6.75) is a zeroth order perturbative expansion once removed the “+Virasoro descendants” contributions.

### Composite twist field : $\mathcal{T}\phi$ : at $n = 2$

Let us start with the  $n = 2$  composite twist field :  $\mathcal{T}\phi$  :, which is the only configuration that can be studied with perturbative CFT, since its structure constants require the knowledge of up to four-point CFT correlation functions of the field  $\phi$ . The complete zeroth order perturbative expansion of the two-point correlation function is given by:

$$\langle : \mathcal{T}\phi : (0) : \tilde{\mathcal{T}}\phi : (r) \rangle = r^{-4\Delta_{\mathcal{T}\phi}} \left( 1 + 2C_{\mathcal{T}\phi:\tilde{\mathcal{T}}\phi}^{\Phi_1} r^{2\Delta_{\phi}} \langle \phi \rangle + C_{\mathcal{T}\phi:\tilde{\mathcal{T}}\phi}^{\Phi_{12}} r^{4\Delta_{\phi}} \langle \phi \rangle^2 \right) + \dots \quad (6.112)$$

Using the VEV computed in Section 6.3.2, we can compare the above perturbative expansion with the form factor estimate (up to three particles).

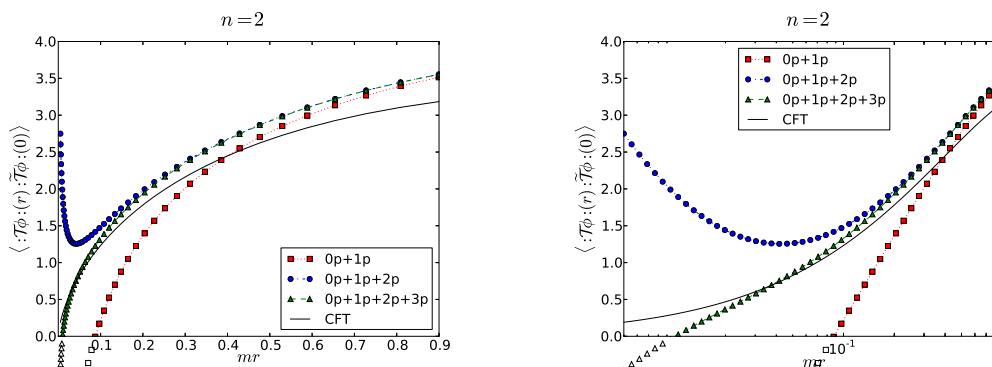


Figure 6.7: Comparison between the perturbative (solid black line) and form factor (coloured points) expansion using linear (left) and logarithmic (right) scales.

From Figure 6.7 it is clear that, while the long range scaling can be easily achieved even with just one particle, the ultraviolet regime requires more particles in order to be more consistent with the perturbative approach. It is important to notice that the normalised form factor expansion used here is affected by *two* truncations. The correlation function itself is computed using a truncated form factor expansion. The vacuum expectation value  $\langle : \mathcal{T}\phi : \rangle$  (which all form factors are proportional to) is estimated using a form factor expansion truncated at the three-particle level.

### Twist Field $\mathcal{T}$ at $n = 2, 3$ and 4

From the qualitative point of view, correlators involving twist fields  $\mathcal{T}$  behave in very similar way to correlation functions of composite fields :  $\mathcal{T}\phi$  :.

The complete perturbative expansion at zeroth order is given by:

$$\begin{aligned} \langle \mathcal{T}(r)\tilde{\mathcal{T}}(0) \rangle &= r^{-4\Delta\tau} \left[ 1 + 4C_{\mathcal{T}\tilde{\mathcal{T}}}^{\Phi_1} r^{2\Delta} \langle \phi \rangle + \left( 4\tilde{C}_{\mathcal{T}\tilde{\mathcal{T}}}^{\Phi_{12}} + 2C_{\mathcal{T}\tilde{\mathcal{T}}}^{\Phi_{13}} \right) r^{4\Delta} \langle \phi \rangle^2 \right. \\ &\quad \left. + 4C_{\mathcal{T}\tilde{\mathcal{T}}}^{\Phi_{123}} r^{6\Delta} \langle \phi \rangle^3 + C_{\mathcal{T}\tilde{\mathcal{T}}}^{\Phi_{1234}} r^{8\Delta} \langle \phi \rangle^4 \right] + \dots \end{aligned} \quad (6.113)$$

Of course, some of the terms of the above equation vanish for  $n$  less than four. For instance, for  $n$  equal to two, non vanishing structure constants involve up to two fields (one for each copy) and the series is truncated after  $C_{\mathcal{T}\tilde{\mathcal{T}}}^{\Phi_{12}}$ .

Using the value of  $\langle \mathcal{T} \rangle$  computed in the previous section, we can now compute the correlation functions using form factors and compare this estimate with the perturbative approach. Since the VEV of  $\mathcal{T}$  is complex for even values of  $n$ , correlators have negative values in such cases. In order to appreciate the different behaviours of the various cases, we plot the correlators with switched sign when needed.

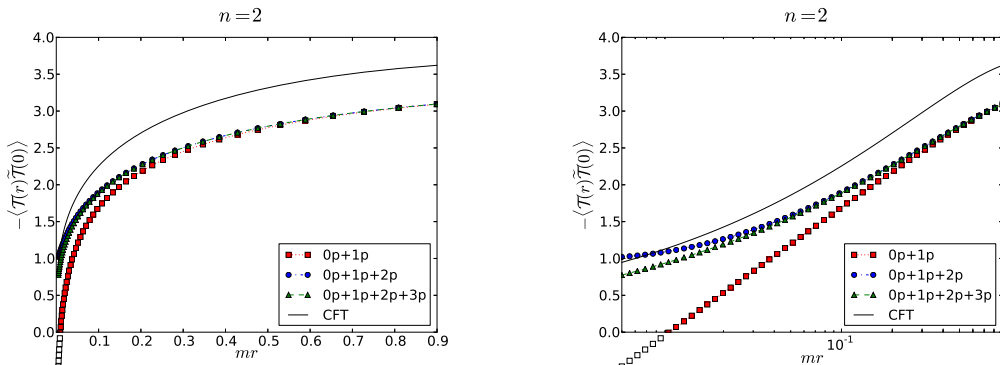


Figure 6.8: Comparison between the perturbative (solid black line) and form factor (coloured points) expansion using linear (left) and logarithmic (right) scales.

Like in the previous case, the form factor expansion does not agree perfectly with the perturbative CFT approach to all values of  $mr$ .

Moreover, some correlators recover the expected ultraviolet scaling better than others. In particular, the agreement is better for lower  $n$ . From a qualitatively point of view, this feature can be explained by the zeroth order truncation. Since the scaling dimension of the field involves increased linearly with  $n$ , sub-leading corrections are more relevant for large  $n$ .<sup>8</sup>

<sup>8</sup>For instance, the first sub-leading correction inside the identity's Virasoro tower is proportional to

$$\int dy \langle \mathcal{T}(0)\tilde{\mathcal{T}}(r)\phi(y) \rangle_{CFT} \propto r^{-4\Delta\tau+2\Delta\phi}$$

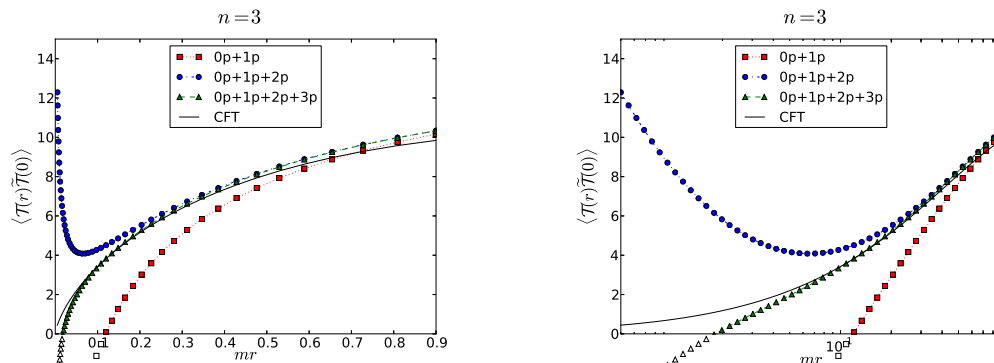


Figure 6.9: Comparison between the perturbative (solid black line) and form factor (coloured points) expansion using linear (left) and logarithmic (right) scales.

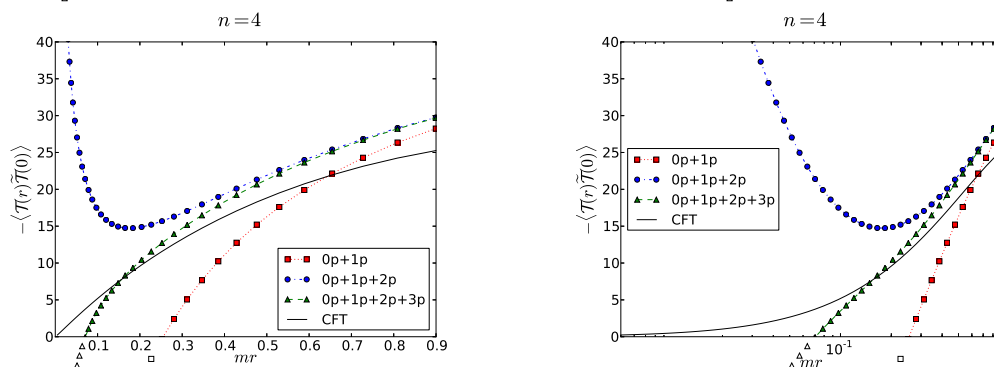


Figure 6.10: Comparison between the perturbative (solid black line) and form factor (coloured points) expansion using linear (left) and logarithmic (right) scales.

In both cases ( $\mathcal{T}$  and  $:\mathcal{T}\phi:$ ) the agreement between the two expansions is not always perfect. This difference is somehow expected and it is due to the different regimes of validity of the two approaches. While the perturbative CFT approach is valid for very small  $mr$ , the form factor approach is naturally more precise in the opposite regime, i.e. for large  $mr$ . Moreover, the conformal perturbative approach we used is truncated at the zeroth order. Such a truncation, even though is very precise at ultraviolet scales, fails to properly describe the infrared regime.

Nevertheless, the comparison is quite encouraging and it is a very strong hint that the form factors we are looking at are the right ones to describe both twist fields of the Lee-Yang model.

We can now address the evaluation of entanglement entropy from the form factor expansion

---

while the zeroth order contribution scales with  $r^{-4\Delta_{\mathcal{T}}}$ . Since  $\Delta_{\mathcal{T}}$  grows with  $n$ , the first order contribution is more relevant for large  $n$ .

sion.

## 6.4 Entanglement Entropy

In previous sections we evaluated form factor expansions for the correlators of both twist fields  $\mathcal{T}$  and  $:\mathcal{T}\phi:$  for the Lee Yang theory.

While the short distance behaviour of the entanglement entropy has a clear universal logarithmic scaling [1], it saturates to a constant in the long distance infrared regime. As long as the mass scale of the system is much greater than the inverse size of the subsystem ( $r \ll \xi = m^{-1}$ ), the entropy scales as if the system was critical:

$$S \sim \frac{c_{\text{eff}}}{3} \log \frac{r}{\varepsilon} \quad (6.114)$$

where  $\varepsilon$  is some ultraviolet normalisation cut-off.

In the opposite regime ( $mr \gg 1$ ) the mass scale breaks completely the conformal invariance and the entropy saturates to a constant:

$$S \sim -\frac{c_{\text{eff}}}{3} \log m\varepsilon \quad (6.115)$$

These two regimes are connected, as they describe the same quantity at two different scales  $mr \ll 1$  and  $mr \gg 1$ . The form factor expansion can be used to estimate how the entropy approaches its saturation value in the intermediate region  $mr \approx 1$ . Even though it saturates to a constant for large values of  $mr$ , we would like to compute the behaviour of the entropy in the intermediate region  $mr \approx 1$ . Using form factors we can analyse the various corrections to this saturation. Given the nature of the form factor expansion, we expect that it will give exponentially decaying corrections to saturation.

### 6.4.1 Saturation

Before addressing the computation of the correction to saturation, we can have a closer look at the saturation value of the entropy (6.115). We know that this constant depends on the mass gap of the system, but we would like to know if it depends also on some other physical properties of the system.

As we have seen in Chapter 5, the entanglement entropy of a non unitary system can be represented via correlation functions involving composite twist fields  $:\mathcal{T}\phi:$  and the

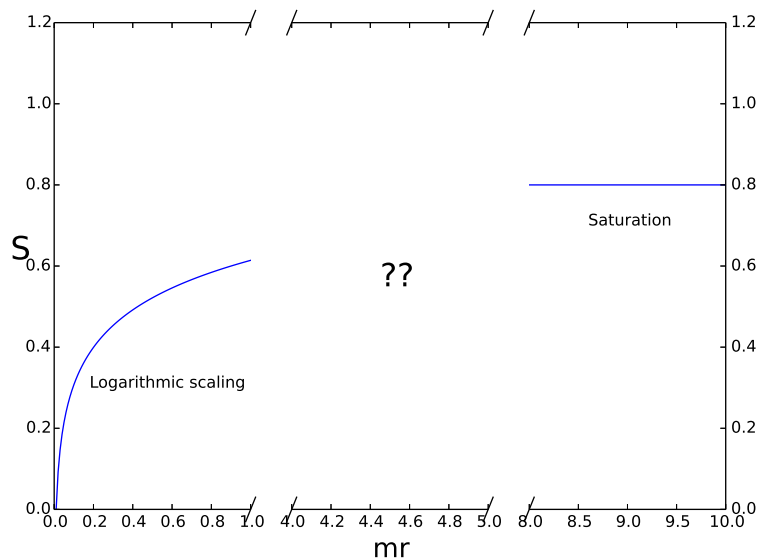


Figure 6.11: Scaling of entanglement entropy at different scales. Near the critical point ( $mr \ll 1$ ) it scales logarithmically according to the CFT prediction. At the other end of the scale, in the infrared regime ( $mr \gg 1$ ), the entropy is constant. Less is known about the behaviour of the entropy in the intermediate region. The form factor expansion can be used to estimate how the entropy tends to its saturation value.

field  $\phi$  responsible for the creation of the ground state:

$$S(r) = - \lim_{n \rightarrow 1} \frac{d}{dn} \left[ \mathcal{Z}_n \varepsilon^{\frac{c_{\text{eff}}}{6} (n - \frac{1}{n})} \frac{\langle : \mathcal{T} \phi : (0) : \tilde{\mathcal{T}} \phi : (r) \rangle}{\langle \phi(0) \phi(r) \rangle^n} \right] \quad (6.116)$$

In order to separate the saturation from its correction, we split the above equation in order to isolate all the terms which depend on  $r$ :

$$S(r) = - \lim_{n \rightarrow 1} \frac{d}{dn} \left[ \mathcal{Z}_n \varepsilon^{\frac{c_{\text{eff}}}{6} (n - \frac{1}{n})} \frac{\langle : \mathcal{T} \phi : \rangle^2}{\langle \phi \rangle^{2n}} \right] - \lim_{n \rightarrow 1} \frac{d}{dn} \frac{A(r, n)}{B(r)^n} \quad (6.117)$$

where the two functions  $A$  and  $B$  are simply rescaled correlators:

$$A(r, n) = \frac{\langle : \mathcal{T} \phi : (0) : \tilde{\mathcal{T}} \phi : (r) \rangle}{\langle : \mathcal{T} \phi : \rangle^2} \quad (6.118)$$

$$B(r) = \frac{\langle \phi(0) \phi(r) \rangle}{\langle \phi \rangle^2} \quad (6.119)$$

These expressions can be further rearranged in order to highlight the various contributions:

$$\begin{aligned}
 S(r) &= -\frac{c_{\text{eff}}}{3} \log m\varepsilon \\
 &- \lim_{n \rightarrow 1} \frac{d}{dn} \left[ m^{-\frac{c_{\text{eff}}}{6}(n-\frac{1}{n})} \frac{\langle : \mathcal{T}\phi : \rangle^2 \left( \frac{C_{\phi\phi}^\phi}{C_{:\mathcal{T}\phi:\mathcal{T}\phi}^{\Phi_{1\dots n}}} \right)^n}{\langle \phi \rangle^{2n}} \right] \\
 &- \lim_{n \rightarrow 1} \frac{d}{dn} \left[ \mathcal{Z}_n - \frac{\left( C_{\phi\phi}^\phi \right)^n}{C_{:\mathcal{T}\phi:\mathcal{T}\phi}^{\Phi_{1\dots n}}} \right]
 \end{aligned} \tag{6.120}$$

Such a rearrangement is not casual: the entire second line can be expressed in terms of form factors. Using equation (6.105) we have

$$\langle : \mathcal{T}\phi : \rangle^2 = m^{4\Delta_{\mathcal{T}\phi}} \frac{C_{:\mathcal{T}\phi:\mathcal{T}\phi}^{\Phi_{1\dots n}} \langle \phi \rangle^n}{K_{:\mathcal{T}\phi}} \tag{6.121}$$

$$\langle \phi \rangle^2 = m^{4\Delta_\phi} \frac{C_{\phi\phi}^\phi}{K_\phi} \tag{6.122}$$

The second line of (6.120) can then be expressed as

$$U \equiv - \lim_{n \rightarrow 1} \frac{d}{dn} \left[ m^{-\frac{c_{\text{eff}}}{6}(n-\frac{1}{n})} \frac{\langle : \mathcal{T}\phi : \rangle^2 \left( \frac{C_{\phi\phi}^\phi}{C_{:\mathcal{T}\phi:\mathcal{T}\phi}^{\Phi_{1\dots n}}} \right)^n}{\langle \phi \rangle^{2n}} \right] = - \lim_{n \rightarrow 1} \frac{d}{dn} \frac{K_\phi^n}{K_{:\mathcal{T}\phi}} \tag{6.123}$$

Thanks to its arbitrariness, the ultraviolet cut-off  $\varepsilon$  can be rescaled in order to absorb the last term of equation (6.120)

$$\frac{c_{\text{eff}}}{3} \log m\varepsilon \rightarrow \frac{c_{\text{eff}}}{3} \log m\epsilon \equiv \frac{c_{\text{eff}}}{3} \log m\varepsilon + \lim_{n \rightarrow 1} \frac{d}{dn} \left[ \mathcal{Z}_n - \frac{\left( C_{\phi\phi}^\phi \right)^n}{C_{:\mathcal{T}\phi:\mathcal{T}\phi}^{\Phi_{1\dots n}}} \right] \tag{6.124}$$

Thanks to this manipulation the entropy is given by

$$S(r) = -\frac{c_{\text{eff}}}{3} \log m\epsilon + U - \lim_{n \rightarrow 1} \frac{d}{dn} \frac{A(r, n)}{B(r)^n} \tag{6.125}$$

Thus, the saturation value of entanglement entropy is given by two contributions: the model dependent constant  $U$  and the logarithmic term which depends on the mass gap  $m$ . Of course, the ultraviolet cut-off  $\epsilon$  still appears in the scaling of the entropy. It is not universal and depends on the physical realisation of the model.<sup>9</sup> This is not a surprise:

<sup>9</sup>For instance, if we consider a field theory as the scaling limit of a lattice model, the short distance cut-off  $\epsilon$  can be interpreted as the lattice spacing.

ultraviolet divergences are often present when predicting observable physical quantities using quantum field theory. Luckily, if we use the same cut-off in both long and short distance scales, we can still extract universal information about entanglement entropy using QFT. Consider the two regimes (without taking into account the corrections to saturation):

$$S(r) \sim \begin{cases} \frac{c_{\text{eff}}}{3} \log \frac{r}{\epsilon} & mr \ll 1 \\ -\frac{c_{\text{eff}}}{3} \log m\epsilon + U & mr \gg 1 \end{cases} \quad (6.126)$$

The short distance scaling can then be used to “calibrate” the model [99]. Suppose, for instance, to study a near-to-critical ( $m \ll 1$ ) system. Using an alternative method (e.g. a numerical computation like DMRG), we can extrapolate the value of  $\epsilon$  from  $S(r) \sim \frac{c_{\text{eff}}}{3} \log \frac{r}{\epsilon}$ . Once the value of  $\epsilon$  is known, it can be used to estimate  $U$ , even though it is not universal but it depends on the microscopic properties of the model studied. Since there is no restriction, we can choose the same ultraviolet cutoff in both regimes.

One of the strengths of the form factor expansion is that we can estimate the universal constant  $U$  (6.123) as:

$$U = -\lim_{n \rightarrow 1} \frac{d}{dn} \frac{K_{\phi}^n}{K_{\mathcal{T}\phi}} \quad (6.127)$$

Since the constant  $K$  can be computed as form factor expansion, the above formula is a powerful recipe, which can also be extended to the unitary case:

$$U = -\lim_{n \rightarrow 1} \frac{d}{dn} \frac{1}{K_{\mathcal{T}}} \quad (6.128)$$

Even though  $K_{\mathcal{T}\phi}$  (or  $K_{\mathcal{T}}$ ) are hard to compute analytically, in principle it is possible to construct an interpolating function from their numerical estimate.

### 6.4.2 Corrections to saturation

We can now address the study of the corrections to saturation, i.e. how the entropy approaches its saturation value at large  $mr$ .

The correction to saturation is given by:

$$\lim_{n \rightarrow 1} \frac{d}{dn} \frac{A(r, n)}{B(r)^n} = \lim_{n \rightarrow 1} \frac{A'(r, n) - A(r, n) \log B(r)}{B(r)^n} = \frac{A'(r, 1)}{B(r)} - \log B(r) \quad (6.129)$$

The above expression cannot be computed directly using form factors. It involves a derivative, a logarithm and a division. These operations can be addressed in a easier way by expanding the functions  $A$  and  $B$ , highlighting each form factor contribution.

Let us expand the functions  $A$  and  $B$  to highlight the one- and two-particle contributions:

$$A(r, n) = 1 + A_1(r, n) + A_2(r, n) + \dots \quad (6.130)$$

$$B(r) = 1 + B_1(r) + B_2(r) + \dots \quad (6.131)$$

Of course, since they are correlators normalised by the VEVs of the fields involved, the zero-particle contribution is one. In our approach, we truncate the expansion at the two-particle level, since, as we will show in this section, the two-particle contribution is already strongly shadowed by the one-particle contribution at large distance  $mr \gg 1$ .

We can now study the explicit expression of the above contributions  $A_i$  and  $B_i$ , whose values at  $n = 1$  (together with their derivative obtained from analytical continuation in  $n$ ) will be used to compute the various contributions to the corrections.

#### **A terms**

Let us now focus on the  $A_i$ s terms, i.e. the ones coming from the form factor expansion of the twist field correlators.

By definition we have

$$A_1(r, n) = - \sum_{i=1}^n \int \frac{d\beta}{2\pi} \left| \frac{F_1^{\mathcal{T}\phi|i}}{\langle \mathcal{T}\phi \rangle} \right|^2 e^{-mr \cosh \beta} = - \frac{n}{\pi} \left| \frac{F_1^{\mathcal{T}\phi|1}}{\langle \mathcal{T}\phi \rangle} \right|^2 K_0(mr) \quad (6.132)$$

where we have used the fact that the one-particle form factor does not depend on the copy number  $j$  or the rapidity  $\beta$ . In the above equation  $K_0$  is a modified Bessel function of the second kind [49]

$$K_\nu(z) = \int_0^\infty dt t^\nu e^{-z \cosh t} \quad (6.133)$$

The two-particle contribution is given by:

$$\begin{aligned}
 A_2(r, n) &= \frac{1}{2!} \sum_{i,j=1}^n \int \frac{d^2\beta}{(2\pi)^2} \left| \frac{F_2^{\mathcal{T}\phi|ij}(\beta_1, \beta_2)}{\langle : \mathcal{T}\phi : \rangle} \right|^2 e^{-mr(\cosh \beta_1 + \cosh \beta_2)} \\
 &= n \sum_{j=1}^n \int_{-\infty}^{\infty} \frac{d\beta}{(2\pi)^2} \left| \frac{F_2^{\mathcal{T}\phi|11}(\beta - 2\pi i(j-1))}{\langle : \mathcal{T}\phi : \rangle} \right|^2 K_0 \left( 2mr \cosh \frac{\beta}{2} \right)
 \end{aligned} \tag{6.134}$$

### B terms

Similarly to the  $A$ s case, we can write explicitly the one- and two-particle contributions of the form factor expansion of the  $\langle \phi(r)\phi(0) \rangle$  correlation function. The form factors for the  $\phi$  field have been computed in [62]. Alternatively, one can use the form factors of  $: \mathcal{T}\phi :$  and set  $n$  to one.

$$\begin{aligned}
 B_1(r) &= - \int_{-\infty}^{\infty} \frac{d\beta}{2\pi} \left| \frac{F_1^\phi}{\langle \phi \rangle} \right|^2 e^{-rm \cosh \beta} = - \frac{1}{\pi} \left| \frac{F_1^\phi}{\langle \phi \rangle} \right|^2 K_0(mr) \\
 &= - \frac{2}{3^{1/2} \pi f(\frac{2\pi i}{3}, 1)^2} K_0(mr)
 \end{aligned} \tag{6.135}$$

The two-particle contribution is given by:

$$\begin{aligned}
 B_2(r) &= \frac{1}{2} \int_{-\infty}^{\infty} \int_{-\infty}^{\infty} \frac{d\beta^2}{(2\pi)^2} \left| \frac{F_2^\phi(\beta_1 - \beta_2)}{\langle \phi \rangle} \right|^2 e^{-rm \cosh \beta_1 - rm \cosh \beta_2} \\
 &= \int_{-\infty}^{\infty} \frac{d\beta}{(2\pi)^2} \left| \frac{F_2^\phi(\beta)}{\langle \phi \rangle} \right|^2 K_0 \left( 2mr \cosh \frac{\beta}{2} \right).
 \end{aligned} \tag{6.136}$$

### Derivatives of $A$ s

The main difficulty in taking the derivative with respect to  $n$  of the one-particle contribution  $A_1$  relies in differentiating the function  $f_n$  (6.17). Its integral representation allows us to directly differentiate with respect to the parameter  $n$ :

$$\frac{df_n(\beta)}{dn} = \left( \int_0^\infty dt \frac{4 \sinh^2 \left( \frac{t}{6} \right) \operatorname{csch}^2(nt) \cos \left( \frac{\beta t}{\pi} \right)}{1 - 2 \cosh \left( \frac{t}{3} \right)} \right) f_n(\beta) \tag{6.137}$$

Since we are interested in the limit  $n \rightarrow 1$ , we can specialise the above expression at  $n = 1$  and  $\beta = \frac{2\pi i}{3}$  (the value of  $\beta$  appearing in the one-particle form factor expression),

obtaining:

$$\lim_{n \rightarrow 1} \frac{df_n(\beta)}{dn} = \left( \frac{11\pi}{72\sqrt{3}} - \frac{1}{2} \right) f_1 \left( \frac{2\pi i}{3} \right) \quad (6.138)$$

We can now compute the  $n \rightarrow 1$  limit of the derivative with respect to  $n$  of the entire one-particle form factor:

$$\begin{aligned} A'_1(r, 1) &= \lim_{n \rightarrow 1} \frac{d}{dn} \left( n \left| \frac{F_1^{\mathcal{T}\phi:|1}}{\langle : \mathcal{T}\phi : \rangle} \right|^2 \right) \\ &= - \left( \frac{F_1^\phi}{\langle \phi \rangle} \right)^2 - 2 \frac{F_1^\phi}{\langle \phi \rangle} \lim_{n \rightarrow 1} \frac{d}{dn} \left( \frac{F_1^{\mathcal{T}\phi:|1}}{\langle : \mathcal{T}\phi : \rangle} \right) \\ &= - \left( \frac{F_1^\phi}{\langle \phi \rangle} \right)^2 - 2 \frac{F_1^\phi}{\langle \phi \rangle} \left[ \frac{i\sqrt{2}}{\sqrt[4]{3} f_1 \left( \frac{2\pi i}{3} \right)} \left( -1 + \frac{\pi}{\sqrt{27}} \right) \right. \\ &\quad \left. - \frac{i\sqrt{2}}{\sqrt[4]{3} f_1 \left( \frac{2\pi i}{3} \right)^2} \lim_{n \rightarrow 1} \frac{df_n \left( \frac{2\pi i}{3} \right)}{dn} \right] \end{aligned} \quad (6.139)$$

Rearranging all the terms we have:

$$A'_1(r, 1) = B_1(r) + \frac{2}{f \left( \frac{2\pi i}{3}, 1 \right)^2} \left( \frac{1}{\pi\sqrt{3}} - \frac{13}{108} \right) K_0(mr) \quad (6.140)$$

The presence of the  $B_1$  term (i.e. the one-particle contribution of the  $\langle \phi(0)\phi(r) \rangle$  form factor expansion) is due to the fact the  $: \mathcal{T}\phi :$  tends to  $\phi$  in the limit  $n \rightarrow 1$ .

We can immediately notice that this term is non-universal. It depends explicitly on the function  $f$  (which depends on the explicit expression of the S-matrix of the theory). This non-universal feature is in contrast with the universal form of the two-particle contribution, which has been computed in [14] for all integrable theories<sup>10</sup> and it is given by:

$$A'_2(r, 1) = \frac{1}{8} K_0(2mr) \quad (6.141)$$

Such a result was obtained from the analytic continuation in the parameter  $n$ .

We can now put together all these results in order to construct the various contributions to the correction to the saturation of the entanglement entropy.

<sup>10</sup>Notice that this result holds also beyond integrability, as shown in [100].

The term  $B^{-1}$  can be Taylor expanded as

$$\begin{aligned} \frac{1}{1 + B_1 + B_2 + \dots} &= 1 - (B_1 + B_2 + \dots) + (B_1 + B_2 + \dots)^2 + \dots \\ &= 1 - B_1 - B_2 + B_1^2 + \dots \end{aligned} \quad (6.142)$$

A Taylor expansion can also be used to compute the logarithmic contribution:

$$\begin{aligned} \log(1 + B_1 + B_2 + \dots) &= (B_1 + B_2 + \dots) - \frac{1}{2}(B_1 + B_2 + \dots)^2 + \dots \\ &= B_1 + B_2 - \frac{1}{2}B_1^2 + \dots \end{aligned} \quad (6.143)$$

Putting all contributions together we have

$$\begin{aligned} \lim_{n \rightarrow 1} \frac{d}{dn} \frac{A(r, n)}{B(r)^n} &= \frac{2}{f_1 \left(\frac{2\pi i}{3}\right)^2} \left( \frac{1}{\pi\sqrt{3}} - \frac{13}{108} \right) K_0(mr) + \frac{1}{8} K_0(2mr) \\ &\quad - \frac{4}{3f_1 \left(\frac{2\pi i}{3}\right)^4} \int_{-\infty}^{\infty} \frac{d\beta}{(2\pi)^2} \left( |F_{\min}(\beta, 1)|^2 - 1 \right) K_0 \left( 2mr \cosh \frac{\beta}{2} \right) \\ &\quad - \frac{13}{3^3 \sqrt{3} \pi f_1 \left(\frac{2\pi i}{3}\right)^4} K_0(mr)^2 + \dots \end{aligned} \quad (6.144)$$

In order to “order” the various contributions, we should consider their large  $mr$  expansion:

$$\begin{aligned} K_0(mr) &= e^{-mr} \left[ \sqrt{\frac{\pi}{2}} \sqrt{\frac{1}{mr}} - \frac{1}{8} \sqrt{\frac{\pi}{2}} \left( \frac{1}{mr} \right)^{3/2} + O \left( \left( \frac{1}{mr} \right)^{5/2} \right) \right] \\ K_0(mr)^2 &= e^{-2mr} \left[ \frac{\pi}{2mr} - \frac{\pi}{8mr^2} + O \left( \left( \frac{1}{mr} \right)^3 \right) \right] \\ K_0(2mr) &= e^{-2mr} \left[ \frac{1}{2} \sqrt{\pi} \sqrt{\frac{1}{mr}} - \frac{1}{32} \sqrt{\pi} \left( \frac{1}{mr} \right)^{3/2} + O \left( \left( \frac{1}{mr} \right)^{5/2} \right) \right] \end{aligned} \quad (6.145)$$

From the above expressions it is clear that the expansion of the function  $K_0(mr)$  is not affected by neither the function  $K_0(mr)^2$  or  $K_0(2mr)$  - the former decays as  $e^{-mr}$  while the latter decay at a much faster rate  $e^{-2mr}$ . Therefore, the  $K_0(mr)$  term is the most relevant term of the correction:

$$\lim_{n \rightarrow 1} \frac{d}{dn} \frac{A(r, n)}{B(r)^n} = \frac{2}{f_1 \left(\frac{2\pi i}{3}\right)^2} \left( \frac{1}{\pi\sqrt{3}} - \frac{13}{108} \right) K_0(mr) + \text{sub-leading corrections} \quad (6.146)$$

The coefficient in front of the Bessel function can be calculated explicitly:

$$\mathbf{a} \equiv \frac{2}{f_1 \left(\frac{2\pi i}{3}\right)^2} \left( \frac{1}{\pi\sqrt{3}} - \frac{13}{108} \right) = 0.0769782\dots \quad (6.147)$$

Concerning the sub-leading corrections, all the factors of order  $\frac{e^{-2mr}}{(2mr)^\alpha}$  can be grouped together. They are given by:

$$\begin{aligned} & \frac{1}{8}K_0(2mr) - \frac{4}{3f_1 \left(\frac{2\pi i}{3}\right)^4} \int_{-\infty}^{\infty} \frac{d\beta}{(2\pi)^2} \left( |F_{\min}(\beta, 1)|^2 - 1 \right) K_0 \left( 2mr \cosh \frac{\beta}{2} \right) \\ & - \frac{13}{3^3\sqrt{3}\pi f_1 \left(\frac{2\pi i}{3}\right)^4} K_0(mr)^2 + \dots \\ & = \left[ \sqrt{\frac{\pi}{2}} \left( \frac{1}{8} - \frac{4}{3f_1 \left(\frac{2\pi i}{3}\right)^4} \int_{-\infty}^{\infty} \frac{d\theta}{(2\pi)^2} \left( |F_{\min}(\theta, 1)|^2 - 1 \right) \right) \right] \frac{e^{-2mr}}{\sqrt{2mr}} \\ & - \left[ \frac{13}{54\sqrt{3}f_1 \left(\frac{2\pi i}{3}\right)^4} \right] \frac{e^{-2mr}}{2mr} \end{aligned} \quad (6.148)$$

where the two constants in front of the two exponential functions can be computed explicitly:

$$\begin{aligned} \mathbf{b} & \equiv \sqrt{\frac{\pi}{2}} \left( \frac{1}{8} - \frac{4}{3f_1 \left(\frac{2\pi i}{3}\right)^4} \int_{-\infty}^{\infty} \frac{d\theta}{(2\pi)^2} \left( |F_{\min}(\theta, 1)|^2 - 1 \right) \right) = 0.326234\dots \\ \mathbf{c} & \equiv \frac{13}{54\sqrt{3}f_1 \left(\frac{2\pi i}{3}\right)^4} = 0.0512159 \end{aligned} \quad (6.149)$$

### 6.4.3 Leading correction to saturation

We have now computed all the contributions needed to build up the complete expression for the next-to-leading order contribution to the entanglement entropy in the large  $mr$  regime:

$$S = -\frac{c_{\text{eff}}}{3} \log m\epsilon + U - \mathbf{a}K_0(mr) - \mathbf{b} \frac{e^{-2mr}}{\sqrt{2mr}} - \mathbf{c} \frac{e^{-2mr}}{2mr} + O \left( \frac{e^{-2mr}}{(2mr)^{3/2}} \right) \quad (6.150)$$

In order to compare these results with the unitary case, let us consider the entropy of a unitary system in the same large  $mr$  regime [14]:

$$\begin{aligned} S &= -\frac{c}{3} \log m\epsilon + U' - \frac{1}{8} K_0(2mr) + \dots \\ &= -\frac{c}{3} \log m\epsilon + U' - \frac{\sqrt{\pi}}{16} \frac{e^{-2mr}}{\sqrt{2mr}} + \dots \end{aligned} \quad (6.151)$$

where  $U'$  is a model-dependent computable constant. Using form factors, it is possible to compute it:

$$U' = - \lim_{n \rightarrow 1} \frac{d}{dn} \frac{1}{K_{\mathcal{T}}} \quad (6.152)$$

Of course, one of the main differences between the two cases is that the central charge  $c$  is substituted by its effective counterpart  $c_{\text{eff}}$  in the non-unitary case. Moreover, the corrections to the respective saturation values scale in different ways. In unitary models the most relevant correction has a universal behaviour: the  $\frac{1}{8}$  coefficient is the same for *any* theory. On the other hand, the non-unitary corrections have a different scaling and the coefficient is no more universal, as it depends explicitly on the features of the model. This feature could play a very important role in the identification of the universality class of the model, as it will be discussed in Section 6.4.4. In order to explain this feature, we should have a look at the main differences between the two cases when evaluating the entanglement entropy. In the non-unitary case the entanglement is given by a correlation function involving composite twist fields  $:\mathcal{T}\phi:$ , which have a much richer structure than the twist fields  $\mathcal{T}$ . Since  $:\mathcal{T}\phi: \rightarrow \phi$  when  $n$  tends to one, the one-particle form factor  $F_1^\phi \neq 0$  of the field  $\phi$  plays an actual role in the study of the large  $mr$  regime. In the unitary case, the entanglement is given by correlators involving twist fields  $\mathcal{T}$  which become the identity  $\mathbf{1}$  when  $n$  tends to one. As noticed in [14], since the one-particle form factor  $F_1^{\mathbf{1}}$  of the identity is equal to zero, it gives no contribution to the entanglement entropy. There are no  $O(e^{-mr})$  corrections to the entanglement entropy in unitary QFTs.

#### 6.4.4 Numerical identification of the universality class

The strong difference between the two cases could be an important help when identifying the universality class of a model from numerical computation of its entanglement entropy. Consider a spin chain and suppose we compute the scaling of its entanglement using some numerical approach (say DMRG). Probably the easiest thing to extract is the (effective) central charge, denoted as  $c_{\text{eff}}$ . Suppose that the numerical estimate gives a result of  $c_{\text{eff}} = 0.71 \pm 0.02$ . Such a result is compatible with either the unitary minimal model  $\mathcal{M}_{4,5}$  with central charge  $c = 7/10 = 0.7$  or with the non unitary  $\mathcal{M}_{3,7}$  model, with effective

central charge  $c_{\text{eff}} = 5/7 = 0.71\dots$ . In order to discriminate between the two models the study of the leading correction to the saturation could be used (if the scaling limit is a massive QFT).

## 6.5 Conclusions

In this chapter we extended the results of Chapter 5 to the massive regime. The form factor recursive equations for the twist fields of the Lee-Yang model have been derived and their solutions found up to the three-particle level. From the recursive equations two distinct series of form factors have been found. These series have been identified with the form factor series of the twist field  $\mathcal{T}$  and its composite variant  $:\mathcal{T}\phi:$ . In order to check this identification, i.e. to check whether the two form factor series have been properly identified with the right field, the scaling of the correlation functions has been studied. We performed a “connected” form factor expansion of the correlation functions, i.e. we studied their logarithm. Using a tool developed by Smirnov [74], we computed the scaling dimensions of the two different twist fields in the ultraviolet regime. In order to check such computations, we developed a perturbative CFT expansion of correlation functions extending previous result known in literature [98, 101]. The form factor expansion of the logarithm of correlation functions, together with the newly developed perturbative CFT approach, allowed us also to estimate the vacuum expectation values of the twist fields in the massive regime. Such a computation, available only in few small  $n$  cases, allowed us to compare directly the perturbative CFT with the numerical form factor expansion of correlation functions involving twist fields. In all the cases studied the agreement was not perfect. We claim that this discrepancy can be explained by some factors, in particular by the truncation of the form factor expansion. Such an expansion can describe very well the large  $mr$  regime, but it fails in accuracy when it is used at short distance scales, when many more form factors may be needed to reconstruct correctly the correlation function. On the other hand, the perturbative CFT approach lacks in precision when trying to describe long range scales. Moreover, all form factors depend explicitly on the vacuum expectation value of the field they are describing. Such a value comes from a form factor expansion itself. The form factor expansion of the correlator is then the results of *two* approximations: one in truncating the actual series and the other in truncating the series to compute the vacuum expectation value. All these numerical computations, while physically relevant on their own for the study of twist field correlation functions at different scales, support the validity of the form factor expression we derived.

Using these expressions, we concluded this chapter studying the saturation of the entanglement entropy at large scales. Using form factor expansions we could formulate a straight recipe for the computation of the saturation constant. Moreover, we used the one-

and two-particle form factors to compute also the corrections to this saturation: since the saturation represents the asymptotic  $mr \rightarrow \infty$  limit, we are also interested in *how* the entanglement tends to a constant. From the results we obtained the non unitarity of the system reveals itself in a very peculiar way. In unitary theories, these corrections have a very universal form. In this non unitary case the corrections decay at a much slower rate and their form is not universal - it depends on the S-matrix of the model. We noticed how this difference arises naturally from the different form factor expressions. The composite twist field  $:\mathcal{T}\phi:$  used for the evaluation of entanglement entropy of non unitary theories has a very different behaviour from the twist field  $\mathcal{T}$ , used in unitary models. We conclude that the non unitarity of models can be manifested in the behaviour of the leading corrections to the saturation of the entanglement entropy of such systems.

## Chapter 7

# Entanglement in Forrester-Baxter RSOS Models

In all previous chapters we studied the entanglement and its features from a field theory point of view. Ideally, we have always had in mind some discrete one-dimensional lattice system, i.e. a spin chain, whose continuum limit can be described by a field theory. In this chapter we will compute the entanglement entropy of some actual spin systems, using the Forrester-Baxter Restricted-Solid-On-Solid (FB RSOS) models. Even if RSOS models are 2D classical statistical systems, they can be interpreted as the euclidean version of some quantum spin chain. Such systems are lattice representation of the non-unitary series of minimal models and their off-critical massive perturbations. Some of the results of this chapter have been already used in another thesis<sup>1</sup>. In particular, the leading logarithmic scaling of Rényi entropy is not original. However, the results here will be presented using a more modern notation and they will be extended to the study of the sub-leading corrections to the logarithmic scaling of the entropy. Moreover, we will compute the entropy of the so-called off-critical logarithmic minimal models, which can be obtained using some special configurations of the FB systems. Additionally, we will also present the explicit formulation of an off critical one dimensional quantum Hamiltonian associated to the RSOS models.

### 7.1 The FB RSOS Models

In this section we will introduce the Forrester-Baxter RSOS models and their properties [102]. Such models, in a particular configuration, provide a lattice realisation of the unitary and non-unitary series of perturbed minimal models  $\mathcal{M}_{m,m'}$ . The RSOS models are clas-

---

<sup>1</sup>Some results of this chapter have been presented in my Master's thesis (D Bianchini, MSc Thesis, University of Bologna, 2013).

sical statistical models defined on a square lattice with a nearest neighbour interaction<sup>2</sup>, also said Interaction Round a Face (IRF) models [11]. As an IRF model, the Boltzmann weight of a single square tile depends only on the configurations of the four corner sites  $i$ ,  $j$ ,  $k$  and  $l$  (see Figure 7.1).

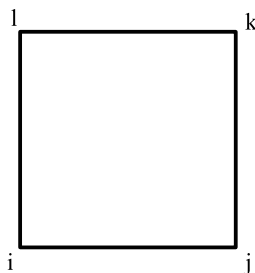


Figure 7.1: Square tile.

On each vertex  $i$  of a RSOS model a local variable, called *local height*  $\ell_i$ , is defined. It runs from 1 to some integer value  $r - 1$  (the same for all vertices of the lattice). Not all configurations of local heights are allowed: any two local heights must differ *exactly* by one if they share one edge.

$$\ell_i - \ell_j = \pm 1 \quad \text{for any } i \text{ and } j \text{ connected by an edge} \quad (7.1)$$

The parameter  $r$  can be seen as the *Coxeter number* [103] of the diagram where the local heights live (in this case  $A_{r-1}$ ). For a more detailed discussion of the interpretation of RSOS models in terms of Dynkin diagrams see, for instance, [104].

We can now define a Boltzmann weight for each tile:

$$W \begin{pmatrix} \ell_l & \ell_k \\ \ell_i & \ell_j \end{pmatrix} = e^{-\beta \varepsilon_{ijkl}} \quad (7.2)$$

From the statistical point of view a Boltzmann weight simply represents the probability of a given configuration of local heights around a tile.

For such models, all the physical parameters of the system (such as the internal parameters of the Hamiltonians) can be rearranged in just two [11]: the *spectral parameter*  $u$  and the *crossing parameter*  $\lambda$ . The former measures the spatial anisotropy of the model, while the

---

<sup>2</sup>In this context, each site can interact with *eight* sites: one above, one below, one right, one left and the four diagonals ones.

latter rules the behaviour of the system when the lattice is rotated by  $\frac{\pi}{2}$ :

$$W \left( \begin{array}{cc|c} \ell_l & \ell_k & u \\ \ell_i & \ell_j & \end{array} \right) = \sqrt{\frac{s(\ell_i \lambda) s(\ell_k \lambda)}{s(\ell_j \lambda) s(\ell_l \lambda)}} W \left( \begin{array}{cc|c} \ell_k & \ell_j & \lambda - u \\ \ell_l & \ell_i & \end{array} \right) \quad (7.3)$$

where the function  $s(x) = \vartheta_1(x; p)$  is the first Jacobi theta function [49] and  $-1 < p < 1$  is a temperature-like parameter which measures the departure from criticality (the system is critical at  $p = 0$ ). In order to be integrable, the Boltzmann weights must satisfy the Yang-Baxter equation[11]<sup>3</sup>. A possible solution can be written in the following form [105, 102]:

$$\begin{aligned} w_{1,a}(u) &\equiv W \left( \begin{array}{cc|c} \ell \pm 1 & \ell & u \\ \ell & \ell \mp 1 & \end{array} \right) = \frac{s(\lambda - u)}{s(\lambda)} \\ w_{2,a}^{\pm}(u) &\equiv W \left( \begin{array}{cc|c} \ell & \ell \pm 1 & u \\ \ell \mp 1 & \ell & \end{array} \right) = \frac{g_{\ell \mp 1} s((\ell \mp 1)\lambda) s(u)}{g_{\ell \pm 1} s(\ell\lambda) s(\lambda)} \\ w_{3,a}^{\pm}(u) &\equiv W \left( \begin{array}{cc|c} \ell & \ell \pm 1 & u \\ \ell \pm 1 & \ell & \end{array} \right) = \frac{s(\ell\lambda \pm u)}{s(\ell\lambda)} \end{aligned} \quad (7.4)$$

where the gauge factor  $g_a$  is an arbitrary function which does not depend on the value of the crossing parameter  $u$ . Since all physical quantities are given by ratios, the actual choice of the gauge parameter does not affect such quantities.

The RSOS models describe a huge variety of physical phenomena. For instance, when fixing  $\lambda = \frac{\pi}{r}$  (the so-called *Andrews-Baxter-Forrester* (ABF) models [105], hereby denoted by  $\text{RSOS}_r$ ), the model can describe four distinct phases, traditionally called *regimes*. In Regime III ( $0 < p < 1$  and  $0 < u < \lambda$ ), the  $\text{RSOS}_r$  model is a lattice realisation of the unitary series of  $\phi_{13}$  thermally perturbed minimal models  $\mathcal{M}_{r-1,r}$ . On the other hand, the Regime I ( $-1 < p < 0$  and  $\lambda < u < 3\lambda$ ) describes the perturbed parafermionic theory  $\mathbb{Z}_{r-2}$ . For example, when specialising to  $r = 4$ , the Regime III of the ABF model it is equivalent to the Ising model.

As we have just seen, the ABF models describe a huge variety of *unitary* models. In order to have a RSOS realisation of non-unitary theories, a further generalisation of the ABF models is needed. We can now introduce the *Forrester-Baxter* (FB) [102] models  $\text{RSOS}_{r,s}$ . In such a case, the crossing parameter depends also on an extra parameter  $s$  (coprime with respect to  $r$  and such that  $1 \leq s < r$ ):

$$\lambda = \frac{s\pi}{r} \quad (7.5)$$

Such FB models have a structure even richer than the ABF models (which can be recovered

<sup>3</sup>also referred to as *star-triangle relation*.

by setting  $s = 1$ ). Among the huge varieties of regimes of the FB models, one configuration is of particular interest to us: the Regime III. In this regime the FB models describe the non-unitary<sup>4</sup> minimal models  $\mathcal{M}_{r-s,r}$  perturbed by the thermal operator  $\phi_{13}$ . Since we are interested in evaluating the entanglement entropy of non-unitary systems we will focus on the Regime III of the FB models. In the following we will always refer to such a regime unless stated otherwise. Of course, a regime II exists also in FB models. However, in this non-unitary case, a complete understanding of the underlying symmetry it is still missing and it is not clear if non unitary parafermions [106] can be used to describe such a phase.

Even if this notation can seem a bit abstract, it is possible to recover some interesting physical quantities from the RSOS models. In particular, we are interested in extracting the correlation length (or the mass gap) of the continuum limit of such theories. Extending the previous results of O'Brien and Pearce [107], we can explicitly relate the correlation length and the temperature-like parameter:

$$e^{-\frac{1}{\xi}} = k' \left( p^{\frac{r}{4s}} \right) \quad (7.6)$$

where  $k'(q)$  is the conjugate elliptic modulus for the elliptic nome  $q$ :

$$k'(q) = \prod_{\ell=1}^{\infty} \left( \frac{1 - q^{2\ell-1}}{1 + q^{2\ell-1}} \right)^4 \quad (7.7)$$

The above results are in perfect agreement with the perturbative CFT approach. The QFT action of the FB model in the continuum limit can be written as

$$S = S_{CFT} + t \int d^2x \phi_{13}(x) \quad (7.8)$$

where  $|t| = p^2$  measures the departure from criticality. A simple dimensional analysis argument gives:

$$m \sim p^{\nu} \quad (7.9)$$

where  $\nu = \frac{1}{2(1-\Delta_{13})} = \frac{r}{4s}$  depends on the conformal dimension of the perturbing operator  $\phi_{13}$ .

The perturbative CFT approach recovers exactly the near-critical expansion (small  $p$ ) of

---

<sup>4</sup>or unitary when  $s = 1$  and the ABF models are recovered.

(7.6):

$$\xi^{-1} = 8p^\nu + \frac{32}{3}p^{3\nu} + \frac{48}{5}p^{5\nu} + \frac{64}{7}p^{7\nu} + O(p^{9\nu}) \quad (7.10)$$

The above equation will play a very important role in the following sections. It will allow us to express the entropy of the FB model (which depends on  $p$ ) using the physical correlation length (or the mass gap).

## 7.2 Entanglement Using Corner Transfer Matrix

In this section we will discuss the relation between a classical 2D and a quantum 1D systems. In the previous section we introduced the Forrester-Baxter RSOS models, a class of lattice 2D models. As entanglement is a genuine quantum feature, it has no proper meaning for classical systems. The entanglement we are computing in this chapter refers to the spin chain whose euclidean time evolution can be described by these FB models. To do so, we need to explain how these two situations (spin chains and classical 2D models) are related. In order to simplify the computation, we will use the so-called *Corner Transfer Matrix* approach.

### 7.2.1 Hamiltonian limit

Let us consider a quantum one-dimensional lattice system (say a spin chain with  $N$  sites). The time evolution with an Hamiltonian  $H$  of a given quantum state  $|\Psi\rangle$  is given by

$$|\Psi\rangle' = e^{-\tau H}|\Psi\rangle \quad (7.11)$$

where  $\tau$  is the euclidean time.

The matrix element between the evolved and the original state is given by

$$\left(\langle\Psi|e^{-\tau H}|\Psi\rangle\right)_{\ell_1\cdots\ell_N}^{\ell'_1\cdots\ell'_N} \quad (7.12)$$

where  $\ell_1\cdots\ell_N \equiv \ell$  is an element of some basis of the spin chain. The above matrix element can be seen as an operator acting on *classical* spin configurations. The quantum 1D evolution operator can then be interpreted as classical row-to-row transfer matrix  $T$  (see next section):

$$T \sim e^{-\tau H} \quad \text{for } \tau \text{ small} \quad (7.13)$$

with

$$[T, H] = 0 \tag{7.14}$$

In other words, each time slice of the evolution of a spin chain can be seen as a row of a 2D classical system and the euclidean time step  $\tau$  can be interpreted as the lattice spacing between two rows.

The process of obtaining a row-to-row transfer matrix (aka a classical 2D system) starting from a quantum 1D Hamiltonian can be reversed. Using such a procedure, called *Hamiltonian limit*, a quantum Hamiltonian can be derived by taking the lattice spacing to zero in the “time” direction. For instance, using the Hamiltonian limit it is possible to show [11] that the eight-vertex model and the XYZ spin chain are related to each other. More precisely the two partition functions (the 2D statistical and the 1D quantum) are equal. Later in this chapter (Section 7.4) we will compute the quantum Hamiltonian associated to the RSOS models, a class of classical 2D system introduced in Section 7.1.

### 7.2.2 Corner transfer matrix

The Corner Transfer Matrix approach is a powerful tool to compute partition and one-point functions in lattice systems. Suppose we have a very large square lattice. The partition function of the entire lattice can be computed using the row-to-row transfer matrix, which is the Boltzmann weight of an entire row of tiles inside the lattice.

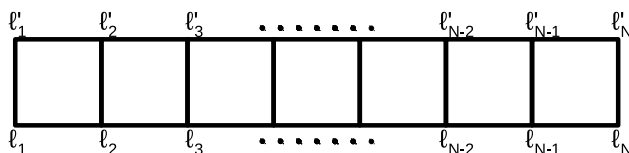


Figure 7.2: A row-to-row transfer matrix between two spin configurations.

The row-to-row transfer matrix can then be expressed as a product of the individual Boltzmann weights of each tile belonging to the row:

$$T_{\ell}^{\ell'} = \prod_{\square \in \text{row}} w(\square) = \prod_{\square \in \text{row}} e^{-\beta \epsilon(\square)} \tag{7.15}$$

In order to take into account the contribution of two adjacent rows, we can consider

the double-row-to-row transfer matrix  $T^2$ , which is composed of two single strips:

$$(T^2)_\ell^{\ell'} = T_\ell^{\ell''} T_{\ell''}^{\ell'} \quad (7.16)$$

where a sum over all possible intermediate configurations  $\ell''$  has been performed.

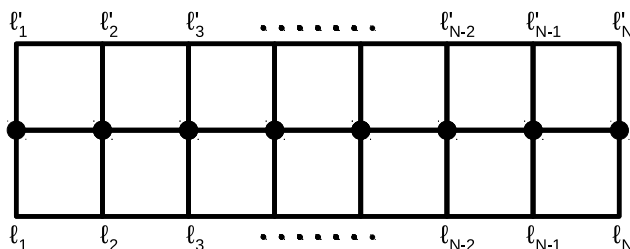


Figure 7.3: A double-row-to-row transfer matrix between two spin configurations. The intermediate spins (black dots) are summed over all possible configurations.

This process can be iterated enough times (say  $M$  times for a rectangular lattice  $N \times M$ ) to cover the entire system.

The entire partition function  $Z$  of the system can then be obtained from the  $M$ -th power of the row-to-row transfer matrix.<sup>5</sup>

The corner transfer matrix (CTM) approach uses the individual Boltzmann weights as building blocks, but they are grouped in a different way than the row-to-row transfer matrix method. Instead of covering the entire lattice by adding rows, this approach is based in covering each of the four corner of the system at a time. For simplicity, consider a diamond shaped lattice, as shown in Figure 7.4.

Let  $2N + 3$  be the horizontal size of the lattice and let  $\ell_0$  be the local height of the central site shared by all corners. When defining a corner transfer matrix, we sum over all possible internal configurations and we keep the values on the edges fixed. In Figure 7.4 the internal sites are denoted by  $\bullet$ , and the states on the edges by  $\circ$ . The partition function of the bottom left corner, denoted by  $A$ , is a corner transfer matrix:

$$A_{\ell\ell'} = \delta_{\ell_0, \ell'_0} \sum_{\bullet} \prod_{\square \in A} W \begin{pmatrix} \ell_i & \ell_k \\ \ell_i & \ell_j \end{pmatrix} \quad (7.17)$$

In the above equation, the  $\delta$  term is inserted because the two edges  $\ell$  and  $\ell'$  share the

<sup>5</sup>The  $M$ -row-to-row transfer matrix  $T^M$  still depends on the two lower and upper configurations  $\ell$  and  $\ell'$ . According to the boundary conditions of the system, some further action can be performed on these two configurations. For instance, they may be left free (for free boundary conditions) or may be identified (for periodic boundary conditions).

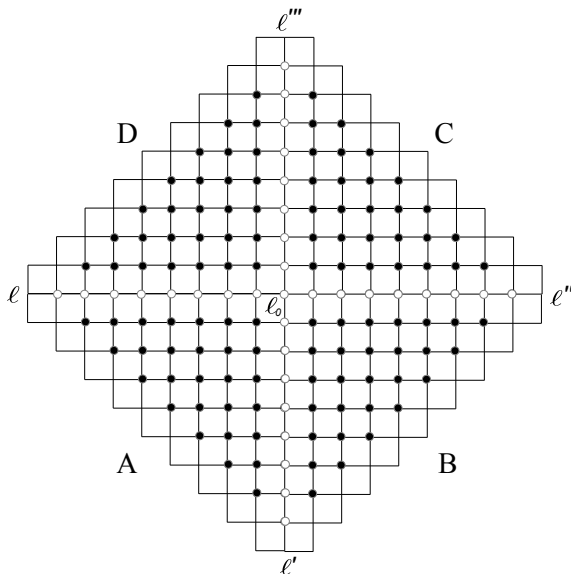


Figure 7.4: Diamond shaped lattice divided into four corners. Each Corner Transfer Matrix depends on the values of the local height on the two edges (denoted by  $\circ$ ). The internal sites ( $\bullet$ ) should be considered already summed over all possible configurations.

central site  $\ell_0 = \ell'_0$ .

To construct the partition function of the lower half of the lattice, we can just “glue” the two corner transfer matrices  $A$  and  $B$  together, summing on all the possible inner configurations  $\ell'$ :

$$Z(\text{lower half})_{\ell\ell''} = \sum_{\ell'} A_{\ell\ell'} B_{\ell'\ell''} = (AB)_{\ell\ell''} \quad (7.18)$$

In order to complete the lattice, we add also the corner transfer matrices  $C$  and  $D$ . To “close” the cycle we sum over the configurations between  $A$  and  $D$ :

$$Z = \sum_{\ell} (ABCD)_{\ell\ell} = \text{tr}(ABCD) \quad (7.19)$$

Evaluating the partition function of the system is then equivalent to computing a matrix product of the four corner transfer matrices.

This tool can also be used to compute the one-point function. Consider the operator  $S_a$ , which acts diagonally on a configuration  $\ell$  and vanishes whenever  $\ell_0$  is different from a given value  $a$ . In other words the operator  $S_a$  checks whether the value of the central height is equal to  $a$  or not. The corner transfer matrix approach gives then immediately

the probability to have  $\ell_0 = a$ :

$$\mathbb{P}(a) = \frac{\text{tr}(S_a ABCD)}{\text{tr}(ABCD)} \quad (7.20)$$

Moreover, the CTM tool can be used to compute the reduced density matrix of a quantum 1D system whose euclidean time evolution is equivalent to the 2D lattice system described by the corner transfer matrices.

### 7.2.3 Reduced density matrix using CTMs

In this section we will introduce the Corner Transfer Matrix approach for the evaluation of the reduced density matrix of a bipartite spin system. It is not always possible to use this tool: it works (i.e. can be used to compute physical quantities) only when studying infinite systems divided into two semi-infinite subsystems.

Consider a given infinite spin chain “living” on the real axis, from  $x = -\infty$  to  $x = +\infty$ . Let us divide our system into two semi-infinite lines: the subsystem  $A$  on the negative  $x$ -axis and its counterpart  $B$  on the positive  $x$ -axis. The Hilbert space then factorises into  $\mathcal{H}_A \otimes \mathcal{H}_B$  and its basis is given by  $\{\ell_A, \ell_B\}$ . Let  $|\Psi_0\rangle$  be the ground state of some quantum Hamiltonian  $H$ . The relative density matrix is then given by

$$\rho = |\Psi_0\rangle\langle\Psi_0| \quad (7.21)$$

The reduced density matrix  $\rho_A$  can be computed by tracing over all degrees of freedom of  $B$ :

$$\rho_A(\ell_A, \ell'_A) = \sum_{\ell_B} \langle \ell_A, \ell_B | \Psi_0 \rangle \langle \Psi_0 | \ell'_A, \ell_B \rangle \quad (7.22)$$

Now we would like to express matrix elements like  $\langle \ell_A, \ell_B | \Psi_0 \rangle$  using corner transfer matrices.

Consider a (not normalised) generic quantum state  $|\Psi\rangle$  and let  $T$  be the row-to-row transfer matrix of the equivalent 2D classical system. We can decompose the state  $|\Psi\rangle$  into the eigenbasis  $\{|\Psi_k\rangle\}_k$  of  $H$  (or  $T$ , since the two operators commute):

$$|\Psi\rangle = |\Psi_0\rangle + \sum_{k \neq 0} C_k |\Psi_k\rangle \quad (7.23)$$

Let  $\{\lambda_k\}_k$  be the eigenvalues of the transfer matrix  $T$ . Since  $|\Psi_0\rangle$  is the ground state of  $H$ , it has the largest eigenvalue  $\lambda_0$  of  $T$ . The action of  $T$  onto  $|\Psi\rangle$  is given by:

$$T|\Psi\rangle = \lambda_0 \left[ |\Psi_0\rangle + \sum_{k \neq 0} C_k \left( \frac{\lambda_k}{\lambda_0} \right) |\Psi_k\rangle \right] \quad (7.24)$$

Applying the row-to-row transfer matrix  $N$  times we have

$$T^N|\Psi\rangle = \lambda_0^N \left[ |\Psi_0\rangle + \sum_{k \neq 0} C_k \left( \frac{\lambda_k}{\lambda_0} \right)^N |\Psi_k\rangle \right] \quad (7.25)$$

Since  $\lambda_k < \lambda_0$ , for large  $N$  the only relevant term is given by

$$T^N|\Psi\rangle \sim \lambda_0^N |\Psi_0\rangle \quad (7.26)$$

On the other hand,  $T^N$  can also be used to compute the lower half partition function of a lattice system:

$$Z(\text{lower half}) = \langle \ell_A, \ell_B | T^N | \Psi \rangle \quad (7.27)$$

where  $|\ell_A, \ell_B\rangle$  represents the state of the upper edge. In other words, if  $\Psi$  is the configuration on of the lower edge of a large lattice, this state can be “time evolved” using the row-to-row transfer matrix until it reaches the upper bound of the lower half of the lattice. Combining the equations (7.26) and (7.27) we have<sup>6</sup>

$$\langle \ell_A, \ell_B | \Psi_0 \rangle \sim Z(\text{lower half}) = (AB)_{\ell_A, \ell_B} \quad (7.28)$$

In a very similar way the term  $\langle \Psi_0 | \ell'_A, \ell_B \rangle$  of equation (7.22) can be written in terms of corner transfer matrices:

$$\langle \Psi_0 | \ell'_A, \ell_B \rangle \sim Z(\text{upper half}) = (CD)_{\ell_B, \ell'_A} \quad (7.29)$$

The matrix element of the reduced density matrix can be computed using corner transfer matrices:

$$\begin{aligned} \rho_A(\ell_A, \ell'_A) &= \sum_{\ell_B} \langle \ell_A, \ell_B | \Psi_0 \rangle \langle \Psi_0 | \ell'_A, \ell_B \rangle \sim \sum_{\ell_B} (AB)_{\ell_A, \ell_B} (CD)_{\ell_B, \ell'_A} \\ &= (ABCD)_{\ell_A, \ell'_A} \end{aligned} \quad (7.30)$$

---

<sup>6</sup>According to the definition of Figure 7.4,  $\ell_A$  and  $\ell_B$  correspond respectively to  $\ell$  and  $\ell'$ .

This result, obtained for the first time by Nishino and Okunishi [12], can be used to compute also various powers of the reduced density matrix.

Of course, there is no guarantee that the reduced density matrix defined in (7.30) is normalised. The *correct* reduced density matrix can be obtained by dividing by the partition function:

$$\rho_A = \frac{ABCD}{\text{tr}ABCD} \quad (7.31)$$

As we have seen in previous chapters, the key object for the evaluation of Rényi entropy is the trace of the  $n$ -th power of the reduced density matrix:

$$\text{tr}\rho_A^n = \frac{\text{tr}(ABCD)^n}{(\text{tr}ABCD)^n} \quad (7.32)$$

In the following section we will evaluate the above quantity for the FB RSOS model in order to compute its Rényi entropy. Notice that the normalisation of the reduced density matrix using CTMs resembles equation (5.3).

### 7.3 Entanglement in Forrester-Baxter Models

In this section we will compute the Rényi entropy of the quantum chain associated with the FB RSOS model using the Corner Transfer Matrix approach. In order to simplify our computations, we will use the so-called *symmetric gauge*  $g_\ell = \sqrt{s(\ell\lambda)}$  in equation (7.4). Since we are interested in perturbed minimal models, we will focus on the Regime III of the FB model:

$$0 < p < 1 \quad 0 < u < \lambda \quad (7.33)$$

The main object to compute is the trace of the reduced density matrix. To do so, we will consider the following quantity

$$Z_n = \text{tr}(ABCD)^n \quad (7.34)$$

With this notation the trace of the reduced density matrix is given by:

$$\text{tr}\rho_A^n = \frac{Z_n}{Z_1^n} \quad (7.35)$$

Following [102], we introduce the following notation:

$$y = e^{\frac{4\pi^2}{\log p}} \quad x = y^{\frac{s}{r}} \quad (7.36)$$

These auxiliary variables  $x$  and  $y$  appear naturally in Forrester's and Baxter's analysis of their model. Moreover it should be noticed that  $x$  and  $y$  are related to  $p$  in a way which resembles modular transformations.

Before computing the thermodynamic limit  $N \rightarrow \infty$  of the matrix element  $(ABCD)_{\ell, \ell'}$ , we should consider its finite version with size  $2N + 3$ . In order to compute the  $n$ th power appearing in (7.34) we can consider the diagonalised version of  $ABCD$ , which has been computed for the first time in [102]:

$$(ABCD)_{\ell, \ell'}^{(diag)} = E(x^{\ell_0}, y) x^{2\Phi(\ell)} \delta_{\ell, \ell'} \quad (7.37)$$

where  $\ell = \{\ell_0, \ell_1, \dots, \ell_{N+1}\}$  represents the string of local heights between the Corner Transfer Matrices  $A$  and  $D$  (see Figure 7.4).

The functions  $E$  and  $\Phi$  are given by

$$\begin{aligned} E(z, q) &= \sum_{k \in \mathbb{Z}} (-1)^k q^{\frac{k(k-1)}{2}} z^k = \prod_{n=1}^{\infty} (1 - q^{n-1} z)(1 - q^n z^{-1})(1 - q^n) \\ \Phi(\ell) &= \sum_{k=1}^N \left( k \frac{|\ell_k - \ell_{k+2}|}{4} + (\ell_k - \ell_{k+1}) \left\lfloor \frac{\ell_k s}{r} \right\rfloor \right) \end{aligned} \quad (7.38)$$

where  $\lfloor x \rfloor$  denotes the integer part of  $x$ .

The partition function  $Z_n$  is then given by

$$\begin{aligned} Z_n &= \text{tr}(ABCD)^n = \sum_{\ell} [(ABCD)^n]_{\ell, \ell} \\ &= \sum_{\ell} E(x^{\ell_0}, y)^n x^{2n\Phi(\ell)} \end{aligned} \quad (7.39)$$

Instead of summing on all possible configurations  $\ell$ , we keep  $\ell_N = b$  and  $\ell_{N+1} = c \equiv b \pm 1$  fixed and we sum over all the other local heights, from  $\ell_0$  to  $\ell_{N-1}$ . Such a fixing will not affect the main results about the scaling of the entropy. However, some non universal constants will depend on the choice of  $b$ .

Equation (7.39) can then be rewritten as

$$Z_n = \sum_{a=1}^{r-1} E(x^a, y)^n D_N(a, b, c; x^{2n}) \quad (7.40)$$

where  $a$  plays the role of the central height  $\ell_0$  and the function  $D_N$  is given by

$$D_N(a, b, c; q) = \sum_{\ell_1, \dots, \ell_{N-1}} q^{\Phi(\ell)} \quad \text{with } \ell_0 = a, \ell_N = b \text{ and } \ell_{N+1} = c \quad (7.41)$$

The sum in equation (7.40) has been denoted with a star  $*$  because it runs only on even or odd values of  $a$ . Since the values of local heights are restricted to differ by one from their neighbours, the allowed values of the central height depend on the value  $b$  on the boundary site.

### 7.3.1 Thermodynamic limit

In order to perform the thermodynamic limit  $N \rightarrow \infty$  we will use some results of [102]. There are two possible results for the thermodynamic limit, according to the two possible boundary conditions  $\ell_N < \ell_{N+1}$  or  $\ell_N > \ell_{N+1}$ .

In the first case we have:

$$\lim_{N \rightarrow \infty} q^{-\frac{kN}{2}} D_N(a, b, b+1; q) = \frac{1}{(q)_\infty} q^{\frac{b(b-1)}{4} - \frac{(k-1)b}{2}} F(a, b-k; q) \quad (7.42)$$

with  $k = \left\lfloor \frac{s(b+1)}{r} \right\rfloor = \left\lfloor \frac{s\ell_{N+1}}{r} \right\rfloor$ .

In the opposite case  $\ell_N > \ell_{N+1}$  the limit is given by:

$$\lim_{N \rightarrow \infty} q^{\frac{kN}{2}} D_N(a, b+1, b; q) = \frac{1}{(q)_\infty} q^{\frac{b(b+1)}{4} - \frac{k(b+1)}{2}} F(a, b-k; q) \quad (7.43)$$

and  $k = \left\lfloor \frac{sb}{r} \right\rfloor = \left\lfloor \frac{s\ell_{N+1}}{r} \right\rfloor$ .

The function  $F$  is given by:

$$\begin{aligned} F(a, d; q) &= q^{\frac{a(a-1)}{4} - \frac{ad}{2}} \left[ E \left( -q^{rd+(r-a)(r-s)}, q^{2r(r-s)} \right) - q^{ad} E \left( -q^{rd+(r-a)(r+s)}, q^{2r(r-s)} \right) \right] \\ &= q^{\frac{a(a-1)}{4} - \frac{ad}{2}} \frac{(q)_\infty}{q^{-\frac{c}{24} + \Delta_{da}}} \chi_{da}(q) \end{aligned} \quad (7.44)$$

where  $(q)_\infty$  is the q-Pochhammer symbol:

$$(q)_\infty = \prod_{k=1}^{\infty} (1 - q^k) \quad (7.45)$$

In equation (7.44),  $\Delta_{da}$  is the conformal dimension of the primary field  $\phi_{da}$  of the minimal model  $\mathcal{M}_{r-s, r}$ . The function  $\chi_{da}$  is its relative Virasoro character, as defined in Chapter 3.

Putting everything together we have

$$\lim_{N \rightarrow \infty} q^{\mp \frac{kN}{2}} D_N(a, b, b \pm 1; q) = q^{f_{\mp}(b,d)} q^{\frac{a(a-1)}{4} - \frac{ad}{2} + \frac{c}{24} - \Delta_{da}} \chi_{da}(q) \quad \text{with } d = b - k \quad (7.46)$$

The two functions  $f_+$  and  $f_-$  are given by

$$\begin{aligned} f_+(b, d) &= \frac{b(b-1)}{4} - \frac{b(k-1)}{2} \\ f_-(b, d) &= \frac{b(b+1)}{4} - \frac{k(b+1)}{2} \end{aligned} \quad (7.47)$$

Since the term  $q^{f_{\mp}}$  does not depend on the central height  $a$ , it can be factorised out of the sum. For this reason, both  $Z_n$  and  $Z_1^n$  will be proportional to  $x^{2nf_{\mp}}$ . For simplicity, we can define new partition functions  $Y_n$ :

$$Y_n = \sum_{a=1}^{r-1} {}^* E(x^a, y)^n x^{2n \left( \frac{a(a-1)}{4} - \frac{ad}{2} - \Delta_{da} \right)} \chi_{da}(x^{2n}) \quad (7.48)$$

which are simpler than  $Z_n$  but preserve the ratio:

$$\text{tr} \rho_A^n = \frac{Z_n}{Z_1^n} = \frac{Y_n}{Y_1^n} \quad (7.49)$$

While (7.48) is enough to compute the Rényi entropy at different temperatures  $p$ , it is not very suitable to study its small  $p$  scaling. Using the elliptic transformation (D.11) on the function  $E$ , an even simpler partition function can be defined:

$$W_n = \sum_{a=1}^{r-1} {}^* \vartheta_1 \left( \frac{\pi a s}{r}, \sqrt{p} \right)^n \chi_{da}(x^{2n}) \quad (7.50)$$

where, as before, all common factors of  $Y_n$  and  $Y_1^n$  have been dropped.

$$\text{tr} \rho_A^n = \frac{Z_n}{Z_1^n} = \frac{Y_n}{Y_1^n} = \frac{W_n}{W_1^n} \quad (7.51)$$

Even though the elliptic theta function  $\vartheta_1$  has a well-behaved expansion around  $p = 0$ , the conformal character  $\chi_{da}$  still depends on  $x = \exp \frac{4\pi^2 s}{\log p r}$ , which tends to 1 for  $p \rightarrow 0$ . This difficulty can be overcome by performing an  $S$  modular transformation of the conformal character  $\chi_{da}$  (3.44):

$$\chi_{a,a'}(\tilde{q}) = \sum_{(b,b') \in \mathcal{J}} \mathcal{S}_{a,a'}^{b,b'} \chi_{b,b'}(q) \quad (7.52)$$

where  $\tilde{q} = x^{2n} = e^{\frac{8\pi^2}{\log p} \frac{s}{r} n}$  and  $\mathcal{S}_{a,a'}^{b,b'}$  is the modular  $S$  matrix. The modular-transformed parameter  $q$  can be extracted from the relation

$$\begin{aligned} q &= e^{2\pi i \tau} \\ \tilde{q} &= e^{-\frac{2\pi i}{\tau}} \end{aligned} \quad (7.53)$$

and is given by

$$q = \left( p^{\frac{r}{2s}} \right)^{\frac{1}{n}} \equiv \omega^{\frac{1}{n}} \quad (7.54)$$

After performing the modular transformation, the partition function  $W_n$  is then given by:

$$W_n = \sum_{a=1}^{r-1} \sum_{(d',a') \in \mathcal{J}} \vartheta_1 \left( \frac{\pi a s}{r}, \sqrt{p} \right)^n \mathcal{S}_{da}^{d'a'} \chi_{d'a'} \left( \omega^{\frac{1}{n}} \right) \quad (7.55)$$

The sum over  $(d',a') \in \mathcal{J}$  can be rewritten as a sum over  $h \in \mathcal{K}$ , i.e. a sum over the dimensions of primary fields of the Kac table  $\mathcal{K}$  (see Chapter 3). The partition function can then be written as

$$\begin{aligned} W_n &= \sum_{a=1}^{r-1} \sum_{h \in \mathcal{K}} \vartheta_1 \left( \frac{\pi a s}{r}, \sqrt{p} \right)^n \mathcal{S}_{da}^{h=(d',a')} \chi_h \left( \omega^{\frac{1}{n}} \right) \\ &= \sum_{h \in \mathcal{K}} \chi_h \left( \omega^{\frac{1}{n}} \right) f_h(n, p) \end{aligned} \quad (7.56)$$

where

$$f_h(n, p) = \sum_{a=1}^{r-1} \vartheta_1 \left( \frac{\pi a s}{r}, \sqrt{p} \right)^n \mathcal{S}_{da}^{d'a'} \quad (7.57)$$

Among the different contributions of equation (7.56) coming from the various dimensions  $h$ s of primary fields, the one coming from the field with the smallest dimension is the most relevant for  $\omega \ll 1$ . Denoting such a dimension as  $\Delta_{\min}$ , it is convenient to rearrange the partition function  $W_n$  as

$$W_n = \chi_{\min} \left( \omega^{\frac{1}{n}} \right) f_{\min}(n, p) \left( 1 + \sum_{h \neq \min} \frac{\chi_h \left( \omega^{\frac{1}{n}} \right)}{\chi_{\min} \left( \omega^{\frac{1}{n}} \right)} \frac{f_h(n, p)}{f_{\min}(n, p)} \right) \quad (7.58)$$

Such a formulation is particularly suitable when studying the scaling of the Rényi entropy:

$$\begin{aligned}
 \mathrm{tr} \rho_A^n &= \log \frac{W_n}{W_1^n} = \log \frac{\chi_{\min}(\omega^{\frac{1}{n}})}{\chi_{\min}(\omega)^n} + \log \frac{f_{\min}(n, p)}{f_{\min}(1, p)^n} \\
 &+ \log \left( 1 + \sum_{h \neq \min} \frac{\chi_h(\omega^{\frac{1}{n}})}{\chi_{\min}(\omega^{\frac{1}{n}})} \frac{f_h(n, p)}{f_{\min}(n, p)} \right) \\
 &- n \log \left( 1 + \sum_{h \neq \min} \frac{\chi_h(\omega)}{\chi_{\min}(\omega)} \frac{f_h(1, p)}{f_{\min}(1, p)} \right)
 \end{aligned} \tag{7.59}$$

Since

$$\frac{\chi_h(\omega)}{\chi_{\min}(\omega)} = \omega^{\Delta_h - \Delta_{\min}} \frac{1 + \dots}{1 + \dots} \ll 1 \tag{7.60}$$

for  $\omega \rightarrow 0$ , the second and third line of the above equation can be easily expanded using Taylor's formula.

From the above expression we can study not only the leading logarithmic scaling of the entropy, but we can also analyse the sub-leading corrections to such logarithmic behaviour. Expanding the Virasoro character:

$$\chi_h(q) = q^{\Delta_h - \frac{c}{24}} \left( 1 + \dots \right) \tag{7.61}$$

we can compute the most relevant contributions to the Rényi entropy

$$\begin{aligned}
 S(n) &= \frac{1}{1-n} \log \mathrm{tr} \rho_A^n = -\frac{c_{\mathrm{eff}}}{24} \frac{n+1}{n} \log \omega + \tilde{A}^{(n)} \\
 &+ \frac{1}{1-n} \log \left( 1 + \sum_{h \neq \min} \frac{\chi_h(\omega^{\frac{1}{n}})}{\chi_{\min}(\omega^{\frac{1}{n}})} \frac{f_h(n, p)}{f_{\min}(n, p)} \right) \\
 &- \frac{n}{1-n} \log \left( 1 + \sum_{h \neq \min} \frac{\chi_h(\omega)}{\chi_{\min}(\omega)} \frac{f_h(1, p)}{f_{\min}(1, p)} \right) + \dots
 \end{aligned} \tag{7.62}$$

All the powers of  $\omega$  greater than one have been dropped from the above expansion, as they are less relevant than each contribution of the kind  $\chi_h/\chi_{\min} \sim \omega^{\Delta_h - \Delta_{\min}}$ .

The constant  $\tilde{A}^{(n)}$  is given by:

$$\tilde{A}^{(n)} = \frac{1}{1-n} \log \frac{\sum_{a=1}^{r-1} \mathcal{S}_{da}^{\min} \sin^n \frac{\pi a s}{r}}{\left( \sum_{a=1}^{r-1} \mathcal{S}_{da}^{\min} \sin \frac{\pi a s}{r} \right)^n} \tag{7.63}$$

and it is well defined in the  $n \rightarrow 1$  limit.

### 7.3.2 “Unusual” corrections

Even though the above expansion of the Rényi entropy recovers a clear logarithmic scaling in the limit  $\omega \rightarrow 0$ , it requires additional manipulation to study further corrections.

As noticed before, since  $\chi_h \ll \chi_{\min}$  when  $\omega$  approaches zero, we can Taylor-expand the second and third line of (7.62). When considering only the most relevant contributions, we have to separate the two cases  $n \lesseqgtr 1$ .

If  $n > 1$  the second line is more relevant and the entropy is given by:

$$S(n) = -\frac{c_{\text{eff}}}{24} \frac{n+1}{n} \log \omega + \tilde{A}^{(n)} + \sum_{h \neq \min} \tilde{B}_h^{(n)} \omega^{\frac{\Delta_h - \Delta_{\min}}{n}} + \dots \quad (7.64)$$

where the constant  $\tilde{B}_h^{(n)}$  is given by

$$\tilde{B}_h^{(n)} = \frac{1}{1-n} \frac{\sum_a \sin^n \frac{\pi a s}{r} \mathcal{S}_{da}^h}{\sum_a \sin^n \frac{\pi a s}{r} \mathcal{S}_{da}^{\min}} \quad (7.65)$$

on the other hand, in the  $n < 1$  regime,  $\omega^{\frac{\Delta_h - \Delta_{\min}}{n}}$  is less relevant than  $\omega^{\Delta_h - \Delta_{\min}}$ . In such a case, the  $\omega \rightarrow 0$  expansion has a slightly different form than before:

$$S(n) = -\frac{c_{\text{eff}}}{24} \frac{n+1}{n} \log \omega + \tilde{A}^{(n)} + \sum_{h \neq \min} \tilde{B}_h^{\prime(n)} \omega^{\Delta_h - \Delta_{\min}} + \dots \quad (7.66)$$

with

$$\tilde{B}_h^{\prime(n)} = \frac{n}{1-n} \frac{\sum_a \sin \frac{\pi a s}{r} \mathcal{S}_{da}^h}{\sum_a \sin \frac{\pi a s}{r} \mathcal{S}_{da}^{\min}} = n \tilde{B}_h^{(1)} \quad (7.67)$$

Regardless of the value of  $n$ , in both expansions a single contribution is the most relevant. The smallest conformal dimension but  $\Delta_{\min}$  - denoted by  $\Delta_1$  in the following - gives rise to the most relevant contribution in the power series (7.64) and (7.66).

As we noticed before, when we introduced the RSOS models, the temperature-like parameter  $p$  and its rescaled version  $\omega$  are not the best quantities to describe the physical behaviour of the system. Using equation (7.10) we can relate  $\omega$  to the correlation length

$\xi$ :

$$\omega = (8\xi)^{-2} + \dots \quad (7.68)$$

The entropy is the given by

$$S(n) = \frac{c_{\text{eff}} n + 1}{12 n} \log \xi + A^{(n)} + B_1^{(n)} \xi^{-\frac{2}{n}(\Delta_1 - \Delta_{\text{min}})} + n B_1^{(1)} \xi^{-2(\Delta_1 - \Delta_{\text{min}})} + \dots \quad (7.69)$$

where the constants  $A^{(n)}$  and  $B_1^{(n)}$  are a simple rescaling of their “tilded” counterparts:

$$A^{(n)} = \tilde{A}^{(n)} + \frac{c_{\text{eff}} n + 1}{4 n} \log 2 \quad (7.70)$$

$$B_1^{(n)} = 8^{-\frac{2}{n}(\Delta_1 - \Delta_{\text{min}})} \tilde{B}_1^{(n)} \quad (7.71)$$

In equation (7.69) both  $B_1$  terms have been taken into account. Of course one of them should be dropped depending on the sign of  $n - 1$ .

The results we obtained (7.69) do not only recover the leading logarithmic scaling of non unitary models studied in Chapters 5 and 6, but they also give interesting information about the corrections of such logarithmic term. A previous result of De Luca and Franchini [108] showed that such a correction scales as  $\xi^{-2\Delta/n}$ , where  $\Delta$  is the conformal dimension of the field responsible for the correction. We believe that the difference is given by the fact that the FB RSOS model is non unitary. The most characteristic non unitary feature is that the ground state  $|gs\rangle$  is not the conformal vacuum  $|\emptyset\rangle$ , but it is an excited state  $|gs\rangle = \phi_{\text{min}}(0)|\emptyset\rangle^7$ . In the same way as the central charge is replaced by its effective counterpart in the leading logarithmic term, a conformal dimension is replaced by its *effective* counterpart:

$$\begin{aligned} c &\rightarrow c_{\text{eff}} = c - 24\Delta_{\text{min}} \\ \Delta &\rightarrow \Delta_{\text{eff}} \equiv \Delta - \Delta_{\text{min}} \end{aligned} \quad (7.72)$$

As expected, the unitary case can be easily recovered by setting  $s$  to one and it is consistent with our results. Of course, in unitary theories, the smallest conformal dimension is equal zero, which implies  $c_{\text{eff}} = c$  and  $\Delta_{\text{eff}} = \Delta$ .

In many areas of one-dimensional systems, two particular regimes can usually have a

---

<sup>7</sup>While this difference is clear at the critical point, a further clarification is needed for the massive regime. If we consider a massive QFT as a perturbation of a given CFT, the ground state will be created by the field  $\phi_{\text{min}}^{QFT}$  which is itself a perturbation of its conformal equivalent  $\phi_{\text{min}}$ .

similar functional scaling. When a system is critical, it is completely “connected” and it is scaling invariant. A typical feature of this case is the power-law scaling of correlation functions. On the other hand, when the system is away from its critical phase, correlator exhibit an exponential decay, which is due to a finite correlation length. The correlation length can be naively interpreted as the scale of the system, or, in other words, as the maximal distance such that two points of the system can “feel” each other. When the system is critical, the correlation length is infinite and then the physical scale of the system is its own size  $\ell$ . As soon as the energy spectrum of the system acquires a mass gap  $m$  - i.e. it becomes critical - the actual physical scale of the system is given by an interplay between its own size  $\ell$  and the correlation length  $\xi = m^{-1}$ . While the system is “not very critical” it still exhibits a critical behaviour. As long as the correlation length “seems infinite” when compared with the physical size ( $\xi \gg \ell$ ), the system “cannot feel” the finiteness of the correlation length, since it is larger than its own size. In the opposite case, when the correlation length is small enough to “seem finite” ( $\xi \ll \ell$ ), each point of the system cannot “see” further than the correlation length. In this case, it can happen that the physical size  $\ell$  of the system is substituted by the correlation length  $\xi$  in the scaling of some physical quantities. For instance, it is well known that the gap between the two lowest eigenenergies of a discrete critical system vanishes as  $\ell^{-1}$ , where  $\ell$  represents the number of sites. On the other hand, when considering an off-critical system, such a gap does not vanish and saturates to the mass gap  $m$ . In particular, when  $\ell \ll \xi = m^{-1}$ , the gap scales as  $\ell^{-1}$  and, when  $\ell \gg \xi$ , it scales as  $\xi^{-1}$ .

Similarly to what happens with the energy gap, the role of the physical scale of a system is played by either the physical size or the correlation length in the two opposite regimes also in the scaling of the entanglement entropy.

The analogy between the large distance critical scaling (as a function of the size  $\ell$ ) and the infinite distance massive case (as a function of the correlation length  $\xi$ ) has been shown in [8] for the unitary case. Such an analogy has been demonstrated by implementing a “c-theorem like” argument, by computing some ground state expectation values of the various components of the stress-energy tensor in the many-particle manifold theory. In the non-unitary case, such an argument faces the same difficulties of a possible proof of the non-unitary version of the c-theorem, i.e. the computation of generic four-point correlation functions involving the stress-energy tensor. Also, proving that the entropy scales in the same way in the two regimes - ( $\ell \gg 1, \xi = \infty$ ) and ( $\ell = \infty, \xi \gg 1$ ) - is very intricate and it has not been achieved yet for non unitary systems. On the other hand, this lattice computation gives a very strong hint that the critical scaling is mimicked in the off-critical massive regime. While such a computation is not completely general, it covers a huge variety of universality classes. The precise analogy between the scaling of

the Rényi entropy in the two regimes suggests that Zamolodchikov's c-theorem can be generalised to the non-unitary case, even though a proof is still missing.

### 7.3.3 Off-critical logarithmic minimal models

One of the most intriguing features of critical Forrester Baxter RSOS models is that, under certain conditions, they provide also a lattice realisation of logarithmic minimal models [109]. In particular, it has been shown that when taking the limit of  $r$  and  $s$  going to infinity while keeping their ratio fixed  $r/s \equiv R/S$ , the FB models at critical point - between Regimes III and IV ( $p = 0$ ,  $0 < u < \lambda$ )- are a lattice realisation of logarithmic minimal models  $\mathcal{LM}_{R-S,R}$ . Interestingly, it is possible to define a  $\phi_{13}$  perturbation of these models, called *Off-critical logarithmic minimal models* [110].

The Rényi entropy of such models can be obtained from (7.69) by taking the  $r, s \rightarrow \infty$  limit:

$$S(n) = \frac{1}{12} \frac{n+1}{n} \log \xi + \bar{A}^{(n)} + \bar{B}_1^{(n)} \xi^{-\frac{2}{n}(\Delta_1 - \Delta_{\min})} + n \bar{B}_1^{(1)} \xi^{-2(\Delta_1 - \Delta_{\min})} + \dots \quad (7.73)$$

where the constant  $\bar{B}_1^{(n)}$  is the simple limit of its non-logarithmic counterpart:

$$\bar{B}_1^{(n)} = \lim_{r,s \rightarrow \infty} B_1^{(n)} \quad (7.74)$$

The main problem that appears when taking such a limit is inside the definition of the modular S matrix (3.44), which is proportional to  $[r(r-s)]^{-1/2} = r^{-1}(1-s/r)^{-1/2}$ . Such a prefactor, which tends to zero in the  $r, s \rightarrow \infty$  logarithmic limit, creates some problems in the definition of the constants in equation (7.73). While the S matrix appears in both the numerator and the denominator with the same power, in the definition of the coefficient  $B_1^{(n)}$  (7.70), it is not the case for the constant  $A^{(n)}$  (7.63). The difference between the two powers at the nominator and the denominator makes the constant  $A^{(n)}$  ill defined when  $r$  and  $s$  tend to infinity.

In order to avoid this divergence, which scales with  $r^{n-1}$ , we can multiply the partition function  $W_n$  by  $r^n$ , in a renormalisation-like approach:

$$W_n \rightarrow r^n W_n \quad (7.75)$$

Such a renormalisation allows  $\bar{A}^{(n)}$  to have a finite value:

$$\bar{A}^{(n)} = \lim_{r,s \rightarrow \infty} \left( A^{(n)} + \log r \right) \quad (7.76)$$

This procedure, which can be interpreted the entropic version of the generalised order parameter for such models [110], lacks of a better understanding from a physical point of view. However, it affects only the numerical value of the constant term and not the functional shape of the  $\xi$  dependence.

The leading logarithmic term of (7.73) depends on the effective central charge - which is identically to one for any choice of  $R$  and  $S$  - in agreement with the CFT prediction (5.24) when the size  $\ell$  of the subsystem  $A$  is replaced by the correlation length  $\xi$ . However, the double logarithmic term predicted in (5.24) is missing in the lattice realisation (7.73). Such a discrepancy can be explained by the fact that off-critical logarithmic FB RSOS models are not *truly* logarithmic. As noticed by Pearce and Seaton [110] the logarithmic feature that logarithmic FB RSOS models enjoy at criticality is lost as soon as the system is perturbed outside its critical region. As explained in Chapter 5, a model is called logarithmic when its Hamiltonian presents non diagonalisable Jordan. Such a feature, which is enjoyed by logarithmic FB RSOS models at criticality, disappears out of criticality. For this reason, the off-critical logarithmic FB RSOS models are not properly logarithmic and they behave as standard non-unitary systems, in agreement with the scaling predicted in Chapter 5.

## 7.4 RSOS Quantum Hamiltonians

In the previous section we computed the Rényi entropy for a very broad class of one-dimensional quantum systems associated with the Forrester Baxter RSOS models. Even though such a computation gives precious and important information about the scaling of the entropy in a huge variety of cases, it is legitimate to investigate which is the underlying one-dimensional quantum Hamiltonian. In this section we will perform a Hamiltonian limit, a procedure to compute a Hamiltonian operator from its corresponding evolution operator, represented by a row-to-row transfer matrix in our case. In our analysis we will specialise to the periodic case (when a single row-to-row transfer matrix is enough to compute the Hamiltonian). However, we should expect to obtain the very same quantum chain also in the open case (double row-to-row transfer matrix). While such a computation had already been performed [111, 112] at the critical point, less is known about the off-critical Hamiltonian. It is well known[112] that the generators  $e_j$  of the Temperley-Lieb

Algebra [113] can be used to build up the critical Hamiltonian for such models:

$$\begin{aligned}
 H_{TL} &= - \sum_{j=1}^N e_j \\
 e_j e_{j\pm 1} e_j &= e_j \\
 e_j^2 &= \beta e_j \\
 e_i e_j &= e_j e_i \quad \text{if } |i - j| > 1
 \end{aligned} \tag{7.77}$$

where the coefficient  $\beta$  is called *loop fugacity* and for RSOS models (ABF and FB) and is equal to  $2\cos \lambda$ . Different representations of such an algebra have been studied [114, 115] and it has been shown that some XXZ spin chains with particular boundary conditions are (in their thermodynamic limit) lattice representations of conformal minimal models. In this section we will perform the Hamiltonian limit outside the critical region and we will provide a consistent formulation of the quantum lattice representation of  $\phi_{13}$  perturbed minimal models. Since we are interested in such models, we will focus on the Regime III ( $0 < p < 1$  and  $0 < u < \lambda$ ) which provides a lattice realisation of off-critical minimal models.

### Building the transfer matrix

In order to build up a row-to-row transfer matrix like the one in Figure 7.2, we introduce the *face transfer operator*. Such operators are the building blocks of various objects (including Corner Transfer Matrices) and represent the Boltzmann weights of a single tile:

$$\mathbb{X}_j(u)_{\ell_{j-1}, \ell_j, \ell_{j+1}}^{\ell'_{j-1}, \ell'_j, \ell'_{j+1}} = \delta_{\ell_{j-1}, \ell'_{j-1}} \delta_{\ell_{j+1}, \ell'_{j+1}} \times \ell_{j-1} \text{---} \begin{array}{c} \ell'_j \\ \diagup \quad \diagdown \\ u \\ \diagdown \quad \diagup \\ \ell_j \end{array} \text{---} \ell_{j+1} \tag{7.78}$$

The red arc at the bottom of the square has the simple role to keep track of the orientation of the tile. Such an operator, which maps the string of local variables  $\ell_{j-1}, \ell_j, \ell_{j+1}$  into  $\ell'_{j-1}, \ell'_j, \ell'_{j+1}$  can be used to compute various objects. In particular it is very useful for the construction of transfer matrices. Such a notation encapsulates graphically the Boltzmann weights (7.4) and it gives a visual taste of the physical meaning of such weights.

Following Baxter [11], in order to build up transfer matrices involving more than just three sites, we should extend the definition of the face operator in order to take into account a

string of  $N$  sites:

$$\begin{aligned}
 \mathbb{X}_j(u)_{\ell}^{\ell'} &= \begin{array}{c} \ell'_1 \quad \ell'_2 \quad \cdots \quad \ell'_{j-2} \quad \ell'_{j-1} \quad \ell'_j \quad \ell'_{j+1} \quad \ell'_{j+2} \quad \cdots \quad \ell'_{N-1} \quad \ell'_N \\ a_1 \quad a_2 \quad \cdots \quad \ell_{j-2} \quad \ell_{j-1} \quad u \quad \ell_{j+1} \quad \ell_{j+2} \quad \cdots \quad \ell_{N-1} \quad \ell_N \\ \ell_j \end{array} \\
 &= \left( \prod_{i \neq j} \delta_{\ell_i \ell'_i} \right) \begin{array}{c} \ell'_j \quad \ell'_{j+1} \\ u \\ \ell_j \end{array} \end{aligned} \tag{7.79}$$

This operator acts non trivially only on the site  $j$  and does not affect all the other local variables. The choice of considering a  $45^\circ$  rotated lattice [11] makes the construction of corner transfer matrices easier. Moreover, with such a convention, they can be represented as local operators - i.e. they act non trivially only on few neighbour sites.

Using the face transfer operators, we can construct explicitly the row-to-row transfer matrix:

$$T(u)_{\ell}^{\ell'} = \prod_{i=1}^N \mathbb{X}_i(u)_{\ell'_i \ell_i \ell_{i+1}}^{\ell'_i \ell'_{i+1} \ell_{i+1}} = \begin{array}{c} \ell'_1 \quad \ell'_2 \quad \ell'_3 \quad \cdots \quad \ell'_{N-1} \quad \ell'_N \quad \ell'_1 \\ \ell_1 \quad \ell_2 \quad \ell_3 \quad \cdots \quad \ell_{N-1} \quad \ell_N \quad \ell_1 \end{array} \tag{7.80}$$

Thanks to the above equation we can compute directly the underlying quantum Hamiltonian<sup>8</sup>

$$H = - \frac{d}{du} \log T(u) \Big|_{u=0} \tag{7.81}$$

Since the RSOS restrictions on the values of the local heights make the analysis quite complicated, it can be convenient to specialise to one simple case first before addressing a more generic computation. Moreover, before addressing the actual computation of the Hamiltonian, it is worth understanding the multiplication rules of the face operators.

### 7.4.1 Multiplying face operators

Let us first consider the case of two face operators acting on the same site  $j$ , for instance the operators  $\mathbb{X}_j(u)$  and  $\mathbb{X}_j(v)$ . We define the product  $\mathbb{X}_j(u)\mathbb{X}_j(v)$  by placing the latter on top of the former and summing over all possible values of the common local height (see

<sup>8</sup>Since the parameter  $u$  represents the anisotropy of the lattice, the  $u \rightarrow 0$  limit represents a lattice with infinitesimal lattice spacing.

equation (7.82)).

$$\mathbb{X}_j(u)\mathbb{X}_j(v) = \begin{array}{c} \begin{array}{c} c' \\ \diagdown \quad \diagup \\ d' \quad v \quad b' \\ \diagup \quad \diagdown \\ d \quad u \quad b \\ a \end{array} \\ \text{---} \\ \begin{array}{c} d' \\ \diagdown \quad \diagup \\ d \quad u \quad b \\ a \end{array} \end{array} \quad (7.82)$$

In the above equation a sum over all possible values of the internal local height  $g$  has been performed. Moreover, since the action of a face operator does not change the values of the external local heights, the product is non vanishing only if the external local heights are the same in the two tiles, i.e.  $d' = d$  and  $b' = b$ .

In order to build up operators like the row-to-row transfer matrix (7.80), we have to multiply face operators acting on different (adjacent sites). As before, the right value of the multiplication will be at the bottom of the left value:

$$\mathbb{X}_{j+1}(u)\mathbb{X}_j(v) = \begin{array}{c} \begin{array}{c} c' \\ \diagdown \quad \diagup \\ d' \quad v \quad c \\ \diagup \quad \diagdown \\ a \quad u \quad b \\ a \end{array} \end{array} \quad (7.83)$$

In this case there is no need to sum, as there are no internal local heights. In order to have a non zero result of the multiplication, the local heights  $d$  and  $c$  have to be the same on both tiles.

Iterating such a definition it is possible to define larger objects, like the row-to-row transfer matrix (7.80).

Moreover, the two multiplication rules can be used to implement explicitly the inversion relation [11]:

$$\mathbb{X}_j(u)\mathbb{X}_j(-u) = \frac{s(\lambda - u)s(\lambda + u)}{s(\lambda)^2} \mathbf{1} \quad (7.84)$$

and the Yang-Baxter equation [11]

$$\mathbb{X}_j(u)\mathbb{X}_{j+1}(u+v)\mathbb{X}_j(v) = \mathbb{X}_{j+1}(v)\mathbb{X}_j(u+v)\mathbb{X}_{j+1}(u) \quad (7.85)$$

Even though the two equations (7.85) and (3.50) - sometimes referred to as *hexagon Yang-Baxter* and *vertex Yang-Baxter*, respectively - are different in form, they are equivalent one to each other [116] and they both guarantee the integrability of the models they are

referring to.

#### 7.4.2 The $r = 5$ case (the $T_2$ quantum chains)

Let us consider first the FB (or ABF) RSOS model with the parameter  $r$  set to 5. Compared to other values of  $r$ , such choice allows a more intuitive representation of the local heights. When considering two neighbour local heights, their values run from 1 to 4 and they have to differ exactly by one. If the first height has one of the central values, say 2, the other height can have *two distinct* values, 1 or 3. On the other hand, if the first height has one of the extremal values, say 1, the other one can have *just one* value, 2. In fact we can classify the values of the local heights into two subgroups: the extremal (1 and 4, denoted by  $\bullet$ ) and the bulk (2 and 3, denoted by  $\circ$ ). When moving from a site to its adjacent, a bulk value can either become an extremal or remain bulk. For instance, the bulk value 2 can either become 1 (extremal) or 3 (still bulk). On the other hand, an extremal value must become bulk. Such restrictions can be encapsulated into the *tadpole* diagram  $T_2$ :

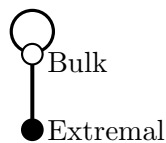


Figure 7.5: Tadpole diagram  $T_2$ .

In order to simplify the notation we can introduce some additional local variables  $\sigma_j$  instead of the local heights  $\ell_j$ :

$$\sigma_j = \begin{cases} 0 & \ell_j = 2, 3 \\ 1 & \ell_j = 1, 4 \end{cases} \quad (7.86)$$

The RSOS restriction  $|\ell_j - \ell_{i+1}| = 1$  is simply translated into  $\sigma_j \sigma_{i+1} = 0$ . If we want to describe as a particle the state  $\sigma_j = 1$  and as a vacuum the state  $\sigma_j = 0$ , the restriction rule implies that there cannot be two adjacent particles. If we consider a periodic system with  $N$  sites ( $\sigma_{i+N} \equiv \sigma_i$ ) the number of allowed configurations with initial site  $\sigma_1 = 0$  is simply given by  $F_{N+1}$ , where  $F_N$  is the  $N$ th term of the Fibonacci sequence:

$$F_N = F_{N-1} + F_{N-2} = 0, 1, 1, 2, 3, 5, 8, 13, 21, 34, \dots \quad (7.87)$$

while the number of allowed configurations starting with  $\sigma_1 = 1$  is given by  $F_{N-1}$ . The total number of allowed configurations (considering both starting points) is given by the  $N$ th Lucas number:

$$L_N = F_{N+1} + F_{N-1} = \varphi^N + (-1)^N \varphi^{-N} = 1, 3, 4, 7, 11, 18, 29, 47, \dots \quad (7.88)$$

where  $\varphi$  is the celebrated golden ratio

$$\varphi = \frac{1 + \sqrt{5}}{2} = 1.6180339887498948482 \dots \quad (7.89)$$

Until now we have not specified the value of the parameter  $s$ . Since different values of such a parameter give rise to quite different models, we will consider the  $s = 1$  and  $s = 3$  cases separately<sup>9</sup>.

### Golden chain

Let us now focus on the  $r = 5$  and  $s = 1$  case, which corresponds to the tricritical Ising model. The critical case has been studied extensively in [111] and it has been identified with the so-called Fibonacci Golden Chain.

The face transfer operator for the  $s = 1$  case is given by<sup>10</sup>

$$\begin{aligned} \mathbb{X}_j(u) &= \text{diamond}(u) \\ &= \frac{s(2\lambda + u)}{s(2\lambda)} \text{tile}_1 + \frac{s(2\lambda - u)}{s(2\lambda)} \text{tile}_2 + \frac{s(\lambda - u)}{s(\lambda)} \left( \text{tile}_3 + \text{tile}_4 \right) \\ &+ \frac{s(\lambda + u)}{s(\lambda)} \text{tile}_5 + \frac{s(u)}{\sqrt{s(\lambda)s(2\lambda)}} \left( \text{tile}_6 + \text{tile}_7 \right) \end{aligned} \quad (7.90)$$

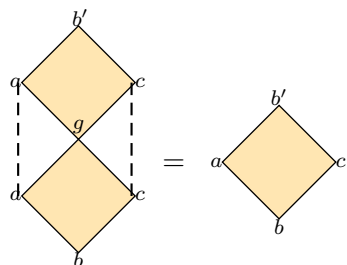
where the yellow tiles (denoted by  $E_j$  in the following) are simple  $\delta_s$  operators which select the right Boltzmann weight for a given configuration. For instance, the Boltzmann weight of the configuration  $\sigma_{j-1} = \sigma_j = \sigma_{j+1} = 0$  and  $\sigma'_j = 1$  is given by  $s(u)/\sqrt{s(\lambda)s(2\lambda)}$ .

It is possible to define a multiplication also for these simple tile operators  $E_j$ . The definition is almost the same as for the face operators (Section 7.4.1). The only difference

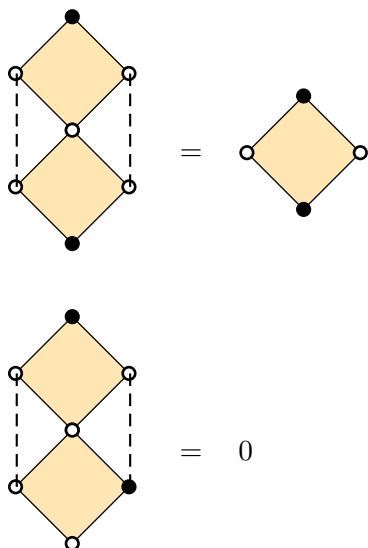
<sup>9</sup>These are the most interesting cases, as they correspond to the thermally perturbed minimal models  $\mathcal{M}_{45}$  and  $\mathcal{M}_{25}$  (the tricritical Ising and the Lee-Yang universality classes).

<sup>10</sup>In this section we chose the symmetric gauge  $g_\ell = \sqrt{s(\ell\lambda)}$  in the Boltzmann weights (7.4).

is that there is no sum over internal configurations. When multiplying two  $E_j$  matrices acting on the same sites, the result is given by:


(7.91)

Of course, such a multiplication vanishes if any of the common local heights are different in the two tiles. For instance, consider the following examples:


(7.92)

When multiplying two yellow tiles acting on adjacent sites, the same convention of Section 7.4.1 applies: the result is not zero if two local heights shared by two tiles have the same value.

The equation (7.90) can be used to compute directly the Hamiltonian:

$$\begin{aligned}
 H &= \sum_{i=1}^N H_j \\
 H_j &= -\frac{d}{du} \log \mathbb{X}_j(u) \Big|_{u=0} = -\mathbb{X}_j(0)^{-1} \frac{d}{du} \mathbb{X}_j(u) \Big|_{u=0} \\
 &= \frac{s'(2\lambda)}{s(2\lambda)} \text{diag}(\circ, \bullet, \circ, \circ) - \frac{s'(2\lambda)}{s(2\lambda)} \text{diag}(\bullet, \circ, \circ, \circ) - \frac{s'(\lambda)}{s(\lambda)} \left( \text{diag}(\circ, \bullet, \circ, \bullet) + \text{diag}(\bullet, \circ, \bullet, \circ) \right) \\
 &+ \frac{s'(\lambda)}{s(\lambda)} \text{diag}(\bullet, \bullet, \circ, \circ) + \frac{s'(0)}{\sqrt{s(\lambda)s(2\lambda)}} \left( \text{diag}(\bullet, \circ, \circ, \bullet) + \text{diag}(\circ, \bullet, \bullet, \circ) \right)
 \end{aligned} \tag{7.93}$$

Notice that in the above calculation the prefactor  $\mathbb{X}_j(0)^{-1}$  plays a trivial role, since<sup>11</sup>

$$\mathbb{X}_j(0) = \text{diag}(\circ, \bullet, \circ, \circ) + \text{diag}(\bullet, \circ, \circ, \circ) + \text{diag}(\circ, \bullet, \circ, \bullet) + \text{diag}(\bullet, \circ, \bullet, \circ) + \text{diag}(\bullet, \bullet, \circ, \circ)$$

(7.94)

is a projector onto all possible configuration and it is, in fact, the identity operator.

From the particle-hole point of view, the various terms of the above Hamiltonian have a very physical meaning. In particular, terms like

$$\text{diag}(\bullet, \circ, \circ, \circ)$$

(7.95)

simply measure the presence (or absence) of a particle in the central site  $j$ . On the other hand, the operators

$$\text{diag}(\bullet, \bullet, \circ, \circ) \quad \text{diag}(\circ, \bullet, \bullet, \circ)$$

(7.96)

have a much more interesting action: they act like creation and annihilation operators. In fact, they transform the site  $j$  from  $\circ$  to  $\bullet$  and vice versa.

Such a formulation allows us also to perform a  $p \rightarrow 0$  limit towards the critical point.

---

<sup>11</sup> $s(0) = 0$ .

The critical Hamiltonian is then given by

$$H_j = a + be_j \tag{7.97}$$

where  $a$  and  $b$  are two simple numerical constants. The operator  $e_j$  is given by

$$e_j = \begin{array}{c} \circ \\ \diagup \quad \diagdown \\ \circ \quad \circ \\ \diagdown \quad \diagup \\ \circ \end{array} + \frac{1}{\beta} \begin{array}{c} \bullet \\ \diagup \quad \diagdown \\ \circ \quad \circ \\ \diagdown \quad \diagup \\ \bullet \end{array} + \beta \begin{array}{c} \circ \\ \diagup \quad \diagdown \\ \bullet \quad \bullet \\ \diagdown \quad \diagup \\ \circ \end{array} + \frac{1}{\sqrt{\beta}} \left( \begin{array}{c} \bullet \\ \diagup \quad \diagdown \\ \circ \quad \circ \\ \diagdown \quad \diagup \\ \bullet \end{array} + \begin{array}{c} \circ \\ \diagup \quad \diagdown \\ \bullet \quad \bullet \\ \diagdown \quad \diagup \\ \circ \end{array} \right) \tag{7.98}$$

where  $\beta = 2 \cos \frac{\pi}{5}$ .

Using the multiplication rules defined above for the yellow tiles, it is possible to show that the operator  $e_j$  (as defined in (7.98) using the  $E_j$  operators) satisfy

$$\begin{aligned} e_j^2 &= \beta e_j \\ e_j e_{j\pm 1} e_j &= e_j \\ e_i e_j &= e_j e_i \quad \text{for } |i - j| > 1 \end{aligned} \tag{7.99}$$

Such relations show that the Hamiltonian we obtained can be expressed as a representation of the Temperley-Lieb algebra. At the critical point, our computation then recovers the Golden Chain anyonic Hamiltonian [111].

### The Lee-Yang off-critical chain

Using the same particle-hole interpretation used in the last section, we can compute also the quantum Hamiltonian of the Lee-Yang regime ( $r = 5$  and  $s = 3$ ).

In this context the face operator and the quantum Hamiltonian are very similar to the previous case ( $s = 1$ ). The only difference relies in the different Boltzmann weight associated to two symmetric configurations. In order to simplify the notation, we will consider the simpler, non symmetric gauge choice of  $g_\ell = 1$ . The face operator in this case is given

by

$$\begin{aligned}
 \mathbb{X}_j(u) &= \text{diamond}(u) = \frac{s(2\lambda + u)}{s(2\lambda)} \text{diamond}(u) + \frac{s(2\lambda - u)}{s(2\lambda)} \text{diamond}(u) \\
 &+ \frac{s(\lambda - u)}{s(\lambda)} \left( \text{diamond}(u) + \text{diamond}(u) \right) + \frac{s(\lambda + u)}{s(\lambda)} \text{diamond}(u) \\
 &+ \frac{s(u)}{s(2\lambda)} \text{diamond}(u) + \frac{s(u)}{s(\lambda)} \text{diamond}(u)
 \end{aligned} \tag{7.100}$$

and the Hamiltonian can be obtained immediately from it:

$$\begin{aligned}
 H &= - \sum_{i=1}^N H_j \\
 H_j &= \frac{s'(2\lambda)}{s(2\lambda)} \text{diamond}(u) - \frac{s'(2\lambda)}{s(2\lambda)} \text{diamond}(u) - \frac{s'(\lambda)}{s(\lambda)} \left( \text{diamond}(u) + \text{diamond}(u) \right) \\
 &+ \frac{s'(\lambda)}{s(\lambda)} \text{diamond}(u) + \frac{s'(0)}{s_1(2\lambda)} \text{diamond}(u) + \frac{s'(0)}{s(\lambda)} \text{diamond}(u)
 \end{aligned} \tag{7.101}$$

The main difference between this Hamiltonian and the previous one (7.93) lies in the last two terms of each operator. While in the unitary version (7.93) the creation and annihilation operators appear with the same numerical coefficient, it is not the case for the non unitary case (7.101). It can be argued that this discrepancy is due to the different gauge choice. However, it should be noticed that the numerical coefficient in front of the creation/annihilation operator - whilst it is the same for both operators - becomes purely imaginary in the Lee Yang case when choosing the symmetric gauge  $g_\ell = \sqrt{s(\ell\lambda)}$ . On the other hand, the choice of the asymmetric gauge  $g_\ell = 1$  in the unitary case leads to different coefficients for the creation and annihilation operators, even though they are still purely real. In conclusion, it is possible to fix the gauge in both cases in order to have a meaningful physical interpretation. In the Lee Yang case it is preferable to choose the asymmetric gauge fixing in order have real coefficients. In order to interpret these terms as creation/annihilation operators, the coefficients in front of them - i.e. the energy lost/gained when creating/annihilating a particle - have to be real.

Of course, the critical Hamiltonian can be obtained by performing the  $p \rightarrow 0$  limit. As

before, the Hamiltonian can be written in terms of  $e_j$  operators:

$$H_j = a + be_j \quad (7.102)$$

where the operator  $e_j$  is given by

$$e_j = \begin{array}{c} \circ \\ \diagup \quad \diagdown \\ \circ \quad \circ \\ \diagdown \quad \diagup \\ \circ \end{array} + \frac{1}{\beta} \begin{array}{c} \bullet \\ \diagup \quad \diagdown \\ \circ \quad \circ \\ \diagdown \quad \diagup \\ \bullet \end{array} + \beta \begin{array}{c} \circ \\ \diagup \quad \diagdown \\ \bullet \quad \bullet \\ \diagdown \quad \diagup \\ \circ \end{array} + \frac{1}{\beta} \begin{array}{c} \bullet \\ \diagup \quad \diagdown \\ \bullet \quad \bullet \\ \diagdown \quad \diagup \\ \bullet \end{array} + \begin{array}{c} \circ \\ \diagup \quad \diagdown \\ \bullet \quad \bullet \\ \diagdown \quad \diagup \\ \circ \end{array} \quad (7.103)$$

and the loop fugacity  $\beta$  is equal to  $2 \cos \frac{3\pi}{5}$ .

Once again, the multiplication rules can be used to check that the above operators  $e_j$  belong to a representation of the Temperley-Lieb algebra:

$$\begin{aligned} e_j^2 &= \beta e_j \\ e_j e_{j\pm 1} e_j &= e_j \\ e_i e_j &= e_j e_i \quad \text{for } |i - j| > 1 \end{aligned} \quad (7.104)$$

#### The $r = 5$ Hamiltonians using Pauli matrices

Once we have computed the Hamiltonians of the two  $r = 5$  cases studied using the tiles operators, it is worth translating these Hamiltonians into a Pauli matrix formalism. Such a formalism is also used in the study of quantum critical chains representing the so-called *Fibonacci Anyons* [111]. In particular, let  $n_j$  be the (inverse) number operator (defined as  $n_j(\circ) = 1$  and  $n_j(\bullet) = 0$ ) and  $\sigma_j^x$  be the flipping operator (defined as  $\sigma_j^x(\circ) = \bullet$  and  $\sigma_j^x(\bullet) = \circ$ ). With this notation it is possible to rewrite the Hamiltonian (7.93) as

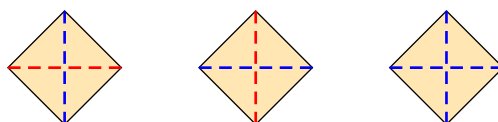
$$\begin{aligned} H_j &= -2 \frac{s'(\lambda)}{s(\lambda)} (n_{i-1} + n_{i+1} - \mathbf{1}) \\ &+ n_{i-1} n_{i+1} \left[ \frac{s'(0)}{s(\lambda)s(2\lambda)} \sigma_j^x + 2 \frac{s'(2\lambda)}{s(2\lambda)} n_j + \left( 3 \frac{s'(\lambda)}{s(\lambda)} - \frac{s'(2\lambda)}{s(2\lambda)} \right) \right] - \frac{s'(\lambda)}{s(\lambda)} \mathbf{1} \end{aligned} \quad (7.105)$$

The critical limit  $p \rightarrow 0$  of the above Hamiltonian is equal to the Fibonacci Hamiltonian (up to a multiplicative and an additive constants) studied in [111]. The above Hamiltonian can then be seen as the off-critical perturbation of the Fibonacci Hamiltonian.

Even though the Hilbert space is not given by  $\mathbb{C}^{2N}$  (since two neighbour particles are forbidden) a formulation using Pauli matrices could be more intuitive from the physical point of view.

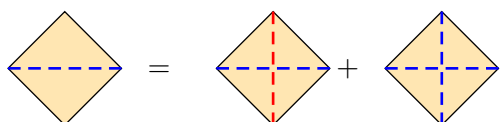
### 7.4.3 The generic case

Once we have analysed the  $r = 5$  case, we can address the computation of the quantum off-critical Hamiltonian for a wider class of models. A generic base vector can be represented by a collection of  $N$  local heights, each of them running from 1 to  $r - 1$  with the condition that two neighbour heights must differ exactly by one. While the  $r = 5$  model allows a nice physical interpretation in terms of particles and holes, such a representation is missing when studying the FB RSOS models with generic values of  $r$  and  $s$ . Nevertheless it is possible to classify the various configurations around a tile using the values of the local heights. In particular, we are interested whether opposite local heights have the same value. In this section, we will denote with a blue dashed line a couple of opposite local heights with the same value. On the other hand, a red dashed line indicates that the couple of local heights have different values. Thus, the possible configurations of local heights around a tile are just three:



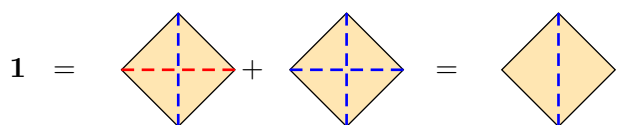
$$(7.106)$$

Additionally, when one of the two dashed lines are missing, all possible configurations are considered. For instance, consider the following example of a tile with just one dashed line:



$$(7.107)$$

Moreover, we can notice that the identity <sup>12</sup> is the operator which leaves the three local heights unaffected:



$$(7.108)$$

---

<sup>12</sup>Intended as an operator mapping the lower configuration into the upper one.

Using this compact notation for the yellow tiles, we can write explicitly the face operator for generic values of  $r$  and  $s$ :

$$\mathbb{X}_j(u) = \begin{array}{c} c \\ \diagup \quad \diagdown \\ u \\ \diagdown \quad \diagup \\ a \end{array} = \omega_{1,b}(u) \begin{array}{c} b' \\ \diagup \quad \diagdown \\ \quad \quad \quad \\ \diagdown \quad \diagup \\ a \quad c \\ \quad \quad \quad \\ b \end{array} + \omega_{2,a}(u) \begin{array}{c} b' \\ \diagup \quad \diagdown \\ \quad \quad \quad \\ \diagdown \quad \diagup \\ \quad \quad \quad \\ b \end{array} + \omega_{3,a}(u) \begin{array}{c} b' \\ \diagup \quad \diagdown \\ \quad \quad \quad \\ \diagdown \quad \diagup \\ \quad \quad \quad \\ b \end{array} \quad (7.109)$$

Once again, we can perform the Hamiltonian limit of the transfer matrix to obtain an explicit expression of the off-critical Hamiltonian. In order to avoid imaginary coefficients in the Hamiltonian, we choose the asymmetric  $g_\ell = 1$  gauge fixing. The Hamiltonian is then given by:

$$H = - \sum_{i=1}^N H_j$$

$$H_j = \left[ \frac{s'(0)}{s(\lambda)} F_j + G_j \right] \quad (7.110)$$

where the operators  $F_j$  and  $G_j$  are given by

$$F_j = \frac{s(b'\lambda)}{s(c\lambda)} \begin{array}{c} b' \\ \diagup \quad \diagdown \\ \quad \quad \quad \\ \diagdown \quad \diagup \\ a \quad c \\ \quad \quad \quad \\ b \end{array}$$

$$G_j = \left[ \frac{s'(\lambda)}{s(\lambda)} - \frac{s'(0)}{s(\lambda)} \frac{s(b'\lambda)}{s(c\lambda)} + (b' - c) \frac{s'(c\lambda)}{s(c\lambda)} \right] \begin{array}{c} b' \\ \diagup \quad \diagdown \\ \quad \quad \quad \\ \diagdown \quad \diagup \\ \quad \quad \quad \\ b \end{array} \quad (7.111)$$

Also in this very generic case we can set  $p$  to zero in order to analyse the critical Hamiltonian. In such a regime the  $G_j$  vanishes and the Hamiltonian is simply given by

$$H_j = \frac{s'(0)}{s(\lambda)} F_j \quad (7.112)$$

Decomposing the yellow tile using (7.107) it is possible to show that the operator  $F_j$  is a representation of the Temperley-Lieb algebra with fugacity  $\beta = 2 \cos \lambda = 2 \cos \frac{s\pi}{r}$ :

$$F_j^2 = \beta F_j$$

$$F_j F_{i\pm 1} F_j = F_j$$

$$F_i F_j = F_j F_i \quad \text{for } |i - j| > 1 \quad (7.113)$$

In conclusion, even in the generic case we are able to derive a precise form of an off-critical Hamiltonian associated with off-critical minimal models (unitary and non unitary). Even though these operators are not always symmetric (or hermitian) they are suitable Hamiltonians. For instance, their eigenspectrum is real and the Hamiltonian itself can be diagonalised, once subtleties have been considered. For instance, it is well known [114, 115] that the so-called *quantum group reduction* has to be implemented in order to diagonalise the critical version of the above Hamiltonians. In the off-critical case, even though such a process can be implemented in a case-by-case study, a general formulation is far from complete. This is mainly due to the fact that the underlying symmetry of the critical case (the quantum group) has been widely studied and developed. On the other hand, a complete understanding of the symmetries of the off-critical case is still missing.

## 7.5 Conclusions

While all other chapters focus on evaluation of entanglement using field theory techniques, in this Chapter we used a lattice oriented approach. In particular, we computed the scaling of entanglement entropy of infinite off-critical systems at different values of the mass gap using the so-called Corner Transfer Matrix approach. The lattice system we analysed are the so-called Forrester Baxter RSOS models. In a particular configuration (called Regime III) these models provide a lattice realisation of thermally perturbed non unitary minimal models. While such a computation has already been performed in some similar unitary systems [108], the non unitary generalisation has never been attempted.

As expected, we found that the leading term of the entropy scales logarithmically, as in the unitary case. The main difference is that the central charge has been replaced by its effective counterpart. From the physical point of view, the reason for this replacement is the same as in the non unitary critical case: the conformal vacuum is different from the physical ground state. Additionally, we could also analyse the first corrections to the logarithmic scaling. We showed that non unitarity affects not only the logarithmic scaling, but also its corrections. While in the unitary case such corrections are related to the conformal dimension  $\Delta$  of a certain field, we found that in the non unitary case they are affected also by the non trivial ground state. We introduced then also the notation of effective conformal dimension  $\Delta \rightarrow \Delta_{\text{eff}} = \Delta - \Delta_{\text{min}}$ , which, like the effective central charge, takes into account the non trivial action of the ground state. Moreover, we computed the entropy of the so-called off-critical logarithmic minimal models, which can be easily realised by a particular limit of the FB RSOS models.

While quantum one dimensional Hamiltonians associated with conformal minimal models have been known in the literature for a long time, less is known about the off critical case. In order to have a better understanding of the quantum chain the FB RSOS models

represent, we performed a Hamiltonian limit of such systems. With this tool we managed to compute the explicit expressions of one-dimensional quantum chains associated with generic off critical minimal models. Even though the notation used might seem not very intuitive from a physical point of view, we showed that few cases known in the literature can be recovered from our results. In particular, the critical limit of the FB RSOS Hamiltonians matches perfectly with a class of Hamiltonians known to be a spin chain representation of minimal models. Furthermore, we showed that the so-called Fibonacci chain can be easily recovered from our results.

## Chapter 8

# Logarithmic Negativity and Entanglement Entropy in Free Boson Theories

In the previous sections of this thesis (Chapters 5, 6 and 7) we focused on the evaluation of the entanglement entropy of non unitary theories. In such cases we focused on the bipartite case, i.e. when the system is divided in just two regions. In this Chapter we study the entanglement of non-compactified free boson systems in various configurations. In particular, we consider the bipartite entanglement entropy of a single interval and the logarithmic negativity between two disjoint semi-infinite intervals. These entanglement measures can be computed using correlation functions of twist fields and we probe both the critical and massive regimes using form factor expansions.

### 8.1 Logarithmic Negativity

As we have seen in Chapter 2, entanglement entropy - one of the most celebrated entanglement measures - fails to measure the amount of quantum entanglement between non complementary subsystems. As previously explained, another measure of entanglement must be introduced. A suitable quantity is the logarithmic negativity (2.44) [28, 31]:

$$\mathcal{E} = \lim_{n_e \rightarrow 1} \log \text{tr}_{A \cup B} \left( \rho_{A \cup B}^{T_B} \right)^{n_e} \quad (8.1)$$

where  $T_B$  denotes the partial transposition of the degrees of freedom belonging to the subsystem  $B$  (see Section 2.3).

As in the entanglement entropy case, logarithmic negativity can be expressed as a correlation functions involving twist fields. In particular, when considering a system  $A \cup B \cup C$ ,

the partial transpose of the reduced density matrix is given by [31]:<sup>1</sup>

$$\text{tr} \left( \rho_{A \cup B}^{T_B} \right)^n = \left\langle \mathcal{T}(a_1) \tilde{\mathcal{T}}(a_2) \tilde{\mathcal{T}}(b_1) \mathcal{T}(b_2) \right\rangle \quad (8.2)$$

where  $A = [a_1, a_2]$ ,  $B = [b_1, b_2]$ . Such a formulation can also be extended to a much simpler case. If we consider a gapped system made of two disjoint semi infinite regions  $A = ]-\infty, 0]$  and  $B = [r, +\infty[$  (see Figure 8.2), the four-point correlation function factorises into a much simpler two-point correlator:

$$\lim_{\substack{a_1 \rightarrow -\infty \\ b_2 \rightarrow +\infty}} \left\langle \mathcal{T}(a_1) \tilde{\mathcal{T}}(0) \tilde{\mathcal{T}}(r) \mathcal{T}(b_2) \right\rangle = \langle \mathcal{T} \rangle \langle \tilde{\mathcal{T}}(0) \tilde{\mathcal{T}}(r) \rangle \langle \mathcal{T} \rangle = \langle \mathcal{T} \rangle^2 \langle \mathcal{T}(a) \mathcal{T}(b) \rangle \quad (8.3)$$

thanks to the fact that  $\langle \tilde{\mathcal{T}}(0) \tilde{\mathcal{T}}(r) \rangle = \langle \mathcal{T}(0) \mathcal{T}(r) \rangle$ .

In this chapter we study the scaling of entanglement of a free bosonic system in various configurations through the analysis of the correlators  $\langle \mathcal{T}(0) \tilde{\mathcal{T}}(r) \rangle$  and  $\langle \mathcal{T}(0) \mathcal{T}(r) \rangle$ , which can be expanded into a form factor series.

The value of the vacuum expectation value  $\langle \mathcal{T} \rangle$ , while it is usually difficult to compute exactly in QFT, it can be estimated through the methods discussed in Section 3.3.2.

<sup>1</sup>In the following, the subscript  $A \cup B$  will be dropped from the expressions involving traces.

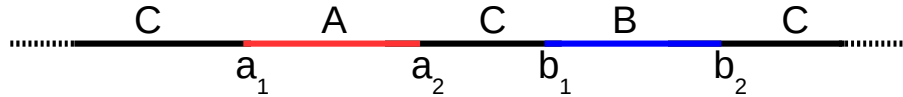


Figure 8.1: Tripartite system. Using logarithmic negativity we can compute the amount of entanglement between the subsystems  $A$  and  $B$  even though they are embedded into  $C$ .



Figure 8.2: Tripartite system in Figure 8.1 in the limit  $A = ]-\infty, 0]$ ,  $B = [r, \infty[$ .

### 8.1.1 The $\langle \mathcal{T}(0)\tilde{\mathcal{T}}(r) \rangle$ short distance scaling

The scaling of the  $\langle \mathcal{T}(0)\tilde{\mathcal{T}}(r) \rangle$  correlation function has been identified in previous chapters and it is given by

$$\log \left( \frac{\langle \mathcal{T}(0)\tilde{\mathcal{T}}(r) \rangle}{\langle \mathcal{T} \rangle^2} \right) = -4\Delta_n \log r - 2 \log \langle \mathcal{T} \rangle_n \quad \text{for } mr \rightarrow 0 \quad (8.4)$$

where the conformal dimension  $\Delta_n$  of  $\mathcal{T}$  is given by [8]

$$\Delta_n = \frac{c}{24} \left( n - \frac{1}{n} \right) \quad (8.5)$$

In this chapter we are using a slightly different notation from the previous ones<sup>2</sup>. In particular, we denote with  $\Delta_n$  the conformal dimension of the twist field and with  $\langle \mathcal{T} \rangle_n$  its vacuum expectation values. From this short distance scaling it is possible to numerically estimate  $\langle \mathcal{T} \rangle_n$  using a form factor expansion (see Section 8.4). While for free fermionic theories there is an explicit interpretation of twist fields in terms of simpler fields<sup>3</sup>, such an interpretation is still missing for free bosonic theories. All the correlation functions are defined on the multi-copied theory  $(\mathcal{L}^{(n)}, \mathbb{C})$  (using the notation of Chapter 4).

### 8.1.2 The $\langle \mathcal{T}(0)\mathcal{T}(r) \rangle$ short distance scaling

While the short distance behaviour of the  $\langle \mathcal{T}(0)\tilde{\mathcal{T}}(r) \rangle$  correlation function has been exhaustively discussed in Section 6.2, less is known about the correlation function between two identical twist fields  $\mathcal{T}$ . It has already been noticed that the branch cut created by  $\mathcal{T}$  and  $\tilde{\mathcal{T}}$  becomes smaller and smaller as the two fields get close to each other. On the other hand, when two fields  $\mathcal{T}$  come close together, the “long range” picture of their geometrical effect is a “double” branch cut. As noticed in [31, 117], such a double cut can be associated to a double twist field  $\mathcal{T}^2$ . From an operational point of view, the first contribution to the conformal OPE is given by:

$$\mathcal{T}(0)\mathcal{T}(r) \sim r^{-2(2\Delta_n - \Delta'_n)} C_{\mathcal{T}\mathcal{T}}^{\mathcal{T}^2} \langle \mathcal{T}^2 \rangle_n \quad (8.6)$$

where  $\Delta'_n$  is the conformal dimension of the  $\mathcal{T}^2$  field.

One of the most surprising features of this new field is that it behaves in quite different ways in systems with even or odd number of copies  $n$ . In particular, if the number of copies  $n$  is odd, a double cut gives rise to a simple rearrangement of the theory with a

---

<sup>2</sup>In previous chapters (especially in Chapter 6) we focused on the difference between twist fields  $\mathcal{T}$  and their composite versions  $\mathcal{T}\phi$ . In this chapter our focus is on single  $\mathcal{T}$  and double  $\mathcal{T}^2$  twist fields, whose difference is linked to the number of copies they are acting on.

<sup>3</sup>See Appendix B of [14]

single cut. For instance, in a system with  $n = 3$  copies, the cut connects the first sheet with the third, the third with the second and the second with first, closing the cycle. From an operator point of view, when a particle  $p_1$  belonging to a copy (say the first) crosses the branch cut created by a  $\mathcal{T}^2$  field, it ends up in the third copy. Crossing again such a cut, it visits the second copy end, if crosses the cut a third time, it comes back to the original one. If the number of copies is odd, the a particle can visit all the copies through a double branch cut created by  $\mathcal{T}^2$ . The only difference between  $\mathcal{T}$  and  $\mathcal{T}^2$  when  $n$  is odd is a rearrangement of the order with which the various sheets are visited. For this reason, we would expect  $\mathcal{T}^2$  to have the same scaling dimension  $\Delta_n$  of  $\mathcal{T}$ . On the other hand, in the even  $n$  case, the situation is quite different. Every time a particle cross the  $\mathcal{T}^2$  branch cut, its “parity” is conserved: the cut connects even sheets with even sheets and odd with odd. In this case there is no rearrangement of the copies, they are actually split into two separate sets. The operator  $\mathcal{T}^2$  is then equivalent to two copies of  $\mathcal{T}$ , and each copy acts on a different set of  $n/2$  sheets. Thus we expect that the field  $\mathcal{T}^2$  has twice the conformal dimension  $\Delta_{\frac{n}{2}}$  of a single field  $\mathcal{T}$  with half of the number of copies. The short-distance scaling of the  $\langle \mathcal{T}(0)\mathcal{T}(r) \rangle$  correlation function is then given by

$$\log \frac{\langle \mathcal{T}(0)\mathcal{T}(r) \rangle}{\langle \mathcal{T} \rangle^2} = \begin{cases} -2\Delta_n \log r + \log \left( \frac{c_{\mathcal{T}\mathcal{T}}^{\mathcal{T}^2}}{\langle \mathcal{T} \rangle_n} \right) & n \text{ odd} \\ -4(\Delta_n - \Delta_{\frac{n}{2}}) \log r + \log \left( \frac{\langle \mathcal{T} \rangle_{\frac{n}{2}}^2 c_{\mathcal{T}\mathcal{T}}^{\mathcal{T}^2}}{\langle \mathcal{T} \rangle_n^2} \right) & n \text{ even} \end{cases} \quad \text{for } mr \rightarrow 0 \quad (8.7)$$

where we have used the fact that  $\langle \mathcal{T}^2 \rangle_n = \langle \mathcal{T} \rangle_{\frac{n}{2}}^2$  for  $n$  even and  $\langle \mathcal{T}^2 \rangle_n = \langle \mathcal{T} \rangle_n$  for  $n$  odd.

## 8.2 Form Factor Expansion of Twist Field Correlation Functions

Using the techniques introduced in Chapter 3, we can study the twist field correlators in the massive regime. In order to recover the ultraviolet conformal scaling of such correlators, we can perform a short distance expansion of the form factor series.

### 8.2.1 Form factors in the massive free boson theory

In order to construct the complete form factor series, we need to compute the two-particle contribution. The S-matrix for free bosons is identically one and the two-particle form

factor is given by:

$$F_2^{\mathcal{T}|11}(\beta_1, \beta_2) = \frac{\sin \frac{\pi}{n}}{2n \sinh\left(\frac{i\pi - \beta_1 + \beta_2}{2n}\right) \sinh\left(\frac{i\pi + \beta_1 - \beta_2}{2n}\right)} = F_2^{\tilde{\mathcal{T}}|11}(\beta_1, \beta_2) \quad (8.8)$$

In this Chapter we are using a more compact notation:

$$f(\beta_1 - \beta_2; n) := F_2^{\mathcal{T}|11}(\beta_1, \beta_2) \quad (8.9)$$

As we have seen in Chapter 4, form factors of particles belonging to different copies are simply related to the form factors of particles in the same copy (say the copy one):

$$\begin{aligned} F_2^{\mathcal{T}|p_1 p_2}(\beta) &= f(-\beta + 2\pi i(p_2 - p_1); n) \\ F_2^{\tilde{\mathcal{T}}|p_1 p_2}(\beta) &= f(\beta + 2\pi i(p_2 - p_1); n) \end{aligned} \quad (8.10)$$

Moreover, thanks to the  $\mathbb{Z}_2$  symmetry of the bosonic Lagrangian, all odd-particle form factors vanish. Even-particle form factors can be obtained as sums of products of two-particle form factors using the Wick's theorem [118]:

$$F_{2\ell}^{11\dots 1}(\beta_1, \dots, \beta_{2\ell}) = \sum_{\sigma \in S_{2\ell}} f(\beta_{\sigma(1)\sigma(2)}; n) \cdots f(\beta_{\sigma(2\ell-1)\sigma(2\ell)}; n) \quad (8.11)$$

where  $S_{2\ell}$  is the set of all permutations of  $\{1, 2, \dots, 2\ell\}$ .

Once we have an explicit expression for the all terms of the form factor expansion, we can compute the correlation functions.

### 8.2.2 Connected correlation functions

In order to analyse the behaviour of the connected correlation functions, we can focus on their expansions:

$$\begin{aligned} \log \left( \frac{\langle \mathcal{T}(0) \tilde{\mathcal{T}}(r) \rangle}{\langle \mathcal{T} \rangle^2} \right) &= \sum_{\ell=1}^{\infty} c_{2\ell}^{\mathcal{T}\tilde{\mathcal{T}}}(r, n) \\ \log \left( \frac{\langle \mathcal{T}(0) \mathcal{T}(r) \rangle}{\langle \mathcal{T} \rangle^2} \right) &= \sum_{\ell=1}^{\infty} c_{2\ell}^{\mathcal{T}\mathcal{T}}(r, n) \end{aligned} \quad (8.12)$$

## 8.2. Form Factor Expansion of Twist Field Correlation Functions

where the functions  $c_{2\ell}$  encapsulate all the contributions from a given number of particles. Their explicit expressions are given by

$$\begin{aligned} c_{2\ell}^{\mathcal{T}\tilde{\mathcal{T}}}(r, n) &= \frac{1}{(2\ell)!(2\pi)^{2\ell}} \sum_{p_1, \dots, p_{2\ell}=1}^n \int d^{2\ell}\beta H_{2\ell}^{\mathcal{T}\tilde{\mathcal{T}}|p_1 \dots p_{2\ell}}(\beta_1, \dots, \beta_{2\ell}) e^{-mr \sum_{i=1}^{2\ell} \cosh \beta_i} \\ c_{2\ell}^{\mathcal{T}\mathcal{T}}(r, n) &= \frac{1}{(2\ell)!(2\pi)^{2\ell}} \sum_{p_1, \dots, p_{2\ell}=1}^n \int d^{2\ell}\beta H_{2\ell}^{\mathcal{T}\mathcal{T}|p_1 \dots p_{2\ell}}(\beta_1, \dots, \beta_{2\ell}) e^{-mr \sum_{i=1}^{2\ell} \cosh \beta_i} \end{aligned} \quad (8.13)$$

where  $H_{2\ell}$  are the ‘‘connected’’ functions introduced in Section 3.3.2:

$$\begin{aligned} H_1^{\mathcal{O}_1 \mathcal{O}_2 | p}(\beta) &= F_1^{\mathcal{O}_1 | p_1}(\beta) (F_1^{\mathcal{O}_2^\dagger | p_1}(\beta))^* \\ H_2^{\mathcal{O}_1 \mathcal{O}_2 | p_1 p_2}(\beta_1, \beta_2) &= F_2^{\mathcal{O}_1 | p_1 p_2}(\beta_1, \beta_2) (F_2^{\mathcal{O}_2^\dagger | p_1 p_2}(\beta_1, \beta_2))^* \\ &\quad - H_1^{\mathcal{O}_1 \mathcal{O}_2 | p_1}(\beta_1) H_1^{\mathcal{O}_1 \mathcal{O}_2 | p_2}(\beta_2) \end{aligned} \quad (8.14)$$

The simplicity of the higher-particle form factors allows a tremendous simplification of the above equations. Such a feature is unique of free theories and has already been exploited in the study of twist fields in free fermionic theories [70].

The first contribution to  $H_{2\ell}^{\mathcal{T}\tilde{\mathcal{T}}}$  is given by

$$\begin{aligned} &F_{2\ell}^{\mathcal{T}|p_1 \dots p_{2\ell}}(\beta_1 \dots \beta_{2\ell}) (F_{2\ell}^{\mathcal{T}|p_1 \dots p_{2\ell}}(\beta_1 \dots \beta_{2\ell}))^* \\ &= \left( \sum_{\sigma \in S_{2\ell}} F_2^{\mathcal{T}|p_1 p_2}(\beta_{\sigma(1)}, \beta_{\sigma(2)}) \dots F_2^{\mathcal{T}|p_{2\ell-1} p_{2\ell}}(\beta_{\sigma(2\ell-1)}, \beta_{\sigma(2\ell)}) \right) \\ &\times \left( \sum_{\sigma \in S_{2\ell}} (F_2^{\mathcal{T}|p_1 p_2}(\beta_{\sigma(1)}, \beta_{\sigma(2)}))^* \dots (F_2^{\mathcal{T}|p_{2\ell-1} p_{2\ell}}(\beta_{\sigma(2\ell-1)}, \beta_{\sigma(2\ell)}))^* \right) \end{aligned} \quad (8.15)$$

while the corresponding term in the  $\langle \mathcal{T}(0) \mathcal{T}(r) \rangle$  correlator is given by

$$\begin{aligned} &F_{2\ell}^{\mathcal{T}|p_1 \dots p_{2\ell}}(\beta_1 \dots \beta_{2\ell}) (F_{2\ell}^{\tilde{\mathcal{T}}|p_1 \dots p_{2\ell}}(\beta_1 \dots \beta_{2\ell}))^* = \left( F_{2\ell}^{\mathcal{T}|p_1 \dots p_{2\ell}}(\beta_1 \dots \beta_{2\ell}; n) \right)^2 \\ &= \left( \sum_{\sigma \in S_{2\ell}} F_2^{\mathcal{T}|p_1 p_2}(\beta_{\sigma(1)}, \beta_{\sigma(2)}) \dots F_2^{\mathcal{T}|p_{2\ell-1} p_{2\ell}}(\beta_{\sigma(2\ell-1)}, \beta_{\sigma(2\ell)}) \right)^2 \end{aligned} \quad (8.16)$$

## 8.2. Form Factor Expansion of Twist Field Correlation Functions

---

Many of these terms are identical up to integration over all rapidities. For instance, for  $2\ell = 4$  we have:

$$\begin{aligned}
& F_4^{\mathcal{T}|p_1 p_2 p_3 p_4}(\beta_1, \beta_2, \beta_3, \beta_4; n) (F_4^{\mathcal{T}|p_1 p_2 p_3 p_4}(\beta_1, \beta_2, \beta_3, \beta_4; n))^* \\
&= \left[ F_2^{\mathcal{T}|p_1 p_2}(\beta_1, \beta_2; n) F_2^{\mathcal{T}|p_3 p_4}(\beta_3, \beta_4; n) + F_2^{\mathcal{T}|p_1 p_3}(\beta_1, \beta_3; n) F_2^{\mathcal{T}|p_3 p_4}(\beta_3, \beta_4; n) \right. \\
&\quad \left. + F_2^{\mathcal{T}|p_1 p_4}(\beta_1, \beta_4; n) F_2^{\mathcal{T}|p_2 p_3}(\beta_2, \beta_3; n) \right] \left[ F_2^{\mathcal{T}|p_1 p_2}(\beta_1, \beta_2; n) F_2^{\mathcal{T}|p_3 p_4}(\beta_3, \beta_4; n) \right. \\
&\quad \left. + F_2^{\mathcal{T}|p_1 p_3}(\beta_1, \beta_3; n) F_2^{\mathcal{T}|p_3 p_4}(\beta_3, \beta_4; n) + F_2^{\mathcal{T}|p_1 p_4}(\beta_1, \beta_4; n) F_2^{\mathcal{T}|p_2 p_3}(\beta_2, \beta_3; n) \right]^* \\
&\stackrel{\text{int}}{=} 6 F_2^{\mathcal{T}|p_1 p_2}(\beta_1, \beta_2; n) (F_2^{\mathcal{T}|p_2 p_3}(\beta_2, \beta_3; n))^* F_2^{\mathcal{T}|p_3 p_4}(\beta_3, \beta_4; n) (F_2^{\mathcal{T}|p_1 p_4}(\beta_1, \beta_4; n))^* \\
&\quad + 3 \left| F_2^{\mathcal{T}|p_1 p_2}(\beta_1, \beta_2; n) \right|^2 \left| F_2^{\mathcal{T}|p_1 p_2}(\beta_3, \beta_4; n) \right|^2
\end{aligned} \tag{8.17}$$

where the notation  $\stackrel{\text{int}}{=}$  means that the two sides are equal up to integration over all rapidities. As we said before, we can express all two particle form factors in term of  $F_2^{\mathcal{T}} = f$ . The equation (8.17) now becomes:

$$\begin{aligned}
& F_4^{\mathcal{T}|p_1 p_2 p_3 p_4}(\beta_1, \beta_2, \beta_3, \beta_4; n) (F_4^{\mathcal{T}|p_1 p_2 p_3 p_4}(\beta_1, \beta_2, \beta_3, \beta_4; n))^* \\
&\stackrel{\text{int}}{=} 6 f(\beta_{12}^{p_1 - p_2}; n) f((- \beta_{23})^{p_2 - p_3}; n) f(\beta_{34}^{p_3 - p_4}; n) f((- \beta_{14})^{p_1 - p_4}; n)^* \\
&\quad + 3 \left| f(\beta_{12}^{p_1 - p_2}; n) \right|^2 \left| f(\beta_{34}^{p_3 - p_4}; n) \right|^2
\end{aligned} \tag{8.18}$$

where we have used the notation

$$\beta^p = \beta + 2\pi i p \tag{8.19}$$

For generic  $\ell$  it is possible to show that there are  $(2\ell - 1)!$  “fully connected” terms. A term is fully connected if factor  $f(\beta^k; n)$  appears only once. For example, in equation (8.18) the term in the second line is fully connected, while the one in the last line it is not. From a Feynman’s diagram point of view, a fully connected diagram cannot be divided into smaller diagrams. For generic  $\ell$ , the contribution coming from all fully connected terms is given by:

$$\begin{aligned}
& \text{fully connected terms of } \left[ \sum_{p_1, \dots, p_{2\ell}=1}^n F_{2\ell}^{\mathcal{T}|p_1 \dots p_{2\ell}}(\beta_1, \dots, \beta_{2\ell}) (F_{2\ell}^{\mathcal{T}|p_1 \dots p_{2\ell}}(\beta_1, \dots, \beta_{2\ell}))^* \right] \\
&\stackrel{\text{int}}{=} (2\ell - 1)! n \sum_{p_1, \dots, p_{2j-1}=0}^{n-1} \left( f_n((- \beta_{12})^{p_1}) f_n(\beta_{12j}^{p_{2j}-1}) \prod_{k=1}^{\ell-1} f_n(\beta_{2k+1, 2k+2}^{p_{2k} - p_{2k+1}}) f_n(\beta_{2k, 2k+1}^{p_{2k} - p_{2k-1}}) \right)
\end{aligned} \tag{8.20}$$

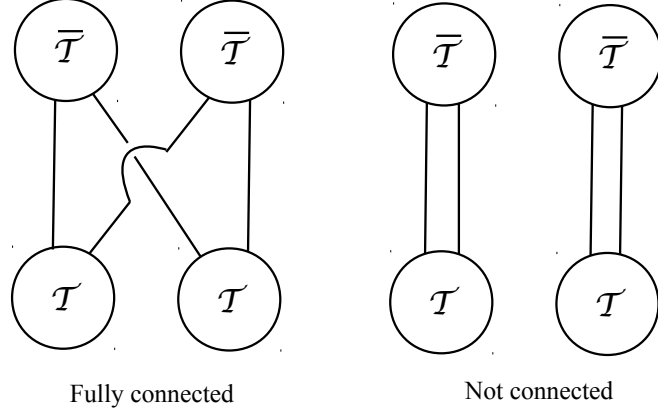


Figure 8.3: Difference between fully connected and not fully connected diagrams. The diagram on the left (right) corresponds to terms like the second (third) line of (8.18). Even though equation (8.18) refers to a  $\langle \mathcal{T}(0)\tilde{\mathcal{T}}(r) \rangle$  correlator, four operators appear in this picture instead of just two. This discrepancy is corrected by the fact that the form factors we are taking into account are normalised by the VEV of  $\mathcal{T}$ .

In the above expression all the  $p_i$ s have been shifted by one in order to make the sums start from zero. Moreover, since all form factors are invariant under a global shift on all their indices, we can set  $p_{2j}$  to one and we can factor out a factor  $n$ . The next crucial step is to observe that the “fully connected” terms are the only ones which survive when the form factors  $H_{2\ell}$  are considered. The fully connected terms are thus the only ones which give contributions to the form factor expansion of the logarithm of the correlation functions. In particular we have:

$$\begin{aligned}
 c_{2\ell}^{\mathcal{T}\tilde{\mathcal{T}}}(r, n) &= \frac{n}{(2\ell)(2\pi)^\ell} \sum_{p_1, \dots, p_{2\ell-1}=0}^{n-1} \int d^{2\ell} \beta e^{-mr \sum_{i=1}^{2\ell} \cosh \beta_i} \\
 &\times \left( f((-\beta_{12})^{p_1}; n) f(\beta_{12\ell}^{p_{2\ell-1}}; n) \prod_{k=1}^{\ell-1} f(\beta_{2k+1, 2k+2}^{p_{2k}-p_{2k+1}}; n) f(\beta_{2k, 2k+1}^{p_{2k}-p_{2k-1}}; n) \right)
 \end{aligned} \tag{8.21}$$

This simplification applies also to the  $\langle \mathcal{T}\mathcal{T} \rangle$  correlation function, when all terms which are not fully connected cancel out:

$$\begin{aligned}
 c_{2\ell}^{\mathcal{T}\mathcal{T}}(r, n) &= \frac{n}{(2\ell)(2\pi)^{2\ell}} \sum_{p_1, \dots, p_{2\ell-1}=0}^{n-1} \int d^{2\ell} \beta e^{-m\ell \sum_{i=1}^{2\ell} \cosh \beta_i} \\
 &\times f(\beta_{12\ell}^{p_1}; n) f(\beta_{2\ell-1, 2\ell}^{p_1-p_2}; n) \cdots f(\beta_{23}^{p_{2\ell-2}-p_{2\ell-1}}; n) f(\beta_{12}^{p_{2\ell-1}}; n)
 \end{aligned} \tag{8.22}$$

This massive simplification of course can be performed thanks to the fact that the theory studied is free and Wick's theorem can be applied. Moreover, we will show how the sum over  $p_i$ s can be performed, leading to an even further simplification of the form factors expansion.

### 8.3 Short Distance Scaling

In this section we will make use of equation (3.103) to compute the scaling dimensions of such correlation functions:

$$x_{\mathcal{O}_1\mathcal{O}_2} = \frac{1}{4\pi} \sum_{\ell=0}^{\infty} \frac{1}{(2\ell)!} \sum_{p_1 \cdots p_{2\ell}=1}^n \int \frac{d^{2\ell-1}\beta}{(2\pi)^{2\ell-1}} H_{2\ell}^{\mathcal{O}_1\mathcal{O}_2|p_1 \cdots p_{2\ell}}(0, \beta_1, \dots, \beta_{2\ell-1}) \quad (8.23)$$

Due to the great simplification of the free Bosonic system, it is worth sketching again the tool introduced in Section 3.3.2. Even though the underlying strategy is exactly the same, the notation will differ a bit from the one used in Chapters 3 and 6.

#### 8.3.1 The two-point function $\langle \mathcal{T}(0)\tilde{\mathcal{T}}(r) \rangle$

Let us start the study of the  $\langle \mathcal{T}(0)\tilde{\mathcal{T}}(r) \rangle$  correlation function. The logarithm of the correlator is given by

$$\log \left( \frac{\langle \mathcal{T}(0)\tilde{\mathcal{T}}(r) \rangle}{\langle \mathcal{T} \rangle^2} \right) = \sum_{\ell=1}^{\infty} c_{2\ell}^{\mathcal{T}\tilde{\mathcal{T}}}(r, n) \quad (8.24)$$

In order to simplify the above equation we rearrange the variables in the following way:

$$\begin{aligned} \beta_{j,j+1} &\equiv \beta_j - \beta_{j+1} = x_j & \text{for } j = 1, 2, \dots, 2\ell - 1 \\ \beta_{2\ell} &= x_{2\ell} \end{aligned} \quad (8.25)$$

whose inverse is given by

$$\beta_j = \sum_{p=j}^{2\ell} x_p \quad \text{for } j \neq 2\ell \quad (8.26)$$

In the new variables we have:

$$\begin{aligned}
 & \sum_{p_1, \dots, p_{2\ell-1}=0}^{n-1} \left( f((- \beta_{12})^{p_1}; n) f(\beta_{12}^{p_{2\ell-1}}; n) \prod_{k=1}^{\ell-1} f(\beta_{2k+1}^{p_{2k}-p_{2k+1}}; n) f(\beta_{2k}^{p_{2k}-p_{2k-1}}; n) \right) \\
 = & \sum_{p_1, \dots, p_{2\ell-1}=0}^{n-1} \left( f((-x_1)^{p_1}; n) f((x_1 + \dots + x_{2\ell-1})^{p_{2\ell-1}}; n) \right. \\
 \times & \left. \prod_{k=1}^{\ell-1} f(x_{2k+1}^{p_{2k}-p_{2k+1}}; n) f(x_{2k}^{p_{2k}-p_{2k-1}}; n) \right) \\
 = & \sum_{p_1, \dots, p_{2\ell-1}=0}^{n-1} \left[ f((-x_1)^{p_1}; n) f(x_3^{p_2-p_3}; n) f(x_5^{p_4-p_5}; n) \dots f(x_{2\ell-1}^{p_{2\ell-2}-p_{2\ell-1}}; n) \right. \\
 \times & \left. f((x_1 + \dots + x_{2\ell-1})^{p_{2\ell-1}}; n) f(x_2^{p_2-p_1}; n) f(x_4^{p_4-p_3}; n) \dots f(x_{2\ell-2}^{p_{2\ell-2}-p_{2\ell-3}}; n) \right] \\
 = & \sum_{p_1, \dots, p_{2\ell-1}=0}^{n-1} \left[ f((-x_1)^{p_1}; n) f(x_2^{p_2-p_1}; n) f(x_3^{p_2-p_3}; n) f(x_4^{p_4-p_3}; n) f(x_5^{p_4-p_5}; n) \dots \right. \\
 \dots & \left. f(x_{2\ell-1}^{p_{2\ell-2}-p_{2\ell-1}}; n) f(x_{2\ell-1}^{p_{2\ell-2}-p_{2\ell-1}}; n) f((x_1 + \dots + x_{2\ell-1})^{p_{2\ell-1}}; n) \right]
 \end{aligned} \tag{8.27}$$

This summation can be computed using equation (E.2) with  $y_{2\ell} = x_1 + x_2 + \dots + x_{2\ell-1}$  and  $y_i = x_i$ :

$$\begin{aligned}
 & \sum_{p_1, \dots, p_{2\ell-1}=0}^{n-1} \left[ f((-x_1)^{p_1}; n) f(x_2^{p_2-p_1}; n) f(x_3^{p_2-p_3}; n) f(x_4^{p_4-p_3}; n) f(x_5^{p_4-p_5}; n) \dots \right. \\
 \dots & \left. f(x_{2\ell-1}^{p_{2\ell-2}-p_{2\ell-1}}; n) f(x_{2\ell-1}^{p_{2\ell-2}-p_{2\ell-1}}; n) f((x_1 + \dots + x_{2\ell-1})^{p_{2\ell-1}}; n) \right] \\
 = & \frac{in}{\ell(4\pi)^{2\ell}} \frac{\mathfrak{F}_\ell(\sum_{p=1}^{\ell} x_{2p-1}, n) \sinh(\sum_{p=1}^{\ell} x_{2p-1})}{\cosh \frac{\sum_{p=1}^{2\ell-1} x_p}{2} \prod_{i=1}^{2\ell-1} \cosh \frac{x_p}{2}}
 \end{aligned} \tag{8.28}$$

where the function  $\mathfrak{F}_\ell$  is given by (see Appendix E)

$$\mathfrak{F}_\ell(x, n) = \sum_{p=1}^{\ell} (-1)^p \binom{2\ell-1}{\ell-p} [f(2x + (2p-1)i\pi; n) - f(2x - (2p-1)i\pi; n)] \tag{8.29}$$

The correlation function thus becomes:

$$\begin{aligned}
 & \log \left( \frac{\langle \mathcal{T}(0) \tilde{\mathcal{T}}(r) \rangle}{\langle \mathcal{T} \rangle^2} \right) \\
 &= \sum_{\ell=1}^{\infty} \frac{in}{\ell(4\pi)^{2\ell}} \int d^{2\ell-1} x \left[ \frac{\mathfrak{F}_{\ell} \left( \sum_{p=1}^{\ell} x_{2p-1}, n \right) \sinh \left( \sum_{p=1}^{\ell} x_{2p-1} \right)}{\cosh \frac{\sum_{p=1}^{2\ell-1} x_p}{2} \prod_{i=1}^{2\ell-1} \cosh \frac{x_p}{2}} \right. \\
 & \times \left. \int_{-\infty}^{\infty} dx_{2\ell} e^{-mr [\cosh(\sum_{i=1}^{2\ell} x_i) + \cosh(\sum_{i=2}^{2\ell} x_i) + \dots + \cosh x_{2\ell}]} \right] \quad (8.30)
 \end{aligned}$$

Since the variable  $x_{2\ell}$  appears only in the exponential function, we can easily integrate such a variable. After the integration we have

$$\begin{aligned}
 & \log \left( \frac{\langle \mathcal{T}(0) \tilde{\mathcal{T}}(r) \rangle}{\langle \mathcal{T} \rangle^2} \right) \\
 &= \sum_{\ell=1}^{\infty} \frac{2in}{\ell(4\pi)^{2\ell}} \int d^{2\ell-1} x \left[ \frac{\mathfrak{F}_{\ell} \left( \sum_{p=1}^{\ell} x_{2p-1}, n \right) \sinh \left( \sum_{p=1}^{\ell} x_{2p-1} \right)}{\cosh \frac{\sum_{p=1}^{2\ell-1} x_p}{2} \prod_{i=1}^{2\ell-1} \cosh \frac{x_p}{2}} K_0(mr d_{\ell}(x_1, \dots, x_{2\ell-1})) \right]
 \end{aligned}$$

where the function  $d_{\ell}$  is given by

$$d_{\ell}^2(x_1, \dots, x_{2\ell-1}) = \left[ \sum_{i=1}^{2\ell-1} \cosh \left( \sum_{j=1}^{2\ell-1} x_j \right) + 1 \right]^2 - \left[ \sum_{i=1}^{2\ell-1} \sinh \left( \sum_{j=1}^{2\ell-1} x_j \right) \right]^2 \quad (8.31)$$

With the same spirit of Section 3.3.2, we can extract the short-distance scaling of the correlation function:

$$\log \left( \frac{\langle \mathcal{T}(0) \tilde{\mathcal{T}}(r) \rangle}{\langle \mathcal{T} \rangle^2} \right) \quad (8.32)$$

$$\begin{aligned}
 &= (-\log r) \sum_{\ell=1}^{\infty} \frac{2in}{\ell(4\pi)^{2\ell}} \int d^{2\ell-1}x \left[ \frac{\mathfrak{F}_{\ell}(\sum_{p=1}^{\ell} x_{2p-1}, n) \sinh(\sum_{p=1}^{\ell} x_{2p-1})}{\cosh \frac{\sum_{p=1}^{2\ell-1} x_p}{2} \prod_{i=1}^{2\ell-1} \cosh \frac{x_p}{2}} \right] \\
 &+ \sum_{\ell=1}^{\infty} \frac{2in}{\ell(4\pi)^{2\ell}} \int d^{2\ell-1}x \left[ \frac{\mathfrak{F}_{\ell}(\sum_{p=1}^{\ell} x_{2p-1}, n) \sinh(\sum_{p=1}^{\ell} x_{2p-1})}{\cosh \frac{\sum_{p=1}^{2\ell-1} x_p}{2} \prod_{i=1}^{2\ell-1} \cosh \frac{x_p}{2}} \left( \gamma_E + \log \frac{md_{\ell}}{2} \right) \right]
 \end{aligned} \tag{8.33}$$

where  $\gamma_E = 0.5772\dots$  is the Euler-Mascheroni constant.

### Scaling dimension

We can now use equation (8.33) to estimate directly the scaling dimension of the  $\langle \mathcal{T}(0)\tilde{\mathcal{T}}(r) \rangle$  correlator. From (8.33) it immediately follows that:

$$\langle \mathcal{T}(0)\tilde{\mathcal{T}}(r) \rangle \sim (mr)^{-4x_{\mathcal{T}\tilde{\mathcal{T}}}} \quad \text{for } mr \rightarrow 0 \tag{8.34}$$

with

$$x_{\mathcal{T}\tilde{\mathcal{T}}} = \sum_{\ell=1}^{\infty} \frac{2in}{\ell(4\pi)^{2\ell}} \int d^{2\ell-1}x \left[ \frac{\mathfrak{F}_{\ell}(\sum_{p=1}^{\ell} x_{2p-1}, n) \sinh(\sum_{p=1}^{\ell} x_{2p-1})}{\cosh \frac{\sum_{p=1}^{2\ell-1} x_p}{2} \prod_{i=1}^{2\ell-1} \cosh \frac{x_p}{2}} \right] \tag{8.35}$$

Even though such integrals can be directly computed numerically (as we have done in Chapter 6 for the Lee-Yang theories), the symmetries that free Bosonic systems enjoy allow an even further simplification.

It is convenient to perform the following change of variables:

$$\begin{aligned}
 x_j \rightarrow y_j &= x_j \quad j \neq 2\ell \\
 x_{2\ell} \rightarrow y &= \sum_{j=1}^{\ell} x_{2j-1}
 \end{aligned} \tag{8.36}$$

The form factor expansion of the scaling dimension now becomes:

$$\begin{aligned}
 x_{\mathcal{T}\tilde{\mathcal{T}}} &= \sum_{\ell=1}^{\infty} \frac{2in}{\ell(4\pi)^{2\ell}} \int_{-\infty}^{\infty} dy_1 \cdots \int_{-\infty}^{\infty} dy_{2\ell-2} \int_{-\infty}^{\infty} dy \mathfrak{F}_{\ell}(y, n) \sinh y \\
 &\times \left[ \operatorname{sech} \left( \frac{y + \sum_{p=1}^{\ell-1} y_{2p}}{2} \right) \operatorname{sech} \left( \frac{y - \sum_{p=1}^{\ell-1} y_{2p-1}}{2} \right) \prod_{p=1}^{\ell-1} \operatorname{sech} \frac{y_{2p}}{2} \operatorname{sech} \frac{y_{2p-1}}{2} \right]
 \end{aligned} \tag{8.37}$$

We can now use the following identity [14] to perform all but one integral:

$$\begin{aligned}
 G_{\ell}(y) &= \int_{-\infty}^{\infty} dx_1 \cdots \int_{-\infty}^{\infty} dx_{\ell-1} \operatorname{sech} \left( \frac{\pm y + \sum_{p=1}^{\ell-1} x_p}{2} \right) \prod_{p=1}^{\ell-1} \operatorname{sech} \frac{x_p}{2} \\
 &= \frac{(2\pi)^{\ell-1}}{(\ell-1)!} \begin{cases} \frac{y}{\pi} \operatorname{cosech} \frac{y}{2} \prod_{p=1}^{\frac{\ell}{2}-1} \left( \frac{y^2}{\pi^2} + (2p)^2 \right) & \text{for } \ell \text{ even} \\ \operatorname{sech} \frac{y}{2} \prod_{p=1}^{\frac{\ell-1}{2}} \left( \frac{y^2}{\pi^2} + (2p-1)^2 \right) & \text{for } \ell \text{ odd.} \end{cases}
 \end{aligned} \tag{8.38}$$

Thus, the scaling dimension  $x_{\mathcal{T}\tilde{\mathcal{T}}}$  can be expressed as a sum of integrals:

$$x_{\mathcal{T}\tilde{\mathcal{T}}} = \sum_{\ell=1}^{\infty} \frac{2in}{\ell(4\pi)^{2\ell}} \int_{-\infty}^{\infty} dy \mathfrak{F}_{\ell}(y, n) G_{\ell}(y)^2 \sinh y \tag{8.39}$$

Such a simple formulation allows us to compute with very high precision the scaling dimension from its form factor expansion (some results could be found in Table 8.1).

$n$	2	3	4	6
$4\Delta_{\mathcal{T}}$	$\frac{1}{4} = 0.25$	$\frac{4}{9} = 0.444$	$\frac{5}{8} = 0.625$	$\frac{35}{36} = 0.972$
$x_{\mathcal{T}\tilde{\mathcal{T}}}$	0.246	0.438	0.608	0.953

Table 8.1: Numerical evaluation of (8.39). The sum has been truncated at  $\ell = 2000$  and it shows a very good agreement with the expected scaling dimension (8.5).

### Analytic continuation

Since a limit for  $n$  tending to one is involved in the definition of entanglement entropy (and logarithmic negativity), an analytical continuation of (8.39) is needed to take into

account the non-integer  $n$  cases. As discussed in [14], the analytical continuation of the function  $x_{\mathcal{T}\bar{\mathcal{T}}}$  can be performed by adding the residues of poles which appear in  $\mathfrak{F}_\ell(y, n)$  for non integer values of  $n$ . In particular, there is a set of poles which approaches the real axis when  $n$  goes from large values to one. The function  $\mathfrak{F}_\ell(y, n)$  presents kinematic poles at

$$\begin{aligned} 2y \pm (2p - 1)i\pi &= (2k + 1)i\pi \\ 2y \pm (2p - 1)i\pi &= (2k - 1)i\pi \end{aligned} \quad (8.40)$$

for all values of  $k \in \mathbb{Z}$ .

Such poles can be divided into four families:

$$\begin{aligned} y_1 &= (kn + 1 - p)i\pi \\ y_2 &= (kn - p)i\pi \\ y_3 &= (kn - 1 + p)i\pi \\ y_4 &= (kn + p)i\pi \end{aligned} \quad (8.41)$$

The corresponding residues are given by:

$$R_{1,4} = -R_{2,3} = \frac{i}{2} \sum_{p=1}^{\ell} (-1)^p \binom{2\ell - 1}{\ell - p} \quad (8.42)$$

We should now investigate whether any of these poles become real in the limit  $n \rightarrow 1^+$ . In particular, since the imaginary part of the above poles is positive (negative) for  $k \geq 1$  ( $k \leq -1$ ) when  $n$  is large enough, we should study the conditions under which the imaginary part changes sign. Once again, four families of conditions appear:

$$\begin{aligned} kn + 1 - p < 0 &\Rightarrow 1 \leq k < \frac{p-1}{n} \\ kn - p < 0 &\Rightarrow 1 \leq k < \frac{p}{n} \\ kn - 1 + p < 0 &\Rightarrow -\frac{p-1}{n} < k \leq -1 \\ kn + p < 0 &\Rightarrow -\frac{p}{n} < k \leq -1 \end{aligned} \quad (8.43)$$

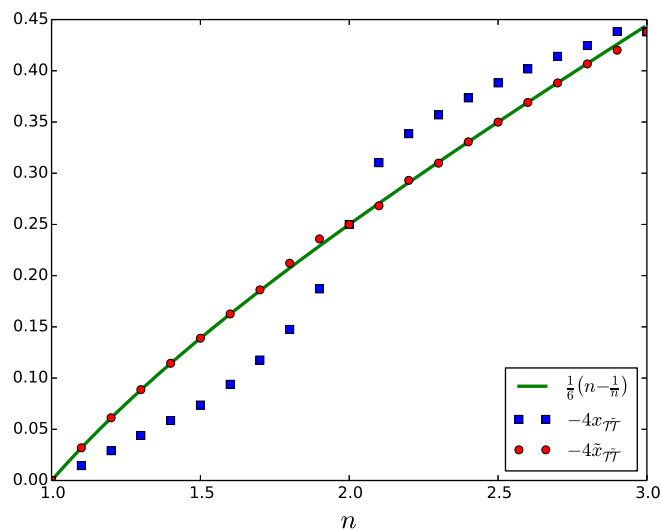


Figure 8.4: Numerical evaluation of the scaling dimension  $-4x_{\mathcal{T}\tilde{\mathcal{T}}}$  for integer and non integer values of  $n$ . In order to compute the sum (8.44) for a very high value of  $\ell$ , the actual values have been computed through a numerical fit. We computed and summed the first 150 terms of (8.44), then we completed the sum by fitting the logarithm of each term from  $\ell=20$  to  $\ell=150$  against  $\log \ell$ .

Taking into account these residues, equation (8.39) becomes:

$$\begin{aligned}
 & x_{\mathcal{T}\tilde{\mathcal{T}}} \rightarrow \tilde{x}_{\mathcal{T}\tilde{\mathcal{T}}} \\
 = & x_{\mathcal{T}\tilde{\mathcal{T}}} - \sum_{\ell=1}^{\infty} \sum_{p=1}^{\ell} \sum_{k=1}^{\lfloor \frac{\ell}{n} \rfloor - q_1} \frac{in}{\ell(4\pi)^{2\ell-1}} \binom{2\ell-1}{\ell-p} \sinh(i\pi nk) G_{\ell}^2((nk-p+1)i\pi) \\
 + & \sum_{\ell=1}^{\infty} \sum_{p=1}^{\ell} \sum_{k=1}^{\lfloor \frac{\ell}{n} \rfloor - q_2} \frac{in}{\ell(4\pi)^{2\ell-1}} \binom{2\ell-1}{\ell-p} \sinh(i\pi nk) G_{\ell}^2((nk-p)i\pi) \quad (8.44)
 \end{aligned}$$

The shift  $q_1$  ( $q_2$ ) is equal to one if  $p(p-1)$  is a multiple of  $n$  and to zero otherwise.

In principle, both (8.39) and (8.44) can be used to compute the scaling of the  $\langle \mathcal{T}\tilde{\mathcal{T}} \rangle$  correlation function for non integer values of  $n$ . While the contributions of the residues vanish for integer values of  $n$ , of course it is not the case when  $n$  is not integer.

From a direct comparison of the two expansions (see Figure 8.4) it is clear that the residue contributions play a very important role in the form factor expansion of the scaling dimension.

### 8.3.2 The two-point function $\langle \mathcal{T}(0)\mathcal{T}(r) \rangle$

Like in the previous section, we can simplify the expression of the correlator  $\langle \mathcal{T}(0)\mathcal{T}(r) \rangle$  using equation (E.2). To do so, let us consider the sum:

$$\sum_{p_1, p_2, \dots, p_{2\ell-1}=0}^{n-1} f(\beta_{1,2\ell}^{p_1}; n) f(\beta_{2\ell-1,2\ell}^{p_1-p_2}; n) \cdots f(\beta_{23}^{p_{2\ell-2}-p_{2\ell-1}}; n) f(\beta_{12}^{p_{2\ell-1}}; n) \quad (8.45)$$

In order to recover an expression compatible with equation (E.2), we should perform the following change of variables:

$$\begin{aligned} \beta_{1,2\ell} &= -x_{2\ell} \\ \beta_{2\ell-1,2\ell} &= x_{2\ell} \\ &\dots \\ \beta_{23} &= x_{2\ell-1} \\ \beta_{12} &= x_1 \end{aligned} \quad (8.46)$$

With the new variables, equation (8.45) becomes:

$$\sum_{p_1, p_2, \dots, p_{2\ell-1}=0}^{n-1} f((-x_1)^{p_1}; n) f(x_2^{p_1-p_2}; n) \cdots f(x_{2\ell-1}^{p_{2\ell-2}-p_{2\ell-1}}; n) f(x_{2\ell}^{p_{2\ell-1}}; n) \quad (8.47)$$

While it is tempting to apply directly the formula (E.2), it should be noticed that since  $\sum_{i=1}^{2\ell} x_i = \beta_{1,2\ell} + \beta_{2\ell-1,2\ell} + \cdots + \beta_{23} + \beta_{12} = 0$ . Such a peculiar condition makes the formula (E.2) ill defined and it requires a particular limit to overcome the difficulty, as explained in Appendix E<sup>4</sup>. Using equation (E.3) we have then (once the integration over  $x_{2\ell}$  has been performed):

$$\begin{aligned} &\log \left( \frac{\langle \mathcal{T}(0)\mathcal{T}(r) \rangle}{\langle \mathcal{T} \rangle^2} \right) \\ &= \sum_{\ell=1}^{\infty} \frac{n h(\ell, n)}{\ell (2\pi)^{2\ell}} \int d^{2\ell-1} x \operatorname{sech} \left( \frac{\sum_{p=1}^{2\ell-1} x_p}{2} \right) \prod_{p=1}^{2\ell-1} \operatorname{sech} \frac{x_p}{2} K_0(mr d(x_1, \dots, x_{2\ell-1})) \end{aligned} \quad (8.48)$$

<sup>4</sup>In Appendix E the limit  $\sum_{i=1}^{2\ell} x_i \rightarrow 0$  is performed.

where the function  $h$  is given by (E.4):

$$h(\ell, n) = \frac{1}{2^{2\ell-1}} \left( \binom{2\ell-1}{\ell-1} + \sum_{p=1}^{\lfloor \frac{\ell}{n} \rfloor} (-1)^{pn} \binom{2\ell}{\ell-pn} \right) \quad (8.49)$$

As before, we can expand the Bessel function  $K_0$  inside (8.48) to extrapolate the scaling dimension of the correlation function. After such a procedure we obtain:

$$x_{\mathcal{T}\mathcal{T}} = \sum_{\ell=1}^{\infty} \frac{n h(\ell, n)}{\ell(2\pi)^{2\ell}} \int d^{2\ell-1}x \operatorname{sech} \left( \frac{\sum_{p=1}^{2\ell-1} x_p}{2} \right) \prod_{p=1}^{2\ell-1} \operatorname{sech} \frac{x_p}{2} \quad (8.50)$$

A further simplification comes from the following identity:

$$\int d^{2\ell-1}x \operatorname{sech} \left( \frac{\sum_{p=1}^{2\ell-1} x_p}{2} \right) \prod_{p=1}^{2\ell-1} \operatorname{sech} \frac{x_p}{2} = \frac{(4\pi)^{2\ell-1}}{(2\ell-1)!} \frac{1}{\pi} ((\ell-1)!)^2 \quad (8.51)$$

which reduces (8.50) to

$$x_{\mathcal{T}\mathcal{T}} = \frac{n}{4\pi^2} \sum_{\ell=1}^{\infty} \frac{2^{2\ell} h(\ell, n) ((\ell-1)!)^2}{\ell(2\ell-1)!} \quad (8.52)$$

Since the scaling of the  $\langle \mathcal{T}(0)\mathcal{T}(r) \rangle$  correlator changes with the parity of  $n$  (8.7), it is worth analysing the two cases separately. For  $n$  even, we can use E.6, and the scaling  $x_{\mathcal{T}\mathcal{T}}$  becomes:

$$\begin{aligned} x_{\mathcal{T}\mathcal{T}}^e &= \frac{n}{2\pi^2} \sum_{\ell=1}^{\infty} \frac{((\ell-1)!)^2}{\ell(2\ell-1)!} \left[ \binom{2\ell-1}{\ell-1} + \sum_{p=1}^{\lfloor \frac{\ell}{n} \rfloor} \binom{2\ell}{\ell-pn} \right] \\ &= \frac{n}{2\pi^2} \sum_{\ell=1}^{\infty} \frac{1}{\ell^2} + \frac{n}{2\pi^2} \sum_{\ell=1}^{\infty} \sum_{p=1}^{\lfloor \frac{\ell}{n} \rfloor} \frac{((\ell-1)!)^2}{\ell(2\ell-1)!} \binom{2\ell}{\ell-pn} \\ &= \frac{n}{12} + \frac{n}{2\pi^2} \sum_{p=1}^{\infty} \sum_{\ell=np}^{\infty} \frac{((\ell-1)!)^2}{\ell(2\ell-1)!} \binom{2\ell}{\ell-pn} = \frac{n}{12} + \frac{1}{6n} \end{aligned} \quad (8.53)$$

For  $n$  odd we can implement E.6, which gives

$$x_{\mathcal{T}\mathcal{T}}^o = \frac{n}{12} - \frac{1}{12n} \quad (8.54)$$

#### 8.4. The Vacuum Expectation Value $\langle \mathcal{T} \rangle$ and The Structure Constant $C_{\mathcal{T}\mathcal{T}}^{\mathcal{T}^2}$

In this very particular case a complete summation of the form factor series has been performed and the results are a perfect match with the expected CFT prediction (8.7)

$$\begin{aligned}\langle \mathcal{T}(0)\mathcal{T}(r) \rangle &= r^{-4\left(\frac{n}{12} + \frac{1}{6n}\right)} && \text{for } n \text{ even} \\ \langle \mathcal{T}(0)\mathcal{T}(r) \rangle &= r^{-4\left(\frac{n}{12} - \frac{1}{12n}\right)} && \text{for } n \text{ odd}\end{aligned}\tag{8.55}$$

The different scaling in the odd and even cases is another signal of the intrinsic difference between the two cases.

Such a complete summation of the form factor series is almost unique, since in the majority of cases only truncated series can be actually computed.

Moreover, this result has been obtained for generic  $n$  and thus can be used directly to compute the scaling of logarithmic negativity. In particular, the limit  $n \rightarrow 1$  of  $x_{\mathcal{T}}^e$  is equal to  $1/4$ , in perfect agreement with the prediction of the scaling of negativity in bosonic systems [31, 117, 118].

#### 8.4 The Vacuum Expectation Value $\langle \mathcal{T} \rangle$ and The Structure Constant $C_{\mathcal{T}\mathcal{T}}^{\mathcal{T}^2}$

The form factor expansion can be used not only to extract the leading scaling of correlation functions, but also to evaluate the numerical values of other constants involved in the scaling. In particular, it is possible to compute the constants appearing in (8.4,8.7) in terms of form factor series. Let us define:

$$\begin{aligned}\kappa_{\mathcal{T}\tilde{\mathcal{T}}} &= \log K_{\mathcal{T}\tilde{\mathcal{T}}} = 2 \log \langle \mathcal{T} \rangle_n \\ \kappa_{\mathcal{T}\mathcal{T}}^o &= \log K_{\mathcal{T}\mathcal{T}}^o = -\log \left( \frac{C_{\mathcal{T}\mathcal{T}}^{\mathcal{T}^2}}{\langle \mathcal{T} \rangle_n} \right) \\ \kappa_{\mathcal{T}\mathcal{T}}^e &= \log K_{\mathcal{T}\mathcal{T}}^e = \log \left( \frac{\langle \mathcal{T} \rangle_n^2 C_{\mathcal{T}\mathcal{T}}^{\mathcal{T}^2}}{\langle \mathcal{T} \rangle_n^2} \right)\end{aligned}\tag{8.56}$$

In the same spirit of Section 3.3.2, we can compute the constants above using a form factor expansion. Combining these results, we can estimate the numerical values of the vacuum expectation value  $\langle \mathcal{T} \rangle_n$  and the structure constant  $C_{\mathcal{T}\mathcal{T}}^{\mathcal{T}^2}$  in both  $n$  even and odd cases.

### 8.4.1 The $\langle \mathcal{T}(0)\tilde{\mathcal{T}}(r) \rangle$ correlation function

Let us start with the correlation function  $\langle \mathcal{T}(0)\tilde{\mathcal{T}}(r) \rangle$ . Such a correlator and its related constant  $\kappa_{\mathcal{T}\tilde{\mathcal{T}}}$  can be used to estimate the numerical values of the vacuum expectation value  $\langle \mathcal{T} \rangle_n$  for various values of  $n$ . From equation (8.33) we have:

$$\kappa_{\mathcal{T}\tilde{\mathcal{T}}} = x_{\mathcal{T}\tilde{\mathcal{T}}} \left( \log \frac{m}{2} + \gamma_E \right) + \sum_{\ell=1}^{\infty} \frac{2n u_{\ell}(n)}{\ell(4\pi)^{2\ell}} \quad (8.57)$$

where the coefficients  $u_{\ell}(n)$  are given by the following integrals:

$$u_{\ell}(n) = \int d^{2\ell-1}x \frac{i\mathfrak{F}_{\ell}(\sum_{p=1}^{\ell} x_{2p-1}, n) \sinh(\sum_{p=1}^{\ell} x_{2p-1})}{\cosh \frac{\sum_{p=1}^{2\ell-1} x_p}{2} \prod_{p=1}^{2\ell-1} \cosh \frac{x_p}{2}} \log d_{\ell} \quad (8.58)$$

These integrals can be computed using the Vegas variant of the Monte Carlo Algorithm (see Appendix C). In order to speed up the computation process we used a tool described in Appendix G. For instance, the values of such integrals for  $n = 3$  and  $n = 5$  are shown in Figure 8.5.

The coefficients  $u_{\ell}(n)$  exhibit a clear exponential scaling, and we can attempt to fit them (see Appendix F):

$$u_{\ell}^{\text{fit}}(n) = (4\pi)^{2\ell + a_n + \frac{b_n}{\ell}} \quad (8.59)$$

where the two numbers  $a_n$  and  $b_n$  are the interpolation constants for  $u_{\ell}(n)$  and depend on  $n$ . Interestingly, the linear term  $2\ell$  is the same for all  $u_{\ell}(n)$ . The precision of such an interpolation can be seen in Figure 8.6.

Unfortunately, it is clear that the sum  $\sum_{\ell=1}^{\infty}$  of (8.57) is divergent, since (from the interpolation) each term is given by

$$\frac{u_{\ell}^{\text{fit}}(n)}{\ell(4\pi)^{2\ell}} = \frac{(4\pi)^{a_n + \frac{b_n}{\ell}}}{\ell} \quad (8.60)$$

which gives rise to a divergent series. However, as we will see in the next sections, also the infinite summation appearing in (8.61) presents a clear divergent behaviour. Since the structure constant  $C_{\mathcal{T}\mathcal{T}}^{\mathcal{T}^2}$  can be obtained from a combination of (8.57) and (8.61), it is possible to extract some meaningful physical information.

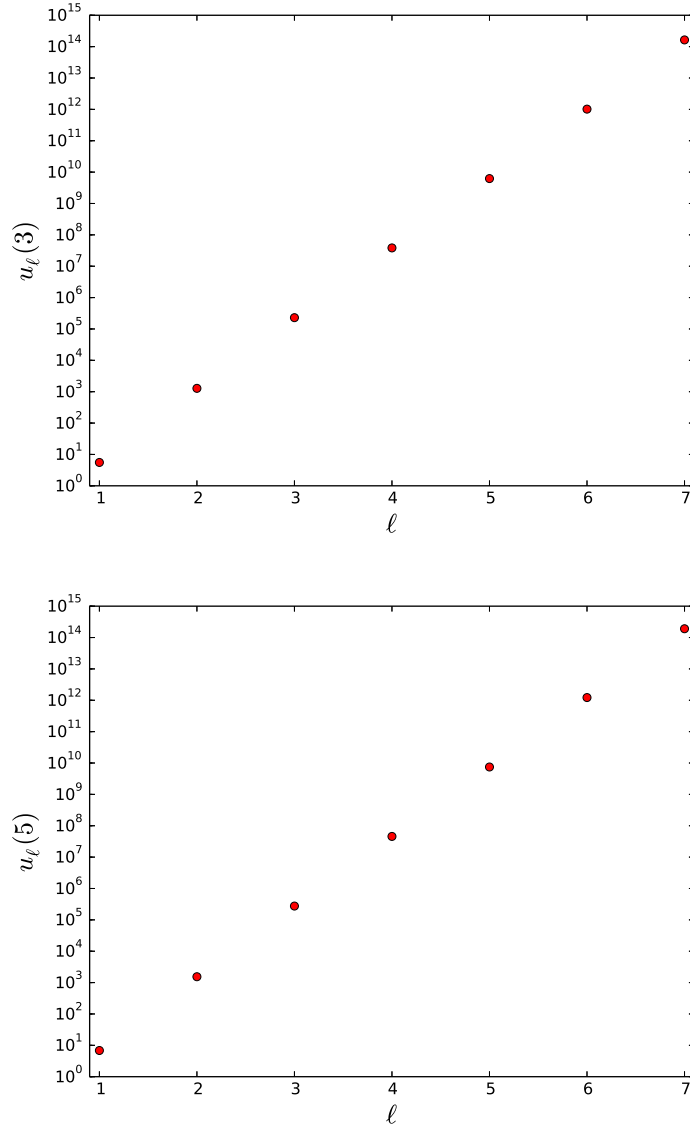


Figure 8.5: Values of  $u_\ell(3)$  and  $u_\ell(5)$  in linear-logarithmic scale.

#### 8.4.2 The $\langle \mathcal{T}(0)\mathcal{T}(r) \rangle$ correlation function

Let us focus now on the  $\langle \mathcal{T}(0)\mathcal{T}(r) \rangle$  correlation function. From equation (8.48) we can extract the value of  $\kappa_{\mathcal{T}\mathcal{T}}$  as a form factor expansion (regardless of the parity of  $n$ ):

$$\kappa_{\mathcal{T}\mathcal{T}} = x_{\mathcal{T}\mathcal{T}} \left( \log \frac{m}{2} + \gamma_E \right) + \sum_{\ell=1}^{\infty} \frac{n h(\ell, n) v_\ell}{\ell (2\pi)^{2\ell}} \quad (8.61)$$

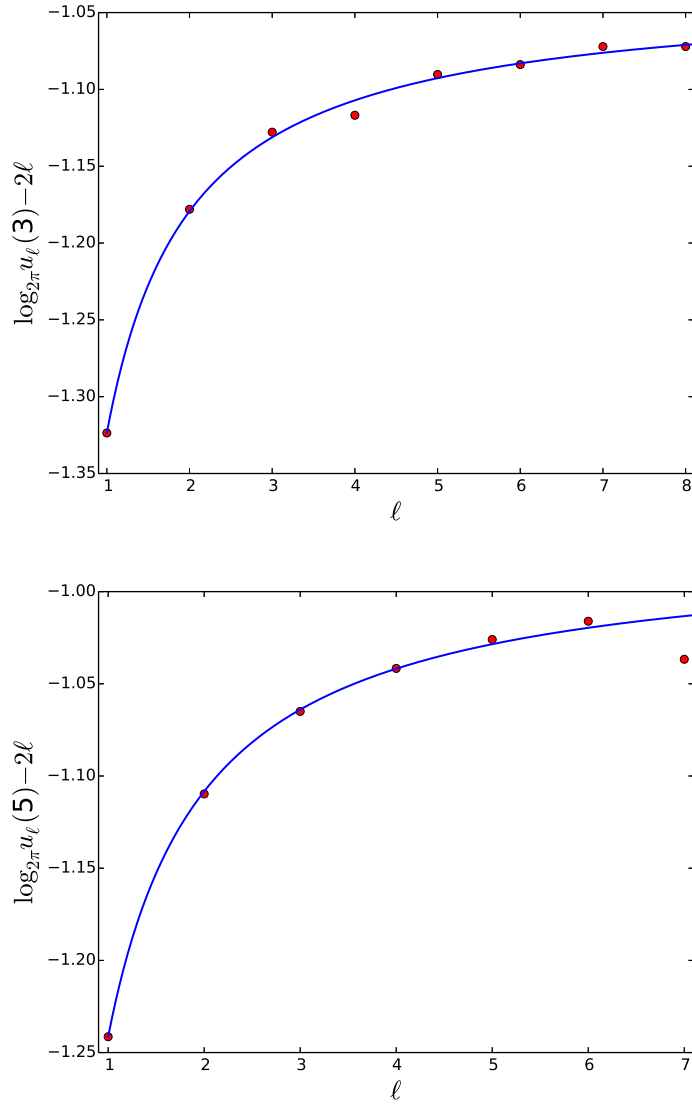


Figure 8.6: Values (rescaled) of  $u_\ell(3)$  and  $u_\ell(5)$  (red dots) in linear scale checked against the fit (8.59) (blue line).

where the coefficients  $v_\ell$  are given by

$$v_\ell = \int d^{2\ell-1}x \operatorname{sech} \left( \frac{\sum_{p=1}^{2\ell-1} x_p}{2} \right) \prod_{p=1}^{2\ell-1} \operatorname{sech} \frac{x_p}{2} \log d_\ell \quad (8.62)$$

These integrals can be evaluated using the Vegas-Monte Carlo algorithm (see Appendix C) and their values are shown in Figure 8.4.2.

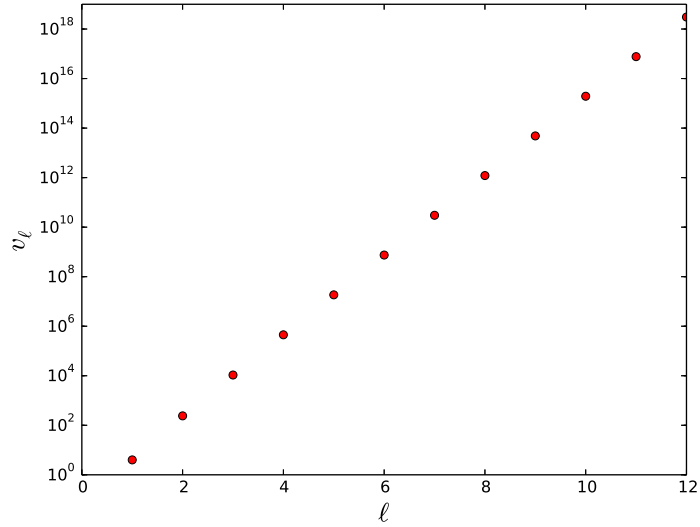


Figure 8.7: The values of the integrals  $v_\ell$  in linear-logarithmic scale.

The values of  $v_\ell$ , which do not depend on  $n$ , exhibit a clear exponential scaling, which can be easily interpolated as

$$v_\ell^{\text{fit}} = (2\pi)^{2\ell - 0.806996 - \frac{0.4363331}{\ell}} \quad (8.63)$$

The precision of such an interpolation can be inferred from Figure 8.4.2, in which the data and the interpolating function are rescaled in order to focus on the corrections beyond the  $(2\pi)^{2\ell}$  term.

Using the interpolation (8.63) we can compute the sum appearing in equation (8.61) with large values of  $\ell$  without actually computing all the integrals (8.62).

The numerical evaluation of the constants  $K_{\mathcal{T}}$  and  $K_{\mathcal{T}\hat{\mathcal{T}}}$  can then be used to compute the structure constant  $C_{\mathcal{T}\mathcal{T}}^{\mathcal{T}^2}$ .

### 8.4.3 The $C_{\mathcal{T}\mathcal{T}}^{\mathcal{T}^2}$ structure constant

We can now address the numerical evaluation of the structure constants  $C_{\mathcal{T}\mathcal{T}}^{\mathcal{T}^2}$  by combining the results of previous sections concerning the coefficients  $K_{\mathcal{T}}$  and  $K_{\mathcal{T}\hat{\mathcal{T}}}$ . Since the odd and even  $n$  cases are intrinsically different, we will discuss the two cases separately.

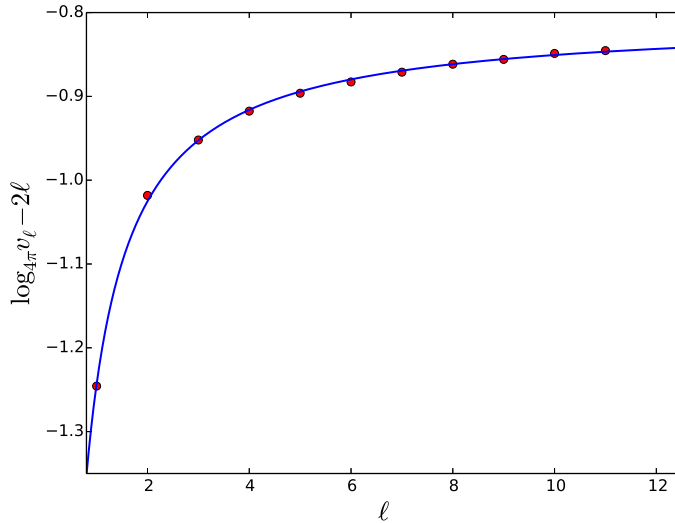


Figure 8.8: The (rescaled) values of  $v_\ell$  (red dots) checked against the interpolating function (8.63) (blue line) in linear scale.

### The odd $n$ case

Let us start with the odd  $n$  case. Even though it is not used for the computation of the logarithmic negativity, its analysis provides us with interesting information about the replica QFT content of the system.

First of all, we can compute the constant  $\kappa_{\mathcal{T}\mathcal{T}}^o$  from the expression (8.61) and using the odd variant  $h^o$  (E.6) of the function  $h$ . Since  $h^o$  tends to zero for large  $\ell$

$$\lim_{\ell \rightarrow \infty} h^o(\ell, n) = 0 \quad (8.64)$$

the sum appearing in (8.61) is convergent for  $n$  odd. Some values of  $\kappa_{\mathcal{T}\mathcal{T}}^o$  are reported in Table 8.2. Since the only non trivial  $n$  dependence of  $\kappa_{\mathcal{T}\mathcal{T}}^o$  is encapsulated in  $h^o$ , we can

$n$	3	5	7	9	11	13	15	17	19
$\kappa_{\mathcal{T}\mathcal{T}}^o$	0.345	0.760	1.183	1.607	2.033	2.459	2.885	3.311	3.737

Table 8.2: Numerical values of  $\kappa_{\mathcal{T}\mathcal{T}}^o = -\log\left(\frac{C_{\mathcal{T}\mathcal{T}}^{\mathcal{T}^2}}{\langle T \rangle_n}\right)$  for  $n$  odd. These values have been computed from equation (8.61) summing up to  $\ell = 1000$  using the interpolation (8.63).

easily compute it also for non integer values of  $n$ . The simple dependence on  $n$  of such a

#### 8.4. The Vacuum Expectation Value $\langle \mathcal{T} \rangle$ and The Structure Constant $C_{\mathcal{T}\mathcal{T}}^{\mathcal{T}^2}$

constant is emphasised by the simple fit

$$\kappa_{\mathcal{T}\mathcal{T}}^{o,\text{fit}} = -0.34 + 0.215n + 0.13/n \quad (8.65)$$

which is shown in Figure 8.4.3 together with some values of  $\kappa_{\mathcal{T}\mathcal{T}}^o$  computed for integer and non integer values of  $n$ .

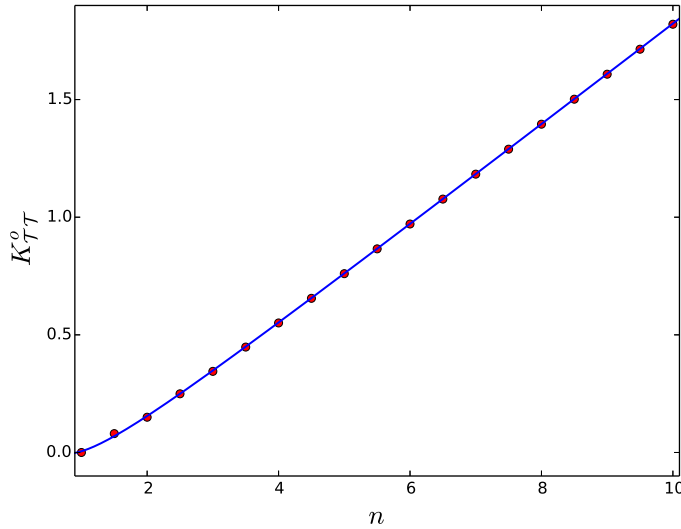


Figure 8.9: Numerical values of  $\kappa_{\mathcal{T}\mathcal{T}}^o$  (red dots) for different integer and non integer values of  $n$ . The blue line represent the best fit  $-0.34 + 0.215n + 0.13/n$ .

Thanks to the linear scaling of  $\kappa_{\mathcal{T}\mathcal{T}}^o$  in the large  $n$  regime, it is clear that the ratio between  $C_{\mathcal{T}\mathcal{T}}^{\mathcal{T}^2}$  and  $\langle \mathcal{T} \rangle_n$  decays exponentially for large  $n$ .

Moreover, if we specialise to the  $n = 1$  case (in which  $h^o(\ell, n = 1) = 0$ ), we have

$$\log \frac{C_{\mathcal{T}\mathcal{T}}^{\mathcal{T}^2}}{\langle \mathcal{T} \rangle_n} = 0 \quad \text{for } n = 1. \quad (8.66)$$

Such a ratio can also be computed without taking into account any form factor expansion. Since at  $n = 1$  the twist field  $\mathcal{T}$  is equal to the identity  $\mathbf{1}$ , we have  $\Delta_1 = 0$  and  $\langle \mathcal{T} \rangle_1 = 1$ . Since  $\mathcal{T}^2 = \mathcal{T}$  when  $n$  is odd, we have  $C_{\mathcal{T}\mathcal{T}}^{\mathcal{T}^2} = C_{\mathcal{T}\mathcal{T}}^{\mathcal{T}} = C_{\mathbf{1}\mathbf{1}}^{\mathbf{1}} = 1$ , which matches perfectly with (8.66).

For odd values of  $n$  we can then compute exactly the ratio between two universal QFT quantities: the structure constant  $C_{\mathcal{T}\mathcal{T}}^{\mathcal{T}^2} = C_{\mathcal{T}\mathcal{T}}^{\mathcal{T}}$  and the vacuum expectation value  $\langle \mathcal{T} \rangle_n$ . While the sum (8.57) is divergent, the sum (8.61) seems pretty convergent for odd values

#### 8.4. The Vacuum Expectation Value $\langle \mathcal{T} \rangle$ and The Structure Constant $C_{\mathcal{T}\mathcal{T}}^{\mathcal{T}^2}$

of  $n$ . For this reason, while the ratios between the two constants (the structure constant and the VEV) is convergent, the VEV itself is divergent. In order to have a consistent interpretation, the structure constant has to diverge as well.

##### The even $n$ case

While the constant  $\kappa_{\mathcal{T}\mathcal{T}}^{\mathcal{O}}$  can be expressed as a convergent sum (thanks to the behaviour of  $h^{\mathcal{O}}$  for large  $\ell$ ), the even case is more complicated.

Since  $h^e$  does not tend to zero for large values of  $\ell$

$$\lim_{\ell \rightarrow \infty} h^e(\ell, n) = \frac{1}{2} \quad (8.67)$$

the sum appearing in (8.61) seems divergent. Luckily, as we have seen in Section 8.4.1, the constant  $\kappa_{\mathcal{T}\tilde{\mathcal{T}}}$  looks divergent as well. For this reason, while the two constants are divergent on their own, the structure constant (which can be obtained from a combination of the two  $\kappa$ s constants) is itself convergent.

In particular, we can extract  $C_{\mathcal{T}\mathcal{T}}^{\mathcal{T}^2}$  by combining the equations (8.56):

$$\log C_{\mathcal{T}\mathcal{T}}^{\mathcal{T}^2} = -n \sum_{\ell=1}^{\infty} \left( \frac{h^e(\ell, n)v_{\ell}}{\ell(2\pi)^{2\ell}} + \frac{u_{\ell}(\frac{n}{2}) - 2u_{\ell}(n)}{\ell(4\pi)^{2\ell}} \right) \quad (8.68)$$

whose actual values can be computed by employing the fitted function  $v_{\ell}^{\text{fit}}$  and  $u_{\ell}(n)^{\text{fit}}$  (Figure 8.10). In particular, for  $n = 2$  we have

$$u_{\ell}(2) = 2^{2(\ell-1)}v_{\ell} \quad (8.69)$$

Such an equality can be used to simplify further the equation (8.68):

$$\log C_{\mathcal{T}\mathcal{T}}^{\mathcal{T}^2} = \sum_{j=1}^{\infty} \frac{(1 - 2h^e(j, 2))v_j}{j(2\pi)^{2j}} \quad \text{for } n = 2 \quad (8.70)$$

Since  $h^e(2, \ell)$  is identically equal to  $1/2$  for any value of  $\ell$ , we have:

$$\begin{aligned} \log C_{\mathcal{T}\mathcal{T}}^{\mathcal{T}^2} &= 0 & \text{for } n = 2 \\ C_{\mathcal{T}\mathcal{T}}^{\mathcal{T}^2} &= 1 & \text{for } n = 2 \end{aligned} \quad (8.71)$$

As it has been noticed in [119], in the  $n = 2$  case, the squared twist field  $\mathcal{T}^2$  is nothing but the identity operator (it maps each copy in itself). In such a case  $C_{\mathcal{T}\mathcal{T}}^{\mathcal{T}^2} = C_{\mathcal{T}\mathcal{T}}^1$  and it has to be equal to one (as imposed by the CFT normalisation of correlation functions<sup>5</sup>).

<sup>5</sup>In CFT normalisation  $\langle \mathcal{O}(r)\mathcal{O}(0) \rangle = \frac{1}{r^{4\Delta_{\mathcal{O}}}}$ .

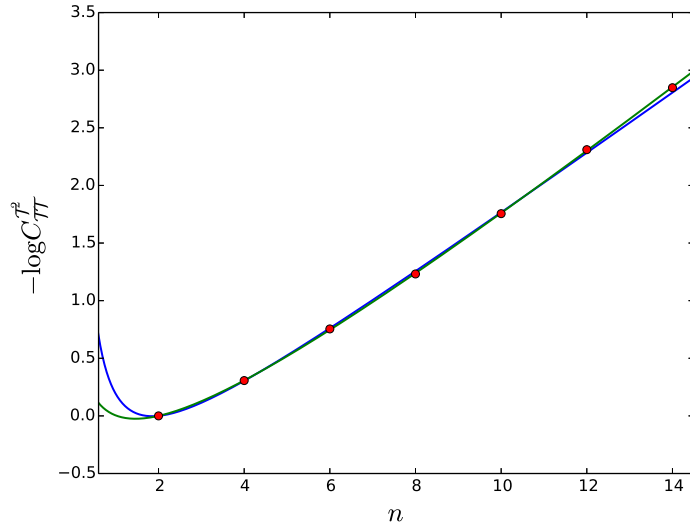


Figure 8.10: Numerical values of  $-\log C_{TT}^{\mathcal{T}^2}$  for some even values of  $n$  (red dots). Both interpolating functions (blue and green lines) provide a very good fit of the data.

### Continuation to $n=1$

As shown in Figure 8.10, the logarithm of the structure constant exhibits a clear linear behaviour in  $n$ . Such a linear scaling can be interpolated using the fit:

$$\log \left( C_{TT}^{\mathcal{T}^2} \right)^{\text{fit},1} = a + b n + \frac{c}{n} \quad (8.72)$$

Alternatively, we can consider another fitting function:

$$\log \left( C_{TT}^{\mathcal{T}^2} \right)^{\text{fit},2} = a + b n + c \log n \quad (8.73)$$

Such fitting functions can then be used to extrapolate the value of the structure constant at  $n = 1$ .

Many sources of error are present in computing the structure constants. First of all, the infinite series (8.68) converges very slowly, inducing a truncation error. Furthermore, the various terms of (8.68) come from various interpolations themselves. Probably, the main source of error is given by the systematic truncation of the form factor expansion at  $\ell = 2000$  particles. As can be noticed in table 8.1, the difference between the theoretical prediction and the form factor expansion of the scaling dimension is around 2%. Using a similar truncation, we should expect a similar error also for the value of the constants  $\kappa_{TT}$  and  $\kappa_{T\bar{T}}$ . Since the logarithm of the structure constant can be estimated combining

#### 8.4. The Vacuum Expectation Value $\langle T \rangle$ and The Structure Constant $C_{TT}^{\mathcal{T}^2}$

three values of  $\kappa$ , the systematic error associated with the truncation of the form factor expansion (8.68) should be at least 6%<sup>6</sup>. This amount is only a lower bound for the actual error. As we said before, there is an additional uncertainty coming from the fact that the various terms of (8.68) come themselves from a fitting extrapolation. We believe then the values of  $\log C_{TT}^{\mathcal{T}^2}$  we computed should be considered with an error of about 10%. It is clear from (F.4), (F.5), (F.9) and (F.10) that the final error associated with the fitting constant is proportional to the error of the  $\log C_{TT}^{\mathcal{T}^2}$  values, if they are all the same as percentage of the actual value.

Using the the formulae of Appendix F, we can compute the values of the fitting constants and their relative errors.

When using a polynomial function (8.72), the fitting parameters are (using a 10% error)<sup>7</sup>:

$$\begin{aligned} a &= -1.0 \pm 0.2 \\ b &= 0.27 \pm 0.02 \\ c &= 0.9 \pm 0.2 \end{aligned} \tag{8.74}$$

On the other hand, the fitting parameters of (8.73) are given by (using a 10% error)<sup>7</sup>:

$$\begin{aligned} a &= -0.31 \pm 0.02 \\ b &= 0.31 \pm 0.03 \\ c &= -0.46 \pm 0.12 \end{aligned} \tag{8.75}$$

Both fitting can be used to extrapolate the value of  $C_{TT}^{\mathcal{T}^2}$  in the limit  $n_e \rightarrow 1$ . When considering the fit (8.72), the structure constant is given by:

$$C_{TT}^{\mathcal{T}^2} = 0.8 \pm 0.3 \tag{8.76}$$

while the fitting (8.73) gives:

$$C_{TT}^{\mathcal{T}^2} = 1.00 \pm 0.06 \tag{8.77}$$

These estimates lie below the analytical value of 1.20184... found in [117] and the numerical value of 1.38... which can be extracted using numerical data of [15]. This result has been obtained in [117] for a compactified free boson theory. The above numerical value is

---

<sup>6</sup>In other words, the value of  $\log C_{TT}^{\mathcal{T}^2}$  comes from three series: one in  $v_\ell$  and two in  $u_\ell$  (see equation (8.68)).

<sup>7</sup>The  $n = 2$  value is not affected by truncation error, as all terms of the series (8.70) are identically zero. We set the numerical error of this value to  $10^{-8}$ , as an exactly zero error makes the fitting formulae divergent (see Appendix F).

computed by performing the  $n \rightarrow 1$  limit before the taking the compactification radius to infinity. The derivation of such values will be sketched in Sections 8.5.1 and 8.5.2. This discrepancy should not surprise, as our form factor computations if affected by a number of systematic errors and truncations. Moreover, it is common for form factor predictions to approach the expected value from below (see, for instance Figure 6.5), as all series involved are positive-definite.

## 8.5 Interpretation of Divergent Series

In previous sections we encountered some divergent series when studying some physical quantities using form factors. In particular, we showed that the form factor expansion of

$$\log \langle \mathcal{T} \rangle_n \tag{8.78}$$

and

$$\log \frac{\langle \mathcal{T} \rangle_{n_e}^2 C_{\mathcal{T}\mathcal{T}}^{\mathcal{T}^2}}{\langle \mathcal{T} \rangle_{n_e}^2} \tag{8.79}$$

diverge for  $n_e$  even. We believe that such divergences arise from the presence of extra logarithmic terms in the two-point correlation function. In particular, when we extracted the form factor expansion of  $\log \langle \mathcal{T} \rangle_n$  from (8.33) by a direct comparison with the scaling (8.34), we allow only power-law terms in the short distance scaling. If, on the other hand, extra logarithmic terms are present, the definition of the constant  $K_{\mathcal{O}\mathcal{O}}$  (8.56) is ambiguous. In particular, if such terms are present, we should consider an alternative short distance expansions:

$$\log \left( \frac{\langle \mathcal{T}(0) \tilde{\mathcal{T}}(r) \rangle}{\langle \mathcal{T} \rangle_n^2} \right) = -4\Delta_n \log r - \rho_1(n) \log(p \log r) - 2 \log \langle \mathcal{T} \rangle_n \tag{8.80}$$

and

$$\log \left( \frac{\langle \mathcal{T}(0) \mathcal{T}(r) \rangle}{\langle \mathcal{T} \rangle_n^2} \right) = \begin{cases} -2\Delta_n \log r + \log \frac{C_{\mathcal{T}\mathcal{T}}^{\mathcal{T}^2}}{\langle \mathcal{T} \rangle_n} & \text{for } n \text{ odd} \\ -4 \left( \Delta_n - \Delta_{\frac{n}{2}} \right) \log r + \log \frac{\langle \mathcal{T} \rangle_{\frac{n}{2}}^2 C_{\mathcal{T}\mathcal{T}}^{\mathcal{T}^2}}{\langle \mathcal{T} \rangle_n^2} & \\ -\rho_2(n) \log(p \log r) & \text{for } n \text{ even} \end{cases} \tag{8.81}$$

where  $\rho_1(n)$  and  $\rho_2(n)$  are unknown functions and  $p$  is an unknown parameter. Of course, the presence of such parameters implies a redefinition of the constants  $\kappa_{\mathcal{T}\tilde{\mathcal{T}}}$  and  $\kappa_{\mathcal{T}\mathcal{T}}$ , leading to an ambiguity in the identification of the structure constant and the vacuum expectation value of twist fields. It should be noticed that an extra logarithmic divergence can be found only when the associated form factor expansion for the computation of the constant term is divergent. In particular, it appears in the expansion of  $\langle \mathcal{T}(0)\tilde{\mathcal{T}}(r) \rangle$  and  $\langle \mathcal{T}(0)\mathcal{T}(r) \rangle$  ( $n$  even), while no such term is present for the  $\langle \mathcal{T}(0)\mathcal{T}(r) \rangle$  ( $n$  odd) correlation function. An analytic derivation of the extra logarithmic scaling in the correlation function (8.80) will appear on [120]. Even though the functions  $\rho_1(n)$  and  $\rho_2(n)$  are unknown, it is possible to make same assumptions based on the convergence of some combined series. In particular, the fact that the series (8.68) is convergent implies that

$$\rho_1(n) + \rho_1\left(\frac{n}{2}\right) = \rho_2(n) \quad (8.82)$$

Additionally, preliminary results of [120] suggests that

$$\log \frac{\langle \mathcal{T} \rangle_n}{\langle \mathcal{T} \rangle_2^{n-1}} \quad (8.83)$$

admits a convergent form factor expansion (even though the individual vacuum expectation values  $\langle \mathcal{T} \rangle_n$  themselves are divergent). The convergence of such factor implies:

$$\rho_1(n) - (n-2)\rho_1(2) = 0 \quad (8.84)$$

which is equivalent to

$$\rho_1(n) = \rho(n-1) \quad (8.85)$$

with  $\rho$  constant.

Moreover, since the series (8.57) diverges positively, the constant  $\rho$  should be positive.

The presence of double logarithmic terms in the short distance scaling of branch point twist fields should not surprise, as the underlying theory is (at critical point) a logarithmic CFT [90]. Double logarithmic terms can be found when studying the logarithmic negativity of non compactified massless free boson theories [117]. Furthermore, it has been shown in [1] (see Chapter 5) that extra double logarithmic terms in the form  $\rho \log \log r$  are always present in the scaling of the Rényi entropy in logarithmic CFT. In such a context the coefficient  $\rho$ , a positive integer, is related to the algebraic structure of the CFT. Additionally, such double logarithmic divergences can be directly derived using some results of [121]. In particular, combining equation (4) and (66) of [121], it is possible to study a

particular four-point function of twist fields in compactified free boson theory in the large compactification radius  $R \gg 1$  regime:

$$\left\langle \mathcal{T}(-r_1) \tilde{\mathcal{T}}(0) \mathcal{T}(r_2) \tilde{\mathcal{T}}(r_2 + r_3) \right\rangle = \frac{g(r_1, r_2, r_3)^{4\Delta_n} R^{n-1}}{\prod_{k=1}^{n-1} {}_2F_1\left(\frac{k}{n}, 1 - \frac{k}{n}, 1; x\right) {}_2F_1\left(\frac{k}{n}, 1 - \frac{k}{n}, 1; 1 - x\right)} \quad (8.86)$$

where  ${}_2F_1$  is an hypergeometric function [49],  $x = \frac{r_1 r_3}{(r_1 + r_2)(r_2 + r_3)}$  is the usual cross ratio and  $g$  is a known ratio of the positions  $r_1$ ,  $r_2$  and  $r_3$ .

It is possible to expand the correlation function (8.86) around  $r_2 \approx 0$  (equivalent to  $x \approx 1$ ):

$$\begin{aligned} \left\langle \mathcal{T}(-r_1) \tilde{\mathcal{T}}(0) \mathcal{T}(r_2) \tilde{\mathcal{T}}(r_2 + r_3) \right\rangle &\approx \frac{(r_2(r_1 + r_3))^{-4\Delta_n} R^{n-1}}{\prod_{k=1}^n \frac{-\log(1-x)}{\Gamma(\frac{k}{n})\Gamma(1-\frac{k}{n})}} \\ &= \frac{(r_2(r_1 + r_3))^{-4\Delta_n} (2\pi R)^{n-1}}{n(-\log(1-x))^{n-1}} \end{aligned} \quad (8.87)$$

The von Neumann entropy of two disjoint intervals with the rest of the system can be computed by taking the  $n \rightarrow 1$  limit of the correlator (8.87):

$$\begin{aligned} \lim_{n \rightarrow 1} \frac{\log \left\langle \mathcal{T}(-r_1) \tilde{\mathcal{T}}(0) \mathcal{T}(r_2) \tilde{\mathcal{T}}(r_2 + r_3) \right\rangle}{1 - n} &= \frac{1}{3} \log(r_2(r_1 + r_3)) + \log(-\log(1-x)) \\ &- \log(2\pi R) \end{aligned} \quad (8.88)$$

which suggests that  $\rho = 1$  and

$$\begin{aligned} \rho_1(n) &= n - 1 \\ \rho_2(n) &= \frac{n}{2} \end{aligned} \quad (8.89)$$

In conclusion, we believe that the divergences appearing in some form factors expansions are closely related to the presence of extra logarithmic terms in the short distance scaling of the associated correlation functions. Moreover, thanks to the expansion (8.87) (that follows from [121]) and to suggestions coming from [120], we propose that the Rényi entropy of the non compactified massless free boson scales as:

$$S_n(r) \sim \frac{n+1}{6n} \log r + \log \log r \quad (8.90)$$

Like other logarithmic CFTs, the double logarithmic term [1] does not depend on the number  $n$  of copies and it appears also in the von Neumann entropy. It would be very interesting to investigate such scaling numerically, even though, as suggested in [110],

logarithmic properties usually hold only at the critical point and any perturbation could make logarithmic corrections vanish. Since numerical simulations (like DMRG [32]) creates a small mass gap, recovering logarithmic corrections could be very challenging.

### 8.5.1 Three-point structure constant of $C_{\mathcal{T}\bar{\mathcal{T}}\mathcal{T}}^{\mathcal{T}^2}$ and logarithmic negativity

The analytical value of the three-point structure constant has been derived in [117]. In particular, they showed that in massless non compactified free boson theories the logarithmic negativity of two adjacent regions (of size  $r_1$  and  $r_2$ ) scales as:

$$\mathcal{E}(r_1, 0, r_2) \sim \frac{1}{4} \log y - \frac{1}{2} \log \left( \frac{1}{2} \log y \right) - \log P_1 \quad (8.91)$$

where  $y = r_1 r_2 / (r_1 + r_2)$  and  $P_1$  is the inverse of the structure constant<sup>8</sup>

$$(P_1)^{-1} = C_{\mathcal{T}\bar{\mathcal{T}}^2\mathcal{T}}(n=1) = C_{\mathcal{T}\mathcal{T}}^{\mathcal{T}^2}(n=1)$$

Notice that the above scaling is a generalisation of (8.81) to finite subsystems. The double logarithmic term appears with the predicted coefficient of  $\rho_2(1) = 1/2$ . As we said before, the presence of the coefficient  $p$  (equal to  $1/2$  in this case), makes ambiguous the identification of the structure constant. Moreover, the value of constant  $P_1$  can be extended beyond the  $n \rightarrow 1$  limit and their values can be compared against equation (8.68). The generic expression for  $P_n$  can be found in [117] and it is equal to:

$$P_n = \frac{2\pi^{\frac{n-3}{2}}}{\sqrt{n}} \exp \int_0^\infty \frac{dt}{t} e^t \left[ \frac{1}{1-e^{-t}} \left( \frac{e^{\frac{t}{2}} - 1}{e^{\frac{t}{n}} - 1} - \frac{n}{2} \right) - \frac{n-2}{8} \right] \quad (8.92)$$

As we said before the analytic value of the structure constant has been obtained by performing the  $n \rightarrow 1$  limit before taking to infinity the compactification radius  $R$ . While the radius  $R$  disappears in the  $n \rightarrow 1$  limit, it plays a non trivial role for  $n \neq 1$ . In particular, when considering the scaling of logarithmic negativity for compactified free boson theories, a  $R^{(n-1)/2}$  factor is always present. For this reason, it is hard to compare (8.68) and (8.92), as a divergent constant appears when decompactifying the theory. In order to perform a meaningful comparison, we should impose some constraints. In particular, we impose that  $P_2$  correctly recover the  $n = 2$  case (8.70). In order to satisfy such a requirement, we introduce a modified version of the function  $P_n$ :

$$P_n \rightarrow \tilde{P}_n \equiv \left( \frac{\pi}{2} \right)^{\frac{n-1}{2}} P_n \quad (8.93)$$

---

<sup>8</sup>The equivalence between the two structure constants can be found in [119].

which satisfies the required property:

$$\tilde{P}_2 = 1 \quad (8.94)$$

Additionally, the two versions of the function  $P_n$  coincide at  $n = 1$ :

$$\tilde{P} = P_1 \quad (8.95)$$

We can now compare the form factor expansion (8.68) and the function  $\tilde{P}_n$  (see Figure 8.11).

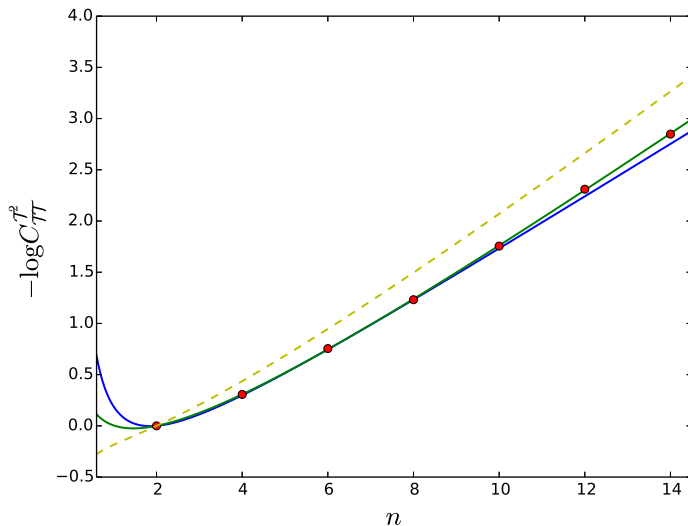


Figure 8.11: Numerical values (red dots) of the logarithm of the three-point structure constant computed using equation (8.68). The blue and green solid line the  $-1.0 + 0.27n + 0.9/n$  and  $-0.31 + 0.31n - 0.46 \log n$  fitting functions, respectively. These values are checked against  $\log \tilde{P}_n$  (yellow dashed line).

The values of  $\tilde{P}_n$  are very close to the form factor expansion of the three-point structure constant  $C_{\mathcal{T}\mathcal{T}}^{\mathcal{T}^2}$ , especially in the large  $n$  regime. This agreement suggests that our identification

$$\left(\tilde{P}_n\right)^{-1} = C_{\mathcal{T}\mathcal{T}}^{\mathcal{T}^2}(n) \quad (8.96)$$

is correct. As usual, the form factor expansion fails to recover completely the analytic values of conformal quantities. In particular, form factor computations approach by below (as absolute value) the true values. Nevertheless, the linear and the logarithmic contributions

of the large  $n$  expansion of  $\log \tilde{P}_n$  match the logarithmic fit of the form factor expansion:

$$\begin{aligned} \left(\log \tilde{P}_n\right)_{n \gg 1} &= -1.25 + 0.34 - 0.5 \log n \\ \left(-\log C_{\mathcal{T}\mathcal{T}}^{\mathcal{T}^2}\right)^{\text{fit}} &= -0.31 + 0.31n - 0.46 \log n \end{aligned} \quad (8.97)$$

### 8.5.2 Three-point structure constant of $C_{\mathcal{T}\mathcal{T}}^{\mathcal{T}^2}$ and out of equilibrium systems

The three-point structure constant can also be probed studying how negativity changes after a quantum quench. In a particular set up [15], two harmonic chains at inverse temperature  $\beta$  are connected (at time  $t = 0$ ) and let evolve unitarily. As can be seen in Figure 8.12, the negativity grows logarithmically:

$$\mathcal{E} \sim \frac{1}{2} \log t + c_1 \quad (8.98)$$

for a short period of time and then reaches a temperature dependant plateau:

$$\mathcal{E} \sim \frac{1}{2} \log \beta + c_2 \quad (8.99)$$

In [119] it has been shown that, even though the constant  $c_1$  and  $c_2$  are non universal,

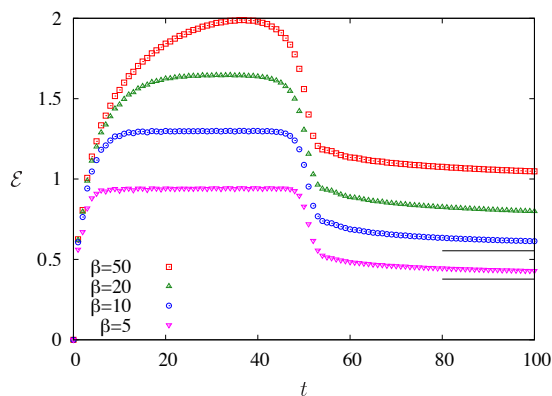


Figure 8.12: Time evolution of logarithmic negativity after a quench at equal temperature  $\beta^{-1}$ . Picture taken from [15] with permission from the authors.

their difference is related to the value of the structure constant at  $n = 1$ :

$$-2 \lim_{n_e \rightarrow 1} \log C_{\mathcal{T}\mathcal{T}}^{\mathcal{T}^2} = c_1 - c_2 - \frac{1}{2\pi} \quad (8.100)$$

From the raw numerical data it is possible to extrapolate the constants  $c_1$  and  $c_2$ . In particular, by looking at the various plateaus (red, green, blue and purple points in Figure 8.12) and solving equation (8.99), we can infer the value of  $c_2 \approx 0.119$ . Such a result has been obtained as an average of the four values of  $c_2$  (one for each plateau). Moreover, the constant  $c_1$  can be extrapolated from the short time logarithmic growth (red points):

$$c_1 \approx 0.47 \tag{8.101}$$

Using the extrapolated data it is possible to compute the structure constant:

$$C_{\mathcal{T}\mathcal{T}}^{\mathcal{T}^2} \approx 1.33 \tag{8.102}$$

The constant  $c_1$  has been obtained fitting the first ten points (up to  $t = 10$ ) of the time evolution of the negativity. As shown in [119], the logarithmic growth (8.98) holds in the short time regime  $t \ll L$ , where  $L$  is the smallest size of the system. In [15] two subsystems of 50 sites each have been considered.

Even though such an estimate relies on numerical (non exact) information, the agreement with the analytical predictions (see Section 8.5.1) is remarkable. Moreover, the theoretical explanation [119] of the time evolution of logarithmic negativity does not take into account the double logarithmic correction. As suggested in [110], the non diagonalisability condition of the Hamiltonian underlying the logarithmic theory can be easily broken and in some cases it appears only at the critical point. It is possible that finite size corrections destroy the logarithmic feature of the boson model studied in [15].

## 8.6 Conclusions

In this chapter we have performed a number of form factor expansion to study different correlation functions of twist fields in the free Boson theory. In particular, we were able to compute the scaling dimensions  $x$  of the correlators:

$$\begin{aligned} \frac{\langle \mathcal{T}(0)\tilde{\mathcal{T}}(r) \rangle}{\langle \mathcal{T} \rangle^2} &\sim K_{\mathcal{T}\tilde{\mathcal{T}}} r^{-4x_{\mathcal{T}\tilde{\mathcal{T}}}} \\ \frac{\langle \mathcal{T}(r)\mathcal{T}(0) \rangle}{\langle \mathcal{T} \rangle^2} &\sim K_{\mathcal{T}\mathcal{T}} r^{-4x_{\mathcal{T}\mathcal{T}}} \quad \text{for } n \text{ even} \\ \frac{\langle \mathcal{T}(r)\tilde{\mathcal{T}}(0) \rangle}{\langle \mathcal{T} \rangle^2} &\sim K_{\mathcal{T}\tilde{\mathcal{T}}} r^{-4x_{\mathcal{T}\tilde{\mathcal{T}}}} \quad \text{for } n \text{ odd} \end{aligned}$$

Thanks to the simple nature of the various terms of the form factor expansion, we could represent each contribution of the  $x_{\mathcal{T}\tilde{\mathcal{T}}}$  expansion as a single integral, regardless of the

number of particles. Such a simplification allowed us to truncate the expansion at a very high number of particles. The form factor expansion of the scaling of the correlator  $\langle \mathcal{T}(0)\mathcal{T}(r) \rangle$  is even simpler. It can be computed exactly taking into account all terms. In this even simpler case the form factor series is computable analytically. The agreement between such an expansion and the short distance prediction provides a powerful test for the twist fields approach to the evaluation of entanglement. Moreover, we showed that such scaling dimension can be computed not only for integer values of the number of copies  $n$ , but we managed to perform also an analytic continuation to non integer values of  $n$ . In the same spirit of Chapter 5, we computed also the form factor expansion of the constant  $K$ . We found that, with the exception of  $K_{\mathcal{T}\mathcal{T}}$  with  $n$  odd, the form factor series of the constant  $K$  diverges, even though very slowly. We believe that such a divergence is associated with the peculiar features of the free boson theory. In particular, the non compactified massless free boson can be described by a logarithmic CFT and its entanglement entropy has an extra double logarithmic correction (see Chapter 5). It has been shown in [117] that massless twist fields correlator present logarithmic divergences at small scales in free boson theories. Logarithmic scaling are usually associated with a degeneracy in the values of the scaling dimensions. In particular, all composite fields of the form  $:\mathcal{T}\phi^k:$  with  $k = 0, 1, 2, \dots$  have the same conformal dimension. Here  $\phi$  is the free boson field with conformal dimension 0. The composite field  $:\mathcal{T}\phi^k:$  is the leading field appearing in the OPE between  $\mathcal{T}$  and  $\phi^k$  and it has been discussed in Chapters 5 and 6. Such double logarithmic corrections were implicit in the scaling of Rényi and von Neumann entanglement entropy [121] and they have now been independently derived in [120]. When taking into account these extra divergences, the short distance expansion of twist fields becomes:

$$\begin{aligned} \frac{\langle \mathcal{T}(0)\tilde{\mathcal{T}}(r) \rangle}{\langle \mathcal{T} \rangle^2} &\sim K_{\mathcal{T}\tilde{\mathcal{T}}} r^{-4x_{\mathcal{T}\tilde{\mathcal{T}}}} (\log r)^{1-n} \\ \frac{\langle \mathcal{T}(r)\mathcal{T}(0) \rangle}{\langle \mathcal{T} \rangle^2} &\sim K_{\mathcal{T}\mathcal{T}} r^{-4x_{\mathcal{T}\mathcal{T}}} (\log r)^{-\frac{n}{2}} \quad \text{for } n \text{ even} \\ \frac{\langle \mathcal{T}(r)\mathcal{T}(0) \rangle}{\langle \mathcal{T} \rangle^2} &\sim K_{\mathcal{T}\mathcal{T}} r^{-4x_{\mathcal{T}\mathcal{T}}} \quad \text{for } n \text{ odd} \end{aligned}$$

The actual power of the logarithmic term has been fixed using some constraints derived in [117] and [120].

Even though we were not able to compute a form factor expansion for the new constants  $K$  (with the exception of  $K_{\mathcal{T}\mathcal{T}}$  with  $n$  odd case), we managed to calculate some interesting ratios. In particular, we wrote a form factor expansion for the three-point structure constant  $C_{\mathcal{T}\mathcal{T}}^{\mathcal{T}^2}$  for  $n$  even. Like the dimensions  $x$ , the constants  $C_{\mathcal{T}\mathcal{T}}^{\mathcal{T}^2}$  can be expressed as infinite sum. While the expansion of the scaling dimensions  $x$  are simple enough to allow us to calculate them with arbitrary precision, the expansion of the structure constants  $C_{\mathcal{T}\mathcal{T}}^{\mathcal{T}^2}$

(equation 8.68) is more complicated. Using the fitted values of the coefficients  $u_\ell$  and  $v_\ell$  we computed the structure constant at different even values of  $n$  using 2000 particles. Even though the even  $n$  series is very well behaving, the structure constant seems divergent for  $n$  odd.

In order to extrapolate the value of the structure constant  $C_{\mathcal{T}\mathcal{T}}^{\mathcal{T}^2}$  in the limit  $n_e \rightarrow 1$ , we compute its values for  $n$  even. We compared our extrapolation with both analytical [117] and numerical [15] results. In [15], the authors studied how the logarithmic negativity of an harmonic chain changes after a quench. Using the CFT description of such quench [119], it is possible to compute the structure constant  $C_{\mathcal{T}\mathcal{T}}^{\mathcal{T}^2}$  from the time evolution of logarithmic negativity. Even though our extrapolation is affected by a number of truncation and fitting, there is a reasonable agreement between our and previous results. Even if no double logarithmic corrections has been taken into account in the study of the time evolution of the logarithmic negativity, the value of the structure constant extrapolated from [15] data is in good agreement with the analytical prediction [117]. Additionally, we compared our even  $n$  results for the structure constant  $C_{\mathcal{T}\mathcal{T}}^{\mathcal{T}^2}$  with the analytical prediction [117] finding a good agreement, especially in the large  $n$  regime.

It is quite remarkable how the form factor expansion of correlators involving twist fields in free Boson theory can be actually computed with so many particles (in some case also with an infinite number). In contrast, we managed to sum only up to three particles in the form factor expansion in the Lee-Yang theory (see Chapter 6).

## Chapter 9

# Conclusions

Through the various chapters of the thesis, we presented a number of results regarding the scaling of entanglement. After a brief introduction to the various measures of entanglement (Chapter 2) and to integrable field theory techniques (Chapter 3), some known results have been presented. In particular, as discussed in Chapter 4 it is known that if a unitary one-dimensional quantum system has a critical point described by a conformal field theory with central charge  $c$ , the entanglement between a subsystem and the rest of the system scales as [7, 8]:

$$S \sim \frac{c}{3} \log \frac{r}{\epsilon} \quad r \ll \xi \quad (9.1)$$

$$S \sim \frac{c}{3} \log \frac{\xi}{\epsilon} \quad r \gg \xi \quad (9.2)$$

where  $r$  is the size of the subsystem and  $\xi$  is the correlation length<sup>1</sup>. These scalings describe two very different regimes: when the system is critical  $\xi = \infty$  (or almost critical  $r \ll \xi$ ) and when the system is so far from the critical point that the correlation length is much smaller than the size of the subsystem  $\xi \ll r$ . Moreover, it is known that in an intermediate regime  $r \sim \xi$ , entanglement scales as [14]:

$$S \sim \frac{c}{3} \log \frac{\xi}{\epsilon} - \frac{1}{8} K_0 \left( \frac{2r}{\xi} \right) \quad (9.3)$$

where  $K_0$  is a modified Bessel's function of the second kind. While the logarithmic saturation depends on the central charge  $c$  of the particular theory, the scaling of the corrections, including the pre-factor  $1/8$ , is universal. The above entropy has been computed by evaluating a correlation function of particular fields called branch point twist fields  $\mathcal{T}$  using a

---

<sup>1</sup>If particles with different masses are present, the correlation length is given by the inverse of the lightest mass.

---

form factor expansion (see Chapter 3). In particular, it is known that:

$$S \sim \lim_{n \rightarrow 1} \frac{d}{dn} \langle \mathcal{T}(0) \tilde{\mathcal{T}}(r) \rangle \quad (9.4)$$

One of the main achievements of this thesis is the extension of these results to the non unitary case. From the CFT point of view, the main difference between unitary and non unitary theories is given by different ground state structures. In unitary CFT, the physical ground state  $|\text{gs}\rangle$  (i.e. the state with the lowest energy) coincides with the conformal vacuum  $|\emptyset\rangle$ . This is so because the identity operator is the field with the smallest conformal dimension ( $\Delta_1 = 0$ ). In non unitary CFTs the smallest conformal dimension  $\Delta_{\min}$  is negative and the ground state is then created by the relative primary field  $\phi$ :

$$|\text{gs}\rangle = \phi(0)|\emptyset\rangle \quad (9.5)$$

In Chapter 5 we showed how this feature affects the scaling of entanglement entropy in non unitary CFT:

$$S \sim \frac{c_{\text{eff}}}{3} \log \frac{r}{\epsilon} \quad (9.6)$$

which is reminiscent of what happens in the scaling of the ground state energy (see Section 3.1.6). As the ground state energy, entanglement entropy represents a physical quantity and its scaling is governed by the effective central charge  $c_{\text{eff}}$ . We also proposed an interpretation in terms of modified twist fields  $:\mathcal{T}\phi:$ , which includes also the field  $\phi$  responsible for the creation of the ground state. A more general definition of entanglement entropy which holds also in the non unitary case has been proposed:

$$S \sim \lim_{n \rightarrow 1} \frac{d}{dn} \frac{\langle : \mathcal{T}\phi : (0) : \tilde{\mathcal{T}}\phi : (r) \rangle}{\langle \phi(0)\phi(r) \rangle^n} \quad (9.7)$$

The above ratio suggests a new prescription in defining additional “physical” correlators in CFT when the ground state differs from the conformal vacuum:

$$\langle\langle \mathcal{O}_1(x_1)\mathcal{O}_2(x_2) \rangle\rangle \equiv \frac{\langle : \mathcal{O}_1\phi : (x_1) : \mathcal{O}_2\phi : (x_2) \rangle}{\langle \phi(x_1)\phi(x_2) \rangle} \quad (9.8)$$

While  $\langle \mathcal{O}_1(x_1)\mathcal{O}_2(x_2) \rangle$  scales in an “unphysical way”, i.e. it diverges at large distances, its modified version behaves in the usual way (it vanishes at infinity and it diverges at short distance).

Like in (9.7), it is possible that such “improved” correlation functions should be studied in order to probe physical features of a non unitary system, even though this assumption requires further investigations.

---

Additionally, we computed the scaling of entanglement in logarithmic CFT. In particular we showed that, if the underlying CFT is logarithmic, entanglement entropy scales as:

$$S \sim \frac{c_{\text{eff}}}{3} \log \frac{r}{\epsilon} + p \log \log \frac{r}{\epsilon} \quad (9.9)$$

Moreover, we checked the scaling (9.6) in an actual spin chain using an exact diagonalisation approach.

In Chapter 6 we evaluated the entanglement entropy in the massive Lee-Yang model, the simplest non unitary integrable quantum field theory. In particular, we performed a form factor expansion of the correlators (9.7), obtaining:

$$S \sim \frac{c_{\text{eff}}}{3} \log \frac{\xi}{\epsilon} + \mathfrak{a} K_0 \left( \frac{r}{\xi} \right) \quad r \gg \xi \quad (9.10)$$

where  $\mathfrak{a}$  is a non universal constant which depends on the theory considered. Apart from the presence of the effective central charge, the main difference from the unitary case is that the leading correction to saturation is not universal. We showed that this non universal behaviour is due to the presence of modified twist fields. While a direct numerical verification of the scaling (9.3) has already been performed in [99], such a check is still missing in the non unitary case, mainly because it is not easy to handle the few non unitary off critical spin chains known in the literature [77, 4].

In Chapter 7 we continued the analysis of the scaling of entanglement in non unitary systems by implementing the Corner Transfer Matrix tool on the Forrester-Baxter RSOS models. In a particular regime, such models provide a lattice realisation of perturbed non unitary minimal models. The RSOS model is a two-dimensional classical theory which can be interpreted as the euclidean time evolution of the one-dimensional quantum system we are referring to when evaluating the entanglement. We showed non only that the effective central charge plays an important role in the entropy, but also that the corrections to the logarithmic scaling are affected by the non unitary nature of such models:

$$S_n(\xi) \sim \frac{c_{\text{eff}}}{12} \frac{n+1}{n} \log \frac{\xi}{\epsilon} + A_n + B_n \left( \frac{\xi}{\epsilon} \right)^{-\frac{\Delta_{\text{eff}}}{6}} \quad (9.11)$$

where we introduced the  $\Delta_{\text{eff}} = \Delta - \Delta_{\text{min}}$  *effective conformal dimension*. As for the effective central charge, we interpret the presence of an effective conformal dimension as a consequence of the non trivial ground state. Moreover, we extended the above computation to the off critical logarithmic case. Even though double logarithmic corrections to entropy are expected according to (9.9), they do not appear in the FB RSOS case. This absence is in perfect agreement with the observation [110] that all the logarithmic features of logarithmic FB RSOS minimal models hold only at the critical point. Off critical

---

minimal models are only few of the many theories described by the various regimes of the FB RSOS model. In the unitary case [108], entanglement has been computed not only in the off critical minimal model regime, but also in other cases, like the one described by parafermionic theories. In the non unitary case, the computation of the entanglement in other regimes is still missing.

Since entanglement is a genuine quantum phenomenon, we need to know which is the quantum Hamiltonian we are considering when computing the entanglement. For this reason, we also derived the quantum chain whose euclidean time evolution can be represented by the RSOS models. Such an Hamiltonian extends some previous results and provides the first one dimensional quantum realisation of a generic off critical minimal model.

In Chapter 8 we studied the scaling of twist field correlation functions in non compactified massive free boson theories. In particular, we analysed the  $\langle \mathcal{T}(0)\tilde{\mathcal{T}}(r) \rangle$  correlator (to compute the entanglement entropy) and the  $\langle \mathcal{T}(0)\mathcal{T}(r) \rangle$  (to compute the logarithmic negativity) using form factor expansions. The simple nature of the free boson theory allowed us to compute all form factor expansions with a tremendous amount of contributions. Usually, just few form factor contributions can be actually computed. For instance, in Chapter 6, only three contributions have been considered. In this chapter we could sum all terms of some series while we considered few thousand contributions in others. Even though such expansions recover very well the scaling dimensions of these correlators, they seem to diverge when computing other physical constants relative to the same correlation functions. We interpret such divergences as a signal of the presence of extra double logarithmic corrections in the scaling of entanglement entropy and logarithmic negativity. We suppose that such extra corrections, which have the same form of (9.9) are due to the logarithmic nature of the non compactified free boson theory. Even though these extra logarithmic terms make the computation of physical quantities very hard, some universal ratios can be computed as a form factor expansion. In particular, the three point structure constant  $C_{\mathcal{T}\mathcal{T}}^{\mathcal{T}^2}$

$$\mathcal{T}(0)\mathcal{T}(r) \sim C_{\mathcal{T}\mathcal{T}}^{\mathcal{T}^2} r^{-2(2\Delta_{\mathcal{T}}-\Delta_{\mathcal{T}^2})} \mathcal{T}^2(0) \quad (9.12)$$

can be expressed using an infinite series of form factor contributions.

The computation of such constant for even values of  $n$  and its continuation at  $n = 1$  allows us to directly access the scaling of logarithmic negativity. Using a numerical fitting, we extrapolated its numerical value at  $n = 1$  and we found a reasonable agreement with previous analytical [117] and numerical results [15]. Even though the form factor expansion and the CFT computation [117] clearly show the presence of extra logarithmic corrections in the scaling of logarithmic negativity, such corrections have not been observed in numer-

---

ical simulations yet.

The study of entanglement in quantum systems is an invaluable source of information for both unitary and non unitary theories. Even though non unitary systems have always been regarded as “non physical”, in recent years they have been attracting the attention of many scholars. From the many-body point of view, they constitute a magnificent playground, especially because (at the critical point) their ground state is not the conformal vacuum [50, 77].

Many questions are still open. For instance, an effective description of logarithmic negativity in non unitary quantum field theory is still missing. If we accept the prescription (9.8), we can naively obtain the non unitary version of each formula including twist fields<sup>2</sup> by substituting each field  $\mathcal{T}$  with its counterpart  $\mathcal{T}\phi$  and dividing by the correct normalising correlation function. While this assumption provides an intuitive prescription, there is no formal proof whether such a recipe could work or not. More work in this direction is still needed to have a full picture of entanglement in non unitary theories.

Moreover, entanglement is a powerful probe to extract information about the conformal properties of a system quenching through a critical point [122, 123, 124]. A further generalisation of such non equilibrium mechanisms could help us understand better non unitary theories. From a numerical point of view, these phenomena can be studied using quantum Hamiltonians like [77] or the new class of Hamiltonians derived in Chapter 7.

Of course, the computation of entanglement in non unitary theories is not restricted only to one dimensional systems. Interesting results in this direction for specific two dimensional non unitary quantum models have been recently developed [125].

---

<sup>2</sup>Like equation (10) in [31].

## Appendix A

### Values of $A_i$

Residue equations (6.30) and (6.39) for the polynomial  $Q_3$  can be solved using the guess (6.45). The solution in terms of the coefficients  $A_i$  is given by:

$$\begin{aligned}
 A_6 &= A_7 = 0, \quad A_1 = A_4 = \frac{\alpha F_1^{\mathcal{O}|1} (C_0(n) \cos^2 \frac{\pi}{3n} - \alpha \langle \mathcal{O} \rangle^{-1} F_1^{\mathcal{O}|1} H_1(n) \cos^2 \frac{\pi}{2n})}{\sin \frac{\pi}{6n} \sin \frac{5\pi}{6n}}, \\
 A_2 &= \frac{\alpha F_1^{\mathcal{O}|1} (\alpha \langle \mathcal{O} \rangle^{-1} F_1^{\mathcal{O}|1} H_1(n) - C_0(n))}{4 \sin \frac{\pi}{6n} \sin \frac{5\pi}{6n}}, \\
 A_3 &= -\frac{\alpha C_0(n) F_1^{\mathcal{O}|1} (5 \cos \frac{\pi}{6n} + 4 \cos \frac{\pi}{2n} + 2 \cos \frac{5\pi}{6n} + 6 \cos \frac{7\pi}{6n} + \cos \frac{11\pi}{6n} + \cos \frac{13\pi}{6n} - \cos \frac{5\pi}{2n})}{4 \cos \frac{\pi}{2n} \sin \frac{\pi}{6n} \sin \frac{5\pi}{6n}} \\
 &\quad + \frac{\alpha^2 \langle \mathcal{O} \rangle^{-1} (F_1^{\mathcal{O}|1})^2 H_1(n) (11 \cos \frac{\pi}{2n} + 6 \cos \frac{3\pi}{2n} + \cos \frac{5\pi}{2n})}{4 \cos \frac{\pi}{2n} \sin \frac{\pi}{6n} \sin \frac{5\pi}{6n}}, \\
 A_5 &= \frac{\alpha C_0(n) F_1^{\mathcal{O}|1} (2 \cos \frac{\pi}{n} + 1)^2 (\cos \frac{\pi}{6n} + \cos \frac{\pi}{2n} + 2 \cos \frac{7\pi}{6n} - \cos \frac{3\pi}{2n} + \cos \frac{11\pi}{6n} - \cos \frac{13\pi}{6n})}{4 \cos \frac{\pi}{2n} \sin \frac{\pi}{6n} \sin \frac{5\pi}{6n}} \\
 &\quad - \frac{\alpha^2 \langle \mathcal{O} \rangle^{-1} (F_1^{\mathcal{O}|1})^2 H_1(n) (2 \cos \frac{\pi}{n} + 1)^3}{4 \sin \frac{\pi}{6n} \sin \frac{5\pi}{6n}} \tag{A.1}
 \end{aligned}$$

## Appendix B

# Structure Constants

In this appendix we will compute some conformal structure constants involved in the OPE of simple and composite twist fields of the Lee-Yang theory. Even though the following results are computed for the Lee-Yang theory, they can be very easily extended to different systems. To do so, we will implement the actual definition of the twist field itself:

$$\frac{\langle \mathcal{T}(x_1) \tilde{\mathcal{T}}(x_2) \mathcal{O}_k(x_3) \rangle}{\langle \mathcal{T}(x_1) \tilde{\mathcal{T}}(x_2) \rangle} = \langle \mathcal{O}(x_3; \text{sheet } k) \rangle \quad (\text{B.1})$$

Such a situation describes a multi-copied theory with branch cut between  $x_1$  and  $x_2$ . By definition, all correlators involving twist fields are defined on  $\mathbb{C}$  in the multi-copied theory and the index  $k$  in  $\mathcal{O}_k(x_3)$  refers to the number of the copy. On the other hand, correlator involving operators in the form  $\mathcal{O}(x_3; \text{sheet } k)$  are computed on the Riemann manifold  $\mathcal{M}_n(x_1, x_2)$  (see Chapter 4). The manifold  $\mathcal{M}_n(x_1, x_2)$  can be mapped onto  $\mathbb{C}$  using the conformal map  $g$ :

$$\begin{aligned} g : \mathcal{M}_n(x_1, x_2) &\rightarrow \mathbb{C} \setminus \{0, \infty\} \\ g(z) &= \left( \frac{z - x_1}{z - x_2} \right)^{\frac{1}{n}} \\ \partial g(z) := \frac{\partial g}{\partial z}(z) &= \frac{1}{n} \frac{y_2 - y_1}{(z - y_1)(z - y_2)} \left( \frac{z - y_1}{z - y_2} \right)^{1/n} \end{aligned} \quad (\text{B.2})$$

We can now compute the conformal structure constants involving Twist Fields by a direct comparison between correlation functions computed with different methods.

The main idea is to compute ratios like

$$\frac{\langle \mathcal{T}(x_1) \tilde{\mathcal{T}}(x_2) \mathcal{O}_k(x_3) \rangle}{\langle \mathcal{T}(x_1) \tilde{\mathcal{T}}(x_2) \rangle} \quad (\text{B.3})$$

using the OPE between twist fields as define in Chapter 6 and to compare the results with (B.1).

$\Delta = -1/5$  is the conformal dimension of the field  $\phi$ .  $\Delta_{\mathcal{T}}$  and  $\Delta_{:\mathcal{T}\phi}$  are the conformal dimensions of the twist fields  $\mathcal{T}$  and  $:\mathcal{T}\phi$  .:

## B.1 Structure Constants of Twist Fields $\mathcal{T}$

In the following section we will compute various correlation functions involving “simple” Twist Fields  $\mathcal{T}$ . When two or more fields appear in the same correlation functions, the correlator itself can be factorised if the fields belong to different copies. For instance:

$$\langle \phi_1(x_1) \phi_2(x_2) \phi_2(x_3) \rangle = \langle \phi_1(x_1) \rangle \langle \phi_2(x_2) \phi_2(x_3) \rangle \quad (\text{B.4})$$

### B.1.1 The $C_{\mathcal{T}\tilde{\mathcal{T}}}^{\Phi_1}$ structure constant

Let us consider the following correlation function in the short distance limit:

$$\begin{aligned} \frac{\langle \mathcal{T}(x_1) \tilde{\mathcal{T}}(x_2) \phi_1(x_3) \rangle}{\langle \mathcal{T}(x_1) \tilde{\mathcal{T}}(x_2) \rangle} &\stackrel{x_1 \rightarrow x_2}{\sim} \tilde{C}_{\mathcal{T}\tilde{\mathcal{T}}}^{\Phi_1} |x_1 - x_2|^{2\Delta} \sum_{j=1}^n \langle \phi_j(x_2) \phi_1(x_3) \rangle \\ &= \tilde{C}_{\mathcal{T}\tilde{\mathcal{T}}}^{\Phi_1} |x_1 - x_2|^{2\Delta} \langle \phi(x_2) \phi(x_3) \rangle \\ &= \tilde{C}_{\mathcal{T}\tilde{\mathcal{T}}}^{\Phi_1} |x_1 - x_2|^{2\Delta} |x_2 - x_3|^{-4\Delta} \end{aligned} \quad (\text{B.5})$$

Of course, there are other terms in the OPE of the Twist Fields, but all of them vanish when the correlation function is evaluated. For instance, the following term:

$$\begin{aligned} \sum_{j=2}^{\lfloor \frac{n}{2} \rfloor + 1} \tilde{C}_{\mathcal{T}\tilde{\mathcal{T}}}^{\Phi_{1,j}} \langle \Phi_{1j}(x_2) \phi_1(x_3) \rangle &= \sum_{j=2}^{\lfloor \frac{n}{2} \rfloor + 1} \frac{\tilde{C}_{\mathcal{T}\tilde{\mathcal{T}}}^{\Phi_{1,j}}}{\#_{1j}} \langle \phi_1(x_2) \phi_j(x_2) \phi_1(x_3) \rangle \\ &= \langle \phi_1(x_2) \phi_1(x_3) \rangle \sum_{j=2}^{\lfloor \frac{n}{2} \rfloor + 1} \frac{\tilde{C}_{\mathcal{T}\tilde{\mathcal{T}}}^{\Phi_{1,j}}}{\#_{1j}} \langle \phi_j(x_2) \rangle \end{aligned} \quad (\text{B.6})$$

always vanishes, since one-particle correlators are always equal to zero in CFT.

In particular, all the other terms of the OPE contain a string of fields belonging to different sheets. All these fields but one factorise into one-point correlation functions, which are identically zero in CFT.

On the other hand, the above correlator can be computed using the definition (B.1):

$$\begin{aligned} \frac{\langle \mathcal{T}(x_1) \tilde{\mathcal{T}}(x_2) \phi_1(x_3) \rangle}{\langle \mathcal{T}(x_1) \tilde{\mathcal{T}}(x_2) \rangle} &= \langle \phi(x_3; \text{sheet } k) \rangle \\ &= |\partial g(x_3)|^{2\Delta} \left\langle \phi \left( e^{\frac{2\pi i k}{n}} g(x_3) \right) \right\rangle \end{aligned} \quad (\text{B.7})$$

The last correlation function is defined on the complex plane. Any one-point function in CFT vanishes identically for any value of  $x_3$ . Comparing the two results for the correlation functions it is clear that

$$C_{\mathcal{T}\tilde{\mathcal{T}}}^{\Phi_1} = 0 \quad (\text{B.8})$$

The exponential factor  $\exp \frac{2\pi i k}{n}$  has a geometric interpretation coming from the conformal map (B.2). The idea is to map each sheet into a Riemann sphere with a cut between the two poles. Each of these cut spheres can be contracted into a slice and the all slices can be packed together into a sphere. Such a sphere can be mapped back to a plane. For this reason, the exponential factor is needed to keep track of the original sheet.

### B.1.2 The $C_{\mathcal{T}\tilde{\mathcal{T}}}^{\Phi_{1j}}$ structure constant

The  $C_{\mathcal{T}\tilde{\mathcal{T}}}^{\Phi_{1j}}$  structure constant, which is the first non-trivial involving twist fields, can be computed in the same way as the  $C_{\mathcal{T}\tilde{\mathcal{T}}}^{\Phi_1}$  constant.

Consider the following short distance scaling, with  $k \neq 1$ :

$$\begin{aligned} \frac{\langle \mathcal{T}(x_1) \tilde{\mathcal{T}}(x_2) \phi_1(x_3) \phi_k(x_4) \rangle}{\langle \mathcal{T}(x_1) \tilde{\mathcal{T}}(x_2) \rangle} &\underset{x_1 \rightarrow x_2}{\sim} |x_1 - x_2|^{4\Delta} \sum_{j=2}^{\lfloor \frac{n}{2} \rfloor + 1} \tilde{C}_{\mathcal{T}\tilde{\mathcal{T}}}^{\Phi_{1,j}} \langle \Phi_{1,j}(x_2) \phi_1(x_3) \phi_k(x_4) \rangle \\ &= \tilde{C}_{\mathcal{T}\tilde{\mathcal{T}}}^{\Phi_{1,k}} |x_1 - x_2|^{4\Delta} \langle \Phi_{1,k}(x_2) \phi_1(x_3) \phi_k(x_4) \rangle \\ &= \tilde{C}_{\mathcal{T}\tilde{\mathcal{T}}}^{\Phi_{1,k}} |x_1 - x_2|^{4\Delta} (|x_2 - x_3| |x_2 - x_4|)^{-4\Delta} \end{aligned} \quad (\text{B.9})$$

As before, all other terms of the OPE vanish when inserted in such a correlation function. In all terms but one, at least one one-point function can be factorised out of the correlator. In order to evaluate the conformal structure constant, we compute the correlation function

involving twist fields using (B.1):

$$\begin{aligned}
& \frac{\langle \mathcal{T}(x_1) \tilde{\mathcal{T}}(x_2) \phi_1(x_3) \phi_k(x_4) \rangle}{\langle \mathcal{T}(x_1) \tilde{\mathcal{T}}(x_2) \rangle} = |\partial g(x_3)|^{2\Delta} |\partial g(x_4)|^{2\Delta} \langle \phi(e^{\frac{2\pi i}{n}} g(x_3)) \phi(e^{\frac{2\pi i k}{n}} g(x_4)) \rangle \\
& = \frac{n^{-4\Delta} |x_2 - x_1|^{4\Delta} \langle \phi(e^{\frac{2\pi i}{n}} g(x_3)) \phi(e^{\frac{2\pi i k}{n}} g(x_4)) \rangle}{|x_3 - x_1|^{2\Delta(1-\frac{1}{n})} |x_3 - x_2|^{2\Delta(1+\frac{1}{n})} |x_4 - x_1|^{2\Delta(1-\frac{1}{n})} |x_4 - x_2|^{2\Delta(1+\frac{1}{n})}} \\
& = \frac{n^{-4\Delta} |x_2 - x_1|^{4\Delta} \left| e^{\frac{2\pi i}{n} \left( \frac{x_3 - x_1}{x_3 - x_2} \right)^{\frac{1}{n}}} - e^{\frac{2\pi i k}{n} \left( \frac{x_4 - x_1}{x_4 - x_2} \right)^{\frac{1}{n}}} \right|^{-4\Delta}}{|x_3 - x_1|^{2\Delta(1-\frac{1}{n})} |x_3 - x_2|^{2\Delta(1+\frac{1}{n})} |x_4 - x_1|^{2\Delta(1-\frac{1}{n})} |x_4 - x_2|^{2\Delta(1+\frac{1}{n})}} \\
& \stackrel{x_1 \rightarrow x_2}{\sim} \frac{n^{-4\Delta} |x_2 - x_1|^{4\Delta} \left| e^{\frac{2\pi i}{n}} - e^{\frac{2\pi i k}{n}} \right|^{-4\Delta}}{|x_3 - x_2|^{4\Delta} |x_4 - x_2|^{4\Delta}}
\end{aligned} \tag{B.10}$$

Comparing the two results we obtain:

$$\tilde{C}_{\mathcal{T}\tilde{\mathcal{T}}}^{\Phi_{1,k}} = n^{-4\Delta} \left| 1 - e^{\frac{2\pi i(k-1)}{n}} \right|^{-4\Delta} \tag{B.11}$$

### B.1.3 Higher-point structure constants

From the previous case it is possible to recover a general formula to compute the  $J$ -point structure constants. The general rule is given by

$$C_{\mathcal{T}\tilde{\mathcal{T}}}^{\Phi_{k_1 \dots k_J}} = n^{-2J\Delta} \left\langle \phi \left( e^{\frac{2\pi i k_1}{n}} \right) \phi \left( e^{\frac{2\pi i k_2}{n}} \right) \dots \phi \left( e^{\frac{2\pi i k_J}{n}} \right) \right\rangle \tag{B.12}$$

Of course, the above constant cannot be computed for an arbitrary value of  $J$ , since it will involve a many-point correlation function.

## B.2 Structure Constants of Composite Twist Fields : $\mathcal{T}\phi$ :

The structure constants involving composite fields :  $\mathcal{T}\phi$  : are a bit more complicated than their not composite  $\mathcal{T}$  counterparts, even though the strategy to evaluate them is the same. The main difference will be the implementation of the definition (5.18) of composite twist fields:

$$: \mathcal{T}\phi : (x) \equiv n^{2\Delta-1} \lim_{y \rightarrow x} |x - y|^{2\Delta(1-\frac{1}{n})} \mathcal{T}(x) \sum_{j=1}^n \phi_j(y) \tag{B.13}$$

**The structure constant**  $\tilde{C}_{\mathcal{T}\phi:\tilde{\mathcal{T}}\phi}^{\Phi_1}$

As before, let us consider the following correlation function:

$$\frac{\langle :\mathcal{T}\phi:(x_1) : \tilde{\mathcal{T}}\phi:(x_2)\phi_1(x_3) \rangle}{\langle \mathcal{T}(x_1)\tilde{\mathcal{T}}(x_2) \rangle} \quad (\text{B.14})$$

As usual, we can study its short distance scaling looking at its OPE or by implementing the definition B.1 of twist field.

The only non vanishing terms of its OPE are given by:

$$\begin{aligned} \frac{\langle :\mathcal{T}\phi:(x_1) : \tilde{\mathcal{T}}\phi:(x_2)\phi_1(x_3) \rangle}{\langle \mathcal{T}(x_1)\tilde{\mathcal{T}}(x_2) \rangle} &\stackrel{x_1 \rightarrow x_2}{\sim} \tilde{C}_{\mathcal{T}\phi:\tilde{\mathcal{T}}\phi}^{\Phi_1} |x_1 - x_2|^{2\Delta - 4\Delta_{\mathcal{T}\phi}} \frac{\langle \phi_1(x_2)\phi_1(x_3) \rangle}{\langle \mathcal{T}(x_1)\tilde{\mathcal{T}}(x_2) \rangle} \\ &= \tilde{C}_{\mathcal{T}\phi:\tilde{\mathcal{T}}\phi}^{\Phi_1} |x_1 - x_2|^{2\Delta(1 - \frac{2}{n})} |x_2 - x_3|^{-4\Delta} \end{aligned} \quad (\text{B.15})$$

Additionally we can implement the definitions (5.18) and (B.13) to factor the normal twist fields  $\mathcal{T}$  from their composite counterparts :  $\mathcal{T}\phi$  : from the above equation:

$$\begin{aligned} \frac{\langle :\mathcal{T}\phi:(x_1) : \tilde{\mathcal{T}}\phi:(x_2)\phi_1(x_3) \rangle}{\langle \mathcal{T}(x_1)\tilde{\mathcal{T}}(x_2) \rangle} &= n^{4\Delta - 2} \lim_{y_i \rightarrow x_i} |x_1 - y_1|^{2\Delta(1 - \frac{1}{n})} |x_2 - y_2|^{2\Delta(1 - \frac{1}{n})} \\ &\times \sum_{j_1, j_2=1}^n \frac{\langle \mathcal{T}(x_1)\tilde{\mathcal{T}}(x_2)\phi_{j_1}(y_1)\phi_{j_2}(y_2)\phi_1(x_3) \rangle}{\langle \mathcal{T}(x_1)\tilde{\mathcal{T}}(x_2) \rangle} \end{aligned} \quad (\text{B.16})$$

Once we have reached this point, we can proceed in the same way of the previous sections:

$$\begin{aligned}
& \frac{\langle : \mathcal{T}\phi : (x_1) : \tilde{\mathcal{T}}\phi : (x_2) \phi_1(x_3) \rangle}{\langle \mathcal{T}(x_1) \tilde{\mathcal{T}}(x_2) \rangle} \\
&= n^{4\Delta-2} \lim_{y_i \rightarrow x_i} |x_1 - y_1|^{2\Delta(1-\frac{1}{n})} |x_2 - y_2|^{2\Delta(1-\frac{1}{n})} |\partial g(y_1)|^{2\Delta} |\partial g(y_2)|^{2\Delta} |\partial g(x_3)|^{2\Delta} \\
&\times \sum_{j_1, j_2=1}^n \langle \phi(e^{\frac{2\pi i j_1}{n}} g(y_1)) \phi(e^{\frac{2\pi i j_2}{n}} g(y_2)) \phi(e^{\frac{2\pi i}{n}} g(x_3)) \rangle \\
&= \tilde{C}_{\phi\phi}^{\phi} n^{4\Delta-2} n^{-4\Delta} \lim_{y_i \rightarrow x_i} |x_2 - y_2|^{4\Delta(1-\frac{1}{n})} |\partial g(x_3)|^{2\Delta} \\
&\quad \sum_{j_1, j_2=1}^n \left( |e^{\frac{2\pi i j_1}{n}} g(y_1) - e^{\frac{2\pi i j_2}{n}} g(y_2)| |e^{\frac{2\pi i j_1}{n}} g(y_1) - e^{\frac{2\pi i}{n}} g(x_3)| |e^{\frac{2\pi i j_2}{n}} g(y_2) - e^{\frac{2\pi i}{n}} g(x_3)| \right)^{-2\Delta} \\
&= \tilde{C}_{\phi\phi}^{\phi} \lim_{y_i \rightarrow x_i} |x_2 - y_2|^{4\Delta(1-\frac{1}{n})} |\partial g(x_3)|^{2\Delta} (|g(y_2)|^2 |g(x_3)|)^{-\frac{4\Delta}{n}} \\
&= \tilde{C}_{\phi\phi}^{\phi} |x_1 - x_2|^{-\frac{4\Delta}{n}} \lim_{y_i \rightarrow x_i} |\partial g(x_3)|^{2\Delta} |g(x_3)|^{-2\Delta} \\
&= \tilde{C}_{\phi\phi}^{\phi} n^{-2\Delta} |x_1 - x_2|^{2\Delta(1-\frac{2}{n})} |x_3 - x_1|^{-2\Delta} |x_3 - x_2|^{-2\Delta}
\end{aligned} \tag{B.17}$$

Comparing the two results, we can conclude that:

$$\tilde{C}_{:\mathcal{T}\phi: \tilde{\mathcal{T}}\phi}^{\phi} = n^{-2\Delta} \tilde{C}_{\phi\phi}^{\phi} \tag{B.18}$$

**The structure constant  $\tilde{C}_{:\mathcal{T}\phi: \tilde{\mathcal{T}}\phi}^{\Phi_{1,k}}$**

To compute  $\tilde{C}_{:\mathcal{T}\phi: \tilde{\mathcal{T}}\phi}^{\Phi_{1,k}}$  we will evaluate the short distance scaling of:

$$\frac{\langle : \mathcal{T}\phi : (x_1) : \tilde{\mathcal{T}}\phi : (x_2) \phi_1(x_3) \phi_k(x_4) \rangle}{\langle \mathcal{T}(x_1) \tilde{\mathcal{T}}(x_2) \rangle} \tag{B.19}$$

Its short-distance OPE is given by:

$$\begin{aligned}
& \frac{\langle : \mathcal{T}\phi : (x_1) : \tilde{\mathcal{T}}\phi : (x_2) \phi_1(x_3) \phi_k(x_4) \rangle}{\langle \mathcal{T}(x_1) \tilde{\mathcal{T}}(x_2) \rangle} \\
& \stackrel{x_1 \rightarrow x_2}{\sim} C_{:\mathcal{T}\phi: \tilde{\mathcal{T}}\phi}^{\Phi_{1,k}} |x_1 - x_2|^{4\Delta(1-\frac{1}{n})} \langle \phi_1(x_2) \phi_1(x_3) \rangle \langle \phi_k(x_2) \phi_k(x_4) \rangle \\
& = C_{:\mathcal{T}\phi: \tilde{\mathcal{T}}\phi}^{\Phi_{1,k}} |x_1 - x_2|^{4\Delta(1-\frac{1}{n})} (|x_2 - x_3| |x_2 - x_4|)^{-4\Delta}
\end{aligned} \tag{B.20}$$

This correlation function can also be computed via (B.13):

$$\begin{aligned}
& \frac{\langle : \mathcal{T}\phi : (x_1) : \tilde{\mathcal{T}}\phi : (x_2) \phi_1(x_3) \phi_k(x_4) \rangle}{\langle \mathcal{T}(x_1) \tilde{\mathcal{T}}(x_2) \rangle} \\
&= n^{4\Delta-2} \lim_{y_i \rightarrow x_i} |x_1 - y_1|^{2\Delta(1-\frac{1}{n})} |x_2 - y_2|^{2\Delta(1-\frac{1}{n})} |\partial g(y_1)|^{2\Delta} |\partial g(y_2)|^{2\Delta} |\partial g(x_3)|^{2\Delta} |\partial g(x_4)|^{2\Delta} \\
&\times \sum_{j_1, j_2=1}^n \langle \phi(e^{\frac{2\pi i j_1}{n}} g(y_1)) \phi(e^{\frac{2\pi i j_2}{n}} g(y_2)) \phi(e^{\frac{2\pi i}{n}} g(x_3)) \phi(e^{\frac{2\pi i k}{n}} g(x_4)) \rangle \\
&= n^{4\Delta-2} n^{1-4\Delta} \lim_{y_i \rightarrow x_i} |x_2 - y_2|^{-\frac{4\Delta}{n}} |\partial g(x_3)|^{2\Delta} |\partial g(x_4)|^{2\Delta} \\
&\times \sum_{j=1}^n \langle \phi(0) \phi(g(y_2)) \phi(e^{-\frac{2\pi i(j-1)}{n}} g(x_3)) \phi(e^{\frac{2\pi i(k-j)}{n}} g(x_4)) \rangle \\
&= |x_1 - x_2|^{-\frac{4\Delta}{n}} \lim_{y_i \rightarrow x_i} |\partial g(x_3)|^{2\Delta} |\partial g(x_4)|^{2\Delta} |g(x_4)|^{-4\Delta} \mathcal{F} \left( 1 - e^{\frac{2\pi i(k-1)}{n}} \frac{g(x_4)}{g(x_3)} \right) \\
&= n^{-4\Delta} |x_1 - x_2|^{4\Delta(1-\frac{1}{n})} (|x_3 - x_1| |x_4 - x_2|)^{-2\Delta(1-\frac{1}{n})} (|x_3 - x_2| |x_4 - x_1|)^{-2\Delta(1+\frac{1}{n})} \\
&\times \mathcal{F} \left( 1 - e^{\frac{2\pi i(k-1)}{n}} \left( \frac{(x_4 - x_1)(x_3 - x_2)}{(x_4 - x_2)(x_3 - x_1)} \right)^{\frac{1}{n}} \right) \\
&\stackrel{x_1 \rightarrow x_2}{\sim} n^{-4\Delta} |x_1 - x_2|^{4\Delta(1-\frac{1}{n})} |x_3 - x_2|^{-4\Delta} |x_4 - x_2|^{-4\Delta} \mathcal{F} \left( 1 - e^{\frac{2\pi i(k-1)}{n}} \right)
\end{aligned} \tag{B.21}$$

where the function  $\mathcal{F}$  is the conformal block of the four-point function  $\langle \phi\phi\phi\phi \rangle$  (6.87):

$$\mathcal{F}(x) = \lim_{y \rightarrow \infty} |y|^{4\Delta} \langle \phi(0) \phi(1) \phi(y) \phi(x) \rangle \tag{B.22}$$

which can has been computed in [126] and it is given by

$$\mathcal{F}(x) = |x|^{\frac{4}{5}} \left( \left| {}_2F_1 \left( \frac{3}{5}, \frac{4}{5}, \frac{6}{5}; x \right) \right|^2 + (C_{\phi\phi}^\phi)^2 \left| x^{-\frac{1}{5}} {}_2F_1 \left( \frac{3}{5}, \frac{2}{5}, \frac{4}{5}; x \right) \right|^2 \right) \tag{B.23}$$

and  ${}_2F_1$  is an hyperbolic function.

## Appendix C

# Monte Carlo Integration Algorithm

In this appendix we present a very brief introduction to the Monte Carlo Algorithm for the numerical evaluation of integrals.

Let us consider the integral  $I$  of a function  $f$  over a  $d$ -dimensional domain  $D$ :

$$I = \int_D d^d x f(x) \quad (\text{C.1})$$

Let us define a random variable  $y$  as

$$y = \frac{1}{N} \sum_{i=1}^N \frac{f(x_i)}{\rho(x_i)} \quad (\text{C.2})$$

where each of the  $N$  points  $x_i$  is randomly chosen inside  $D$  using a probability distribution with a given probability density  $\rho(x_i)$ .<sup>1</sup>

The probability density of  $y$  itself is then given by

$$\hat{\rho}(y) = \int_{D^N} dx_1 \cdots dx_N \delta \left( y - \frac{1}{N} \sum_{i=1}^N \frac{f(x_i)}{\rho(x_i)} \right) \rho(x_1) \cdots \rho(x_N) \quad (\text{C.3})$$

---

<sup>1</sup>Notice that a point  $x_i$  s.t.  $\rho(x_i) = 0$  will never be chosen using  $\rho$  as a probability density function.

---

The average of  $y$  is equal to the integral  $I$ :

$$\begin{aligned}\langle y \rangle &= \int dy \hat{\rho}(y) y = \int_{D^N} dx_1 \cdots dx_N \left[ \frac{1}{N} \left( \sum_{i=1}^N \frac{f(x_i)}{\rho(x_i)} \right) \rho(x_1) \cdots \rho(x_N) \right] \\ &= \frac{1}{N} \sum_{i=1}^N \int_D dx_i f(x_i) = I\end{aligned}\tag{C.4}$$

Since

$$y \approx \langle y \rangle + \text{Error} = I + \text{Error}\tag{C.5}$$

the integral  $I$  can then be approximated by  $y$ , i.e. by taking  $N$  random points and calculating the average value of the function on these points.

Thanks to the simple random nature of the variable  $y$ , it can be used also to estimate the error of the Monte Carlo algorithm. Consider

$$\langle y^2 \rangle = \int dy \hat{\rho}(y) y^2 = \frac{1}{N^2} \sum_{i,j=1}^N \int_{D^N} dx_1 \cdots dx_N \rho(x_1) \cdots \rho(x_N) \frac{f(x_i) f(x_j)}{\rho(x_i) \rho(x_j)}\tag{C.6}$$

The sum on the RHS of equation (C.6) can be split into the  $i = j$  ( $N$  terms) and the  $i \neq j$  parts ( $N^2 - N$  terms). The former gives rise to  $\int \frac{f^2}{\rho}$  contributions while the latter to  $(\int f)^2$  ones. Taking all terms together we have

$$\langle y^2 \rangle = \frac{1}{N} \int_D dx \frac{f(x)^2}{\rho(x)} + \frac{N-1}{N^2} \left( \int_D dx f(x) \right)^2\tag{C.7}$$

The variance  $\sigma^2$  is then given by

$$\sigma^2 = \langle y^2 \rangle - \langle y \rangle^2 = \frac{1}{N} \left[ \int_D dx \frac{f(x)^2}{\rho(x)} - \left( \int_D dx f(x) \right)^2 \right]\tag{C.8}$$

When approximating  $I$  with  $y$ , the error is  $\sqrt{\sigma}$  and it decreases as  $\frac{1}{\sqrt{N}}$ .

In the basic version of the Monte Carlo routine, usually called *plain Monte Carlo*, the distribution is chosen to be uniform, i.e.  $\rho = \frac{1}{\text{Vol}(D)}$  and the integral  $I$  is then approximated by

$$I \approx \frac{\text{Vol}(D)}{N} \sum_{i=1}^N f(x_i)\tag{C.9}$$

---

## Vegas algorithm

In plain Monte Carlo algorithm the approximation error decreases with the square root of the number of points used to sample the domain. For this reason, to decrease the error by a factor of 10, a 100-fold increase in the number of point is required. In order to increase the precision, some tricks have to be put in place, like the *Vegas Monte Carlo Algorithm*. Instead of using a uniform distribution for  $\rho$ , we can choose a distribution [81] that is peaked around the points where the function  $f$  is more relevant. In particular,  $\rho$  can be chosen as

$$\rho(x) = \frac{|f(x)|}{\int_D dy |f(y)|} \quad (\text{C.10})$$

The variance with this approximation is then given by

$$\sigma^2 = \frac{1}{N} \left[ \left( \int_D dx |f(x)| \right)^2 - \left( \int_D dx f(x) \right)^2 \right] \quad (\text{C.11})$$

Even though the error still scales with as the square root of the number of sampling points,  $\sigma \sim N^{-\frac{1}{2}}$ , the constant coefficient is expected to be very small.

Of course the density (C.10) is not known exactly, since it would require a complete sampling of the function in the whole domain.<sup>2</sup>

---

<sup>2</sup>If a complete sampling of the function in the whole domain was done with a very fine precision, the integral can be calculated directly with a “trapezoid-like” method.

## Appendix D

# Jacobi Elliptic Theta Functions

In this Appendix we list the definitions of Jacobi elliptic theta functions and their elliptic transformations [49].

$$\vartheta_1(z, q) = 2q^{\frac{1}{4}} \sum_{n=0}^{\infty} (-1)^n q^{n(n+1)} \sin[(2n+1)z] \quad (\text{D.1})$$

$$\vartheta_1(z, q) = 2q^{\frac{1}{4}} \sum_{n=0}^{\infty} q^{n(n+1)} \cos[(2n+1)z] \quad (\text{D.2})$$

$$\vartheta_1(z, q) = 1 + 2 \sum_{n=0}^{\infty} q^{n^2} \cos(2nz) \quad (\text{D.3})$$

$$\vartheta_1(z, q) = 1 + 2 \sum_{n=0}^{\infty} (-1)^n q^{n^2} \cos(2nz) \quad (\text{D.4})$$

It could be useful to represent the *nome*  $q$  in terms of a modular parameter  $\tau$ :

$$q = e^{\pi i \tau} \quad (\text{D.5})$$

Theta functions can then be expressed in terms of  $z$  and  $\tau$ :

$$\vartheta_i(z, q) \equiv \theta_i(z|\tau) \quad (\text{D.6})$$

Jacobi  $\theta$  functions enjoy the following modular transformations [37].

$$\theta_1(z| -1/\tau) = \sqrt{-i\tau} e^{\frac{i\tau z^2}{\pi}} \vartheta_1(\tau z|\tau) \quad (\text{D.7})$$

$$\theta_2(z| -1/\tau) = \sqrt{-i\tau} e^{\frac{i\tau z^2}{\pi}} \vartheta_4(\tau z|\tau) \quad (\text{D.8})$$

$$\theta_3(z| -1/\tau) = \sqrt{-i\tau} e^{\frac{i\tau z^2}{\pi}} \vartheta_3(\tau z|\tau) \quad (\text{D.9})$$

$$\theta_4(z| -1/\tau) = \sqrt{-i\tau} e^{\frac{i\tau z^2}{\pi}} \vartheta_2(\tau z|\tau) \quad (\text{D.10})$$

---

Moreover, it should be noticed ([108]) that the function  $E$  (7.38) can be expressed using the Jacobi  $\vartheta_1$  function:

$$E(e^{2iz}, q^2) = iq^{-\frac{1}{4}} e^{iz} \vartheta_1(z, q) \quad (\text{D.11})$$

## Appendix E

# Summation Formulæ

Numerous summation formulæ involving two-particle form factors were derived in [118]. When specialising to the massive free boson case these formulæ become:

$$\begin{aligned} & \sum_{p=0}^{n-1} f(-x + 2\pi ip; n) f(y + 2\pi ip; n) \\ = & -\frac{i}{2} \frac{\sinh \frac{x+y}{2}}{\cosh \frac{x}{2} \cosh \frac{y}{2}} [f(x + y + i\pi; n) - f(x + y - i\pi; n)] \end{aligned} \quad (\text{E.1})$$

where  $f(\beta; n)$  is the two particle form factor (8.9).

Equation (E.1) has been derived by considering the left-hand-side sum as the sum of the residues of a contour integral and by solving such an integral using the kinematic singularities of the two-particle form factor. Formula (E.1) can be generalised by induction to an arbitrary number of sums. This procedure is very similar to the one used in [70] when studying free fermion theories. The generalised summation formula is given by

$$\begin{aligned} & \sum_{p_1, \dots, p_{2\ell-1}=0}^{n-1} f((-y_1)^{p_1}; n) f(y_2^{p_1-p_2}; n) \cdots f(y_{2\ell-1}^{p_{2\ell-2}-p_{2\ell-1}}; n) f(y_{2\ell}^{p_{2\ell-1}}; n) \\ = & \frac{2i \sinh(\frac{1}{2} \sum_{i=1}^{2\ell} y_i)}{\prod_{i=1}^{2\ell} 2 \cosh \frac{y_i}{2}} \sum_{p=1}^{\ell} (-1)^p \binom{2\ell-1}{\ell-p} \left[ f\left(\sum_{i=1}^{2\ell} y_i + (2p-1)i\pi; n\right) \right. \\ & \left. - f\left(\sum_{i=1}^{2\ell} y_i - (2p-1)i\pi; n\right) \right] \end{aligned} \quad (\text{E.2})$$

where  $x^p = x + 2\pi ip$ .

An important property of the above summation formula is its behaviour in the  $\sum_{i=1}^{2\ell} x_i \rightarrow 0$  limit. Even though the sinh term tends to zero, some kinematic poles in the two-particle

form factors appear. Such divergences appear when  $p=1$  (corresponding to the kinematic pole at  $i\pi$ ), when  $p=kn$ , i.e. when  $p$  is a multiple of  $n$ , which correspond to the pole at  $(2n-1)i\pi$ . Thanks to the  $2\pi in$  periodicity of the two-particle form factor, an extra kinematic pole is present when  $p=kn+1$ , which corresponds to the pole at  $(2n+1)i\pi=i\pi \pmod{2\pi in}$ . The number of such poles then depends on the relative value of  $n$  and  $\ell$ :

$$\begin{aligned} & \lim_{\sum_{i=1}^{2\ell} x_i \rightarrow 0} \sum_{p_1, \dots, p_{2\ell-1}=0}^{n-1} f((-y_1)^{p_1}; n) f(y_2^{p_1-p_2}; n) \cdots f(y_{2\ell-1}^{p_{2\ell-2}-p_{2\ell-1}}; n) f(y_{2\ell}^{p_{2\ell-1}}; n) \\ = & h(\ell, n) \operatorname{sech} \left( \frac{\sum_{p=2}^{2\ell} x_p}{2} \right) \prod_{p=2}^{2\ell} \operatorname{sech} \frac{x_p}{2} \end{aligned} \quad (\text{E.3})$$

where the function  $h(\ell, n)$  is given by:

$$h(\ell, n) = \frac{1}{2^{2\ell-1}} \left[ \binom{2\ell-1}{\ell-1} + \sum_{p=1}^{\lfloor \frac{\ell}{n} \rfloor} (-1)^{pn} \binom{2\ell}{\ell-pn} \right] \quad (\text{E.4})$$

From its definition it is clear that when  $\ell < n$  the second term does not contribute.

In case an analytic continuation of the function  $h$  is needed, it is important to distinguish the even  $n$  case from the odd  $n$  case:

$$h^e(\ell, n) = \frac{1}{2^{2\ell-1}} \left[ \binom{2\ell-1}{\ell-1} + \sum_{p=1}^{\lfloor \frac{\ell}{n} \rfloor} \binom{2\ell}{\ell-pn} \right] \quad (\text{E.5})$$

$$h^o(\ell, n) = \frac{1}{2^{2\ell-1}} \left[ \binom{2\ell-1}{\ell-1} + \sum_{p=1}^{\lfloor \frac{\ell}{n} \rfloor} (-1)^{pn} \binom{2\ell}{\ell-pn} \right] \quad (\text{E.6})$$

# Appendix F

## Numerical Fit

In this appendix we discuss the fitting algorithm used to interpolate numerical data. We derive the fitting constants for both polynomial and logarithmic fitting. In the following we consider  $N$  couples  $(y_i, n_i)$  of data with associated error  $\sigma_i$  (relative only to the  $y_i$  values).

### F.1 Fitting Algorithm - Polynomial

In this section we derive the best fitting constants  $a$ ,  $b$  and  $c$  for the polynomial fit:

$$y_i = a + bn_i + \frac{c}{n_i} \quad (\text{F.1})$$

In order to compute the values (and their relative errors) of the fitting constants  $a$ ,  $b$  and  $c$  we perform a least-squared fitting [127]. In particular, the constants  $a$ ,  $b$ , and  $c$  are such that minimise the quantity:

$$\chi^2 = \sum_{i=1}^N \frac{(a + bn_i + \frac{c}{n_i} - y_i)^2}{\sigma_i^2} \quad (\text{F.2})$$

Taking derivatives with respect to the coefficients  $a$ ,  $b$ , and  $c$  we can minimise  $\chi^2$ :

$$\begin{cases} \frac{1}{2} \frac{\partial \chi^2}{\partial a} = a \sum w_i + b \sum w_i n_i + c \sum \frac{w_i}{n_i} - \sum w_i y_i = 0 \\ \frac{1}{2} \frac{\partial \chi^2}{\partial b} = a \sum w_i n_i + b \sum w_i n_i^2 + c \sum w_i - \sum w_i y_i n_i = 0 \\ \frac{1}{2} \frac{\partial \chi^2}{\partial c} = a \sum \frac{w_i}{n_i} + b \sum w_i + c \sum \frac{w_i}{n_i^2} - \sum \frac{w_i y_i}{n_i} = 0 \end{cases} \quad (\text{F.3})$$

where  $w_i = \sigma_i^{-2}$  are the statistical weights of the various points  $y_i$ .

The above system can be easily solved for  $a$ ,  $b$ , and  $c$ :

$$\left\{ \begin{array}{l} a = \frac{1}{\Delta} \left[ \left( (\sum w_i)^2 - \sum \frac{w_i}{n_i^2} \sum w_i n_i^2 \right) \sum w_i y_i + \left( \sum \frac{w_i}{n_i^2} \sum w_i y_i n_i - \sum w_i \sum \frac{w_i y_i}{n_i} \right) \sum w_i n_i \right. \\ \quad \left. - \left( \sum w_i \sum w_i y_i n_i - \sum \frac{w_i y_i}{n_i} \sum w_i n_i^2 \right) \sum \frac{w_i}{n_i} \right] \\ b = \frac{1}{\Delta} \left[ \left( \sum \frac{w_i}{n_i^2} \sum w_i n_i - \sum w_i \sum \frac{w_i}{n_i} \right) \sum w_i y_i - \left( \sum \frac{w_i}{n_i^2} \sum w_i - \left( \frac{w_i}{n_i} \right)^2 \right) \sum w_i y_i n_i \right. \\ \quad \left. - \left( \sum \frac{w_i}{n_i} \sum w_i n_i - (\sum w_i)^2 \right) \sum \frac{w_i y_i}{n_i} \right] \\ c = -\frac{1}{\Delta} \left[ \left( \sum w_i \sum w_i n_i - \sum \frac{w_i}{n_i} \sum w_i n_i^2 \right) \sum w_i y_i + \left( \sum \frac{w_i}{n_i} \sum w_i n_i - (\sum w_i)^2 \right) \sum w_i y_i n_i \right. \\ \quad \left. - \left( (\sum w_i n_i)^2 - \sum w_i \sum w_i n_i^2 \right) \sum \frac{w_i y_i}{n_i} \right] \\ \Delta = \sum \frac{w_i}{n_i^2} (\sum n_i w_i)^2 - 2 \sum \frac{w_i}{n_i} \sum w_i \sum w_i n_i - \sum \frac{w_i}{n_i^2} \sum w_i \sum w_i n_i^2 + \left( \sum \frac{w_i}{n_i} \right)^2 + (\sum w_i)^3 \end{array} \right. \quad (\text{F.4})$$

Since only the  $y_i$  values are affected by error, the associated error of the  $a$ ,  $b$ , and  $c$  constants is given by:

$$\left\{ \begin{array}{l} \Delta a = \sqrt{\sum_i \left( \frac{\partial a}{\partial y_i} \sigma_i \right)^2} \\ \Delta b = \sqrt{\sum_i \left( \frac{\partial b}{\partial y_i} \sigma_i \right)^2} \\ \Delta c = \sqrt{\sum_i \left( \frac{\partial c}{\partial y_i} \sigma_i \right)^2} \end{array} \right. \quad (\text{F.5})$$

## F.2 Fitting Algorithm - Logarithm

Following the steps of the previous section, we derive the fitting constants  $a$ ,  $b$  and  $c$  for the linear-logarithmic fit:

$$y_i = a + b n_i + c \log n_i \quad (\text{F.6})$$

As before, we minimise the  $\chi^2$  value to find the best values for the fitting constants:

$$\chi^2 = \sum_{i=1}^N \frac{(a + b n_i + c \log n_i - y_i)^2}{\sigma_i^2} \quad (\text{F.7})$$

We can now take some derivatives of  $\chi^2$  respect with  $a$ ,  $b$  and  $c$ :

$$\left\{ \begin{array}{l} \frac{1}{2} \frac{\partial \chi^2}{\partial a} = a \sum w_i + b \sum w_i n_i + c \sum w_i \log n_i - \sum w_i y_i = 0 \\ \frac{1}{2} \frac{\partial \chi^2}{\partial b} = a \sum w_i n_i + b \sum w_i n_i^2 + c \sum w_i n_i \log n_i - \sum w_i y_i n_i = 0 \\ \frac{1}{2} \frac{\partial \chi^2}{\partial c} = a \sum w_i \log n_i + b \sum w_i n_i \log n_i + c \sum w_i (\log n_i)^2 - \sum w_i y_i \log n_i = 0 \end{array} \right. \quad (\text{F.8})$$

Such a linear system can be easily solved:

$$\left\{ \begin{array}{l}
 a = \frac{1}{\Delta} [\sum w_i \log n_i (\sum w_i n_i^2 \sum w_i y_i \log n_i - \sum w_i n_i \log n_i \sum w_i y_i n_i) \\
 + \sum w_i n_i (\sum w_i (\log n_i)^2 \sum w_i y_i n_i - \sum w_i n_i \log n_i \sum w_i y_i \log n_i) \\
 + (\sum w_i n_i \log n_i^2 - \sum w_i (\log n_i)^2 \sum w_i n_i^2) \sum w_i y_i] \\
 b = \frac{1}{\Delta} [\sum w_i (\sum w_i n_i \log n_i \sum w_i y_i \log n_i - \sum w_i (\log n_i)^2 \sum w_i y_i n_i) \\
 + \sum w_i \log n_i^2 \sum w_i y_i n_i - \sum w_i \log n_i \sum w_i n_i \sum w_i y_i \log n_i \\
 - (\sum w_i (\log n_i)^2 \sum w_i n_i - \sum w_i \log n_i \sum w_i n_i \log n_i) \sum w_i y_i] \\
 c = \frac{1}{\Delta} [\sum w_i (\sum w_i n_i^2 \sum w_i y_i \log n_i - \sum w_i n_i \log n_i \sum w_i y_i n_i) \\
 + \sum w_i \log n_i \sum w_i n_i \sum w_i y_i n_i - \sum w_i n_i^2 \sum w_i y_i \log n_i \\
 + (\sum w_i n_i \sum w_i n_i \log n_i - \sum w_i \log n_i \sum w_i n_i^2) \sum w_i y_i] \\
 \Delta = \sum w_i (\sum w_i n_i \log n_i^2 - \sum w_i (\log n_i)^2 \sum w_i n_i^2) \\
 - 2 \sum w_i \log n_i \sum w_i n_i \sum w_i n_i \log n_i + \sum w_i \log n_i^2 \sum w_i n_i^2 + \sum w_i (\log n_i)^2 \sum w_i n_i^2
 \end{array} \right. \quad (\text{F.9})$$

As before, since only  $y_i$  values are affected by an error, the uncertainty associated to the fitting constants  $a$ ,  $b$  and  $c$  is given by:

$$\left\{ \begin{array}{l}
 \Delta a = \sqrt{\sum_i \left( \frac{\partial a}{\partial y_i} \sigma_i \right)^2} \\
 \Delta b = \sqrt{\sum_i \left( \frac{\partial b}{\partial y_i} \sigma_i \right)^2} \\
 \Delta c = \sqrt{\sum_i \left( \frac{\partial c}{\partial y_i} \sigma_i \right)^2}
 \end{array} \right. \quad (\text{F.10})$$

## Appendix G

# Numerical Implementations

In this appendix we sketch the the main problems encountered when evaluating  $u_\ell(n)$  and  $v_\ell$  integrals of Chapter 8.

All numerical integrals have been performed using the Vegas Monte-Carlo integration algorithm (see Appendix C). In particular, we used the GNU Scientific Library implementation [128]. Consider, for instance , the integrals (8.58):

$$\begin{aligned} u_\ell(n) &= \int_{-\infty}^{\infty} dx_1 \cdots \int_{-\infty}^{\infty} dx_{2\ell-1} \frac{i\mathfrak{F}_\ell(\sum_{p=1}^{\ell} x_{2p-1}, n) \sinh(\sum_{p=1}^{\ell} x_{2p-1})}{\cosh \frac{\sum_{p=1}^{2\ell-1} x_p}{2} \prod_{p=1}^{2\ell-1} \cosh \frac{x_p}{2}} \log d_\ell \\ &\equiv \int_{-\infty}^{\infty} dx_1 \cdots \int_{-\infty}^{\infty} dx_{2\ell-1} \mathcal{I}_{n,\ell}(\mathbf{x}) \end{aligned} \quad (\text{G.1})$$

Every time the integration routine calls the function  $\mathcal{I}_{n,\ell}$ , a  $\sum_{p=1}^{\ell}$  sum and a  $\prod_{p=1}^{2\ell-1}$  product have to be performed. Since the variables  $x_i$  are stored as pointers, every single time of the function  $\mathcal{I}_{n,\ell}$  is called, the following loops are implemented:

```
double sum = 0.;
for(p=0;p<ell-1;p++) {
    sum += x[2*p];
}

double prod = 1.;
for(p=0;p<2*1-2;p++) {
    prod *= cosh(x[p]/2.);
}
```

Since the integration routine requires thousands of calls to the function, performing integrals directly in the form (8.62) becomes quite demanding in terms of computation time.

---

In order to speed up the code, we implemented the following procedure<sup>1</sup>

1. We wrote a Mathematica code whose role is to simplify the function  $\mathcal{I}_{n,\ell}$  for various values of  $n$  and  $\ell$  and to store the results in an header file `functions_U.h` in a C++ readable format. Once the Mathematica code has been executed, the file `functions_U.h` contains the definitions of all the functions  $\mathcal{I}_{n,\ell}$  without any implicit sum or product.
2. We wrote a C++ code (`integrate.cpp`) which integrates a generic function, whose declaration is inside another header file `function.h`, which include all the definitions of the  $\mathcal{I}_{n,\ell}$  functions. The program `integrate.cpp` is able to integrate with arbitrary precision.
3. We wrote two additional C++ codes (`creator_function.cpp` and `creator.cpp`). The latter program loop over all values of  $n$  and  $\ell$  and compute the integral. For each couple  $(n, \ell)$ , `creator.cpp` performs the following operations:
  - Modify `function.h` (using `creator_function.cpp`), wrapping the correct function to integrate.
  - Compile `integrate.cpp`. At this stage, the correct function is selected at the **compilation** stage. The executable is compiled and optimised for that specific function.
  - Execute `integrate.cpp`

Through this tool the computation time is widely reduced and we managed to compute form factor contributions up to 24-particle level <sup>2</sup>.

---

<sup>1</sup>For simplicity, in the following we refer to a source code and the relative executable using the source code's file name.

<sup>2</sup>24 for  $v_\ell$  integrals.  $u_\ell(n)$  integrals give reliable results up to 12-20 particles (the low  $n$  cases perform better).

# Bibliography

- [1] D. Bianchini, O. A. Castro-Alvaredo, B. Doyon, E. Levi, and F. Ravanini. Entanglement entropy of non-unitary conformal field theory. *J.Phys.*, A48:04FT01, 2015.
- [2] D. Bianchini, O. A. Castro-Alvaredo, and B. Doyon. Entanglement entropy of non-unitary integrable quantum field theory. *Nuclear Physics B*, 896:835–880, 2015.
- [3] D. Bianchini and F. Ravanini. Entanglement entropy from corner transfer matrix in forrester–baxter non-unitary rsos models. *Journal of Physics A: Mathematical and Theoretical*, 49(15):154005, 2016.
- [4] D. Bianchini, E. Ercolessi, P. A. Pearce, and F. Ravanini. Rsos quantum chains associated with off-critical minimal models and  $\mathbb{Z}_n$  parafermions. *Journal of Statistical Mechanics: Theory and Experiment*, 2015(3):P03010, 2015.
- [5] D. Bianchini and O. A. Castro-Alvaredo. Branch point twist field correlators in the massive free boson theory. *Nuclear Physics B*, 913:879 – 911, 2016.
- [6] G. Vidal, J. I. Latorre, E. Rico, and A. Kitaev. Entanglement in quantum critical phenomena. *Phys. Rev. Lett.*, 90:227902, 2003.
- [7] C. Holzhey, F. Larsen, and F. Wilczek. Geometric and renormalized entropy in conformal field theory. *Nuclear Physics B*, 424(3):443 – 467, 1994.
- [8] P. Calabrese and J. L. Cardy. Entanglement entropy and quantum field theory. *J. Stat. Mech.*, 0406:P002, 2004.
- [9] M. Karowski and P. Weisz. Exact form factors in (1+1)-dimensional field theoretic models with soliton behaviour. *Nuclear Physics B*, 139(4):455 – 476, 1978.
- [10] F. A. Smirnov. Form Factors In Completely Integrable Models Of Quantum Field Theory. *Form Factors In Completely Integrable Models Of Quantum Field Theory. Series: Advanced Series in Mathematical Physics. World Scientific, Edited by F A Smirnov, vol. 14*, 1992.

- 
- [11] R. J. Baxter. *Exactly solved models in Statistical Mechanics*. Academic Press, 1982.
- [12] T. Nishino and K. Okunishi. Corner transfer matrix algorithm for classical renormalization group. *Journal of the Physical Society of Japan*, 66(10):3040–3047, 1997.
- [13] I. Peschel, M. Kaulke, and Ö. Legeza. Density-matrix spectra for integrable models. *Annalen der Physik*, 8(2):153–164, 1999.
- [14] J. L. Cardy, O. A. Castro-Alvaredo, and B. Doyon. Form factors of branch-point twist fields in quantum integrable models and entanglement entropy. *Journal of Statistical Physics*, 130(1):129–168, 2007.
- [15] V. Eisler and Z. Zimborás. Entanglement negativity in the harmonic chain out of equilibrium. *New Journal of Physics*, 16(12):123020, 2014.
- [16] de Broglie, L. La mécanique ondulatoire et la structure atomique de la matière et du rayonnement. *J. Phys. Radium*, 8(5):225–241, 1927.
- [17] W. Gerlach and Otto Stern. Der experimentelle nachweis der richtungsquantelung im magnetfeld. *Zeitschrift für Physik*, 9(1):349–352, 1922.
- [18] J. S. Bell. On the Einstein Podolski Rosen paradox. *Physics*, 1:195–200, 1964.
- [19] A. Aspect, P. Grangier, and G. Roger. Experimental tests of realistic local theories via Bell’s theorem. *Phys. Rev. Lett.*, 47:460–463, 1981.
- [20] B. Hensen, H. Bernien, A. E. Dréau, A. Reiserer, N. Kalb, M. S. Blok, J. Ruitenberg, R. F. L. Vermeulen, R. N. Schouten, C. Abellán, W. Amaya, V. Pruneri, M. W. Mitchell, M. Markham, D. J. Twitchen, D. Elkouss, S. Wehner, T. H. Taminiau, and R. Hanson. Experimental loophole-free violation of a Bell inequality using entangled electron spins separated by 1.3 km. *Nature*, 526:682–686, 2015.
- [21] A. Garg and N. D. Mermin. Detector inefficiencies in the einstein-podolsky-rosen experiment. *Phys. Rev. D*, 35:3831–3835, 1987.
- [22] C. H. Bennett, G. Brassard, C. Crépeau, R. Jozsa, A. Peres, and W. K. Wootters. Teleporting an unknown quantum state via dual classical and einstein-podolsky-rosen channels. *Phys. Rev. Lett.*, 70:1895–1899, 1993.
- [23] D. Bouwmeester, J. Pan, K. Mattle, M. Eibl, H. Weinfurter, and A. Zeilinger. Experimental quantum teleportation. *Nature*, 390(6660):575–579, 1997.
- [24] D. Boschi, S. Branca, F. De Martini, L. Hardy, and S. Popescu. Experimental realization of teleporting an unknown pure quantum state via dual classical and einstein-podolsky-rosen channels. *Phys. Rev. Lett.*, 80:1121–1125, 1998.

- 
- [25] J. von Neumann. *Mathematical foundations of quantum mechanics*. Princeton University Press, 1955.
- [26] A. Rényi. On measures of entropy and information. In *Proceedings of the Fourth Berkeley Symposium on Mathematical Statistics and Probability, Volume 1: Contributions to the Theory of Statistics*, pages 547–561, Berkeley, Calif., 1961. University of California Press.
- [27] M. Horodecki, P. Horodecki, and R. Horodecki. Limits for entanglement measures. *Physical Review Letters*, 84(9):2014, 2000.
- [28] G. Vidal and R. F. Werner. Computable measure of entanglement. *Physical Review A*, 65(3):032314, 2002.
- [29] M. B. Plenio. Logarithmic negativity: A full entanglement monotone that is not convex. *Phys. Rev. Lett.*, 95:090503, 2005.
- [30] K. Audenaert, J. Eisert, M. B. Plenio, and R. F. Werner. Entanglement properties of the harmonic chain. *Phys. Rev. A*, 66:042327, 2002.
- [31] P. Calabrese, J. Cardy, and E. Tonni. Entanglement negativity in quantum field theory. *Phys. Rev. Lett.*, 109:130502, 2012.
- [32] S. R. White. Density matrix formulation for quantum renormalization groups. *Phys. Rev. Lett.*, 69:2863–2866, 1992.
- [33] H. W. J. Blöte, John L. Cardy, and M. P. Nightingale. Conformal invariance, the central charge, and universal finite-size amplitudes at criticality. *Phys. Rev. Lett.*, 56:742–745, 1986.
- [34] I. Affleck. Universal term in the free energy at a critical point and the conformal anomaly. *Phys. Rev. Lett.*, 56:746–748, 1986.
- [35] H. Bethe. Zur theorie der metalle. *Zeitschrift für Physik*, 71(3):205–226, 1931.
- [36] W. K. Wootters. Entanglement of formation of an arbitrary state of two qubits. *Phys. Rev. Lett.*, 80:2245–2248, Mar 1998.
- [37] P. Di Francesco, P. Mathieu, and D. Senechal. *Conformal Field Theory*. Springer, 1997.
- [38] A. A. Belavin, A. M. Polyakov, and A. B. Zamolodchikov. Infinite Conformal Symmetry in Two-Dimensional Quantum Field Theory. *Nucl. Phys.*, B241:333–380, 1984.

- 
- [39] J. L. Cardy. Conformal Field Theory and Statistical Mechanics. In *Les Houches Summer School: Session 89: Exact Methods in Low-Dimensional Statistical Physics and Quantum Computing Les Houches, France, June 30-August 1, 2008*, 2008.
- [40] P. H. Ginsparg. Applied Conformal Field Theory. In *Les Houches Summer School in Theoretical Physics: Fields, Strings, Critical Phenomena Les Houches, France, June 28-August 5, 1988*, 1988.
- [41] A. B. Zamolodchikov. Integrable field theory from conformal field theory. *Adv. Stud. Pure Math.*, 19:641–674, 1989.
- [42] G. Mussardo. *Statistical field theory: an introduction to exactly solved models in statistical physics*. Oxford Graduate Texts. Oxford Univ. Press, New York, NY, 2010.
- [43] P. Dorey. Exact S-matrices. *ArXiv High Energy Physics - Theory e-prints*, 1998.
- [44] G. Mussardo. Off-critical statistical models: Factorized scattering theories and bootstrap program. *Physics Reports*, 218(5):215 – 379, 1992.
- [45] H. M. Babujian, A. Foerster, and M. Karowski. The form factor program: A review and new results—the nested su (n) off-shell bethe ansatz. *SIGMA*, 2:082, 2006.
- [46] K. D. Rothe E. Abdalla, M. C. B. Abdalla. *Non-perturbative Methods in 2 Dimensional Quantum Field Theory*. World Scientific, 1991.
- [47] V. Riva and J. L. Cardy. Scale and conformal invariance in field theory: a physical counterexample. *Physics Letters B*, 622(3–4):339 – 342, 2005.
- [48] A. Cappelli, C. Itzykson, and J. B. Zuber. The a-d-e classification of minimal and a 1 (1) conformal invariant theories. *Communications in Mathematical Physics*, 113(1):1–26, 1987.
- [49] M. Abramowitz and I. A. Stegun. Handbook of mathematical functions with formulas, graphs, and mathematical tables. *United States Department of Commerce*, 1964.
- [50] C. Itzykson, H. Saleur, and J.-B. Zuber. Conformal invariance of nonunitary 2d-models. *EPL (Europhysics Letters)*, 2(2):91, 1986.
- [51] S. H. Simon, E. H. Rezayi, N. R. Cooper, and I. Berdnikov. Construction of a paired wave function for spinless electrons at filling fraction  $\nu = 2/5$ . *Phys. Rev. B*, 75:075317, 2007.

- [52] F. C. Alcaraz and M. J. Martins. Conformal invariance and the operator content of the xxz model with arbitrary spin. *Journal of Physics A: Mathematical and General*, 22(11):1829, 1989.
- [53] H. B. G. Casimir. On the Attraction Between Two Perfectly Conducting Plates. *Indag. Math.*, 10:261–263, 1948. [Kon. Ned. Akad. Wetensch. Proc.100N3-4,61(1997)].
- [54] E. Fermi. Versuch einer theorie der  $\beta$ -strahlen. i. *Zeitschrift für Physik*, 88(3):161–177, 1934.
- [55] S. Parke. Absence of particle production and factorization of the s-matrix in 1 + 1 dimensional models. *Nuclear Physics B*, 174(1):166 – 182, 1980.
- [56] E. Witten. Nonabelian bosonization in two dimensions. *Comm. Math. Phys.*, 92(4):455–472, 1984.
- [57] D. Iagolnitzer. Factorization of the multiparticle  $s$  matrix in two-dimensional space-time models. *Phys. Rev. D*, 18:1275–1285, 1978.
- [58] A. B. Zamolodchikov and Al. B. Zamolodchikov. Factorized s-matrices in two dimensions as the exact solutions of certain relativistic quantum field theory models. *Annals of Physics*, 120(2):253 – 291, 1979.
- [59] G. Delfino. Fields, particles and universality in two dimensions. *Annals of Physics*, 360:477 – 519, 2015.
- [60] C. N. Yang. Some exact results for the many-body problem in one dimension with repulsive delta-function interaction. *Phys. Rev. Lett.*, 19:1312–1315, 1967.
- [61] R. J. Baxter. One-dimensional anisotropic heisenberg chain. *Annals of Physics*, 70(2):323 – 337, 1972.
- [62] Al.B. Zamolodchikov. Two-point correlation function in scaling lee-yang model. *Nuclear Physics B*, 348(3):619 – 641, 1991.
- [63] A. Fring, G. Mussardo, and P. Simonetti. Form factors for integrable lagrangian field theories, the sinh-gordon model. *Nuclear Physics B*, 393(1):413 – 441, 1993.
- [64] V.P. Yurov and Al. B. Zamolodchikov. Correlation functions of integrable 2d models of the relativistic field theory: Ising model. *International Journal of Modern Physics A*, 06(19):3419–3440, 1991.

- 
- [65] A. Koubek and G. Mussardo. On the operator content of the sinh-Gordon model. *Physics Letters B*, 311(1):193 – 201, 1993.
- [66] J. L. Cardy and G. Mussardo. Form factors of descendent operators in perturbed conformal field theories. *Nuclear Physics B*, 340(2):387 – 402, 1990.
- [67] G. Delfino and G. Niccoli. Matrix elements of the operator in integrable quantum field theory. *Nuclear Physics B*, 707(3):381 – 404, 2005.
- [68] O. A. Castro-Alvaredo and A. Fring. Identifying the operator content, the homogeneous sine-Gordon models. *Nuclear Physics B*, 604(1):367–390, 2001.
- [69] E. Levi. Composite branch-point twist fields in the ising model and their expectation values. *Journal of Physics A: Mathematical and Theoretical*, 45(27):275401, 2012.
- [70] O. A. Castro-Alvaredo and B. Doyon. Bi-partite Entanglement Entropy in Massive QFT with a Boundary: the Ising Model. *Journal of Statistical Physics*, 134(1):105–145, 2009.
- [71] G. Delfino and G. Mussardo. The spin-spin correlation function in the two-dimensional ising model in a magnetic field at  $t = t_c$ . *Nuclear Physics B*, 455(3):724 – 758, 1995.
- [72] G. Delfino and P. Simonetti. Correlation functions in the two-dimensional ising model in a magnetic field at  $t = t_c$ . *Physics Letters B*, 383(4):450 – 456, 1996.
- [73] G. Delfino. Topical Review: Integrable field theory and critical phenomena: the Ising model in a magnetic field. *Journal of Physics A: Mathematical and General*, 37(14):R45, 2004.
- [74] F.A. Smirnov. Reductions of the sine-gordon model as a perturbation of minimal models of conformal field theory. *Nuclear Physics B*, 337(1):156 – 180, 1990.
- [75] H. Babujian and M. Karowski. Towards the construction of wightman functions of integrable quantum field theories. *International Journal of Modern Physics A*, 19(supp02):34–49, 2004.
- [76] J.L. Cardy and G. Mussardo. S matrix of the yang-lee edge singularity in two-dimensions. *Phys. Lett.*, B225:275–278, 1989.
- [77] C. Korff and R.A. Weston. PT symmetry on the lattice: The Quantum group invariant XXZ spin-chain. *J.Phys.*, A40:8845–8872, 2007.

- 
- [78] V. G. Knizhnik. Analytic fields on riemann surfaces. ii. *Comm. Math. Phys.*, 112(4):567–590, 1987.
- [79] P. A. Griffin J. J. Atick, L. J. Dixon and D. D. Nemeschansky. Multi-loop twist field correlation functions for zn orbifolds. *Nuclear Physics B*, 298(1):1 – 35, 1988.
- [80] V.G Kac and M. Wakimoto. Braching functions for winding subalgebras and tensor products. *Acta Appl. Math.*, 21:3, 1990.
- [81] W. K. Hastings. Monte carlo sampling methods using markov chains and their applications. *Biometrika*, 57(1):97–109, 1970.
- [82] C. M. Bender. Making sense of non-Hermitian Hamiltonians. *Reports on Progress in Physics*, 70:947–1018, 2007.
- [83] C. F. M. Faria and A. Fring. Non-Hermitian Hamiltonians with real eigenvalues coupled to electric fields: From the time-independent to the time-dependent quantum mechanical formulation. *Laser Physics*, 17:424–437, 2007.
- [84] A. Mostafazadeh. Pseudo-Hermitian Representation of Quantum Mechanics. *International Journal of Geometric Methods in Modern Physics*, 7:1191, 2010.
- [85] F.G. Scholtz, H.B. Geyer, and F.J.W. Hahne. Quasi-hermitian operators in quantum mechanics and the variational principle. *Annals of Physics*, 213(1):74 – 101, 1992.
- [86] Carl M. Bender and Stefan Boettcher. Real spectra in non-hermitian hamiltonians having  $\mathcal{PT}$  symmetry. *Phys. Rev. Lett.*, 80:5243–5246, 1998.
- [87] B. Doyon, M. Hoogeveen, and D. Bernard. Energy flow and fluctuations in non-equilibrium conformal field theory on star graphs. *Journal of Statistical Mechanics: Theory and Experiment*, 3:03002, 2014.
- [88] O. A. Castro-Alvaredo, B. Doyon, and E. Levi. Arguments towards a c-theorem from branch-point twist fields. *ArXiv e-prints*, 2011.
- [89] M. A. I. Flohr. On modular invariant partition functions of conformal field theories with logarithmic operators. *International Journal of Modern Physics A*, 11:4147–4172, 1996.
- [90] V. Gurarie. Logarithmic operators in conformal field theory. *Nuclear Physics B*, 410(3):535 – 549, 1993.
- [91] B. Berg, M. Karowski, and P. Weisz. Construction of green’s functions from an exact  $s$  matrix. *Phys. Rev. D*, 19:2477–2479, 1979.

- 
- [92] G. Delfino, P. Simonetti, and J. L. Cardy. Asymptotic factorisation of form factors in two-dimensional quantum field theory. *Phys. Lett.*, B387:327–333, 1996.
- [93] O. A. Castro-Alvaredo and E. Levi. Higher particle form factors of branch point twist fields in integrable quantum field theories. *Journal of Physics A: Mathematical and Theoretical*, 44(25):255401, 2011.
- [94] M. Caselle, G. Delfino, P. Grinza, O. Jahn, and N. Magnoli. Potts correlators and the static three-quark potential. *Journal of Statistical Mechanics: Theory and Experiment*, 2006(03):P03008, 2006.
- [95] R. Guida and N. Magnoli. All order i.r. finite expansion for short distance behavior of massless theories perturbed by a relevant operator. *Nuclear Physics B*, 471(1–2):361–385, 1996.
- [96] R. Guida and N. Magnoli. All order i.r. finite expansion for short distance behavior of massless theories perturbed by a relevant operator. *Nuclear Physics B*, 471(1–2):361–385, 1996.
- [97] A.I.B. Zamolodchikov. *ITEP preprint*, pages 144–89, 1989.
- [98] M. Headrick. Entanglement rényi entropies in holographic theories. *Phys. Rev. D*, 82:126010, 2010.
- [99] E. Levi, O. A. Castro-Alvaredo, and B. Doyon. Universal corrections to the entanglement entropy in gapped quantum spin chains: A numerical study. *Phys. Rev. B*, 88:094439, 2013.
- [100] B. Doyon. Bipartite entanglement entropy in massive two-dimensional quantum field theory. *Phys. Rev. Lett.*, 102:031602, 2009.
- [101] M. A. Rajabpour and F. Gliozzi. Entanglement entropy of two disjoint intervals from fusion algebra of twist fields. *Journal of Statistical Mechanics: Theory and Experiment*, 2012(02):P02016, 2012.
- [102] P. J. Forrester and R. J. Baxter. Further exact solutions of the eight-vertex SOS model and generalizations of the Rogers-Ramanujan identities. *Journal of statistical physics*, 38(3-4):435–472, 1985.
- [103] H. S. M. Coxeter. *Regular polytopes*. Courier Corporation, 1973.
- [104] S. Warnaar and B. Nienhuis. Solvable lattice models labelled by dynkin diagrams. *Journal of Physics A: Mathematical and General*, 26(10):2301, 1993.

- 
- [105] G. E. Andrews, R. J. Baxter, and P. J. Forrester. Eight-vertex sos model and generalized rogers-ramanujan-type identities. *Journal of Statistical Physics*, 35(3):193–266, 1984.
- [106] D. Gepner and Z. Qiu. Modular invariant partition functions for parafermionic field theories. *Nuclear Physics B*, 285:423 – 453, 1987.
- [107] David L O’Brien and Paul A Pearce. Surface free energies, interfacial tensions and correlation lengths of the abf models. *Journal of Physics A: Mathematical and General*, 30(7):2353, 1997.
- [108] A. De Luca and F. Franchini. Approaching the restricted solid-on-solid critical points through entanglement: One model for many universalities. *Phys. Rev. B*, 87:045118, 2013.
- [109] P. A. Pearce, J. Rasmussen, and J.-B. Zuber. Logarithmic minimal models. *Journal of Statistical Mechanics: Theory and Experiment*, 2006(11):P11017, 2006.
- [110] P. A. Pearce and K. A. Seaton. Off-critical logarithmic minimal models. *Journal of Statistical Mechanics: Theory and Experiment*, 2012(09):P09014, 2012.
- [111] A. Feiguin, S. Trebst, A. W. W. Ludwig, M. Troyer, A. Kitaev, Z. Wang, and M. H. Freedman. Interacting anyons in topological quantum liquids: The golden chain. *Phys. Rev. Lett.*, 98:160409, 2007.
- [112] V. Pasquier and H. Saleur. Symmetry of the xxz chain and quantum su(2). *Ecole d’ete de Physique Théorique*, Field, Strings and Critical Phenomena(Session XLIX), 1988.
- [113] H. N. V. Temperley and E. H. Lieb. Relations between the ‘percolation’ and ‘colouring’ problem and other graph-theoretical problems associated with regular planar lattices: Some exact results for the ‘percolation’ problem. *Proceedings of the Royal Society of London A: Mathematical, Physical and Engineering Sciences*, 322(1549):251–280, 1971.
- [114] V. Pasquier and H. Saleur. Common structures between finite systems and conformal field theories through quantum groups. *Nucl. Phys.*, B330:523, 1990.
- [115] C. Korff and R.A. Weston. PT symmetry on the lattice: The Quantum group invariant XXZ spin-chain. *J.Phys.*, A40:8845–8872, 2007.
- [116] C. Gómez, M. Ruiz-Altaba, and G. Sierra. *Quantum groups in two-dimensional physics*. Cambridge University Press, 2005.

- [117] P. Calabrese, J. Cardy, and E. Tonni. Entanglement negativity in extended systems: A field theoretical approach. *J. Stat. Mech.*, 1302:P02008, 2013.
- [118] O. Blondeau-Fournier, O.A. Castro-Alvaredo, and B. Doyon. Universal scaling of the logarithmic negativity in massive quantum field theory. *J. Phys.*, A49(12):125401, 2016.
- [119] M. Hoogeveen and B. Doyon. Entanglement negativity and entropy in non-equilibrium conformal field theory. *Nucl. Phys.*, B898:78–112, 2015.
- [120] O. Blondeau-Fournier and B. Doyon. Expectation values of twist fields in integrable quantum field theory and universal entanglement saturation. *arXiv:1612.04238*, 2016.
- [121] P. Calabrese, J. Cardy, and E. Tonni. Entanglement entropy of two disjoint intervals in conformal field theory. *J. Stat. Mech.*, 0911:P11001, 2009.
- [122] T W B Kibble. Topology of cosmic domains and strings. *Journal of Physics A: Mathematical and General*, 9(8):1387, 1976.
- [123] W. H. Zurek. Cosmological experiments in superfluid helium? *Nature*, 317:505–508, 1985.
- [124] P. Calabrese and J. Cardy. Entanglement and correlation functions following a local quench: a conformal field theory approach. *Journal of Statistical Mechanics: Theory and Experiment*, 10:10004, October 2007.
- [125] B. Estienne, N. Regnault, and B. A. Bernevig. Correlation lengths and topological entanglement entropies of unitary and nonunitary fractional quantum hall wave functions. *Phys. Rev. Lett.*, 114:186801, 2015.
- [126] J. L. Cardy. Conformal invariance and the Yang-Lee Edge singularity in two dimensions. *Phys. Rev. Lett.* **54**, pages 1354–1356, 1985.
- [127] J. Taylor. *Introduction to Error Analysis, the Study of Uncertainties in Physical Measurements, 2nd Edition*. 1997.
- [128] M. Galassi et al. *GNU Scientific Library Reference Manual (3rd edition)*.